Mechanistic Insights on Inhibitors Targeting the RNA Helicase eIF4A

By

Jennifer Chu
Department of Biochemistry
McGill University, Montreal
November 2019

A thesis submitted to McGill University
in partial fulfillment of the requirements of the degree of Doctor of Philosophy

ABSTRACT

Protein synthesis (also known as translation) is a core step in the gene expression pathway that allows cells to rapidly alter the proteome in response to intra- and extracellular cues, and deregulation of this process can severely reduce cellular fitness or lead to malignant transformation. The rate-limiting step for protein synthesis is the initiation phase, which can be broken down into 4 phases: 1) activation of the mRNA through association of the eIF4F complex (comprised of the cap-binding protein, eIF4E, the scaffolding protein, eIF4G, and the RNA helicase, eIF4A) to the 5' cap; 2) recruitment of the 40S ribosome; 3) scanning of the 40S ribosome; 4) start codon recognition and joining of the 60S ribosomal subunit. Because the availability of eIF4F is limiting, the competitive ability of an mRNA to associate with this complex is a major determinant for how efficiently it gets translated. As well, eIF4F availability is under the regulation of several different signalling cascades, and perturbance of these pathways can dramatically alter the make-up of the translatome. For these reasons, this complex is considered to be an attractive target for anti-neoplastic therapy.

Small molecules belonging to the rocaglate family of compounds have garnered considerable interested in recent years. In this dissertation, we provide genetic evidence demonstrating that eIF4A1 is the primary cellular target of rocaglates. These compounds appear to inhibit protein synthesis by stimulating eIF4A RNA binding activity, and it had been proposed that mRNAs with purine-rich 5' leaders display heightened sensitivity towards these compounds. However, we discovered that this bias is not shared among all rocaglates, indicating that although these compounds have a common cellular target, their mechanism of action may not be entirely identical. Lastly, we offer a model that provides a rationale for how stimulation of eIF4A activity leads to inhibited protein synthesis.

RÉSUMÉ

La synthèse protéine (aussi appelée traduction) est une étape essentielle de la voie d'expression des gènes qui permet aux cellules de modifier rapidement le protéome en réponse à des signaux intra et extracellulaires, et la dérégulation de ce processus peut réduire considérablement l'aptitude cellulaire ou entraîner une transformation maligne. L'étape qui limite le taux de synthèse des protéines est la phase d'initiation, qui peut être décomposée en 4 phases : 1) activation de l'ARNm par association du complexe eIF4F (composé de la protéine qui ce fixe au coiffe en 5', eIF4E, de la protéine d'échafaudage, eIF4G, et de l'hélicase d'ARN, eIF4A) au coiffe en 5' ; 2) recrutement du ribosome 40S ; 3) balayage du ribosome 40S ; 4) reconnaissance du codon de démarrage et liaison de l'unité ribosomale 60S. Comme la disponibilité du eIF4F est limitée, la capacité concurrentielle d'un ARNm à s'associer à ce complexe est un facteur déterminant de l'efficacité avec laquelle il est traduit. De plus, la disponibilité de l'eIF4F est soumise à la régulation de plusieurs cascades de signalisation différentes, et la perturbation de ces voies peut modifier considérablement la composition du translatome. Pour ces raisons, ce complexe est considéré comme une cible attrayante pour le traitement anti-néoplasique.

Les petites molécules de la famille des rocaglates ont suscité beaucoup d'intérêt ces dernières années. Dans cette thèse, nous fournissons des preuves génétiques démontrant que l'eIF4A1 est la principale cible cellulaire des roacglates. Ces composés semblent inhiber la synthèse des protéines en stimulant l'activité de liaison de l'ARN eIF4A, et il a été proposé que les ARNm avec des leaders en 5' riches en purine présentent une sensibilité accrue envers ces composés. Cependant, nous avons découvert que ce biais n'est pas partagée par tous les rocaglates, ce qui indique que même si ces composés ont une cible cellulaire commune, leur mécanisme d'action est probablement pas

entièrement identique. Enfin, nous proposons un modèle qui explique comment la stimulation de l'activité eIF4A conduit à une inhibition de la synthèse des protéines.

ACKNOWLEDGEMENTS

I would like to thank my supervisor, Dr. Jerry Pelletier, who has gone above and beyond in guiding my development young scientist. I am grateful to him for being more or less available at all hours of the day to discuss anything science-related, be it experimental results or a hypothetical off-the-wall idea. Beyond technical guidance, I am also greatly appreciative of Jerry for driving me to talks/conferences, helping me move and providing career (and occasional life) advice. Jerry's own passion for research and his incredible work ethic has also provided great inspiration for me to always push myself to improve and to never feel complacent.

I would also like to thank all members of the Pelletier lab (past and present). Unfortunately, there are too many to name, but every person has aided me in one way or another. In particular, I am gracious for all the people who guided me during my early years as a graduate student and set me on the right path in my development as a researcher. Notably, I thank Gaby Galicia-Vázquez for being an attentive and patient teacher who taught me how to conduct every eIF4A-related assay performed in this thesis. To John R. Mills, whose mentorship during my first year in graduate school greatly influenced the way that I approach experiments now. Much appreciation also goes towards the stalwarts of the Pelletier lab, Francis Robert, Regina Cencic, and Patrick Sénéchal, for their consistent technical assistance. I would also like to express deep gratitude towards my good friend, Alex Katigbak, for providing unpaid therapy and for reliably consuming various forms of carbohydrates with me in moments of joy and misery. In the same vein, I am also incredibly gracious to have crossed paths with Abba Malina, who has been (and still is) an incredible resource for scientific discourse and unsolicited baking advice.

Additionally, I thank the lab of Dr. John Porco for their longstanding collaboration with our lab. Without their contributions, this thesis simply would not exist. Much appreciation also goes towards members of Pasha Baranov's lab for their bioinformatic expertise. I also thank members of my research advisory committee, Dr. Nahum Sonenberg and Dr. Bushan Nagar for their valuable input.

Beyond the lab, I would like to thank my friends and family for all the emotional support I have received. As an avid consumer of audio journalism (particularly during long experiments), I would also like to thank Ira Glass and This American Life for paving way for all of the wonderful podcasts that have come out in recent years. Most of all, I would like to thank my parents and my sister for their unwavering support and encouragement.

TABLE OF CONTENTS

LIST OF FIGURES

LIST OF TABLES

PREFACE

This is a manuscript-based thesis which consists of three published research articles (Chapters 2, 3, and 4), and one research article that is currently under revision (Chapter 5), for which I am the first author. Certain sections in the introduction (Chapter 1) and the discussion (Chapter 6) were adapted from two literature reviews and one book chapter, for which I am the first author.

Chapter 1:

Chu, J., and Pelletier, J. (2015). Targeting the eIF4A RNA helicase as an anti-neoplastic approach. *Biochimica et biophysica acta* **1849**, 781-791.

Chu, J., Cargnello, M., Topisirovic, I., and Pelletier, J. (2016). Translation Initiation Factors: Reprogramming Protein Synthesis in Cancer. *Trends in cell biology* **26**, 918-933.

Chapter 2:

Chu J., Cencic R., Wang W., Porco J. A. Jr., and Pelletier J. (2016). Translation Inhibition by Rocaglates is Independent of eIF4E Phosphorylation Status. *Mol. Cancer. Ther.* **15(1):** 136-141.

Chapter 3:

Chu J., Galicia-Vázquez G., Cencic R., Mills J. R., Katigbak A., Porco J. A. Jr., and Pelletier J. (2016). CRISPR-Mediated Drug-Target-Validation Reveals Selective Pharmacological Inhibition of the RNA helicase eIF4A. *Cell Rep.* **15(11):** 2340-2347

Chapter 4:

Chu J., Zhang W., Cencic R., Devine W. G., Beglov D., Henkel T., Brown L. E., Vajda S., Porco J. A. Jr., and Pelletier J. (2016). Translation Inhibition by Rocaglates is Independent of eIF4E Phosphorylation Status. *Cell Chem. Biol.* **In Press**

Chapter 5:

Chu J., Zhang W., Cencic R., O'Connor P. B. F., Robert F., Devine W. G., Selznick A., Henkel T., Merrick W. C., Brown L. E., Porco J. A. Jr., and Pelletier J. (2019). Rocaglates Cause Gain-of-Function Alterations to eIF4A and eIF4F, *Cell Rep.* **Under Revision**

Chapter 6:

Chu, J., and Pelletier, J. (2015). Targeting the eIF4A RNA helicase as an anti-neoplastic approach. *Biochimica et biophysica acta* **1849**, 781-791.

Chu, J., Cargnello, M., Topisirovic, I., and Pelletier, J. (2016). Translation Initiation Factors: Reprogramming Protein Synthesis in Cancer. *Trends in cell biology* **26**, 918-933.

Chu, J., and Pelletier, J. (2018). Chemical and CRISPR/Cas9 Tools for Functional Characterization of RNA Helicases. *Applied RNA Bioscience*, S. Masuda, and Izawa S., ed. (Springer), pp. 221-245

CONTRIBUTION OF AUTHORS

Chapter 2:

I performed all experiments and generated all reagents with the following exceptions: The small molecules shown in Figure 2.1B were synthesized by the lab of Dr. John Porco and the panel in Figure 2.3 was produced by Dr. Regina Cencic. All work was completed under the supervision of Dr. Jerry Pelletier.

Chapter 3:

I performed all experiments and generated all reagents with the following exceptions: All rocaglates were synthesized by the lab of Dr. John Porco. The retroviral complementation vector (Figure 3.2A) was made by Dr. John Mills. The CRISPR-modified cell lines were generated by Dr. Gabriela Galicia Vazquez. Drug administration in the *in vivo* xenograft experiments and tumor measurements (Figure 3.4B) were performed by Dr. Regina Cencic. All work was completed under the supervision of Dr. Jerry Pelletier.

Chapter 4:

I performed all experiments and generated all reagents with the following exceptions: All rocaglates were supplied by the labs of Dr. John Porco and Dr. Thomas Henkel. *In silico* docking was performed by Dr. Dmitri Beglov and Dr. Sandor Vajda (Figure 4.3C). *In vivo* studies were executed by Dr. Regina Cencic. All work was completed under the supervision of Dr. Jerry Pelletier.

Chapter 5:

I performed all experiments and generated all reagents with the following exceptions. All rocaglates were supplied by the labs of Dr. John Porco and Dr. Thomas Henkel. Cloning of the mRNA reporters was done with the assistance of Asher Selznick. Dr. Regina Cencic performed the experiment shown in Figure 5.2B. Analysis of ribosome profiling data was performed by Dr. Patrick O'Connor and Dr. Pavlov Baranov. Purified eIF4F complexes were supplied by Dr. William C. Merrick. Dr. Francis Robert performed the dissociation experiments shown in Figure S5.1E. All work was completed under the supervision of Dr. Jerry Pelletier.

ORIGINAL CONTRIBUTION TO KNOWLEDGE

Chapter 2:

- ERK phosphorylation is altered by the presence of rocaglates. However, certain cell types display increased phosphorylation of ERK (e.g. NIH/3T3 cells), whereas others show decreased phosphorylation levels (e.g. Jurkat T cells).
- Regardless of ERK phosphorylation status, phosphorylation of eIF4E is not affected by rocaglates.
- Cells deficient in eIF4E phosphorylation are similarly responsive to rocaglates compared to wild type cells.

Chapter 3:

- The eIF4A mutant, eIF4A1 (F163L), shows similar enzymatic activity as the wildtype protein but does not respond to silvestrol *in vitro*.
- Introduction of the eIF4A1 (F163L) mutant into cells confers resistance to silvestrol.
- Tumors harboring the eIF4A1 F163L point mutation do not respond to silvestrol *in vivo*.
- Silvestrol preferentially inhibits the translation of MYC in an eIF4A-dependent mechanism.

Chapter 4:

- eIF4A1 and eIF4A2 respond similarly to >200 different rocaglate analogues.
- Both eIF4A1 and eIF4A2 display inherent bias towards binding purine rich RNAs.
- Amidino-rocaglates represent a novel subclass of synthetic rocaglates with promising *in vivo* anti-tumor activity.

Chapter 5

- Stimulation of eIF4A binding towards polypurine-rich RNA is a good, but not perfect, predictor of the efficacy of a given rocaglate as an inhibitor of protein synthesis.
- All active rocaglates exert their mechanism through an eIF4A1-dependent manner.
- Rocaglates vary with respect to their bias in inhibiting the translation of mRNAs with purine-rich 5' leaders.
- Rocaglates increase the retention time of the entire eIF4F complex onto 5' caps. In doing so, this exerts a *trans*-inhibitory effect as the levels of available eIF4F is diminished.

LIST OF ABBREVIATIONS

4EHP	eIF4E Homologous Protein
ABCB1	ATP-Binding Cassette Sub-Family B1
ADR	Amidino-Rocaglate
AKT	AKR Thymoma Cell Line Kinase (Protein Kinase B)
ALL	Acute Lymphoblastic Leukemia
AML	Acute Myeloid Leukemia
AMP	Adenosine Monophosphate
AMPK	AMP-Activated Protein Kinase
AMPPNP	Adenylyl-Imidodiphosphate
ASO	Antisense Oligonucleotide
ATG7	Autophagy Related 7
ATL	Adult T-Cell Lymphoma
ATM	Ataxia Telangiectasia Mutated Kinase
ATP	Adenosine Triphosphate
BCL	B-Cell Lymphoma, or Bcl-2 like
BC1	Brain Cytoplasmic 1 RNA
BiP	Binding Immunoglobulin Protein
BSA	Bovine Serum Albumin
CAT	Chloramphenicol Acetyltransferase
CBC	Cap Binding Complex
CCR4	CC Chemokine Receptor 4
CDK1	Cyclin-Dependent Kinase 1
CDS	Coding Sequence
CDX	Cell Line-Derived Xenograft
CETSA	Cellular Thermal Shift Assay
CNOT1	CCR4-Negative Regulator of Transcription Subunit 1
CITE	Cap Independent Translation Enhancer
CLIP	Crosslinking Immunoprecipitation
CPV	Cytoplasmic Polyhedrosis Virus
CRD-BP	Coding Region Determinant-Binding Protein
CRISPR	Clustered Regularly Interspaced Short Palindromic Repeats
CTD	C-Terminal Domain
CTP	Cytosine Triphosphate
CUL3	Cullin 3
DEAD	Aspartate Glutamine Alanine Aspartate
DMDA-PatA	Des-Methyl, Des-Amino Pateamine A
DNA	Deoxyribonucleic Acid
DSF	Differential Scanning Fluorimetry
EDTA	Ethylenediaminetetraacetic acid
eEF2	Elongation Factor 2
EGFR	Epidermal Growth Factor Receptor

EGTA	Ethylene Glycol-Bis(β-aminoethyl ether)-N,N,N′,N′-Tetraaceti Acid
eIF	Eukaryotic Initiation Factor
EJC	Exon Junction Complex
EMCV	Encephalomyocarditis Virus
EMT	Epithelial to Mesenchymal
ERK	Extracellular Signal-Regulated Kinase
FAM	Fluorescein
FBS	Fetal Bovine Serum
FDA	Federal Drug Administration
FGF	Fibroblast Growth Factor
FKBP	FK506-Binding Proteins
FMDV	Foot and Mouth Disease Virus
FRET	Forster Resonance Energy Transfer
GAP	Guanine Activating Protein
GAPDH	Glyceraldehyde 3-Phosphate Dehydrogenase
GCN	General Control Nonderepressible
GDP	Guanosine Diphosphate
GEF	Guanine Exchange Factor
GFP	Green Fluorescent Protein
GMP	Guanine Monophosphate
GTP	Guanine Triphosphate
HCV	Hepatitis C Virus
HDR	Homology Directed Repair
HEAT	Huntingtin, Elongation Factor 3, Protein Phosphatase 2A, Tor1 Repeat Structure
HEK	Human Embryonic Kidney
HEPES	4-(2-Hydroxyethyl)-1-Piperazineethanesulfonic Acid
HIF	Heat Inducible Factor
HMEC	Human Mammary Epithelial Cells
HNSCC	Head and Neck Squamous Cell Carcinoma
HPDE	Human Pancreatic Ductal Epithelial
HRI	Heme-Regulated Inhibitor Kinase
HTLV	Human T-Lymphotropic Virus
iNOS	Inducible Nitric Oxide Synthase
IPTG	Isopropyl β- d-1-Thiogalactopyranoside
IRES	Internal Ribosomal Entry Site
IRS	Insulin Receptor Substrate
ISR	Integrated Stress Response
KEAP1	Kelch Like ECH Associated Protein 1
KRAS	Kirsten Rat Sarcoma
LDS	Lithium Dodecyl Sulfate
lncRNA	Long Non-Coding RNA
MAP	Mitogen Activated Protein

MAPK	Mitogen Activated Protein Kinase
MAX	MYC Associated Factor X
MCL	Myeloid Leukemia Cell
MDR	Multi-Drug Resistance 1
MEF	Mouse Embryonic Fibroblast
MEK	Mitogen-Activated Protein Kinase Kinase
MES	2-Ethanesulfonic Acid
MFC	Multifactor Complex
miRNA	Micro RNA
MMP	Matrix Metalloproteinase
MNK	MAP Kinase-Like Interacting Protein
mRNA	Messenger RNA
MTOR	Mammalian Target of Rapamycin
MYC	Myelocytomasis Viral Oncogene
NF-kB	Nuclear Factor Kappa-Light-Chain-Enhancer of Activated B Cells
NMD	Nonsense Mediated Decay
NMR	Nuclear Magnetic Resonance
NRF2	Nuclear Factor Erythroid 2-Related Factor 2
NOT	Negative Regulator of Transcription
NSCLC	Non-Small-Cell Lung Carcinoma
NTD	N-Terminal Domain
NTP	Nucleoside Triphosphate
ODC	Ornithine Decarboxylase
ODN	Oligo DNA Nucleotides
ORF	Open Reading Frame
PABP	Poly A Binding Protein
PAGE	Protein Acrylamide Gel Electrophoresis
PAM	Protospacer Adjacent Motif
PAP	Poly A Polymerase
PAR	Photo-Activatable Ribonucleoside
PatA	Pateamine A
PBS	Phosphate-Buffered Saline
PCR	Polymerase Chain Reaction
PDB	Protein Data Bank
PDCD4	Programmed Cell Death 4
PDL	Population Doubling Levels
PDX	Patient Derived Xenograft
PEI	Polyethyleneimine
PERK	PKR-Like Endoplasmic Reticulum Kinase
PGP1	P-Glycoprotein-1
PHB	Prohibitin
PIC	Preinitiation Complex
PIM	Proviral Integration Site MuLV
PKR	Protein Kinase R

PLB	Passive Lysis Buffer
PMSF	Phenylmethanesulfonylfluoride Fluoride
PTEN	Phosphatase and Tensin Homolog
PVDF	Polyvinylidene Fluoride
RAF	Rapidly Accelerated Fibrosarcoma (MAP Kinase Kinase)
RAS	Rat Sarcoma
RBP	RNA Binding Protein
RCV	Retroviral Complementation Vector
RHT	Rohitinib
RICTOR	Rapamycin-Insensitive Companion of mTOR
RIPA	Radioimmunoprecipitation Assay
RISC	RNA-Induced Silencing Complex
RLU	Relative Light Units
RNA	Ribonucleic Acid
RocA	Rocaglate A
ROS	Reactive Oxygen Species
RPD	RNA Pulldown
RRL	Rabbit Reticulocyte Lysate
RSK	Ribosomal S6 Kinase
RT	Reverse Transcription
S6K	S6 Kinase
SAM	S-Adenosyl-L-Methionine
SAR	Structure-Activity-Relationship
SDS	Sodium Dodecyl Sulfate
SG	Stress Granule
snRNA	Small Nuclear RNA
siRNA	Small Interfering RNA
SRB	Sulforhodamine B
STRAP	Serine/Threonine Kinase Receptor Associated Protein
TIA	T-Cell Restricted Intracellular Antigen
TIAR	TIA Related
TISU	Translation Initiator of Short 5'UTR
TLC	Thin Layer Chromatography
TOP	Terminal Oligopyrimidine
TOR	Target of Rapamycin
TRAIL	TNF-Related Apoptosis-Inducing Ligand
TRCP	Transducin Repeats-Containing Protein
TREX	Transcription/Export Complex
TSC	Tuberous Sclerosis Protein
TSS	Translation Start Site
TUNEL	Terminal Deoxynucleotidyl Transferase
ULK1	Unc-51-Like Autophagy Activating Kinase 1
uORF	Upstream Open Reading Frame
UTP	Uridine Triphosphate

UTR	Untranslated Region
VEGF	Vascular Endothelial Growth Factor
XIAP	X-Linked Inhibitor of Apoptosis Protein
XRN1	5'-3' Exoribonuclease 1

CHAPTER 1 GENERAL INTRODUCTION

Selected Sections Published in:

Chu, J., and Pelletier, J. (2015). Targeting the eIF4A RNA helicase as an anti-neoplastic approach. *Biochimica et biophysica acta* **1849**, 781-791.

With copyright permission from Elsevier

Chu, J., Cargnello, M., Topisirovic, I., and Pelletier, J. (2016). Translation Initiation Factors: Reprogramming Protein Synthesis in Cancer. *Trends in cell biology* **26**, 918-933.

With copyright permission from Elsevier

1.1 Features of a Mature Eukaryotic mRNA

1.1.1 The Advent of mRNA Biology

The concept of a messenger RNA was more or less a non-entity until Dr. Francis Crick first publicly proposed its existence during a seminal lecture on September 19, 1957. Prior to this, the mechanism of protein synthesis was shrouded in mystery. Crick had speculated that the assembly of amino acids occurs sequentially in manner dictated by the genetic code, but given that DNA was compartmentalized within the nucleus while protein synthesis was observed to take place within cytoplasm (as first shown by Jean Brachet in 1933), he reasoned that RNA localized within the cytoplasm may serve as intermediary templates that deliver genetic information encoded within DNA to the protein synthesis machinery. In 1957, there was little evidence proving this but Crick's hypothesis was eventually confirmed during the early 1960s when Sydney Brenner, Francois Jacob, and Matthew Meselson demonstrated that upon bacteriophage infection, small, transient RNAs are synthesized from phage DNA *de novo,* and become associated with pre-existing translation machinery derived from the host to produce protein. The discovery of the "messenger" RNA (mRNA) was a pivotal moment in the budding field of protein synthesis, and since then, scientists have uncovered that in addition to carrying the coding information for polypeptide assembly, mRNAs also possess a number of regulatory non-coding elements that can influence gene expression.

1.1.2 The 5' Cap

The 5' methylated cap, now understood to be a key feature of all eukaryotic mRNAs, was not discovered until the 1970s. Prior to then, in the early days of mRNA research, large quantities of intact eukaryotic mRNA proved to be difficult to isolate due to the ubiquitous presence of RNAses and, as

a result, much of the research was done using bacterial systems. Because mRNAs derived from bacteria and bacteriophages were generally triphosphorylated (pppN) at its 5' ends with no additional modifications, this was also presumed to be the case for eukaryotic mRNAs. In 1973, the presence of a 5' methylated cap was first observed when Furuichi and Miura discovered that the addition to the methyl donor, S-adenosyl-L-methionine (SAM) into *in vitro* transcription reactions of cytoplasmic polyhedrosis virus (CPV) mRNA stimulated transcription ~100 fold and yielded transcripts with methylated 5' termini (Furuichi, 1974, 2015). It soon became evident this methylated structure was not just a feature of viral transcripts but instead, the m7GpppN cap was found to be a conserved feature present in all eukaryotic cellular mRNAs (Furuichi, 2015).

The addition of the 5' cap is an early co-transcriptional event that precedes all other mRNA processing events. Newly synthesized RNAs transcribed by RNA polymerase II initially possess a triphosphorylated 5' end (pppN) but upon the incorporation of the 25th to 30th nucleotide, the capping machinery is recruited to the nascent RNA (Cho et al., 1997). The RNA is then capped through three catalytic events. First, the γ-phosphate at the 5' terminus (pppN) is removed by a RNA triphosphatase, resulting in a diphosphate end (ppN) (Furuichi and Shatkin, 2000). Next, a guanylyltransferase incorporates a GMP molecule to form the guanosine cap (GpppN) (Furuichi and Shatkin, 2000). Lastly, the guanosine cap is methylated by guanine-N7 methyltransferase at the N-7 position (m7GpppN) (Furuichi and Shatkin, 2000).

The cap modification is a hallmark of all RNA pol II transcripts which, in addition to mRNA, includes microRNAs (miRNAs) and small nuclear RNAs (snRNA) (Cai et al., 2004). In the case for miRNAs, the cap is either removed during processing or is excluded from loading onto RISC (RNA-induced silencing complex)(Treiber et al., 2019; Xie et al., 2013). Through the recruitment of various

nuclear and cytoplasmic cap-binding proteins, cap structure is an essential mediator of several aspects of mRNA metabolism, including pre-mRNA splicing (Lewis et al., 1996; Pabis et al., 2013), nuclear export (Nojima et al., 2007), protection against exonucleolytic degradation, mRNA turnover, and, the focal point of this thesis, protein synthesis. Many of these processes are made possible through the association of two major cap binding complexes: CBC (cap-binding complex) and eIF4F (eukaryotic initiation factor 4F).

CBC is predominantly nuclear complex comprised of two subunits, Cbp20, which interacts with the cap structure, and Cbp80, which interacts with the CTD of pol II. Shortly after the addition of the cap, CBC is recruited to the nascent pre-mRNA and promotes spliceosome assembly onto the 5' proximal intron (Lewis et al., 1996; Visa et al., 1996). CBC is also involved in mRNA 3' end processing by promoting pre-mRNA cleavage at the poly(A) site and stabilizing the polyadenylation complex (Flaherty et al., 1997). Upon the completion of pre-mRNA processing, CBC remains associated to the 5' cap and interacts with the transcription-export complex (TREX) to promote cytoplasmic export (Cheng et al., 2006). Additionally, CBC is hypothesized direct the pioneer round of translation, and consequently is also thought to mediate nonsense mediated decay (NMD)—an important surveillance mechanism that takes place during the pioneer round of translation to eliminate transcripts containing premature termination codons (Maquat, 2005). In doing so, NMD prevents the accumulation of truncated proteins that may possess toxic cellular effects. Following the pioneer round of translation, CBC is displaced by the cytoplasmic cap-binding protein eIF4E whose role will be covered in more detail in section 1.2.1.1 but in short, eIF4E drives the subsequent rounds of translation that account for the majority of proteins synthesized.

Finally, the life cycle of a mRNA is often terminated when the cap structure is removed by decapping enzymes (Coller and Parker, 2004). With an exposed 5' monophosphate, the mRNA is now highly vulnerable to 5' to 3' degradation mediated by the exonuclease, XRN1 (Coller and Parker, 2004). Overall, the terminal m7GpppN structure is plays a pivotal role throughout the mRNA life cycle, from transcription and mRNA maturation, to cytoplasmic export, translation and turnover. Consequently, the interplay between the 5' cap and the complexes that bind it possess a large regulatory influence over proteome composition and cellular homeostasis.

1.1.3 The 5' Leader Region

The 5' leader region (also commonly known as the 5' untranslated region (UTR)) represents the stretch of nucleotides spanning from the methylated cap to the initiating codon. In the canonical scanning model of eukaryotic translation, the 43S pre-initiation complex scans through this region in a 5' to 3' manner until it encounters a start codon, which is usually the most 5' proximal AUG (Kozak, 1989). The extent of conservation of the 5' leaders of orthologous transcripts between different organisms, while not as high as the coding region, is more conserved compared to untranscribed regions of the genome, suggesting that this portion of the mRNA may play a role in gene regulation (Shabalina et al., 2004). In accordance with this, decades of experimental work support a hypothesis in which translation initiation is modulated by various features of the 5' leader, as summarized in Table 1.1. For instance, long, GC-rich, and highly structured 5' leaders are considered to be barriers for the scanning ribosome and result in inefficient translation initiation compared to mRNAs with shorter and less structured 5' leaders (Leppek et al., 2018). The average human 5' leader possesses 60% GC content and is approximately ~200 nts long (Shabalina et al., 2004; Zhang et al., 2004). In

contrast, yeast mRNAs tend to be less GC rich (40%) and are much shorter (median length of 53 nts) (Leppek et al., 2018; Zhang et al., 2004). This divergence in the 5' leader conservation may be attributed to differing requirements in gene regulation between higher and lower eukaryotes, and highlights that although several core principles of yeast translation are applicable to mammalian translation, several regulatory mechanisms are organism specific.

1.1.3.1 Upstream Translation Start Sites

Protein synthesis typically initiates at the 5' most proximal AUG, but this is not always the case. When the 5' most proximal AUG is positioned within a non-ideal context, the ribosome can bypass this codon and continue scanning (Kozak, 1989). In turn, these upstream AUG (uAUG) elements modulate the translation efficiency at the downstream authentic start site. During the late 1980s, Marilyn Kozak systematically surveyed the 5' leaders of 699 vertebrate UTRs and determined that the optimal sequence for efficient translation initiation to be GCCRCCAUGG (where R denotes a purine), and mutagenesis of these surrounding nucleotides, especially the purine in position -3 and the G in position +4, dramatically affected the rate of initiation at that AUG (Kozak, 2001). In addition to AUG, translation initiation events can take place at near-cognate codons, such as CUG or GUG, albeit at a lower efficiency (Asano, 2014; Ingolia et al., 2011; Kearse and Wilusz, 2017; Tang et al., 2017).

Many transcripts may also possess one or more AUGs positioned upstream of the main open reading frame and in humans it is estimated that approximately 10% of all mRNAs contain at least one uAUG (Pesole et al., 2001). However, the frequency of observed uAUGs is less than what one would expect by chance, suggesting that this feature is selected against during the evolutionary process

(Iacono et al., 2005; Rogozin et al., 2001). uAUGs are generally considered to be negative regulatory elements for translation initiation that compete with the main AUG for the scanning ribosome, but if uAUG is situated within an unfavourable sequence context, it tends to be bypassed (this phenomenon is referred to as 'leaky scanning') (Morris and Geballe, 2000). The frequency of leaky scanning can be determined by availability of translation factors and is modulated by cues such as cellular stressors and the presence growth factors and non-incidentally, numerous uAUG-bearing transcripts encode for stress response proteins (Morris and Geballe, 2000). Proto-oncogenes are also overrepresented among transcripts containing uAUGs, and it is possible that these negative cis-acting elements are important in regulating the expression of these genes (Kozak, 1987).

When an uAUGs is also shortly followed by an in-frame stop codon, it is referred to as an upstream open reading frame (uORF). Upon encountering the stop codon of the uORF, the ribosome can either dissociate from the mRNA or alternatively, remain associated and resume scanning until it reaches the main open reading frame and reinitiates translation (Morris and Geballe, 2000). The frequency of reinitiation varies between mRNAs and is influenced by number of variables, including codon usage of the uORF, nucleotide composition surrounding the terminating codon, and distance between the uORF and the main ORF (Wethmar et al., 2014).

Another exception to the "first AUG" rule is exemplified by AUGs positioned extremely closely to the 5' cap and, in general, the translation of mRNAs with 5' leaders shorter than 20 nts long is inefficient (Kozak, 1991). It is possible that additional contacts between the ribosome and upstream sequences of the mRNA are required for efficient initiation and indeed, crosslinking experiments reveal that when the 40S ribosome is positioned at the start codon, interactions are also formed 17 nucleotides upstream of the initiation site (Pisarev et al., 2008). The discrimination against extremely

5’ proximal AUGs also appears to be mediated by eukaryotic initiation factor (eIF)1 availability as supplementation of eIF1 to *in vitro* translation reactions promotes scanning to a more downstream AUG , while removal of eIF1 in toeprinting assays enabled efficient recognition at the cap-proximal AUG (Elfakess et al., 2011; Pestova and Kolupaeva, 2002).

1.1.3.2 TISU elements

The experiments first conducted by Kozak demonstrate that initiation tends to be inefficient at extremely cap-proximal start sites, but more recently, it was shown that mRNAs with TISU (translation initiator of short 5’ leader) elements do not abide by this. TISU-bearing mRNAs are characterized by extremely short 5’ leaders (median length = 12 nucleotides) and a SAAS<u>AUG</u>GCGGC (where S = G or C) consensus motif flanking the underlined initiating AUG (Elfakess and Dikstein, 2008). How TISU elements are able to evade leaky scanning is not well understood but eIF1 appears to be involved as removal of this factor abrogated TISU-mediated translation initiation, which is the exact opposite effect seen with non-TISU cap-proximal start sites (Sinvani et al., 2015). TISU-bearing mRNAs are generally enriched for transcripts that encode for proteins involved in RNA metabolism, protein synthesis, and mitochondrial activity, and it is thought TISU elements play an important regulatory function in the translation of these proteins under certain physiological conditions (Elfakess and Dikstein, 2008). For example, during nutrient deprived states when overall protein synthesis is repressed, the translation of mRNAs with TISU elements is somehow sustained, and, given the nature of the transcripts involved, this effect may help mitigate the response of the cell towards energetic stress (Sinvani et al., 2015).

1.1.3.3 TOP mRNAs

TOP (5' terminal oligopyrimidine) motifs are another example of a cis-acting element that confers unique regulatory properties to a mRNA. Approximately 100 TOP-containing mRNAs have been identified and this class of transcripts is enriched for components of the translation machinery (Meyuhas and Kahan, 2015). An unique and defining aspect of this class of transcripts is hypersensitivity towards mTOR signalling (Meyuhas and Kahan, 2015). Unlike most eukaryotic mRNAs, which are capped by m7GpppG or m7GpppA, TOP mRNAs possess a m7GpppC 5' terminus followed by a stretch of 4-15 pyrimidines (Meyuhas and Kahan, 2015). The TOP motif is often followed by a GC-rich region which appears to be necessary for TOP-mediated regulation (Avni et al., 1994). There is some controversy regarding the underlying mechanisms of the regulation of TOP mRNA translation. In ribosome profiling studies, it was observed that loss of 4E-BP rendered TOP mRNAs recalcitrant towards pharmacological inhibition of mTOR signaling, leading to the hypothesis that TOP mRNA hypersensitivity towards mTOR is attributed to poor competitive efficacy for eIF4E binding (Hsieh et al., 2012; Thoreen et al., 2012). Another protein that has been implicated in the regulation of TOP mRNA translation is the LARP1 (La-related protein 1) (Fonseca et al., 2015; Lahr et al., 2017; Philippe et al., 2018). LARP-1 is an RNA-binding protein that associates with TOP motifs and is thought to repress their translation upon inhibited mTOR signalling (Fonseca et al., 2015; Lahr et al., 2017; Philippe et al., 2018). Consistent with this notion, deletion of LARP1 was found to decrease TOP sensitivity towards mTOR inhibition (Philippe et al., 2018)

1.1.3.4 Cap Independent Translation

In some instances, the 5' leader can form higher order tertiary structures that can promote initiate translation in a cap-independent manner. Picornaviral mRNAs, for instance, are transcribed without a 5' methylated cap and often possess multiple uAUGs embedded within their 5' leader. In spite of these inhibitory features, these mRNAs are capable of initiating translation efficiently in the absence of cap structure as they harbor an internal ribosomal entry site (IRES), which is an RNA element that enables direct recruitment of ribosome to the mRNA (Jang et al., 1989; Pelletier and Sonenberg, 1988). By employing a cap-independent mechanism, IRES-bearing mRNAs are translated under circumstances in which global protein synthesis is compromised. For example, a number of picornaviruses express 2A proteases that cleave the eIF4G subunit of the eIF4F cap-binding complex (Haghighat et al., 1996). As a result, picornaviral infection leads to a global repression of cap-dependent translation but conversely, IRES-mediated translation of the picornaviral mRNA is enhanced, possibly due to the increased availability of ribosomes (Ohlmann et al., 1995). IRESes have also been found to be present in other viral families, such as Flaviviridae and Herpesviridae (Low et al., 2001; Thurner et al., 2004).

To date, the most highly active IRESes are found in viruses but eukaryotic IRESes have also been reported. The first cellular IRES was found within the 5' leader of Binding immunoglobulin protein (BiP) in the early 90s (Macejak and Sarnow, 1991), and since then, several additional cellular IRESes have been identified with some reports predicting that IRESes can be found within 10% of all cellular mRNAs (Weingarten-Gabbay et al., 2016). The existence of cellular IRESes offers an attractive explanation for why certain transcripts are able to sustain their translation under conditions in which global protein synthesis is compromised but in spite of this, many researchers remain apprehensive

about the notion of a cellular IRESes. Compared to viral IRESes, cellular IRESes exhibit very low activity, which raises the question of the actual contribution of IRES-driven translation towards protein production. Indeed, experiments comparing m7GpppG capped or ApppG capped reporters with putative cellular IRESes often illustrate that levels of translation mediated by the IRES in question are miniscule compared to cap-dependent translation (Shatsky et al., 2018). However, it is plausible that a cellular mRNA can translate predominantly through a cap-dependent mechanism during permissive conditions but switch to a cap-independent mechanism when the translation machinery becomes limiting (Svitkin et al., 2005). In addition, studies characterizing putative cellular IRESes often rely too strongly on assays that are known to give rise to false positives without using complementary approaches to thoroughly rule out artifacts or alternative explanations. Sources of false positives include the presence of unexpected cryptic splice sites or weak promoter activity (Baranick et al., 2008).

Cap-independent translation enhancers (CITE) offer an alternative explanation to IRESes for sustained protein synthesis during inhibition of cap dependent translation (Shatsky et al., 2018). CITEs are RNA elements with high binding affinity towards translation initiation factors but in contrast to IRESes, CITEs cannot directly recruit the initiation complex onto an RNA sequence and require a free 5'end to direct initiation (Shatsky et al., 2018). Instead, CITEs are thought to increase the local concentration of initiation factors near the 5' end of the transcript, and in doing so, the translation of the mRNA becomes less cap-dependent (Shatsky et al., 2018).

Table 1.1 Examples of Cis-Acting Regulatory Features of 5' leaders

5' leader Element	Comments	Notable Examples
Length	Median human 5' leader = 218 nts (Leppek et al., 2018). Inverse correlation between length and TE	VEGFA (1kb (Gandin et al., 2016)), c-Myc (525 nts (Gandin et al., 2016))

GC Content/Thermostability	Average GC% in human 5' leader = 60% (Zhang et al., 2004). Inverse correlation between GC content/thermostability and TE	Arf6 (74% GC (Gandin et al., 2016), CCND1 (73%, (Gandin et al., 2016)
Upstream TSS	Negative regulation of initiation during normal conditions but is often bypassed in the presence of cellular stress.	ATF4, GADD34
TISU Elements	Promotes the initiation of mRNAs with very short 5' leaders (Elfakess and Dikstein, 2008)	Enriched in genes involved in mitochondrial function (e.g. ATP5O)
TOP Motifs	Confers hypersensitivity towards mTORC1 signalling	Enriched in mRNAs encoding for translation machinery (e.g. eEF2)
IRESes	Enables cap-independent initiation events through direct recruitment of the 40S ribosome. Does not require a free 5' end.	CrPV, EMCV
CITES	Reduces cap-dependency by increasing the local concentration of initiation factors. Requires a free 5' end (Shatsky et al., 2018)	Apaf-1 (Andreev et al., 2012)

1.1.4 The Coding Region

The coding region or the coding sequence (CDS) encompasses the section of the mRNA that functions as the blueprint for amino acid assembly. This information of transferred through the ribosome in triplets of nucleotides known as codons. Given how there are 64 possible combinations of codons ($4^3 = 64$) to encode for 20 amino acids, in addition to the translation termination signal, there is a level of redundancy or degeneracy in the genetic code. Synonymous codons usually differ in the second or third nucleotide position and out of the 20 amino acids, 18 are encoded by multiple codons (Chaney and Clark, 2015).

The representation of synonymous codons is not equal across the transcriptome and some codons appear far more frequently than others (Chaney and Clark, 2015). This phenomenon is known as codon bias and its existence is rationalized through two prevailing models. Under the selective model, codon bias is attributed to an evolutionary pressure to optimize for translation efficiency and

fidelity (Duret, 2002). In contrast, the mutational or neutral model theorizes that bias in codon usage is attributed to the inherent variability in mutation patterns across the genome (Duret, 2002). However, these two models are not necessarily mutually exclusive, and it is likely that both contribute to existence of codon bias. For instance, because it is observed that commonly occurring codons also tend to be recognized by more highly expressed tRNAs, the selective model posits that this bias exists to optimize ribosome elongation rate and efficiency (Bulmer, 1987). Additionally, the selection model posits that abundant proteins are under higher selective pressure and accordingly, codon bias is observed to correlate with relative gene expression (Bulmer, 1987). On the other hand, the selective model does not provide an explanation as to why the identity of the nucleotide at the third codon position (which is often varied between synonymous codons) tends to correspond with the GC content of neighboring intergenic regions (Chen et al., 2004). Because these intergenic regions are untranscribed and do not affect elongation rates, it would appear that the neutral model is at play since it reflects imbalances in mutation patterns intrinsic to different regions of the genome rather than selective pressure (Chen et al., 2004; Duret, 2002).

In addition to providing the ribosome instructions for protein production, regulatory elements are also embedded the CDS. There is evidence suggesting that mRNA stability positively correlates with optimal codon usage as it has been demonstrated that the substitution of optimal codons with synonymous rare codons exert destabilizing effects towards the transcript (Presnyak et al., 2015). The GC content within the CDS was also identified to positively correlate with mRNA abundance and this is supported by the observation that increased GC content scales with enhanced transcription rates (Kudla et al., 2006; Newman et al., 2016). The CDS also contains motifs capable of recruiting regulatory RNA binding proteins that can impact gene expression and mRNA fate. For example,

coding region determinant-binding protein (CRD-BP) can stabilize select transcripts such as c-Myc by binding to a specific element found within the CDS (Doyle et al., 1998). In summary, not only does the CDS carry the genetic information for protein synthesis, but it also possesses important regulatory information that influences gene expression (Lemm and Ross, 2002).

1.1.5 The 3' Untranslated Region (UTR)

The 3'UTR represents the stretch of nucleotides spanning between the stop codon and the polyadenylated tail. Over the course of evolution, average 3'UTR lengths have greatly expanded, suggesting that this region of the mRNA may possess greater regulatory significance in more complex organisms (Mayr, 2017). In humans, the average 3'UTR is 1000 nts in humans (compared to 150 nts in yeast) and is usually the longest region of the transcript (Pesole et al).

The 3'UTR harbours a wide variety of regulatory elements, including mRNA localization signals, microRNA binding sites, and various other sequence motifs capable of recruiting effector proteins (Mayr, 2017; Wilkie et al., 2003). One well characterized example of a regulatory feature found within certain 3'UTRs are adenylate-uridylate-rich elements (AREs), which describe contiguous repeats of A/Us that mediate mRNA stability (Chen and Shyu, 1995; Mayr, 2017). AREs are enriched in genes that require precise spaciotemporal regulation (e.g. proteins involved in cell cycle progression) and the presence of this element drastically reduces the half-life of the mRNA (Chen and Shyu, 1995). In addition to controlling mRNA stability, there have been reports that AREs can also influence translation efficiency (Fukao and Fujiwara, 2017).

Alternative splicing of 3'UTRs allow for differential gene regulation through the inclusion or exclusion of particular elements (Andreassi and Riccio, 2009). Actively proliferating cells tend to express mRNA isoforms with shorter 3'UTRs whereas isoforms with longer 3'UTRs are found in differentiated cells (Sandberg et al., 2008). Consistent with this, there are reports that 3'UTRs are globally shortened in cancer cells and it is speculated that reducing the 3'UTR length can lead to the stabilization of mRNAs encoding for proto-oncogenes due to the loss of repressive regulatory sites (Mayr and Bartel, 2009; Mayr et al., 2007). Taken together, although the 3'UTR does not influence the building blocks of the protein, it functions as a critical mediator of gene expression, with its dysregulation resulting in pathogenic consequences.

1.1.6 The Polyadenylated (Poly A) Tail

The terminal region of mature eukaryotic mRNAs is characterized by a long contiguous stretch of adenosines called the polyadenylated tail (poly A). Unlike the rest of the mRNA body, the addition of the poly A tail is not templated and can be considered as a post-transcriptional modification (Proudfoot, 2011). Towards the end of transcription, the 3' end of the nascent mRNA is cleaved and the poly A polymerase (PAP), in conjunction with numerous accessory factors, is recruited to catalyze the addition of adenosine monophosphates to the free 3' end of the transcript (Colgan and Manley, 1997). The site for mRNA cleavage and polyadenylation is demarcated by a highly conserved polyadenylation signal (AAUAAA) located 10-30 nts upstream, and a GU rich element positioned 20-40 nts downstream (Colgan and Manley, 1997).

The poly A tail of most mRNAs in humans ranges from 150-250 nts long, but gradually shortens upon export to the cytoplasm (Eckmann et al., 2011). By blocking 3' exonucleolytic

degradation and inhibiting 5' decapping, the poly A tail exerts stabilizing effects to the mRNA and could be seen as a timer for mRNA lifespan (Eckmann et al., 2011). The rate of deadenylation varies between transcripts and is accelerated by a multitude of factors, such as the presence of miRNA binding sites, induction of NMD, interactions with destabilizing RBPs, and recruitment into P bodies (Chen and Shyu, 2011; Wilson et al., 1978). However, in some instances, poly A tails can be extended in the cytoplasm, which prolongs the half-life of the transcript (Richter, 1999).

Along with its intrinsic mRNA stabilizing properties, an important function of the poly A tail is to promote translation initiation (Jackson and Standart, 1990). Although the cap structure on its own has a critical role in directing translation, its efficacy is significantly enhanced when a poly A tail is also present, and mRNAs containing both of modifications are translated far more efficiently compared to mRNAs with just one (Gallie, 1991). Given how these two elements are located at opposite ends of the mRNA, the prevailing model rationalizing the synergistic stimulation of translation posits that there exists a bridging element that brings the poly A tail into close proximity with the translation machinery at the 5' end (Jackson and Standart, 1990). This concept is commonly referred to as the "closed-loop model" as the cap-to-tail interaction would circularize the mRNA and is supported by electron-microscopy images illustrating that polyribosomes are oriented in a circular fashion (Christensen et al., 1987). Nevertheless, it is not entirely clear how mRNA looping stimulates translation initiation directly, but it is hypothesized that the formation of a mRNA loop may promote recycling of translation machinery *in cis* by positioning 5' cap near the terminating ribosome and recruiting it back onto the same mRNA (Hinnebusch and Lorsch, 2012). Because recruitment of ribosomes to the 5' end is often considered to be the rate-limiting step for translation, ribosome

recycling can significantly enhance the efficiency of protein synthesis. However, experimental evidence demonstrating this is rather limited.

Poly A binding protein (PABP, or PABPC1, referring to the dominant PABP protein existing in the cytoplasm) is thought to be the key bridging element as it possesses strong affinity for the poly A tail and has also been found to associate with the eIF4G subunit of the eIF4F cap-binding complex. In addition to its role in mRNA looping and potential ribosome recycling, PABP also increases eIF4E affinity towards the cap and 40S recruitment to the mRNA (Kahvejian et al., 2005). PABP is a highly abundant protein, and in HeLa cells, there is approximately 8 x 10^6 PABP molecules per cell (Gorlach et al., 1994). In comparison, HeLa cells possess approximately 5-7 x 10^5 mRNA molecules (Gorlach et al., 1994) but in spite of the fact that PABP exists at a vast abundance, there are very few PABP molecules that are not RNA bound in cells (Sladic et al., 2004). Considering that the average poly A tail is 150-250 nts long and the minimal binding site of PABP is 12 nts (Sachs et al., 1987), multiple PABP proteins can bind to a single poly A tail. It is possible that PABP multimerization enhances the association of eIF4F complex to the mRNA and in support of this, it has been documented that the extension of the poly A tail leads to stimulation in translation efficiency (Preiss et al., 1998).

1.2 Eukaryotic Translation Initiation

In the canonical model of eukaryotic translation initiation, the 40S ribosome binds to the 5' end of a mRNA and, upon doing so, moves through the 5' leader in a unidirectional manner until a start codon is encountered. This is commonly referred to as the "scanning mechanism" and requires several essential initiation factors, but in essence, this model can be broken down to 4 parts: 1) association of the eIF4F complex to the 5' m7GpppN; 2) recruitment of the 43S preinitiation complex

(PIC), comprised of the 40S ribosome in association with several initiation factors 5' cap of the mRNA; 3) scanning of the 43S PIC through the 5' leader in search of a start codon; 4) start codon recognition (Figure 1.1). It worth noting, however, that although the scanning model is supported by an ample amount of biochemical data, our understanding of initiation is not complete, and several aspects of the underlying molecular mechanisms of this process remain to be fully characterized. In the sections that follow, the core factors involved in each step (as summarized in Table 1.2), along with any gaps in our knowledge, will be described in more detail.

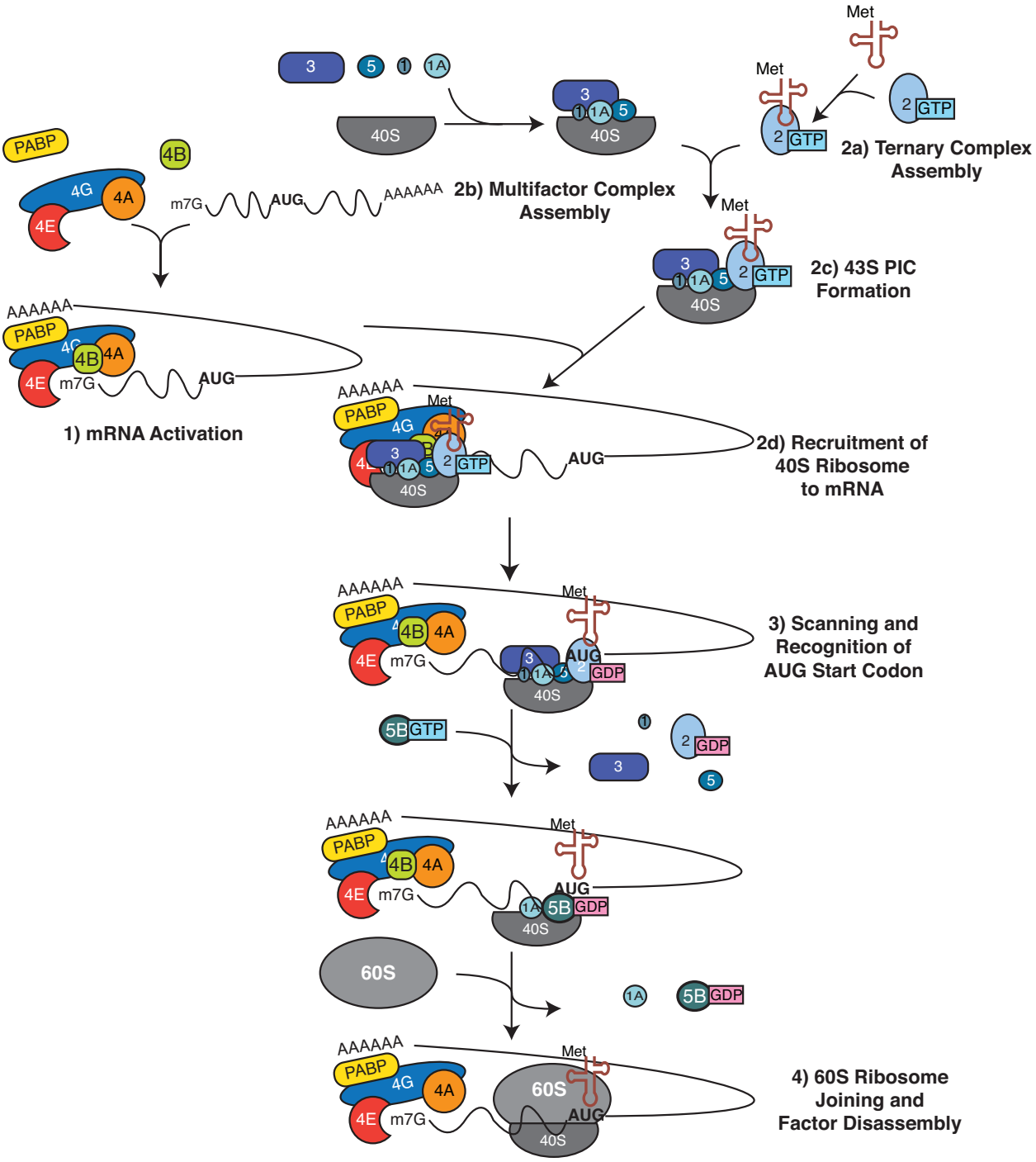

Figure 1.1 Schematic of Eukaryotic Translation Initiation

The mechanism of translation initiation in eukaryotes is a multi-step process involving the coordination of several essential factors: 1) association of eIF4F to the 5' cap 'activates' the mRNA for initiation; 2a-d) interaction between eIF3 and eIF4G facilitates the recruitment of the 43S PIC to the 5' end of the transcript; 3) with the assistance of eIF2, eIF1, eIF1A and eIF5B, the 43S PIC scans through the 5' leader in search for a proper start codon; 4) recognition of the start codon leads to 60S joining. Hydrolysis by eIF5 and eIF5B promote initiation factor dissociation

Table 1.2 Core Eukaryotic Initiation Factors in Translation

Factor	Size (kDa)	Molecules/cell (Schwanhausser et al., 2011)	Major Interacting Partners	Function
eIF4E	25	8.5×10^5	eIF4G, 4EBP	Interact with the m7GpppN cap
eIF4G	220	6.1×10^5 (eIF4G1); 2.5×10^5 (eIF4G2); 1.1×10^3 (eIF4G3)	eIF4E, eIF4A, eIF3, PABP, MNK1/2	Protein scaffold that bridges the 43S PIC to the eIF4E bound 5' cap.
eIF4A	48	1.3×10^7 (eIF4A1); 4.2×10^4(eIF4A2)	eIF4G, eIF4B, eIF4H, PDCD4	ATP-dependent helicase that unwinds local RNA structures to facilitate 43S binding
eIF4B	80	5.1×10^5	eIF4A, eIF3	Accessory factor that promotes that activity of eIF4A
eIF4H	27	1.6×10^6	eIF4A	Accessory factor that promotes the helicase activity of eIF4A
eIF3	~800	3.8×10^5 (eIF3c) to 1.4×10^6 (eIF3f, -m)	eIF4G, eIF4B, 40S ribosome	Multisubunit complex that brings the 40S ribosome to the cap through interactions with eIF4G
eIF1	12	2.6×10^6	40S, eIF3	"Gatekeeper" that regulates start-codon selection by occluding full accommodation of the initiator tRNA at the P site during scanning
eIF1A	17	1×10^6	40S	Factor that cooperates with eIF1 in maintaining initiation fidelity
eIF2	38	1.4×10^6 (eIF2β) to 2.7×10^6 (eIF2γ)	40S, GTP, Met-tRNA$_i^{Met}$, eIF5, 5MP	Factor that associates with the initiator Met-tRNA$_i^{Met}$
eIF5	58	4.8×10^5	eIF2, eIF3	GAP that hydrolyzes eIF2-GTP
eIF5B	139	2.4×10^5	GTP, 60S	GTP-binding protein that mediates 60S subunit joining

1.2.1 Association of the eIF4F Complex to the 5' Cap

Recruitment of the 43S PIC to the m7GpppN cap of an mRNA is considered to the rate-limiting step in translation initiation (Hershey et al., 2012; Shah et al., 2013). In most situations, 43S PIC recruitment to eukaryotic mRNA is mediated by the eIF4F complex, which is formed by 3

proteins: eIF4E, the cap binding subunit; eIF4G, a scaffolding protein; and eIF4A, an RNA helicase. In order to activate an mRNA for 43S PIC association, eIF4E binds the 5' cap to properly position the eIF4F complex onto the transcript and, upon doing so, the eIF4A subunit is thought to unwind local RNA secondary structures to increase the accessibility of the 5' end. Through interactions formed between eIF4G and eIF3, the 43S PIC then loaded onto the activated 5' end of the mRNA.

1.2.1.1 eIF4E

eIF4E, the major cytoplasmic cap-binding protein, plays a critical role in translation by directing the 40S ribosome to the 5' caps of mRNAs. Under most conditions, eIF4E is the limiting protein in translation initiation, existing at approximately 8×10^5 molecules per cell (measured in HeLa cells) (Duncan et al., 1987). In humans, there are three eIF4E paralogs: eIF4E1, eIF4E2 (also known as 4E homologous protein (4EHP)), and eIF4E3 (Joshi et al., 2004; Morita et al., 2012). Of the three, eIF4E1 possesses the strongest affinity for m7GpppN and is the primary cap-binding protein in the cytoplasm (Osborne et al., 2013; Zuberek et al., 2007). As a result, eIF4E1 is often simply referred to as 'eIF4E' in the literature and, unless indicated otherwise, all mentions of eIF4E in this dissertation will also allude to eIF4E1. Relatively speaking, the physiological roles of the other two eIF4E paralogs are not as extensively characterized. Unlike eIF4E1, eIF4E2 does not interact with eIF4G and has been shown to function as a repressor of translation initiation (Morita et al., 2012; Rom et al., 1998). eIF4E3, on the other hand, is capable of eIF4G binding but because its expression profile is restricted to a number of tissue types (e.g. skeletal muscle, heart and lung), its involvement in translation may be limited and tissue-specific (Hernandez et al., 2012; Joshi et al., 2004).

The major determinant of cap recognition in eIF4E1 is attributed to the presence of two key tryptophan residues (W56 and W102 in human eIF4E1) that sandwich the 7-methylguanine of the cap structure to form strong cation-π interactions (Figure 1.2) (Tomoo et al., 2002). The contribution of methyl group at the N(7) position of the 7-methylguanine base significantly strengthens the stacking interaction with the aromatic residues, thus allowing eIF4E to discriminate between capped and uncapped mRNAs (Niedzwiecka et al., 2002). In eIF4E2 and eIF4E3, W56 is substituted with a tyrosine and a cysteine respectively, and as a result, the affinity of these proteins towards the cap is decreased by over an order of magnitude (Zuberek et al., 2007). eIF4E association with the 7-methylguanine is further stabilized by hydrogen bonding interactions formed by a tryptophan and a conserved glutamate (W102 and E103 in human eIF4E1) (Tomoo et al., 2002). The triphosphate bridge of the mu7GpppN structure also form contacts with the basic residues in the cap binding pocket (R112, R157, K162, K206 in human eIF4E1) (Tomoo et al., 2002) and due to these additional interactions, eIF4E has a greater affinity towards m7GTP (K_{as} x 10^{-6} (M^{-1}) = 108.7 ± 4.0) compared to m7GMP ((K_{as} x 10^{-6} (M^{-1}) = 0.806 ± 0.067) and m7GDP (K_{as} x 10^{-6} (M^{-1}) = 20.4 ± 1.5) (Niedzwiecka et al., 2002).

The dorsal surface of eIF4E, which is positioned at the opposite side of the cap binding pocket, possesses a conserved hydrophobic patch that mediates eIF4E interactions with other proteins (Figure 1.2, dark blue) (Gruner et al., 2016). Notably, eIF4G associates to this hydrophobic patch using a conserved eIF4E binding motif, YXXXXLΦ (where X represents any amino acid, and Φ is an aliphatic residue) (Gruner et al., 2016). In metazoans, additional contacts are formed between the lateral side of eIF4E and a non-canonical loop of eIF4G to stabilize the association between the two proteins (Figure 1.2, cyan) (Gruner et al., 2016). Members of eIF4E binding protein (4E-BPs) family also

interact with eIF4E using a similar bipartite mechanism as eIF4G and as a result, 4E-BPs function as negative regulators of protein synthesis that competitively disrupt eIF4E and eIF4G interaction (Peter et al., 2015).

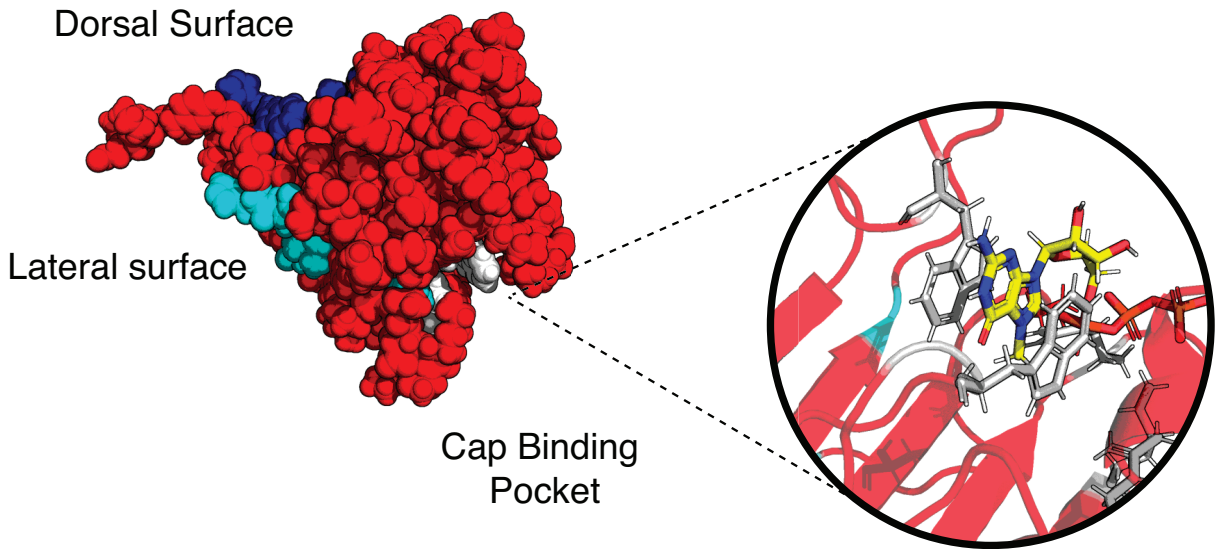

Figure 1.2 Structure of Human eIF4E
Sphere representation of human eIF4E (PDB 5T46, (Gruner et al., 2016)) with the cap binding pocket highlighted in white, the dorsal surface (interacts with the canonical 4E binding motifs of 4E-BP or eIF4G) highlighted in navy blue, and the lateral surface, highlighted in light blue, interacts with the non-canonical binding loop of 4E-BP or eIF4G. The cap binding pocket is magnified to illustrate the pi-pi stacking interactions formed between W56, W102, and the methylated cap (yellow).

1.2.1.2 eIF4G

eIF4G is a large protein with multiple protein binding sites that links the rest of the translation machinery to 5' end of an mRNA. There are 3 different mammalian eIF4G proteins (eIF4G1, eIF4G2/DAP5/p97/NAT1, eIF4G3) and among the 3, eIF4G1 is the dominant contributor towards cap-dependent translation initiation (Hernandez and Vazquez-Pianzola, 2005). The structure of eIF4G1 can be divided into three parts: the amino terminal region (which binds to PABP and eIF4E),

the middle region (which associates with eIF3 and eIF4A), and the carboxy terminal (which interacts with eIF4A and MNK) (Figure 1.3).

The middle portion of eIF4G1 (eIF4G-m) spans aa 635-1105 in the human paralog and harbors the primary interacting surface for eIF4A (aa 762-969) (Korneeva et al., 2000) as well as the eIF3 binding site (Villa et al., 2013). Together, these two subdomains represent the minimal eIF4G module for translation and tethering eIF4G-m alone to uncapped mRNAs is capable of directing initiation (Villa et al., 2013). By binding to eIF3c -d, and -e subunits, eIF4G-m positions the 43S PIC near the 5' end of the mRNA (Villa et al., 2013). The eIF4A binding surface within eIF4G-m is represented by a HEAT domain (named after a structural motif found in Huntingtin, elongation factor 3, protein phosphatase 2A, and Tor1) which primarily interacts with the CTD of eIF4A (Oberer et al., 2005). While eIF4A CTD is sufficient for binding to eIF4G-m, additional contacts are formed between the NTD of eIF4A and eIF4G-m, albeit to a lesser extent (Schutz et al., 2008). According to co-crystal structures of eIF4G-m and eIF4A, eIF4G-m appears to act as a barrier that keeps the NTD of eIF4A near the CTD of eIF4A (Schutz et al., 2008). By confining the two eIF4A domains into close proximity, eIF4G-m promotes eIF4A into adopting an active, 'closed' confirmation, which results in increased eIF4A ATPase, RNA binding, and helicase activities (Schutz et al., 2008). In addition to the eIF3 and eIF4A binding domains, the middle region of eIF4G also carries two putative RNA recognition motifs (RRMs) that may enhance eIF4F association onto capped mRNAs (Yanagiya et al., 2009).

The carboxy third of the mammalian eIF4G (aa 1040-1560) possesses 2 additional HEAT domains (referred to as HEAT-2 and HEAT-3). The HEAT-2 domain also associates with eIF4A, which may suggest that the full-length eIF4G protein harbors two distinct binding sites for eIF4A.

However, binding assays suggest that eIF4G and eIF4A interact in a 1:1 ratio (Li et al., 2001a). Unlike HEAT-1, the HEAT-2 domain is dispensable for translation initiation and is absent in lower eukaryotes (Marintchev and Wagner, 2004; Morino et al., 2000; Schutz et al., 2008). Instead, it appears that the role of HEAT-2 is to modulate eIF4A activity (Marintchev et al., 2009). The HEAT-3 domain, on the other hand, binds to MNK1 and MNK2 kinases. In doing so, this positions these kinases near eIF4E, and promotes eIF4E S209 phosphorylation (Shveygert et al., 2010).

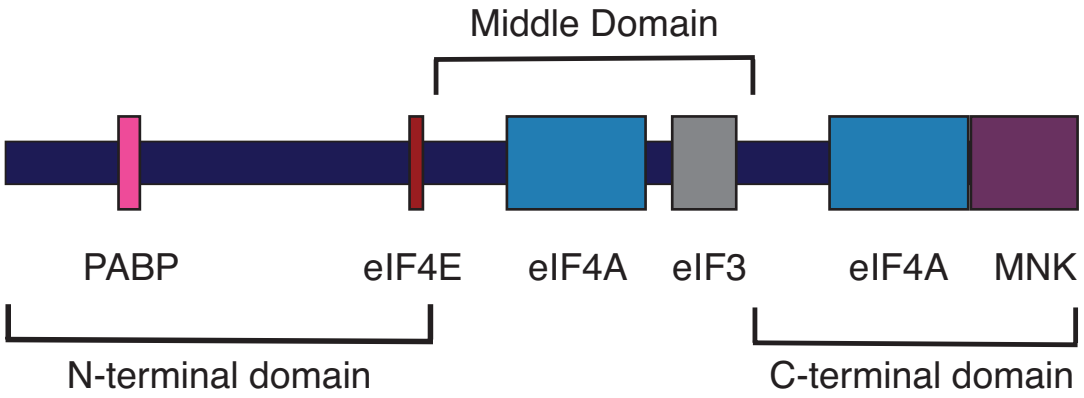

Figure 1.3 Domain Organization of eIF4G1
Schematic of the various protein binding sites of eIF4G1. The middle domain constitutes that minimal region required for 43S PIC recruitment and tethering this domain to RNA is capable of driving initiation in the absence of a cap. The N terminal domain positions eIF4G near the cap and promotes mRNA circularization. The C terminal domain contains sites that function in the regulation of eIF4F activity.

DAP5 (eIF4G2) shares comparable homology with the middle and carboxy regions of eIF4G1 but notably, the eIF4G1 amino region, which carries the binding sites for PABP and eIF4E, is absent (Virgili et al., 2013). Due to its inability to associate with eIF4E, DAP5 is considered to direct cap-independent mechanisms of initiation. Even though the existence of cellular IRESes in eukaryotes remains contentious, there are a number of studies reporting that DAP5, in conjunction with eIF4A and eIF2, promotes the translation of numerous putative cellular IRESes (Liberman et al., 2015; Marash and Kimchi, 2005). As an alternative to promoting IRES-mediated initiation, it has been

proposed that DAP5 can also act as a repressor of cap-dependent translation by sequestering factors such as eIF4A and eIF3 away from eIF4G and the 5' cap (Imataka et al., 1997).

The biological significance of the third eIF4G variant, eIF4G3, has not been extensively explored and this protein is often thought to possess an overlapping role with eIF4G1(Gradi et al., 1998). This assumption is largely based on the fact that eIF4G1 and eIF4G3 are structurally very similar, sharing 56% overall amino acid similarity, with higher degrees of homology observed within the middle and carboxy regions (Gradi et al., 1998). Importantly, eIF4G3 carries the same core binding domains with eIF4G1 and the addition of eIF4G3 is able to restore translation in *in vitro* extracts devoid of eIF4G1 (Gradi et al., 1998). In line with this, ectopic overexpression of eIF4G3 was also capable of rescuing translation inhibition induced by eIF4G1 knockdown (Coldwell et al., 2012). It is possible that eIF4G1 and eIF4G3 mediate the translation of different subsets of mRNAs and it has been observed that HSP70 translation is sensitive towards cleavage of eIF4G3, but not towards eIF4G1 (Castello et al., 2006). However, it remains to be seen if other mRNAs also exhibit this discriminatory effect.

1.2.1.3 eIF4A

RNA helicases are extremely important proteins as they are implicated in every aspect of RNA metabolism, including translation initiation. All eukaryotic RNA helicases fall into either superfamily 1 (SF1) or SF2 and are further categorized into 5 different subfamilies according to their level of shared sequence conservation, substrate specificity, and mechanistic features (Figure 1.4). eIF4A is a member of the DEAD-box family of helicases and is an essential component in cap-dependent translation. Because mRNAs with longer and highly structured 5' leaders are generally more sensitive towards eIF4A or eIF4F inhibition (Rubio et al., 2014), eIF4A is often thought to be

responsible for unwinding secondary structures along the 5' leader to facilitate 43S scanning. A great amount of groundwork has been laid towards understanding the enzymatic properties and cellular regulation of this helicase but many of the parameters measured (e.g. RNA affinity and protein abundance in cells) have raised questions regarding the conventional understanding or eIF4A function in the initiation process.

1.2.1.3.1 The Mechanistic Basis of eIF4A Helicase Activity.

eIF4A belongs to the DEAD-box family of helicases, which constitutes the largest RNA helicase subfamily in mammalian cells and is characterized by 13 common motifs (Figure 1.4) (Fairman-Williams et al., 2010; Linder and Jankowsky, 2011). The DEAD-box family is named after a highly conserved Asp-Glu-Ala-Asp (D-E-A-D) sequence found within motif II, which differentiates them from the DEAH-box family. Structurally, the enzymatic core of DEAD-box helicases is comprised of two tandem RecA-like domains joined by a flexible linker region and many DEAD-box helicases also possess additional N- and/or C- terminal extensions that can confer enhanced enzymatic activity or modulate interactions with accessory proteins (Linder and Jankowsky, 2011). However, eIF4A is a considered to be a prototypical or 'minimal' DEAD-box protein as it only consists of the basic helicase core with a very short (~50 nts) N-terminal extension.

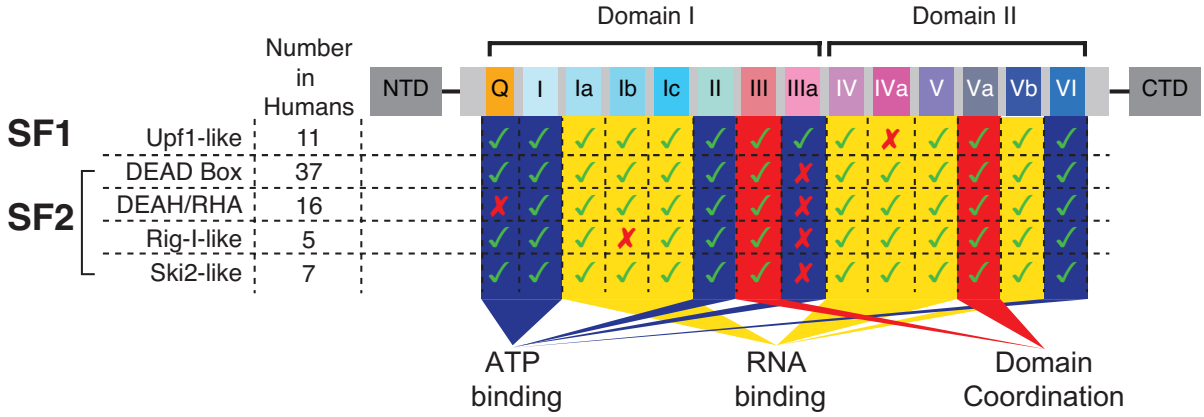

Figure 1.4 Structure of the Conserved RNA Helicase Core.
Domain organization of the 5 RNA helicase families. Motifs involved in ATP binding and RNA binding are indicated by the navy blue and yellow boxes, respectively. Motifs important in domain coordination are denoted by the red boxes. Families are further stratified based on the degree of sequence similarity between common motifs. For instance, the DEAD-box family of RNA helicases are uniquely distinguished by the D-E-A-D motif found within motif II.

The helicase activity of members of the DEAD-box family is ATP dependent and is modulated by conformational cycling of the enzyme (Theissen et al., 2008). The ATP and RNA binding activities these helicases are coupled and association of these two substrates promotes the enzyme to adopt a 'closed' active conformation in which the two RecA domains are brought into close proximity (Lorsch and Herschlag, 1998; Theissen et al., 2008). In this state, the ATP binding pocket is formed between motifs Q, I, and II of the N-terminal RecA domain, and motifs V and VI of the C-terminal RecA domain (Sengoku et al., 2006). The affinity towards RNA is also increased when the closed conformation is adopted as the two RecA domains form continuous RNA binding site (Sengoku et al., 2006).

Much of our understanding behind mechanistic basis of eIF4A helicase activity is inferred from structural studies using other DEAD-box helicases. A co-crystal structure of the DEAD-box

helicase, Vasa, complexed with RNA revealed that the helicase induces a sharp bend to the structure of the RNA upon binding (Sengoku et al., 2006). The presence of this bend makes it thermodynamically unfavorable for the RNA to form duplexed structures, and as a result, base-pairing interactions between nucleotides are destabilized (Sengoku et al., 2006). During the RNA unwinding process, ATP binding promotes transition into the closed 'active' conformation, but ATP hydrolysis, *per se*, is not essential for helicase activity (Liu et al., 2008). Instead, hydrolysis of the ATP molecule induces the enzyme to transition back into the 'open' conformation, leading to dissociation of the protein from the RNA and enzyme turnover (Liu et al., 2008).

Perhaps owing to the lack of ancillary extensions at the N- and C- terminus, eIF4A is an inefficient helicase with poor affinity for RNA (Lorsch and Herschlag, 1998). Even in its 'high'-affinity ATP-bound state, the Kd of eIF4A to RNA is ~125 μM (Lorsch and Herschlag, 1998). The nature of eIF4A helicase activity is also non-processive, meaning that the enzyme dissociates from RNA after a single unwinding event corresponding to ~11 bp (Garcia-Garcia et al., 2015; Rogers et al., 1999). Given its weak and non-processive helicase activity, it is highly unlikely that eIF4A functions alone in unwinding RNA secondary structure during the initiation process. In attempt to rationalize the essential role of eIF4A in translation in spite of its weak enzymatic activity, one hypothesis posits that RNA structures are unwound through a distributive mechanism that is dependent on multiple eIF4A binding events (Rogers et al., 2002). This hypothesis is also consistent with the fact that eIF4A is a highly abundant molecule, existing at an excess of roughly 3 molecules per ribosome (Duncan and Hershey, 1983). However, the enzymatic properties of eIF4A have been shown to be significantly enhanced when associated with eIF4G in conjunction with one of the eIF4A accessory proteins, eIF4B and eIF4H (Garcia-Garcia et al., 2015). This observation suggests that a single eIF4A molecule may

be sufficient in directing the 43S PIC but ultimately, it is currently not conclusive whether eIF4A behaves as a distributive or a processive helicase during initiation.

1.2.1.3.2 The eIF4A1 accessory proteins, eIF4B and eIF4H

eIF4B (69 kDa) and eIF4H (27 kDa) are RNA binding proteins that function as eIF4A accessory proteins. In single molecule helicase assays, unbound eIF4A unwinds approximately 11 nts prior to RNA dissociation, but when bound to eIF4G along with eIF4B or eIF4H, eIF4A is converted into a translocative helicase capable of melting a 72 bp RNA duplex (Garcia-Garcia et al., 2015). Conformational analysis using FRET shows that both eIF4B and eIF4H increase the rate of conformational cycling of eIF4A by promoting the closing its two RecA domains, thus explaining why eIF4A activity is enhanced when associated with eIF4B or eIF4H (Harms et al., 2014; Sun et al., 2014a).

eIF4B and eIF4H are structurally similar proteins but whether they possess overlapping or differential roles in translation is currently unclear. The association of eIF4B or eIF4H to eIF4A is mutually exclusive and pulldown experiments using recombinant eIF4A mutants suggest that eIF4B and eIF4H share the same binding site at the NTD of eIF4A (somewhere between aa 107-229) (Rozovsky et al., 2008). The amino acid sequence of eIF4H is highly homologous to eIF4B, although eIF4B possesses additional N- and C- terminal domains that can form additional protein-protein interactions (Rozovsky et al., 2008). One notable addition in eIF4B is the presence of the DRYG domain (named for the high content of aspartic acid, arginine, tyrosine, and glycine residues within that region) that allows eIF4B to directly associate with eIF3 (Methot et al., 1996). The CTD of eIF4B also contains two phosphorylation sites (S406 and S422) that are modulated by the mTOR and

MAPK pathways (Peng et al., 2007; Raught et al., 2004; Shahbazian et al., 2006). These phosphorylation events are important for eIF4B:eIF3 association and stimulate cap-dependent translation during growth permissive conditions (van Gorp et al., 2009). In contrast, post-translational modifications of eIF4H is largely an unexplored domain within the field of translation. While phosphorylated eIF4H peptides have been detected in mass spectrometry experiments, the significance of these modifications is unclear (Rush et al., 2005).

1.2.1.3.3 The Different Paralogs of eIF4A in Mammals

There are three eIF4A proteins in mammals: eIF4A1 and eIF4A2 (both of which participate in translation initiation), and eIF4A3 (which is not involved in translation initiation but instead functions in splicing and NMD as a core component of the EJC (Chan et al., 2004; Li et al., 1999)). Mammalian eIF4A1 and eIF4A2 share 91% amino acid identity, with most of the divergence existing within the flexible N-terminal extension (Nielsen and Trachsel, 1988). Based on biochemical and *in vitro* translation experiments, eIF4A1 and eIF4A2 appear to be functionally interchangeable as both proteins are capable of assembling into the eIF4F complex and promote translation initiation (Lindqvist et al., 2008b; Yoder-Hill et al., 1993).

Within the cellular context, however, there is evidence demonstrating that eIF4A1 and eIF4A2 are subjected to different regulatory cues, which may indicate that these two highly similar paralogs could possess non-overlapping functions (Galicia-Vazquez et al., 2012). eIF4A1 and eIF4A2 are differentially regulated on the transcription level and the relative expression of these two proteins across different tissues is quite distinct (Galicia-Vazquez et al., 2012). eIF4A1 is an abundant protein (~10^7 eIF4A1 proteins per cell) that is ubiquitously expressed at high levels across virtually all tissues (Nagaraj

et al., 2011; Nielsen and Trachsel, 1988; Schwanhausser et al., 2011). In comparison, eIF4A2 is the less abundant eIF4A paralog (existing at 1-2 orders of magnitude less than eIF4A1) in most adult tissue types, with the exceptions of brain, skeletal muscle, kidney, and ovary (Galicia-Vazquez et al., 2012). eIF4A1 and eI4A2 also respond differently during viral infections as eIF4A1, but not eIF4A2, is cleaved by FMDV 3C protease (Li et al., 2001b). Furthermore, eIF4A2 transcription has been shown to be under the regulation of eIF4A1 activity (Galicia-Vazquez et al., 2012). When eIF4A1 is suppressed either through siRNA or pharmacological inhibition, eIF4A2 mRNA and protein levels become elevated (Galicia-Vazquez et al., 2012). While the disparate patterns of gene expression may suggest eIF4A1 and eIF4A2 could play distinct roles in cell-type specific translation, this link is currently just correlative as there is little to no evidence demonstrating that these two eIF4A proteins can modulate the translation of different subsets of mRNAs.

1.2.2 Recruitment of the 43S preinitiation complex (PIC)

Following mRNA activation through eIF4F binding, the 43S PIC, comprised of eIF1, eIF1A, eIF2, eIF3, eIF5, and the 40S ribosome, is recruited to the 5' cap (Hinnebusch, 2014). This association is largely dependent on the chain of interactions formed by the 5' cap, eIF4E, eIF4G, eIF3 and the 40S ribosome. The 40S ribosome can adopt multiple conformations but is stabilized in an 'open' conformation that is permissive for mRNA interaction when bound to the associating eIFs (Llacer et al., 2015). The sequential order of 43S PIC assembly is still up for debate but it has been observed that eIF1, eIF1A, eIF2, eIF3, and eIF5 can self-assemble into a multifactor complex (MFC) in the absence of the 40S ribosomal, and it is possible that MFC formation precedes 43S assembly (Asano et al., 2001; Sokabe et al., 2012).

There is some debate regarding how an mRNA is initially loaded onto the 43S PIC to form the 48S initiation complex (IC) and there are two main models rationalizing this process. In the "threading model", the transcript enters the mRNA channel of the 40S ribosome through a narrow opening near the A site (Kozak, 1979). However, this model is regarded with some doubt, as the presence of eIF4E at the 5' terminus makes it difficult to imagine how such a bulky complex can thread through the narrow opening of the 40S subunit. Additionally, the threading model cannot explain IRES-mediated translation as these elements enable direct binding of the ribosome to the mRNA in the absence of a free 5' end. The second model for 43S PIC attachment is known as the slotting model, which suggests that transcripts are loaded laterally into the 40S ribosomal channel (Llacer et al., 2015). Ultimately, no conclusions regarding the nature of 43S PIC recruitment can be definitively made as there are no high-resolution structures depicting the stage of translation initiation.

1.2.3 43S PIC Scanning

After attaching to the 5' cap, the 40S ribosome transits along the length of the 5' leader unidirectional manner until it reaches a start codon (Hinnebusch, 2014). This step is thought to be quick, occurring at a rate of ~6 nts/s (as measured in Krebs-2 extracts), but scanning efficiency can be affected by factors such as 5' leader length and thermostability (Pestova and Kolupaeva, 2002; Vassilenko et al., 2011). The key players of the scanning and start codon recognition include eIF4A (and its accessory factors), eIF1, eIF1A, eIF2, eIF5, and eIF5B (Hinnebusch, 2014).

While there a great amount of data that is consistent with the scanning model, it is important to emphasize that 43S PIC scanning has never been definitively proven. Structural data depicting the

scanning ribosome are notably absent due to the fact that there are no small molecules that can reliably block a 43S PIC in motion. The involvement of eIF4A during this process has been particularly unclear and its weak enzymatic activity raises some doubt regarding whether eIF4A actually functions as the primary helicase during scanning. Furthermore, other DEAD-box helicases such as DHX29 can affect translation efficiency and it is possible that these enzymes, rather than eIF4A, are responsible for unwinding steric barriers along the 5' leader (Pisareva et al., 2008). However, toe-printing experiments have demonstrated that the formation of 48S complexes (as defined here as a 43S PIC stabilized onto a start codon) is abrogated in the absence of eIF4A, eIF4G, and eIF4B (Pestova and Kolupaeva, 2002). Additionally, UV-crosslinking experiments show that eIF4A binds up to 52 nts downstream from the cap structure (Lindqvist et al., 2008a). The association of eIF4A with cap-distal RNA sequences was also determined to be cap-dependent and not due to internal binding; these results would support the model in which eIF4A travels with the scanning 43S PIC along the 5' leader (Lindqvist et al., 2008a).

1.2.4 Start Codon Recognition

Delivery of the initiator Met-tRNA$^{Met}_{i}$ to the 43S PIC is mediated by eIF2, a heterotrimeric factor composed of: 1) eIF2α, which contains an important regulatory phosphorylation site; 2) eIF2β, which harbours binding sites for eIF5 and eIF2B; 3) eIF2γ, which possesses a domain for guanine nucleotide binding (Kimball, 1999). Association of eIF2 to Met-tRNA$^{Met}_{i}$ is dependent on the presence of GTP as the affinity of eIF2-GTP for Met-tRNA$^{Met}_{i}$ is 10 times greater compared to that of eIF2-GDP (Walton and Gill, 1975). When a start codon is recognized, eIF2-GTP is hydrolyzed to eIF2-GDP and is released from the translation machinery (Hinnebusch, 2014). In order to be utilized

in subsequent rounds of translation initiation, eIF2-GDP is recycled back into its GTP bound state by the guanine exchange factor (GEF), eIF2B (Price and Proud, 1994).

A major regulatory node of translation initiation hinges on the phosphorylation status of the eIF2α subunit at Ser51 (Figure 1.5) (Wek et al., 2006). When phosphorylated, eIF2-P competitively binds to eIF2B and inhibits its GEF activity (Kimball et al., 1998). As a result, eIF2-GDP is unable to recycle back into eIF2-GTP. Because eIF2-P has higher affinity for eIF2B compared to unphosphorylated eIF2, only a fraction of eIF2 is needed to be phosphorylated in order to inhibit translation (Krishnamoorthy et al., 2001). Phosphorylation of eIF2α S51 is triggered during cellular stress and there are four kinases that mediate this event: general control non-derepressible-2 (GCN2), protein kinase R (PKR), PKR-like endoplasmic reticulum kinase (PERK), and haem-regulated inhibitor (HRI) (Wek et al., 2006). Collectively, the four eIF2α kinases play an integral role in the integrated stress response (ISR) by inhibiting protein synthesis in the presence of unfavourable cellular conditions.(Wek et al., 2006). For example, GCN2 is a nutrient sensor that becomes activated during amino acid deprivation through a mechanism that involves binding to uncharged tRNAs (Dong et al., 2000; Zhang et al., 2002). In contrast, the association with double stranded RNA, which is often a hallmark of viral infection, leads to PKR activation (Lemaire et al., 2008). PERK, an ER transmembrane kinase, is activated by the presence of improperly folded proteins (Harding et al., 1999). Lastly, HRI is activated by heme deficiency, heat shock, and oxidative stress (Lu et al., 2001).

Although protein synthesis is inhibited when eIF2α is phosphorylated, the translation of some mRNAs is maintained or, in some instances, stimulated. One of the best characterized examples is ATF4, a transcriptional regulator that is key in promoting the transcription of stress response mRNAs (Harding et al., 2000; Harding et al., 2003). The 5' leader of the human ATF4 transcript contains

four uORFs and, in the absence of stress, these uORFs act as inhibitory elements that impair the scanning ribosome from efficiently reaching the coding AUG (Vattem and Wek, 2004). However, when eIF2α is phosphorylated and active TCs become limiting, the scanning 43S PIC is able to reinitiate and resume scanning without interruption after recognition of the first uORF (Vattem and Wek, 2004).

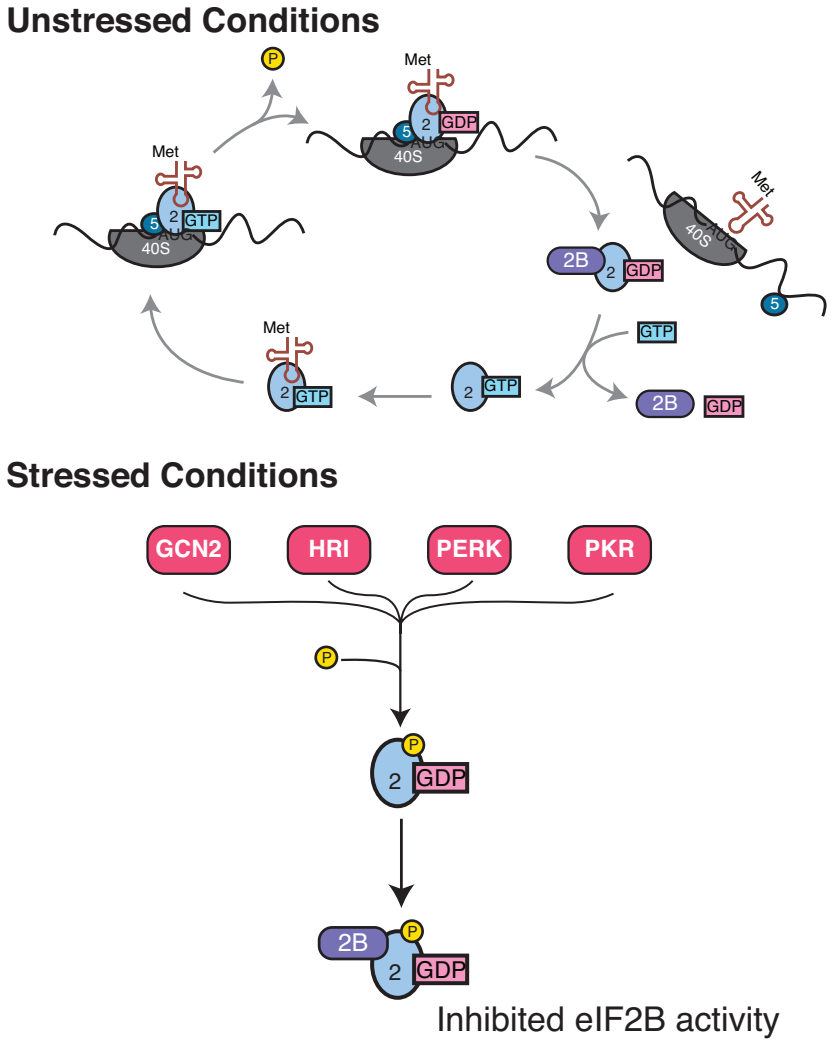

Figure 1.5 Activity and Regulation of eIF2
GTP-bound eIF2 bring the initiator Met-tRNA$^{Met}_{i}$ to the 40S ribosome. Upon recognition of a start codon, eIF5 hydrolyzes the GTP into GDP, causing dissociation of eIF2 from the initiation complex. The GEF, eIF2B, reactivates eIF2 for subsequent rounds of translation by exchanging the GDP to GTP. In the presence of cellular stress, eIF2 is phosphorylated and, in this state, stably binds to eIF2B to inhibits its GEF activity.

Scanning is also mediated by eIF1 and eIF1A, which cooperatively stabilize the 43S PIC in an open conformation that favors mRNA accommodation (Passmore et al., 2007). Additionally, eIF1 and eIF1A are important subunits for start codon selection as mutations in these two initiation factors have been found to result in increased initiation events at non-AUG codons (Cheung et al., 2007; Pestova and Kolupaeva, 2002; Saini et al., 2010). These two factors act as a gatekeepers that sterically blocks the Met-tRNA$^{Met}_{i}$ from stably associating into the P site before an AUG is encountered (Thakur and Hinnebusch, 2018). When a start codon is recognized, eIF1 dissociates from the 43S complex, allowing for full accommodation of Met-tRNA$^{Met}_{i}$ into the P site (Thakur and Hinnebusch, 2018).

In order to enter the elongation phase of translation, the initiation factors must dissociate from the initiation complex which enables the 40S ribosome to adopt a closed conformation. This transitional phase is largely orchestrated by the activities of eIF3c, eIF5, and eIF5B (Hinnebusch, 2014; Obayashi et al., 2017). When a cognate start codon is detected, eIF5 hydrolyzes eIF2-GTP into eIF2-GDP through a catalytic domain found in its NTD, which leads to its dissociation (Paulin et al., 2001). Because the eIF5 NTD is structurally similar to eIF1, it is suggested that eIF5 NTD promotes the dissociation of eIF1 upon start codon recognition by competing for its binding site (Conte et al., 2006; Llacer et al., 2018).

Joining of the 60S subunit to the stabilized 40S ribosome is then mediated by eIF5B (Pestova et al., 2000). After the release of eIF2-GDP from the initiation complex, eIF1A recruits eIF5B-GTP to the stalled 40S ribosome and its presence promotes 60S association (Fringer et al., 2007). Finally, release of eIF5B and eIF1A from the 40S subunit is triggered upon eIF5B-GTP hydrolysis to eIF5B-GDP (Fringer et al., 2007).

1.3 Cellular Regulation of eIF4F

1.3.1 Regulation of initiation by mTOR

The mTOR (mammalian target of rapamycin) pathway functions as a master regulatory node that controls cellular growth, proliferation and energy expenditure in response to a wide variety of cellular conditions (Laplante and Sabatini, 2012; Sabatini, 2006). mTOR is a serine/threonine protein kinase assembles into one of two structurally and functionally distinct complexes, mTORC1 and mTORC2 (Sabatini, 2006). Although these two complexes phosphorylate non-overlapping subsets of substrates, they are operationally defined by their response to rapamycin, where mTORC1 is much more sensitive compared to mTORC2 (Sarbassov et al., 2004). In the presence of growth factors, both mTORC1 and mTORC2 are activated but mTORC1 activity is further modulated by nutrient availability, oxidative stress, DNA damage, and intracellular ATP levels (Saxton and Sabatini, 2017). However, feedback mechanisms enable these two complexes to crosstalk and regulate each other (Sabatini, 2006). For instance, sustained mTORC1 activity leads to inhibition of IRS-1 (insulin receptor substrate), an upstream regulator that promotes PI3K (phosphatidylinositol 3-kinase) signaling (Sabatini, 2006; Tremblay and Marette, 2001). As both mTORC1 and mTORC2 are subjected to the regulation by the PI3K pathway, chronic activation of mTORC1 eventually dampens PI3K activity, which leads to inhibition of both mTORC1/2 (Sabatini, 2006).

With respect to function, mTORC1 is thought to promote cellular growth through the stimulation of anabolic pathways such as protein synthesis and ribosome biogenesis, while suppressing catabolic processes such as autophagy (Sabatini, 2006). The primary roles of mTORC2 is thought to promote cellular proliferation and survival, notably through the phosphorylation of the PI3K effector,

AKT (Sarbassov et al., 2005; Saxton and Sabatini, 2017). Because many tumorigenic promoting lesions lead to the activation of mTORC1/2 as well as the fact that both complexes play important roles in stimulating tumor growth, these two complexes are perceived as highly attractive therapeutic targets.

Crucially, the mTORC1 complex acts as a regulator that links cellular nutrient status to protein synthesis. Both eIF4E and eIF4A are subjected to the regulation by this pathway through the phosphorylation of 4E-BP and S6K respectively (Figure 1.6).

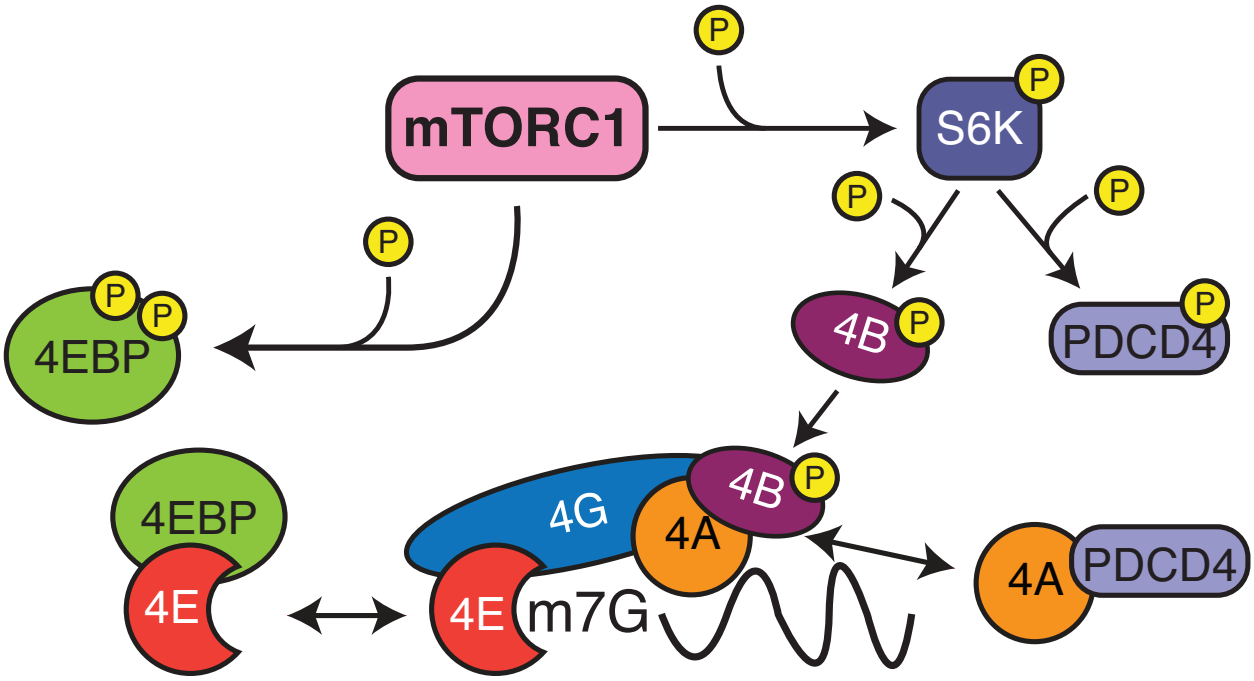

Figure 1.6 Regulation of eIF4F by mTORC1
mTORC1 is a major signalling hub that integrates numerous intracellular and extracellular cues to control cell metabolism, growth, and proliferation. During growth permissive conditions, mTORC1 promotes eIF4F assembly and activity through the phosphorylation 4EBP and S6K. Hyperphosphorylated 4EBP has lowered affinity towards eIF4E and does not effectively inhibit eIF4F formation. S6K is activated upon phosphorylation by mTORC1, which then leads to phosphorylation of several downstream targets such as eIF4B and PDCD4. Phosphorylation of eIF4B is thought to enhance its activity whereas phosphorylation of PDCD4 prevents it from competitively binding to eIF4A.

1.3.1.1 4E-BP

4E-BPs are a family of small (10-12 kDa) proteins that inhibit protein synthesis by competitively binding to the dorsal side of eIF4E and preventing it from associating with eIF4G (Peter et al., 2015). Humans possess 3 different 4E-BP proteins: 4E-BP1, 4E-BP2 (which shares 56% identity with 4E-BP1), and 4E-BP3 (which shares 50% identity with 4E-BP1) (Poulin et al., 1998). Like eIF4G, all three 4E-BPs possess the canonical helical eIF4E binding motif, YXXXXLϕ, a non-canonical motif that associates with the lateral side of eIF4E, and a flexible linker connecting the two motifs together (Gingras et al., 1999b; Peter et al., 2015).

The basis of 4E-BP interaction with eIF4E is determined by its phosphorylation status (Gingras et al., 1999a). Phosphorylation of the 4E-BPs by mTORC1 significantly reduces its affinity towards eIF4E, through conformational changes and, to a lesser extent, electrostatic repulsion (Bah et al., 2015; Gruner et al., 2016). Human 4E-BP1 possesses at least seven phosphorylation sites (T37, T46, S65, T70, S83, S101 and S112) (Gingras et al., 2001; Qin et al., 2016). T37, T46, S65 and T70 are regulated by mTORC1 and are phosphorylated in a sequential manner (Gingras et al., 2001). First, phosphorylation of T37 and T46 (located upstream of the canonical eIF4E-binding motif) represents a priming event that is essential for subsequent modifications (Gingras et al., 1999a; Gingras et al., 2001). NMR experiments of 4E-BP2 reveal that upon phosphorylation of T37 and T46, the canonical YXXXXLϕ eIF4E interacting motif becomes partially buried within a β-strand fold (Bhat et al., 2015). Consequently, this conformational change reduces 4E-BP2 affinity for eIF4E by approximately 2 orders of magnitude (Bah et al., 2015). While phosphorylation of T70 and S65 do not appear to induce major structural changes, these modifications stabilize the β-strand fold induced by T37/T46 phosphorylation and further decrease affinity by roughly 40-fold (Bah et al., 2015).

Phosphorylation of S83, S101 and S112 do not appear to be regulated through mTORC1 and are instead modified by other kinases such as CDK1 and ATM (Heesom et al., 1998; Velasquez et al., 2016; Yang and Kastan, 2000). Compared to the mTOR-sensitive phosphorylation sites, the significance of the phosphorylation at these residues are poorly understood. S83, which forms part of the non-canonical motif that interacts with the lateral side of eIF4E, is phosphorylated during mitosis by CDK1 (Peter et al., 2015; Velasquez et al., 2016). By itself, S83 phosphorylation is insufficient in abrogating 4E-BP:eIF4E association and mutation of this residue to an alanine has no effect on eIF4F formation or translation in cells (Sun et al., 2019; Velasquez et al., 2016). Nonetheless, the S83A mutation is able to confer partial resistance to malignant transformation induced by polyomavirus small T antigen, suggesting that dysregulation of this modification may exert tumor promoting effects (Velasquez et al., 2016).

1.3.1.2 S6K

Mammalian cells possess two S6K orthologs: S6K1 and S6K2. These two proteins share a high degree of homology (83% amino acid identity within the kinase domain) and were long considered to be functionally redundant (Pardo et al., 2001). As a result, the majority of work on S6K biology focused only on S6K1, but more recent evidence suggest that these two kinases may possess non-overlapping roles, through both differential regulation and through their interactions with distinct binding partners (Pardo and Seckl, 2013; Pavan et al., 2016). Furthermore, there is evidence suggesting that while both S6K1 and S6K2 are *bona fide* substrates for mTORC1 phosphorylation, S6K1 is more sensitive towards mTORC1 inhibition (Pardo et al., 2001). In addition to mTORC1, S6K1/2 are also activated by CDK1, PDK1, and the MAPK signaling pathways (Keshwani et al.,

2009; Shah et al., 2003). The S6K proteins phosphorylate a wide array of proteins but with respect to the regulation of translation initiation, the major S6K targets are rpS6 (ribosomal protein S6), PDCD4 (programmed cell death protein 4), and eIF4B.

1.3.1.2.1 rpS6

As the namesake for the kinase, rpS6 is the most well characterized S6K substrate and contains a cluster of 5 phosphorylation sites that are modified by S6K1/2 in a sequential manner (S236 > S235 > S240 > S244 > S247) (Ferrari et al., 1991). rpS6 is a component of the 40S ribosome and its phosphorylation was initially presumed to promote translation initiation by promoting 60S subunit joining. This hypothesis was later disputed as a mouse knock-in model, in which all 5 phosphorylation sites of rpS6 ($rpS6^{P-/-}$) were mutated to alanine, displayed no defect in global protein synthesis (Ruvinsky et al., 2005). However, it is possible that rpS6 phosphorylation affects the translation of specific subsets of mRNAs and it has been observed that the striatum derived from the phosphorylation-deficient mice exhibit impaired translation of transcripts encoding for proteins involved in mitochondrial function (Puighermanal et al., 2017). The absence of rpS6 phosphorylation in $rpS6^{P-/-}$ mice also correlated with smaller cell size, deficiencies in weight gain, muscle weakness, and glucose intolerance (Ruvinsky et al., 2009; Ruvinsky et al., 2005).

1.3.1.2.2 Phosphorylation of eIF4B

S6K1/2 also phosphorylate eIF4B at S422, which is located within its RNA binding domain (Methot et al., 1994). The precise impact of S422 phosphorylation on eIF4B function is still a bit of a mystery, but there is evidence showing that phosphorylation at this site stimulates eIF4B association

with eIF3, which then increases the efficiency of translation initiation (Holz et al., 2005). In support of this, ectopic overexpression of a eIF4B S422D phosphomimetic mutant stimulated cap-dependent translation to a greater extent than overexpression of the wildtype protein (Holz et al., 2005). The eIF4B S422A phosphodeficient mutant, on the other hand, was unable to associate with eIF3 and did not stimulate translation at all (Holz et al., 2005). It is also plausible that the phosphorylation of S422 also enhances eIF4B's ability to stimulate eIF4A activity but this aspect of eIF4B function has not been evaluated. In addition to S6K1/2, eIF4B S422 is also a substrate of kinases belonging to the RSK family, and is therefore subject to the regulation of the MAPK signaling cascade (Shahbazian et al., 2006).

1.3.1.2.3 PDCD4

PDCD4 is a tumor suppressor present in both the nucleus and cytoplasm with distinct functions attributed to these different subcellular sites. In the cytoplasm, PDCD4 has been shown to interact with eIF4A and eIF4G, with both of these interactions leading to depletion of eIF4A from the eIF4F complex (Yang et al., 2003a; Yang et al., 2003b). Structural studies indicate that PDCD4 possesses two tandem domains that bind to the eIF4A NTD in a cooperative fashion (Loh et al., 2009; Suzuki et al., 2008). This interaction prevents the C terminal one-third of eIF4G from associating with eIF4A. Along with interfering with proper assembly of the eIF4F complex, PDCD4 has also been shown to reduce eIF4A's RNA binding capacity and helicase activity (Yang et al., 2003a). Since PDCD4 inhibits the helicase component of eIF4F, it is likely that PDCD4-sensitive mRNAs might be expected to harbor long and/or highly structured 5' leaders but this has not been looked at on a global level.

The availability of PDCD4 for eIF4A inhibition is mediated by both subcellular localization and ubiquitination, which controls its rate of degradation (Bohm et al., 2003; Dorrello et al., 2006). Under conditions of favorable nutrient levels and growth stimuli, PDCD4 is phosphorylated at Ser67 by S6K1 and S6K2 (Dorrello et al., 2006). This event allows PDCD4 to be recognized by the ubiquitin ligase, βTRCP, leading to degradation by the proteasome (Dorrello et al., 2006). Akt has also been found to phosphorylate PDCD4 at Ser67 and Ser457 which in turn drives nuclear localization of PDCD4, sequestering PDCD4 from interacting with eIF4A (Palamarchuk et al., 2005).

In addition to inhibiting eIF4A activity, PDCD4 has also been reported to modulate translation via eIF4A-independent mechanisms. Through its intrinsic RNA binding properties, PDCD4 was demonstrated to directly bind to the XIAP and Bcl-x_L IRESes to suppress their translation (Liwak et al., 2012). PDCD4 can also bind to the coding region of the A-Myb and C-Myb proto-oncogenes and inhibit translation elongation (Biyanee et al., 2014; Singh et al., 2011).

PDCD4 can also modulate transcription and under growth permissive conditions, PDCD4 is predominantly a nuclear protein (Bohm et al., 2003). For instance, PDCD4 suppresses activator protein-1 (AP-1) dependent transcription by binding to c-Jun and inhibiting its transactivation function (Bitomsky et al., 2004; Yang et al., 2003b). The transcriptional regulatory functions of PDCD4 are also exerted by cytoplasmic PDCD4 through sequestration of transcription factors. Cytoplasmic PDCD4 regulates NF-κB transcriptional activity by directly interacting with the NF-κB protein, p65, and inhibiting p65 nuclear localization (Hwang et al., 2014). Overall, it is becoming increasingly apparent that PDCD4 is a multifunctional protein and its tumor suppressing properties may stem from the accumulated effects of affecting gene regulation at multiple levels, including translation initiation.

1.3.2 MAPK Signaling and Translation

The MAPK (mitogen activated protein kinase) signaling cascade integrates extracellular cues to promote cell cycle progression, growth, and proliferation. This pathway influences protein synthesis through MNK1 (MAP kinase interacting protein kinase 1) and MNK2, which lead to eIF4E phosphorylation (Waskiewicz et al., 1999). The physiological significance of this phosphorylation event is currently ambiguous. Deletion of both MNK1 and MNK2 or introduction of a non-phosphorylatable eIF4E mutant (eIF4E S209A) into mice has no effect on viability or development, indicating that this phosphorylation event is not essential (Ueda et al., 2010). However, eIF4E phosphorylation may play a role during tumorigenesis as MNK1/2 double knockout mice, as well as mice harboring the eIF4E S209A knock-in mutation, exhibit impaired tumor development (Furic et al., 2010; Ueda et al., 2010). Additionally, polysome profiling of fibroblasts derived from eIF4E S209A knock-in mice reveal that the absence of eIF4E phosphorylation reduces the translation efficiency of a small subset of mRNAs; among these include transcripts involved in angiogenesis, apoptosis, and metastasis (Furic et al., 2010).

Nevertheless, the molecular basis of how the absence of eIF4E phosphorylation leads to differential effects in translation is not currently well understood. Initially, it was thought that the affinity of eIF4E towards capped mRNAs is increased upon phosphorylation, given how this event is stimulated during growth permissive conditions. Moreover, cocrystal structures of eIF4E complexed with m7GDP show that although S209 does not form direct interactions with the cap structure, it is positioned near the mRNA entrance channel of eIF4E, and phosphorylation of S209 can potentially stabilize the capped mRNA and help position it towards the cap-binding pocket (Marcotrigiano et al.,

1997). In support of this, the phosphomimetic eIF4E mutant, eIF4E S209E, displays increased affinity towards the cap compared to the wild-type protein, (Tomoo et al., 2002). However, surface plasmon resonance experiments later demonstrated that S209 phosphorylation actually impairs eIF4E interaction with capped mRNAs by increasing the dissociation rate 10-fold (Scheper et al., 2002). In light of this, it has been proposed that the increased dissociation rate of phosphorylated eIF4E from the cap structure enables it to detach from the mRNA following 43S recruitment and activate other transcripts for translation more efficiently (Scheper et al., 2002). Alternatively, it is possible that decreased eIF4E affinity towards the cap may allow the eIF4F complex to dissociate from the 5' end during initiation and promote 43S PIC scanning by co-migrating with the complex through the 5' UTR (Scheper et al., 2002). However, at this moment, there is limited experimental evidence to support either hypothesis, and these models remain entirely speculative.

1.3.3 Regulation by Non-Coding RNAs

Non-coding RNAs (ncRNAs) can exert their regulatory influence through complementary binding to mRNA or DNA and/or through RNA structural elements that allow for their interaction with targets (essentially acting as aptamers) (Nakamura et al., 2009). The best characterized and established ncRNAs involved in protein synthesis are undoubtedly rRNAs and tRNAs, but this rapidly growing field has identified new ncRNAs that provide an additional layer of gene regulation. One such example is Brain Cytoplasmic 1 (BC1) RNA, a neuronal ncRNA in rodents that localizes to dendrites and represses translation initiation through its interaction with eIF4A (Lin et al., 2008; Wang et al., 2002). Both BC1 RNA and its proposed human analog, BC200 RNA, directly bind to eIF4A, leading to stimulation of ATPase activity while inhibiting RNA duplex unwinding. BC1 and BC200 thus

inhibit eIF4A by uncoupling ATP hydrolysis from its helicase activity (Lin et al., 2008). As a result, BC1 has been shown to repress general cap-dependent translation, but not eIF4A-independent internal ribosome entry site (IRES)–driven translation (Wang et al., 2002). BC1 is also known to bind to poly (A) binding protein (PABP), although this interaction does not appear to hinder BC1 mediated inhibition of eIF4A activity, as it has been demonstrated that both PABP and eIF4A can bind to BC1 simultaneously (Lin et al., 2008; Wang et al., 2002). Because BC1 is found predominantly in dendritic microdomains of a subset of neurons, the eIF4A/BC1 interaction allows for localized regulation of protein synthesis and may potentially modulate synaptic activity and function (Tiedge et al., 1991).

1.4 Dysregulation of Translation and Pathogenesis

1.4.1 The Role of eIF4F in Cancer

1.4.1.1 eIF4E

The role of translation initiation factors in tumorigenesis was documented over 25 years ago when it was shown that eIF4E overexpression induces neoplastic transformation of immortalized murine fibroblasts (Lazaris-Karatzas et al., 1990). Subsequent studies established eIF4E as a *bona fide* oncogene. eIF4E-overexpression accelerates proliferation and anchorage-independent growth, whereas reduced eIF4E levels prolong the cell cycle and suppress neoplastic growth *in vitro* in a number of cell types (Table 1.3) (De Benedetti et al., 1991; De Benedetti and Rhoads, 1990; Larsson et al., 2007; Rinker-Schaeffer et al., 1993). eIF4E overexpression in mice induces tumorigenesis in a number of tissues and leads to the acceleration of MYC-driven lymphomagenesis (Ruggero et al., 2004; Wendel et al., 2004). In contrast, eIF4E heterozygous mice develop normally, but are more resistant to cancer formation compared to wild-type littermates (Truitt et al., 2015).

Increased eIF4E levels were documented in human cancers, including head and neck squamous cell carcinoma (HNSCC), malignancies of breast, lung, and colon, and leukemias and lymphomas (De Benedetti and Graff, 2004; Silvera et al., 2010). The best-established mechanisms of eIF4E overexpression in neoplasia are gene amplifications in HNSCC and c-MYC-mediated transcriptional upregulation (Haydon et al., 2000; Raught and Gingras, 1999). Importantly, high eIF4E levels correlate with poor prognosis in a number of cancer types, and typically, eIF4E expression is lower in benign lesions (e.g. adenomas of the colon) relative to malignant tumors (adenocarcinoma) in the same tissue (De Benedetti and Graff, 2004; Rosenwald et al., 1999). Moreover, high eIF4E levels have been linked to chemoresistance, and accordingly, forced expression of eIF4E renders cancer cells resistant to a number of chemotherapeutics including those that are widely used in the clinic (e.g. doxorubicin) and targeted therapies (e.g. vemurafenib, Herceptin) (Bhat et al., 2015; Ilic et al., 2011; Wendel et al., 2004; Zindy et al., 2011).

Although eIF4E is required for efficient cap-dependent translation of all nuclear-encoded mRNAs, a subset of mRNAs with long and structured 5' leaders appear to be more sensitive to changes in eIF4E levels compared to those with shorter and less complex 5' leaders. The vast majority of "eIF4E-sensitive mRNAs" that harbor long and structured 5' leaders encode tumor-promoting proteins including oncogenes (e.g. c-MYC) and factors that promote proliferation (e.g. cyclins, ODC), survival (e.g. BCL-2 family members, osteopontin, survivin) and angiogenesis (e.g. VEGF, FGF) (De Benedetti and Graff, 2004; Koromilas et al., 1992a; Silvera et al., 2010). Therefore, eIF4E drives oncogenesis by selectively increasing the translation of mRNAs encoding tumor-promoting proteins, likely because mRNAs harboring complex and long 5' leaders have a heightened dependence on eIF4A helicase activity (Svitkin et al., 2001). eIF4A activity is highly efficient in unwinding secondary RNA

structures only when part of the eIF4F complex (Pause et al., 1994), suggesting that the dependence of eIF4A in the eIF4F complex underpins exceptional sensitivity of mRNAs with long and structured 5' leaders to changes in eIF4E levels (Feoktistova et al., 2013).

While it is generally accepted that eIF4E exerts its oncogenic effects via translational reprogramming, the catalogue of mRNAs that mediate its oncogenic effects is still disputed. Initial studies showed that the length and complexity of 5' leaders are major features that distinguish "eIF4E-senstive" from "eIF4E-insensitive" mRNAs (Koromilas et al., 1992a; Pelletier and Sonenberg, 1985). Indeed, ribosome profiling (a technique that defines global ribosomal occupation on mRNAs through deep-sequencing of ribosome protected mRNA fragments) revealed that the mTORC1/eIF4E pathway almost exclusively regulates translation of mRNAs harboring 5' TOP or 5'TOP-like motifs (Hsieh et al., 2012; Thoreen et al., 2012). In contrast, polysome-profiling (a technique based on microarray analysis of polysome-associated mRNAs) showed that the many mTOR-regulated transcripts do not contain 5'TOP motif (Larsson et al., 2012). A number of mRNAs encoding proteins involved in mitochondrial functions (e.g. components of mitochondrial complex I and V) bearing 5' TISU elements also appear to be highly dependent on eIF4E, but their translation is only marginally sensitive to changes in eIF4A activity (Elfakess et al., 2011; Gandin et al., 2016; Sinvani et al., 2015). Differences in experimental models and technologies can explain these discrepancies (Gandin et al., 2016), but ultimately, future studies are required to carefully catalogue "eIF4E-sensitive" mRNAs and define features that ascribe eIF4E-sensitivity.

Phosphorylation of eIF4E at Ser209 has also been implicated in carcinogenesis and tumor progression as loss of this modification attenuates its oncogenic potential *in vitro* and *in vivo* (Furic et al., 2010; Robichaud et al., 2015; Topisirovic et al., 2004; Wendel et al., 2004). In addition, mice

bearing a nonphosphorylatable eIF4E mutant show delayed development of prostate and breast tumors, and ablation of MNKs 1 and 2 in T cells mitigates lymphomagenesis (Furic et al., 2010; Robichaud et al., 2015; Ueda et al., 2010). It appears that phospho-eIF4E selectively increases translation of mRNAs that encode pro-survival (e.g. MCL-1) and invasion and epithelial-to-mesenchymal transition promoting proteins (e.g. MMP3; SNAIL), and cytokines, which only partially overlap with those induced by eIF4E overexpression (Furic et al., 2010; Robichaud et al., 2015; Wendel et al., 2004). Accordingly, eIF4E phosphorylation has been demonstrated to promote metastatic spread in a breast cancer mouse model (Robichaud et al., 2015).

1.4.1.2 eIF4G

Overexpression of eIF4G1 induces neoplastic transformation in immortalized murine fibroblasts and stimulates neoplastic growth in mouse xenograft models (Fukuchi-Shimogori et al., 1997). As well, levels of eIF4G1 are frequently upregulated in human cancer including malignancies of the breast and lungs (Bauer et al., 2001; Silvera et al., 2009). Although the catalogue of mRNAs whose translation is sensitive to changes in eIF4G1 appears to mostly overlap with those that are also "eIF4E-sensitive" (e.g. cyclin D family members, survivin), there are some notable differences (Braunstein et al., 2007). While the molecular mechanisms underlying this phenomenon remain underexplored, it appears that these discrepancies may stem from the ability of eIF4G1 to stimulate translation of oncogenic mRNAs in a cap-independent manner when the levels of the eIF4F complex are limited by dampened mTORC1 signalling (e.g. during hypoxic conditions) (Braunstein et al., 2007). To this end, eIF4G1 has been proposed to act as a major factor that allows switching from cap-dependent to cap-independent translation when oxygen is limiting (Braunstein et al., 2007). It has

also been suggested that eIF4G1 bolsters tumorigenesis and cancer progression at least in part by selectively modulating cap-dependent translation of mRNAs containing upstream open reading frames (uORFs) and encoding for proteins with crucial roles in energy metabolism (e.g. HIF1-alpha) (Badura et al., 2012; Ramirez-Valle et al., 2008), DNA-damage response (e.g. BRCA1/2 and MRE11) (Badura et al., 2012), and cell cycle regulation (e.g. SKP2, Cyclin D1) (Ramirez-Valle et al., 2008), as well as those that are regulated in a cap-independent manner (e.g. p120 catenin) (Silvera et al., 2009).

1.4.1.3 eIF4B and eIF4H

eIF4B is modulated by several proto-oncogenic pathways including MAPK (Shahbazian et al., 2006), PI3K/mTOR (Raught et al., 2004), and PIM kinases (Peng et al., 2007; Yang et al., 2013a). While the role of eIF4B on translational reprogramming in cancer is still obscure, depletion of eIF4B decreases translation rates and inhibits tumor growth in a K562 leukemic xenograft model (Yang et al., 2013a), whereas its overexpression leads to accelerated cell proliferation (Table 1.3) (Hernandez et al., 2004). Given its apparent role in integrating signals from a number of oncogenic pathways, there may be therapeutic value in developing strategies that target eIF4B activity. For instance, silencing eIF4B sensitizes Abl-transformed cells to imatinib, while ectopic expression of phosphomimetic eIF4B mutants confers resistance to the PIM inhibitor, SMI-4a (Yang et al., 2013a).

The relevance of eIF4H in tumor development and maintenance is rather limited and mostly correlative. In human tissues, there are two alternatively spliced isoforms of eIF4H that differ by the presence of 20 amino acids (exon 5 is alternatively spliced) (Martindale et al., 2000). The shorter isoform (isoform 2) is more prevalent in normal tissues but only isoform 1 is significantly overexpressed in colorectal and esophageal tumor tissues, relative to adjacent non-tumor tissues (Tomonaga et al.,

2004; Wu et al., 2011). However in lung carcinomas, both isoforms are overexpressed (Vaysse et al., 2015) and ectopic overexpression of either eIF4H isoform 1 or isoform 2 stimulates cellular proliferation, induces NIH/3T3 transformation, and inhibits cisplatin or etoposide-induced apoptosis (Vaysse et al., 2015; Wu et al., 2011). It is not known whether the roles of the two isoforms are redundant, but overall, these results may indicate that both possess tumor-promoting properties.

1.4.2 The Role of eIF2 Ternary Complex in Cancer

The role of eIF2α in tumor onset and progression is context dependent and generally not very well understood. The phosphorylation of eIF2α on Ser51 is a cytoprotective mechanism that allows adaptation to stress but depending on the severity and duration of the stress, eIF2α phosphorylation can promote survival or conversely trigger apoptosis (Bi et al., 2005; Donze et al., 2004; Koromilas and Mounir, 2013). The balance between pro-survival and pro-apoptotic signals induced by eIF2α phosphorylation on Ser51 implies that it may be difficult to predict the outcome of targeting this pathway in cancer cells. Indeed, inhibition of eIF2α phosphorylation might prevent adaptive responses to stress and induce cell death and this is exemplified by the anti-neoplastic activity of the PERK inhibitor, GSK2656157 (Atkins et al., 2013). Furthermore, inhibition of the unfolded protein response in Myc-driven tumors attenuated tumor formation (Hart et al., 2012). Contrary to this, the expression of a non-phosphorylatable mutant of eIF2α (S51A) has been shown to transform NIH/3T3 cells (Donze et al., 1995), and sustained eIF2α phosphorylation induced by the PP1 inhibitor salubrinal exhibited pro-apoptotic effects in hepatocellular carcinoma cells (Teng et al., 2014). Interacting partners of eIF2 have also been implicated in tumor progression. For instance, eIF5-mimic protein 1 (5MP-1) is amplified in colorectal cancers and contributes to oncogenesis through

suppressing eIF2 activity (Kozel et al., 2016; Sato et al., 2019). In turn, this suppresses translation initiation at non-AUG codons, while increasing the relative proportion of translation initiation events at downstream start sites (Hiraishi et al., 2014; Kozel et al., 2016; Sato et al., 2019; Tang et al., 2017). Notably, overexpression of 5MP-1 leads to increased expression of ATF4 and c-Myc (Sato et al., 2019).

1.4.3 The Role of eIF3 in Cancer

Several eIF3 subunits (a, b, c, h, i, m) have been documented to be overexpressed in a wide variety of cancers including, but not limited to, breast, prostate, lung, cervical, and gastric cancers (Chen and Burger, 2004; Emmanuel et al., 2013; Goh et al., 2011; Nupponen et al., 1999; Pincheira et al., 2001; Wang et al., 2013). To investigate whether the upregulation of eIF3 observed in cancer is causal for, or a consequence of, tumor progression, John Hershey and colleagues ectopically overexpressed each eIF3 subunit (with the exception of 3m) in NIH/3T3 cells and found that subunits 3a, 3b, 3c, 3h, and 3i stimulated global protein synthesis, accelerated cellular proliferation, and promoted malignant transformation (Zhang et al., 2007). It was also noted that overexpression of 3e and 3f inhibited translation, and decreased cell growth and proliferation (Zhang et al., 2007). Interestingly, eIF3f expression is reduced in several cancer types (Doldan et al., 2008a; Doldan et al., 2008b; Shi et al., 2006) and is thought to possess tumor suppressing activity. Consistent with this, depletion of eIF3f induced transformation of immortalized normal human pancreatic ductal epithelial (HPDE) cells (Wen et al., 2012). On the other hand, the role of eIF3e (also referred to INT6) in tumor onset and maintenance has been more ambiguous—while it has been found that loss of eIF3e promotes transformation and may play a role as a tumor suppressor (Asano et al., 1997; Buttitta et al.,

2005; Gillis and Lewis, 2013; Marchetti et al., 2001; Morris et al., 2012; Suo et al., 2015), it has also been proposed to possess oncogenic properties in certain settings (Grzmil et al., 2010).

Why certain eIF3 subunits promote transformation whereas others appear to be tumor suppressors is not clear. In part, interpretations of studies of individual subunits are complicated by the fact that overexpression or depletion of one subunit can alter the endogenous levels of the other subunits and/or affect eIF3 complex assembly; therefore, this can make it difficult to attribute observed changes directly to one subunit (Hershey, 2015). As well, certain eIF3 subunits have been reported to function outside of translation initiation. eIF3e, for instance, has been shown to interact with ATM and may play a role in the DNA damage response (Morris et al., 2012). Given these findings, it is certainly of interest to further characterize eIF3 outside of its canonical role in translation and better define its role in the oncogenic process.

Table 1.3 Consequences of Aberrant Eukaryotic Initiation Factor Activity/Levels

Factor	Type of alteration	Context and Consequence
eIF4E	Ectopic overexpression	Malignant transformation of NIH/3T3 cells (Lazaris-Karatzas et al., 1990), Rat 2 fibroblasts(Lazaris-Karatzas et al., 1990), and immortalized HMEC/hTERT cells (Larsson et al., 2007); increased cell cycle progression, division, and anchorage-independent growth in HeLa cells(Palamarchuk et al., 2005); cooperation with c-Myc in B-cell lymphomagenesis (Eμ–Myc mouse model) (Ruggero et al., 2004; Wendel et al., 2004); accelerated T-ALL development (murine T-ALL model) (Wolfe et al., 2014)
	Decreased expression	Reversal of transformed properties of RAS-transformed rat embryo fibroblasts (Rinker-Schaeffer et al., 1993); increased cell division times in HeLa cells (De Benedetti et al., 1991)
eIF4G1	Ectopic overexpression	Malignant transformation of NIH/3T3 cells (Fukuchi-Shimogori et al., 1997)
	Decreased activity	Loss of viability; sensitization to dexamethasone in multiple myeloma (Robert et al., 2014)
eIF4A1	Ectopic Overexpression	Accelerated T-ALL development (murine T-ALL model) (Wolfe et al., 2014)

	Decreased expression	Loss of viability in B-cell lymphomas (Eμ–Myc mouse model) (Cencic et al., 2013)
eIF4A2	Ectopic Overexpression	No reported consequence
	Decreased expression	Complete elimination has no reported consequence in NIH/3T3 cells (Galicia-Vazquez et al., 2015)
eIF4H (isoform 1)	Ectopic overexpression	Malignant transformation of NIH/3T3 cells (Wu et al., 2011)
	Decreased expression	Inhibited proliferation of LOVO and RKO colon cancer cell lines (Wu et al., 2011)
eIF4B	Ectopic overexpression	Stimulates proliferation in cultured Drosophila cells (Hernandez et al., 2004)
	Decreased expression	Decreased cell survival, attenuated proliferation, sensitization of cells to genotoxic stress-driven apoptosis (HeLa cells)(Shahbazian et al., 2010)
eIF2	Inhibited/abrogated eIF2α Ser51 phosphorylation	Malignant transformation of NIH/3T3 cells via ectopic overexpression of a dominant negative PKR mutant (Barber et al., 1995; Donze et al., 1995; Koromilas et al., 1992b) or non-phosphorylatable eIF2α S51A (Donze et al., 1995; Perkins and Barber, 2004); transformation of HEK cells stably transduced with hTERT and large T antigen (overexpression of eIF2α S51A) (Perkins and Barber, 2004); inhibition of TRAIL-induced apoptosis in HepG2 cells (Teng et al., 2014); impaired growth of tumors derived from RasV12 transformed *PERK*$^{-/-}$ MEFs (Bi et al., 2005; Hart et al., 2012)
	Increased/constitutive eIF2α Ser51 phosphorylation	Enhanced sensitivity to bortezomib in RPMI 8226 multiple myeloma cells (overexpression of eIF2α S51D) (Schewe and Aguirre-Ghiso, 2009); stimulation of TRAIL-induced apoptosis in HepG2 cells (Teng et al., 2014)
eIF3	Ectopic overexpression	Malignant transformation of NIH/3T3 cells (upon overexpression of subunits 3a, 3b, 3c, 3h, or 3i) (Zhang et al., 2007); inhibition of cell growth and induction of apoptosis in A375 melanoma cells and BxPc3 pancreatic cancer cells (overexpression of 3f) (Shi et al., 2006); malignant transformation of MCF10A or HC11 mammary epithelial cells and NIH cells (overexpression of truncated, but not full length 3e) (Mayeur and Hershey, 2002; Rasmussen et al., 2001)
	Decreased expression	Inhibition of apoptosis (upon knockdown of 3f) in A375 melanoma cells (Shi et al., 2006); malignant transformation of human pancreatic ductal epithelial cells (knockdown of 3f) (Wen et al., 2012)

1.5 Regulation of Translation by Small Molecules

1.5.1 Rationale Behind the Development of Translation Inhibitors

Translation is a central step in the gene expression pathway that can dramatically influence cell fate and its dysregulation can lead to a wide variety of disorders including, but not limited to, cancer, neurodegeneration, diabetes, and anemia (Scheper et al., 2007). Accordingly, small molecules capable of targeting protein synthesis may represent a viable therapeutic avenue for the treatment of these diseases. Tumor cells also often exhibit higher levels of protein synthesis in order to fuel their elevated growth, proliferation rates, and metabolic requirements, and while translation is also essential in non-transformed cells, the heightened dependency of malignant cells towards this process offers a therapeutic window. In particular, eIF4F is an attractive target as many commonly dysregulated signalling pathways converges to the regulation of this complex and additionally, the expression numerous tumor-promoting factors (such as c-Myc, Mcl-1, and XIAP) are highly sensitive towards eIF4F activity.

1.5.2 Small Molecules Targeting Upstream Regulators of eIF4F

1.5.2.1 Rapamycin and its derivatives

Rapamycin, a natural macrolide with broad therapeutic benefits, was first isolated from the soils the Easter Islands during the 1970s—long before mTOR was identified as the cellular target in 1994 (Benjamin et al., 2011). This compound associates with FKBP12 (FK506-binding protein 12) and forms a gain-of-function complex that allosterically inhibits mTOR (Sabatini et al., 1994). As the FKBP12-rapamycin complex does not associate with mTORC2 efficiently, this complex is relatively resistant to rapamycin compared to mTORC1 (Jacinto et al., 2004). Long-term rapamycin exposure

eventually inhibits mTORC2 signaling through preventing free mTOR protein from assembling into the complex (Sarbassov et al., 2006). However, mTORC2 sensitivity towards chronic rapamycin administration varies between different cell types and this appears to be dependent the relative FKBP12 expression levels (Schreiber et al., 2015).

In addition to rapamycin, a number of structural analogs (rapalogs) with improved compound solubility and pharmacokinetic properties have been developed and FDA approved for cancer therapy. For instance, the rapalog everolimus is approved by the FDA for the treatment of metastatic breast cancer, renal cell carcinoma, and pancreatic neuroendocrine cancer (Yao et al., 2011). However, rapalogs have not lived up to initial expectations within the clinical setting and usage of rapalogs in monotherapy tend to stabilize the tumor without causing much regression (Wander et al., 2011). The underperformance of rapalogs has been partially attributed to a number of negative mechanisms and compensatory pathways that become activated during prolonged mTORC1 suppression (Li et al., 2014). Inhibition of mTORC1 activity leads to the accumulation of IRS-1 phosphorylation, which subsequently promotes PI3K-Akt signaling and mTORC2 activity (Gan et al., 2011; Huang and Manning, 2009). Furthermore, certain mTORC1 phosphorylation targets, such as the 4E-BP1 priming sites T36 and T47, are often recalcitrant to rapalog treatment, and this incomplete inhibition of mTORC1 may contribute to the modest effect of rapalogs in clinical applications (Feldman et al., 2009; Kang et al., 2013).

1.5.2.2 Active-site mTOR inhibitors

Second generation mTOR inhibitors target the ATP binding pocket of the mTOR protein and equally suppress the activities of both mTORC1 and mTORC2. The founding members of this

class of inhibitors, Torin1 and PP242, exhibit nanomolar efficacy against tumor cell lines *in vitro* and unlike the rapalogs, are capable of fully inhibiting mTORC1 activity (Feldman et al., 2009; Thoreen et al., 2009). These compounds therefore result in a tighter association of 4E-BP to eIF4E and are more potent inhibitors of cap-dependent translation compared to rapamycin and its derivatives (Feldman et al., 2009; Thoreen et al., 2009). Interestingly, the enhanced efficacy of the active-site mTOR inhibitors are attributed to their capacity to fully inhibit mTORC1 activity rather than their ability to target both mTOR complexes as RICTOR-null fibroblasts exhibit similar sensitivity towards these compounds compared to their wildtype counterparts (Thoreen et al., 2009)

No active-site mTOR inhibitors have been FDA approved at this moment but several are currently being evaluated in clinical trials (Hua et al., 2019). AZD2014 is currently undergoing testing in phase 2 clinical studies as a therapy for metastatic breast cancer and renal cell carcinoma. In pre-clinical animal models, AZD2014 was shown to be well-tolerated and effective against everolimus-resistant tumors (Guichard et al., 2015; Vandamme et al., 2016). In spite of this, a phase 2 trial comparing the efficacy of AZD2014 and everolimus against VEGF-refractory metastatic renal cell carcinoma demonstrated that everolimus outperformed AZD2014 with respect to progression free survival and overall survival (Powles et al., 2016). Similar observations were made in a phase 2 study of advanced metastatic breast cancer in which fluvestrant + AZD2014 treatment was found to be inferior to fluvestrant + everolimus (Schmid et al., 2019). The underlying reasons for these unexpected outcomes are not well understood, but the short half-life of AZD2014 may have limited its efficacy in these studies. Furthermore, resistance towards these inhibitors can be acquired through mutations to changes to the binding pocket of mTOR or through alterations in eIF4E:4E-BP stoichiometry (Alain et al., 2012; Dilling et al., 2002).

1.5.3 Small Molecules Targeting eIF4F

Dysregulation of eIF4F has been identified as a mechanism of resistance against numerous anti-neoplastic therapies but however, pre-clinical studies show that this obstacle in cancer treatment can be circumvented using compounds capable of directly target the eIF4F complex (Boussemart et al., 2014; Malka-Mahieu et al., 2016). Cap analogs represent archetypical inhibitors that interfere with eIF4F activity by competing with the 5' ends of mRNAs for eIF4E association, thus preventing recruitment of the 43S PIC to the transcript. Synthetic cap analogs have proven to be invaluable tools for investigating the underlying molecular mechanisms of cap-dependent translation, splicing, and mRNA decay in *in vitro* studies. However, the efficacy of cap analogs as potential anti-cancer agents is severely limited by their poor membrane permeability.

Alternatively, the eIF4F activity can be inhibited by small molecules that prevent complex assembly. Notably, 4EGI-1 is an allosteric inhibitor that binds near the lateral surface of eIF4E and induces structural alterations that block the ability of eIF4E to associate with eIF4G, but interesting do not affect eIF4E:4E-BP interaction (Moerke et al., 2007; Papadopoulos et al., 2014; Peter et al., 2015). This small molecule has been shown to attenuate tumor growth *in vivo* and is able induce apoptosis in tumor lines resistant to mTOR-targeted therapies (Tamburini et al., 2009).

Although all three components of the eIF4F complex are essential genes, partial suppression of these proteins is generally well-tolerated (Cencic et al., 2009; Chen et al., 2012; Graff et al., 2007; Truitt et al., 2015). Notably, the administration of antisense-oligonucleotides (ASOs) targeting eIF4E into mice is capable of reducing eIF4E levels by 80% in the liver and does not induce illness, distress or changes to organ or overall body weight (Graff et al., 2007). However, the same dosage of 4E-ASO

is able to suppress xenograft tumor growth *in vivo* (Graff et al., 2007). Overall, these results indicate that tumor cells have a higher susceptibility towards eIF4F suppression compared to normal tissues and targeting the eIF4F complex is a viable therapeutic strategy against tumors that is worthy of further exploration.

1.5.4 Small Molecules Targeting eIF4A

1.5.4.1 Hippuristanol

Hippuristanol is a polyoxygenated steroid produced a species of coral known as *Isis hippuris*. It was originally isolated and characterized as a cytotoxic agent in the early 1980s but its mechanism of action as an eIF4A inhibitor was not elucidated until more than 20 years later (Bordeleau et al., 2006b). NMR studies identified the binding pocket to be located within the eIF4A CTD (Lindqvist et al., 2008b). The inhibitory activity of hippuristanol appears to be selective towards eIF4A1 and eIF4A2 as the binding site maps within a region that is poorly conserved among the DEAD-box helicases (Lindqvist et al., 2008b). Accordingly, *in vitro* assays have demonstrated that hippuristanol reduces the activity of eIF4A1 and eIF4A2 at similar concentrations, whereas the IC_{50} of eIF4A3 (DDX48) is 10-fold higher and the ATPase activity of DDX19 and DDX52 is not inhibited at all by this compound (Lindqvist et al., 2008b). Moreover, hippuristanol does not inhibit splicing, transcription or DNA replication, suggesting that it does not affect the activity of RNA helicases involved in these processes (Bordeleau et al., 2006b). Due to these properties, hippuristanol has proven to be a valuable reagent in studies probing the activity of eIF4A (Dauber et al., 2011; Fred et al., 2011; Hoeffer et al., 2013; Linero et al., 2011; Olson et al., 2013; Radtke et al., 2013; Sun et al., 2014b).

The identification of hippuristanol as a specific inhibitor eIF4A has since reignited interest in the evaluation of its potential for cancer therapy. A pre-clinical study assessing the potential of hippuristanol as a therapeutic agent against adult T-cell leukemia (ATL) found it to arrest cells in G_1 (Tsumuraya et al., 2011). Hippuristanol also induced apoptosis of ATL cells but not peripheral blood mononuclear cells (Tsumuraya et al., 2011). Likewise, similar observations were made when hippuristanol was used against primary effusion lymphoma (Ishikawa et al., 2013).

Hippuristanol may also have value in combination strategies. Elevation of anti-apoptotic proteins such as Bcl-2, Bcl-X_L, and Mcl-1 allows malignant cells to evade intrinsic apoptotic signaling and is correlated with resistance to therapeutic strategies dependent on the induction of apoptosis (e.g. DNA damaging agents) (Wilson et al., 2006). However, because the mRNAs of several of these anti-apoptotic proteins are characterized by long, structured 5' leaders and are sensitive to changes in eIF4F levels, targeting eIF4A activity is a reasonable approach to re-sensitize resistant tumors to anti-cancer agents. In an *in vivo* study utilizing the Eμ-Myc lymphoma mouse, hippuristanol was found to synergize with doxorubicin, rapamycin, ABT-737, and cyclophosphamide (Cencic et al., 2013). Furthermore, this synergistic effect was also observed against multiple human lymphoma and leukemia cell lines (Cencic et al., 2013).

While these results appear to be promising, there still remains much to be done with respect to the development and characterization of this compound. Firstly, the potency of hippuristanol can be further improved as reported IC_{50}'s in the aforementioned studies ranged from ~50 - ~300 nM. Additionally, the use of hippuristanol *in vivo* is limited by its relatively low solubility. Although synthetic derivatives have been generated (Ravindar et al., 2010, 2011; Somaiah et al., 2014), none has surpassed the activity of the naturally produced metabolite.

1.5.4.2 Pateamine A

Pateamine A (PatA) is a biologically active metabolite isolated from the sea sponge, *Mycale* sp. that was first found to possess potent and selective cytotoxic activity against tumor cells in 1991 (Northcote et al., 1991). eIF4A was identified as a cellular target of PatA by two independent studies in 2005 (Bordeleau et al., 2005; Low et al., 2005). As the result of a high-throughput screening campaign for novel inhibitors of protein synthesis, our lab identified PatA as a compound capable of inhibiting eIF4A-dependent translation (Bordeleau et al., 2005) whereas Low et al. (Low et al., 2005) utilized a biotinylated-PatA derivative to search for molecular targets and identified eIF4A as the primary binding protein. Although the PatA binding site on eIF4A has yet to be determined, it may be located within the eIF4A NTD since a C-terminal deletion mutant of eIF4A (Δ246-406) is still capable of binding PatA (Low et al., 2007). Unlike hippuristanol, which allosterically inhibits eIF4A RNA binding, the effects of PatA on eIF4A are rather unexpected as it increases its affinity for ATP and RNA and stimulates ATPase and helicase activities (Bordeleau et al., 2005). A mechanism rationalizing these results depicts PatA as a chemical inducer of dimerization that forces non-specific eIF4A-RNA engagements – thereby sequestering eIF4A from the eIF4F complex with concomitant inhibition of cap-dependent translation (Bordeleau et al., 2006a). This mechanism is supported by the observation that administration of PatA disrupts the eIF4A-eIF4G interaction and reduces levels of eIF4A present in the eIF4F complex (Bordeleau et al., 2006a; Low et al., 2005). As an inhibitor of translation, PatA also induces the assembly of stress granules in an manner that did not depend on eIF2α phosphorylation (Dang et al., 2006; Mazroui et al., 2006).

Overall, PatA has been shown to be effective at inhibiting proliferation and inducing apoptosis in many tumor cell lines at sub-nanomolar concentrations *ex vivo* (Low et al., 2005; Northcote et al., 1991). In particular, cells transformed with the Ras oncogene show increased sensitivity to PatA-induced apoptosis (Hood et al., 2001). Synthetic derivatives of PatA are also promising anti-cancer agents as the simplified PatA analog, des-methyl, des-amino PatA (DMDA-PatA) is not as sensitive to the presence of multidrug resistance protein 1 (MDR1) and shows potent anti-proliferative activity *in vitro* against a wide variety of human cancer cell lines (Kuznetsov et al., 2009). However, *in vivo*, the therapeutic activity of DMDA-PatA appears to be more restrictive, as it is cytotoxic against melanoma xenograft models but not towards pancreatic or colorectal xenograft models (Kuznetsov et al., 2009).

Additionally, sub-cytotoxic concentrations of PatA have been recently found to be protective against cachexia-induced muscle wasting (Di Marco et al., 2012). One characteristic feature of muscle wasting is repression of global translation and unexpectedly, low doses of PatA partially reversed this inhibition (Di Marco et al., 2012). This effect was proposed to be the result of selective sequestration of cachexia-promoting mRNAs into stress granules (Di Marco et al., 2012). As such, among mRNAs found within PatA-induced stress granules include inducible nitric oxide synthase (iNOS), a key effector in NF-κB-mediated muscle-wasting that promotes inflammation and degradation of mRNAs associated with muscle maintenance, such as MyoD and myogenin (Di Marco et al., 2012). The selectivity of sequestration is suggested to be mediated by features within the mRNA 5' leader, although it is unknown as to which elements would be the cause of this differential effect.

Although there is quite a bit of compelling data demonstrating that eIF4A1 and eIF4A2 are *bona fide* targets of PatA, there are still questions regarding its specificity. Affinity chromatography with immobilized PatA identified not only eIF4A1 and eIF4A2 as cellular targets of PatA, but also the

serine/threonine kinase receptor associated protein (STRAP), which has been implicated in cap-independent translation (Grimmler et al., 2005; Hunt et al., 1999; Low et al., 2005). However, a recent study identified STRAP as a novel eIF4A-interacting protein, thus raising the possibility that its isolation by PatA affinity chromatography may have been the consequence of direct interaction between STRAP and eIF4A (Vukmirovic et al., 2013). As well, early studies of PatA characterized it as an immunosuppressive compound that inhibits IL-2 production (Romo et al., 1998). In addition, PatA can inhibit nonsense mediated decay as it is known to also target eIF4A3, a related DEAD-box helicase that assembles into EJCs and is involved in NMD (Dang et al., 2006). In sum, it will be important to establish if the anti-cancer effects of PatA are a direct consequence of translation inhibition and/or due to secondary events.

1.5.4.3 Rocaglates

The *Aglaia* genus of the Meliaceae family of angiosperms has garnered much attention as a source of novel therapeutic agents. Many *Aglaia* species are utilized in traditional medicines to treat respiratory diseases and inflammation and since 1970s, extracts from *Aglaia* species have been reported to possess tumor-suppressing properties (Dhar et al., 1973; Ebada et al., 2011). Notably, *Aglaia* species are the exclusive natural source of rocaglates, a class of compounds structurally characterized by a common cyclopenta[*b*]furan skeleton. Rocaglamide (also known as Rocaglamide A or Roc-A) was the first rocaglate isolated from *Aglaia elliptifolia* in 1982 by King and colleagues, and has been found to possess anti-leukemic activity *ex vivo* (King et al., 1982b). In particular, much work has gone towards the characterization of silvestrol, a rocaglate isolated from *Aglaia foveolata* that inhibits translation by targeting eIF4A.

There are three lines of evidence consistent with eIF4A being the primary molecular target of silvestrol. First, in *in vitro* translation extracts and cell based reporter assays, rocaglates inhibit translation of eIF4A-dependent mRNAs while having little effect on expression from eIF4A-independent IRESes (Bordeleau et al., 2008). The mechanism of action of silvestrol appears similar to that of PatA in that it stimulates the RNA-binding and helicase activities of eIF4A (Bordeleau et al., 2008). Second, affinity chromatography using immobilized epi-silvestrol reproducibly and consistently identified eIF4A as the major cellular binding protein (Chambers et al., 2013). Finally, an unbiased genetic selection of rocaglate-resistant yeast variants identified mutations in TIF1 and TIF2, yeast orthologs of eIF4A, as responsible for conferring resistance to the growth inhibitory properties of rocaglates (Sadlish et al., 2013). However, before the studies reported in this thesis were undertaken, it was unclear whether the results observed in yeast would translate (no pun intended) in the mammalian setting.

Preclinical pharmacokinetic studies of silvestrol indicated an overall favorable profile, as it is relatively stable in mouse and human plasma, well tolerated in animals (up to 1.5 mg/kg in mice) and highly potent (effective at nanomolar concentrations in *in vitro* cell culture and less than 0.5 mg/kg daily dosing in murine cancer models) (Cencic et al., 2010; Kogure et al., 2013; Saradhi et al., 2011). However, there are shortcomings with respect to the delivery and absorption of the compound; although the systemic availability of silvestrol when delivered via IP is near 100%, the bioavailability achieved from oral administration is dramatically inferior (1.7%) (Saradhi et al., 2011). When delivered via IP, 60% of silvestrol is bioavailable 6 hrs after injection, and as a single agent, silvestrol has been shown to be an inducer of intrinsic apoptosis and an effective suppressor of solid tumor growth in human breast and prostate cancer xenograft models (Cencic et al., 2009). In an investigation

assessing the effects of silvestrol in a mouse hepatocellular carcinoma model, silvestrol was found to improve median survival in tumor-bearing mice without inducing damage to normal hepatocytes (Kogure et al., 2013).

Are the cytotoxic effects of rocaglates on cancer cells the consequence of inhibiting a large spectrum or a choice number of eIF4F-responsive mRNAs? Current evidence suggests the latter. Detailed analysis of copy number variations across >25 different cancer types identified four known eIF4F transcripts (MYC, MCL1, BCL-XL, and CCND1) to be among the top 20 most amplified genes (Beroukhim et al., 2010). Given the ubiquitous nature of these lesions, and the role that these play in tumor cell maintenance, inhibiting the production of these eIF4F targets is expected to have profound consequences on tumor cell maintenance. Accordingly, silvestrol treatment has been associated with a preferential decrease in the translation of MCL1, CCND1, BCL-XL, and MYC mRNAs in a variety of transformed settings (Cencic et al., 2009).

1.6 Overview and Rationale of Thesis

It is becoming increasingly evident that targeting translation initiation is a viable anti-neoplastic strategy. Members of the rocaglate family of compounds are particularly interesting as they are extremely potent in *in vitro* settings, well tolerated *in vivo*, and are effective in resensitizing resistant tumors towards numerous standard-of-care agents. However, there remains a number of unresolved questions regarding the mechanism of action of these compounds. Although we can observe that silvestrol has a direct effect on eIF4A enzymatic activity, it is unclear whether this effect is relevant for the *in vivo* cytotoxic effects of the compound. Our understanding of rocaglate mechanism of action is further confounded by the alternative hypothesis implicating the MAPK pathway and it is not clear

whether this aspect significantly contributes to rocaglate mediated cytotoxicity. Additionally, the rocaglate family encompasses over 200 naturally and synthetically derived compounds but it is unknown if they operate through a shared mechanism. Lastly, it would be highly beneficial to conduct a structure-activity relationship investigation to better understand what chemical entities are able to improve compound efficacy.

CHAPTER 2 TRANSLATION INHIBITION BY ROCAGLATES IS INDEPENDENT OF EIF4E PHOSPHORYLATION STATUS

Published in:

Chu J., Cencic R., Wang W., Porco J. A. Jr., and Pelletier J. (2016). Translation Inhibition by Rocaglates is Independent of eIF4E Phosphorylation Status. *Mol. Cancer. Ther.* **15(1):** 136-141.

2.1 Preface to Chapter 2

Early biochemical characterization of silvestrol and other naturally occurring rocaglates heavily implicate eIF4A as the mechanistic target for their ability to inhibit translation initiation. While mechanisms of initiation that rely on eIF4A activity (such as cap-dependent initiation or the EMCV IRES) are highly sensitive to the presence of rocaglates, IRESes that do not utilize eIF4A (e.g. CrPV or HCV IRESes) do not respond. Furthermore, *in vitro* assays demonstrate that eIF4A RNA binding and helicase activities are enhanced in the presence of rocaglates; although it is not clear why stimulation of activity would lead to inhibited protein synthesis, this provides evidence that these compounds interact with eIF4A and alters its enzymatic properties.

However, an alternative model suggests that rocaglates inhibit protein synthesis and cell viability by targeting MAPK signalling (Bleumink et al., 2011). It had been observed that rocaglates bind to prohibitin (PHB) 1 and 2, which are reported to interact with c-Raf and stimulate the MAPK pathway (Polier et al., 2012). Because eIF4E phosphorylation is regulated by this signalling cascade, it is inferred that rocaglates reduce levels of phosphorylated eIF4E and in doing so, inhibit protein synthesis. Accordingly, rocaglate exposure has been shown to induce decreased MAPK activity in cells but strangely enough, the eIF4E phosphorylation levels have not been directly evaluated. In this chapter, we assessed whether decreased eIF4E phosphorylation plays a significant role in rocaglate-mediated inhibition of translation and cellular viability. Overall, our results resoundingly contradict this model as we reveal that eIF4E phosphorylation levels do not decrease upon acute rocaglate exposure. In support of this, the response of MNK1/2 knockout MEFs towards rocaglates was also found to be very similar to wildtype MEFs.

2.2 Abstract

Rocaglates are natural products that inhibit protein synthesis in eukaryotes and exhibit anti-neoplastic activity. *In vitro* biochemical assays, affinity chromatography experiments coupled with mass spectrometry analysis, and *in vivo* genetic screens have identified eukaryotic initiation factor (eIF) 4A as a direct molecular target of rocaglates. eIF4A is the RNA helicase subunit of eIF4F, a complex which mediates cap-dependent ribosome recruitment to mRNA templates. The eIF4F complex has been implicated in tumor initiation and maintenance through elevated levels or increased phosphorylation status of its cap-binding subunit, eIF4E, thus furthering the interest towards developing rocaglates as anti-neoplastic agents. Recent experiments have indicated that rocaglates also interact with prohibitins (PHB) 1 and 2; proteins implicated in c-Raf-MEK-ERK signaling. Since increased ERK signaling stimulates eIF4E phosphorylation status, rocaglates are also expected to inhibit eIF4E phosphorylation status, a point that has not been thoroughly investigated. It is currently unknown whether the effects on translation observed with rocaglates are solely through eIF4A inhibition or also a feature of blocking eIF4E phosphorylation. Here, we show that rocaglates inhibit translation through an eIF4E-phophorylation independent mechanism.

2.3 Introduction

Rocaglates are a family of natural products characterized by a common cyclopenta[*b*]furan skeleton that are exclusively found in the *Aglaia* genus of the Meliaceae family of angiosperms (Ebada et al., 2011). Many members of this family are potent inhibitors of translation initiation and exhibit both single agent anti-neoplastic activity in pre-clinical cell and mouse models (Alachkar et al., 2013; Cencic et al., 2009; Lucas et al., 2009) as well as the ability to modulate chemo-responsiveness

(Bordeleau et al., 2008; Chu and Pelletier, 2014; Giaisi et al., 2012; Robert et al., 2014; Rodrigo et al., 2012). A significant body of evidence indicates that these compounds inhibit translation initiation by disabling eIF4F activity and interfering with ribosome recruitment to mRNA templates (Bordeleau et al., 2008; Cencic et al., 2009; Rodrigo et al., 2012).

eIF4F is a hetero-trimeric complex consisting of eIF4E, a cap-binding protein; eIF4A, the RNA helicase target of rocaglates; and eIF4G, a large scaffolding protein. eIF4F is required to unwind cap-proximal secondary structure within the mRNA 5' untranslated region (UTR) as a prelude to 43S pre-initiation complex recruitment. Of all the initiation factors, eIF4E is the least abundant (Duncan and Hershey, 1983; Galicia-Vazquez et al., 2012) and mRNAs must compete for the limiting amounts of eIF4F during the initiation process. A determinant of competitive efficiency is the presence of structural barriers (e.g. stem-loop structures, protein-RNA interactions) within the mRNA 5' UTR, with elevated levels associated with poorly initiating mRNAs. Consequently, translation of these weaker mRNAs is most affected upon inhibition of eIF4F, and hence by rocaglates (Cencic et al., 2009; Liu et al., 2012; Rubio et al., 2014; Wolfe et al., 2014).

eIF4A is an abundant factor that exists as a free form ($eIF4A_f$) or as part of the eIF4F complex ($eIF4A_c$). Biochemical assays using recombinant eIF4A (Bordeleau et al., 2008; Cencic et al., 2009; Rodrigo et al., 2012), affinity chromatography experiments using immobilized epi-silvestrol (Chambers et al., 2013), and chemogenomic profiling in yeast (Sadlish et al., 2013) have identified eIF4A as a predominant target of rocaglates. Rocaglates are thought to deplete eIF4F of its eIF4A subunit by increasing RNA binding of eIF4A, thus restricting efficient recycling of eIF4A through the eIF4F complex (Figure 2.1A) (Chu and Pelletier, 2014).

An alternative mechanism of action of rocaglates on translation initiation has been proposed based on their interactions with prohibitins (PHB) 1 and 2 (Polier et al., 2012). PHB1/2 are involved in a wide variety of cellular processes, including activation of the MAPK signaling cascade through direct interaction with c-RAF (Rajalingam et al., 2005). In the presence of rocaglates, the PHB1/2:c-RAF interaction is inhibited, leading to dampened signaling to MEK and ERK 1/2 (Polier et al., 2012). Since MNKs phosphorylate eIF4E on S209 and are activated by ERK signaling, rocaglates are therefore expected to inhibit eIF4E S209 phosphorylation, although this has yet to be assessed. If correct, this mechanism of action would have profound consequences on our understanding of the anti-neoplastic effects of these compounds since eIF4E phosphorylation is essential to its oncogenic activity (Topisirovic et al., 2004; Wendel et al., 2007). As well, transcriptome wide studies attributing changings in mRNA translational efficiency to inhibition of eIF4A by rocaglates would have to be re-interpreted if inhibition of eIF4E phosphorylation was a significant biological property of rocaglates (Rubio et al., 2014; Wolfe et al., 2014).

However, there are several lines of evidence inconsistent with inhibition of eIF4E phosphorylation contributing to the biological activity of rocaglates. Firstly, rocaglates are potent inhibitors of eIF4A-dependent translation *in vitro* where Ras/MEK/ERK signaling is not maintained (Bordeleau et al., 2008). Secondly, rocaglates have been shown to inhibit encephalomyocarditis (EMC) IRES-driven translation (Bordeleau et al., 2008), an event that is eIF4A, but not eIF4E, dependent (Pestova et al., 1996). Thirdly, rocaglates are potent inhibitors of cap-dependent translation (Bordeleau et al., 2008; Cencic et al., 2009), whereas loss of eIF4E S209 phosphorylation leads to more subtle dampening of select mRNA translation (Furic et al., 2010; Robichaud et al., 2014; Ueda et al., 2010; Wendel et al., 2007). It therefore remains an open question as to whether the reported

suppression of Ras/MEK/ERK signaling by rocaglates represents a primary mechanism of action of these compounds. Herein, we report that the biological activity of rocaglates cannot be explained by modulation of eIF4E phosphorylation.

2.4 Results

Our previous work investigating the consequences of silvestrol (Bordeleau et al., 2008; Cencic et al., 2009), CR-1-31-B [a.k.a. hydroxamate (-)-9] (Rodrigo et al., 2012) and SDS-1-021-(-) (RC., unpublished data) (Figure 2.1B) on translation indicate that these compounds target eIF4A and prevent its entry/recycling into the eIF4F complex (Figure 2.1A). Li-Weber and colleagues (Polier et al., 2012) have reported that rocaglates, such as RocA (Figure 2.1B) can also inhibit PHB1/2 to downregulate ERK activation, although the downstream effects on eIF4E S209 phosphorylation was never reported. We therefore decided to investigate this potential relationship and also took the opportunity to prepare enantio-enriched preparations of RocA to tease out possible biological differences between the stereoisomers (Figure 2.1B).

To assess the relative potencies of the rocaglate series in hand on translation (Figure 2.1B), we performed a series of titrations in NIH/3T3 and Jurkat cells. In Jurkat cells, SDS-1-021-(-) was the most potent rocaglate (IC_{50} < 10 nM) followed by RocA-(-) and CR-1-31-B (Figure 1C). In NIH/3T3 cells, SDS-1-021-(-) and CR-1-31-B showed similar potencies, with IC_{50}'s ~20 nM for translation inhibition under our test conditions (Figure 2.1C). Silvestrol and RocA-(-) were slightly less potent with IC_{50}'s of ~50 nM. RocA-(+) was unable to inhibit translation in both cell lines highlighting the importance of compound stereochemistry for biological activity, as previously noted (Rodrigo et al., 2012). In sum, these results indicate that individual rocaglates exert differences in their ability to

inhibit translation across cell lines, as previously reported (Bordeleau et al., 2008; Rodrigo et al., 2012), but that within this small tested series, SDS-1-021-(-) is the more potent inhibitor.

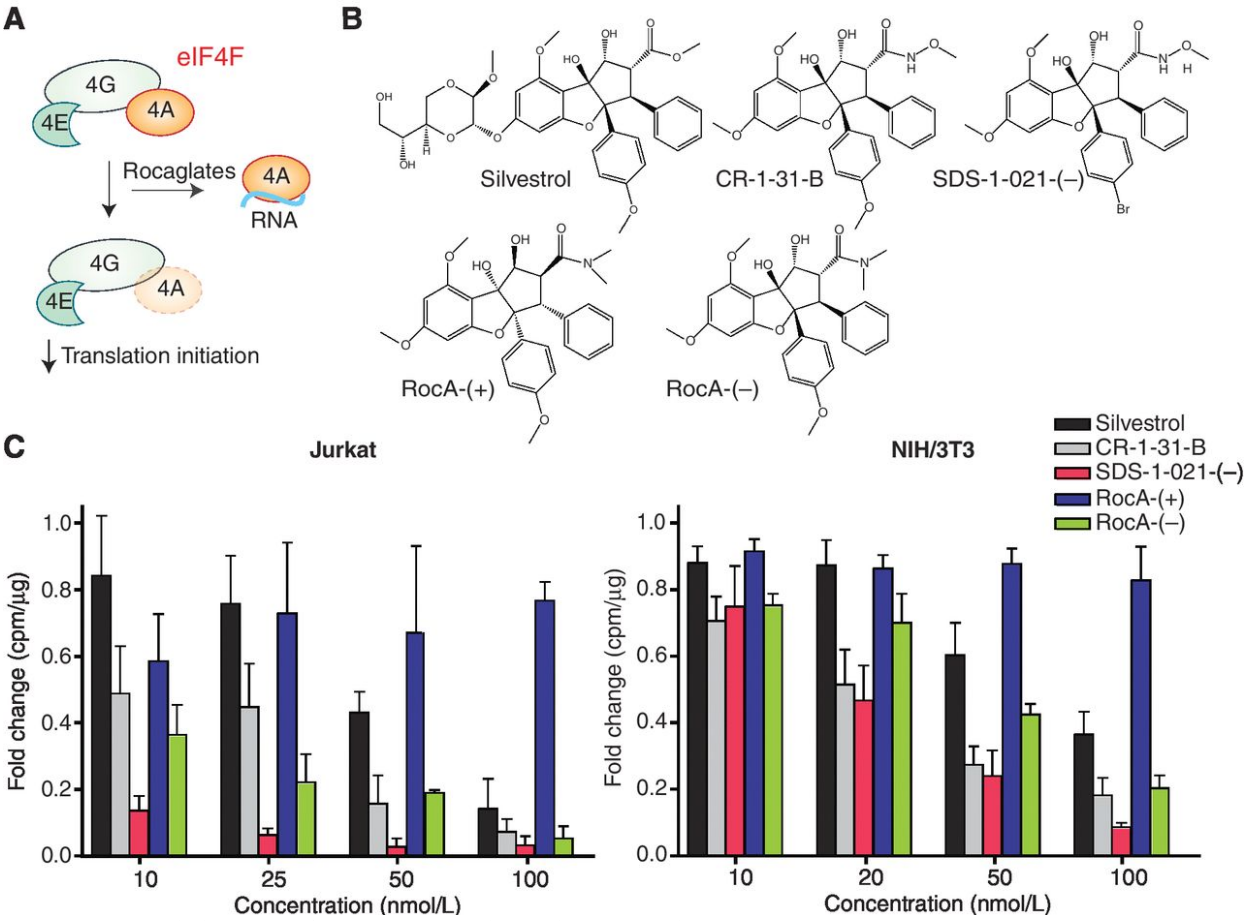

Figure 2.1 Inhibition of Protein Synthesis by Rocaglates

(A) Proposed mechanism of action of rocaglates on eIF4A recycling through the eIF4F complex. In this model, rocaglates stimulate eIF4A RNA binding, rendering it unavailable to enter into the eIF4F complex.

(B) Structures of rocaglates used in this study.

(C) Dose-dependent inhibition of translation by rocaglates in Jurkat and NIH/3T3 cells. Cells were incubated in the presence of compound for a total of 2 hours and protein synthesis rates were determined as described in the Materials and Methods. The relative rates are of translation are calculated by normalizing to DMSO. n = 4; error bars represent the error of the mean.

RocA has been shown to inhibit ERK 1/2 phosphorylation in Jurkat cells (Polier et al., 2012), although its effects on eIF4E phosphorylation have never been reported. We found that, with the exception of RocA-(+), all other rocaglates suppressed ERK 1/2 phosphorylation in Jurkat cells (Figure 2.2A). Silvestrol, CR-1-31-B, and SDS-1-021-(-) completely blocked phosphorylation whereas modest inhibition was observed at 100 nM RocA-(-) (Figure 2.2A). Surprisingly, eIF4E phosphorylation was not inhibited and, contrary to expectation, was stimulated by CR-1-31-B and SDS-1-021. In contrast, in NIH/3T3 cells we observed stimulation, not inhibition, of ERK 1/2 phosphorylation by all rocaglates tested, with the exception of the inactive RocA-(+) enantiomer, compared to vehicle-treated cells (Figure 2.2B). None of the tested rocaglates affected phospho-eIF4E status in NIH/3T3 cells under the tested conditions. These results indicate little correlation between eIF4E phosphorylation status, and the inhibition of translation documented above (Figure 2.1C). One well-characterized activity of rocaglates is stimulation of eIF4A RNA-binding activity in a sequence-independent manner (Bordeleau et al., 2008; Cencic et al., 2009; Rodrigo et al., 2012). To assess whether the rocaglate series under evaluation retained this activity, we performed RNA filter binding assays in vitro using 32P-labeled RNA in the presence of 5 μmol/L of each compound, which is within the concentration range of silvestrol previously shown to stimulate RNA binding of eIF4A ((Cencic et al., 2009); Figure 2.2D). With the exception of the inactive RocA-(+) enantiomer, all rocaglates stimulated binding of eIF4A to RNA, with SDS-1-021-(-) being the most potent compound (Figure 2.2D).

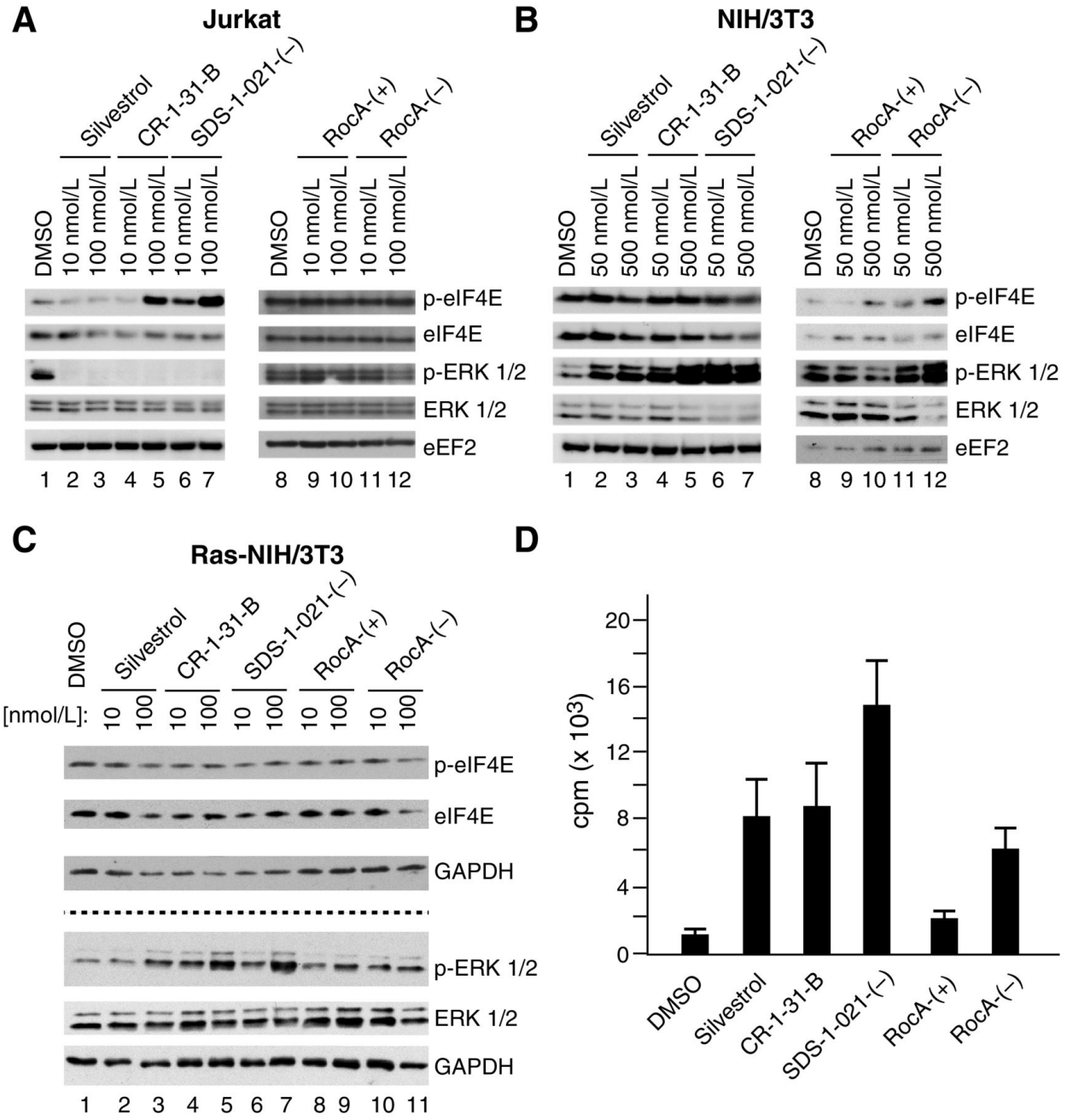

Figure 2.2 Effects of Rocaglates on MAPK Signalling

(A) Effects of rocaglates on eIF4E phosphorylation in Jurkat cells. Cells were incubated in the presence of the indicated compounds for 2 hours, lysed, fractionated on a 10% NuPAGE Bis-Tris gel, and transferred to PVDF membranes for western blotting. Blots were probed using antibodies directed to the proteins indicated to the right of the panel.

(B) Effects of rocaglates on eIF4E phosphorylation status in NIH/3T3 cells. Cells were treated, proteins fractionated, transferred to PVDF membranes, and western blots analyzed as described for Panel A.

(C) Effects of rocaglates on eIF4E phosphorylation status in RAS-transformed NIH/3T3 cells. Cells were treated, proteins fractionated, transferred to PVDF membranes, and western blots analyzed as

described for Panel A. The dashed line indicates that probing for eIF4E and ERK were performed on different membranes. GAPDH levels were used as an internal standard to account for variations in extract levels between lanes.
(D) Stimulation of eIF4A:RNA binding by rocaglates. Recombinant eIF4A (1.3 μM) was incubated with 35 000 cpm of 32P-labelled RNA in the presence of 5 μM rocaglate and processed as described in the Materials and Methods. eIF4A:RNA complexes retained on nitrocellulose filters were quantitated by scintillation counting. N = 3; error bars represent error of the mean.

To further support the notion that eIF4E phosphorylation status is inconsequential to the inhibition of translation observed with rocaglates, we quantitated the effects of rocaglates on protein synthesis in MEFS lacking the two eIF4E kinases, Mnk1 and Mnk2 (Figure 2.3A). Whereas we observed a slight difference in the sensitivities between $Mnk1^{-/-}Mnk2^{-/-}$ and $Mnk1^{+/+}Mnk2^{+/+}$ MEFs (~40%) towards silvestrol, there was no significant difference on translation exerted by the other tested rocaglates in these two cell types (Figure 2.3A). Consistent with our results in Jurkat and NIH/3T3 cells, SDS-1-021-(–) was the most potent inhibitor among the series tested (Figure 2.3A). Western blots of extracts confirmed the complete absence of eIF4E phosphorylation in the $Mnk1^{-/-}Mnk2^{-/-}$ MEFs as well as the absence of diminished eIF4E phosphorylation in $Mnk1^{+/+}Mnk2^{+/+}$ MEFs (Figure 2.3B). As a positive control, we included the Mnk1 inhibitor, CGP57380, and observed reduced phospho-eIF4E levels in $Mnk1^{+/+}Mnk2^{+/+}$ MEFs (Figure 2.3B) (Tschopp et al., 2000).

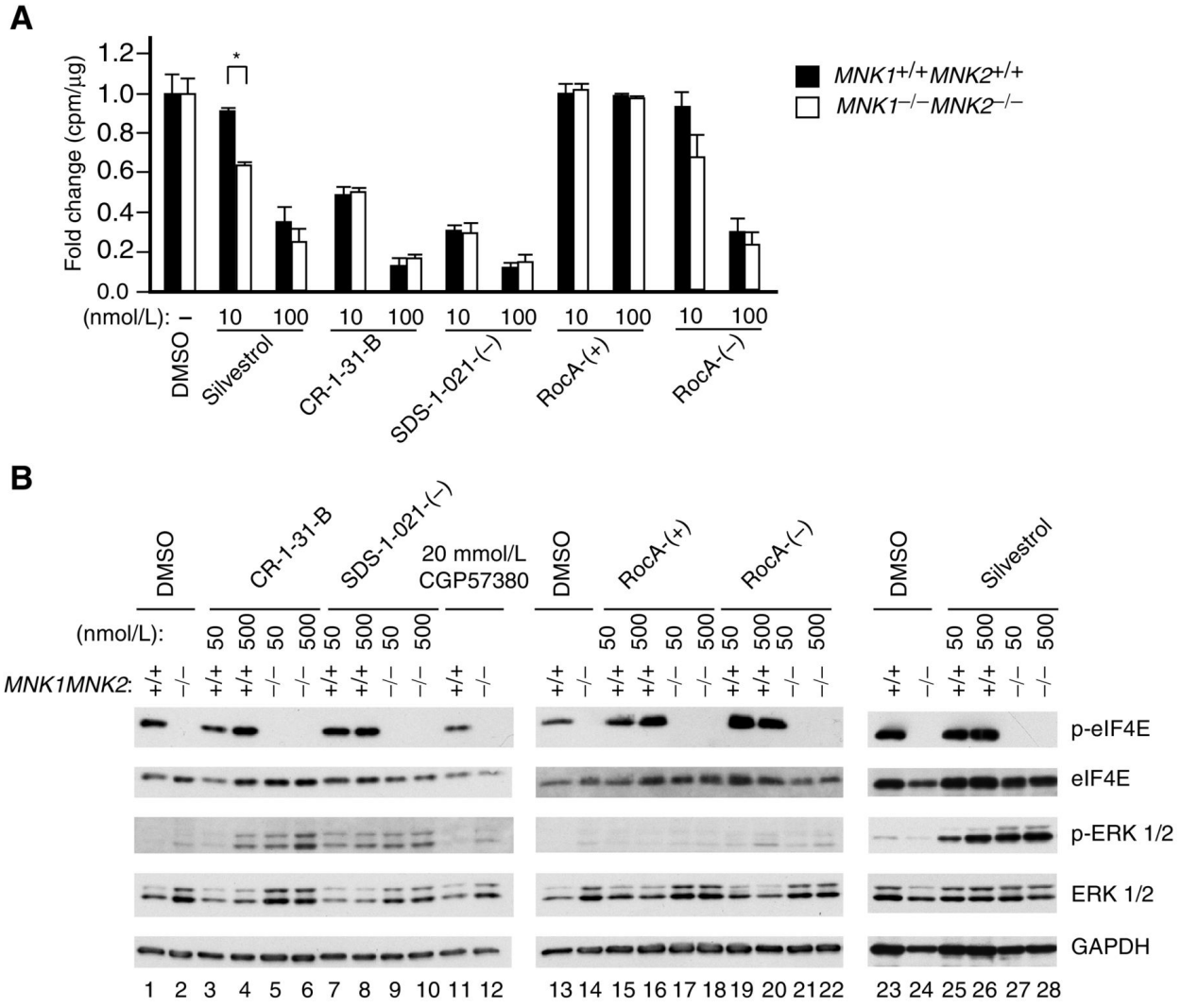

Figure 2.3 Sensitivity of MNK1$^{-/-}$MNK2$^{-/-}$ MEFs towards Rocaglates

(A) Rocaglates inhibit translation in MNK1$^{+/+}$MNK2$^{+/+}$ and MNK1$^{-/-}$MNK2$^{-/-}$ MEFs. Protein synthesis rates were determined as described in Materials and Methods. The relative rates of 35S-Met incorporation are normalized to DMSO. n = 4; error bars, error of the mean. *, P < 0.001 (Student t test).

(B) Effects of rocaglates on eIF4E phosphorylation in MNK1$^{+/+}$MNK2$^{+/+}$ and MNK1$^{-/-}$MNK2$^{-/-}$ cells. Cells were incubated in the presence of the indicated compounds for 2 hours, lysed, resolved on a 10% polyacrylamide gel, and transferred to PVDF membranes for Western blotting. Blots were probed with antibodies directed to the proteins indicated to the right of the panel. GAPDH levels were used as an internal standard to account for variations in extract levels between lanes. Note that lane 24 is slightly underloaded based on the GAPDH internal standard.

2.5 Discussion

In this study, we report that translation inhibition by rocaglates is independent of eIF4E phosphorylation status. Although we have not directly tested the ability of our rocaglate series to inhibit PHB1/2:c-RAF association, RocA has been previously shown to block this interaction (Polier et al., 2012). We find that the effects of rocaglates on p-ERK 1/2 and p-eIF4E status appear cell-type dependent and overall do not correlate with rocaglate-induced translation inhibition (Figure 2.2). It is clear that in the complete absence of eIF4E phosphorylation, the ability of CR-1-31-B, SDS-1-021-(–), and RocA-(–) to inhibit protein synthesis is unperturbed (Figure 2.3). Silvestrol, but not CR-1-31-B, is a known Pgp-1 multi-drug transporter substrate (Cencic et al., 2013). Whether the increased sensitivity of $Mnk1^{-/-}Mnk2^{-/-}$ cells to silvestrol is due to reduced expression of Pgp-1 and/or other drug response modifiers remains to be evaluated (Figure 2.3A).

As reported by Li-Weber and colleagues (Polier et al., 2012), we also find that rocaglates inhibit ERK 1/2 phosphorylation in Jurkat cells (Figure 2.2A). However, in NIH/3T3 cells we observed stimulation, not inhibition, of this post-translational modification (Figure 2.2B, C). The increase in p-eIF4E that we observed with the more potent SDS-1-021-(–) and CR-1-31-B compounds in Jurkat cells is unlinked to p-ERK 1/2 status and may reflect activation of a stress kinase response—an effect that has been previously documented with other translation inhibitors including anisomycin, onnamide A, and theopederin B (Lee et al., 2005; Wang et al., 1998). This increase in p-eIF4E levels is contrary to what would be expected upon ERK 1/2 inhibition, which one would expect to stimulate, not inhibit, selective mRNA translation (Furic et al., 2010; Robichaud et al., 2014; Ueda et al., 2010; Wendel et al., 2007).

Our results do not rule out the possibility that some rocaglate family members not tested here can block eIF4E phosphorylation given the appropriate context. Indeed, the compound RocAR has been reported to exhibit this activity in HTLV-infected ATL (adult T-cell leukemia/lymphoma) cells (Bleumink et al., 2011). However, our data indicate that this is not a general feature of this class of compounds, and that rocaglate-induced translation inhibition is independent of eIF4E phosphorylation status. Taken together with previous data indicating that these compounds also do not inhibit translation by increasing eIF2α phosphorylation (Bordeleau et al., 2008), the consequences of rocaglates on translation appear best explained by their effects on eIF4A activity.

2.6 Materials and Methods

2.6.1 General Methods and Reagents.

Jurkat, NIH/3T3, and MNK1$^{+/+}$MNK2$^{+/+}$ and MNK1$^{-/-}$MNK2$^{-/-}$ MEFs were grown in RPMI 1640 and DMEM, respectively, supplemented with 10% FBS and 100 U/ml penicillin/streptomycin at 37°C and 5% CO_2. Cell extracts were prepared in lysis buffer (20 mM $HEPES_{7.5}$, 150 mM NaCl, 1% Triton-X100, 10% glycerol, 1 mM EDTA, 10 mM tetrasodium pyrophosphate, 100 mM NaF, 17.5 mM β-glycerophosphate, 1mM PMSF, 4 μg/ml aprotinin, 2 μg/ml leupeptin, 2 μg/ml pepstatin). Extracts from Jurkat cells were prepared by lysing cells in 1X NuPAGE LDS sample buffer (26.5 mM Tris $HCl_{8.5}$, 35.25 mM Tris Base, 0.5% LDS, 2.5 % Glycerol, 0.1275 mM EDTA). Protein samples were fractionated on 10% polyacrylamide gels and transferred to PVDF membranes (Bio-Rad). Antibodies used in this study were directed against: p-eIF4E (Ser209) (#9741, Cell Signaling), eIF4E (#9742, Cell Signaling), p-Erk 1/2 (#9106, Cell Signaling), Erk 1/2 (#9102, Cell Signaling), eEF2 (#2332, Cell Signaling), and GAPDH (ab8245, Abcam). ^{35}S-methionine/cysteine protein labeling was

performed as previously described (Galicia-Vazquez et al., 2012). SDS-1-021-(-), RocA-(-), and RocA-(+) were synthesized using biomimetic kinetic resolution of chiral, racemic aglain ketone precursors according to our recent protocol (Stone et al., 2015) followed by amide formation (Gerard et al., 2006). Silvestrol and CR-1-31-B were synthesized as previously reported (Gerard et al., 2007; Rodrigo et al., 2012).

2.6.2 Cell Labeling and TCA Precipitations.

The day prior to metabolic labeling, Jurkat cells were seeded at 500,000 cells/ml and NIH/3T3, $MNK1^{+/+}MNK2^{+/+}$, and $MNK1^{-/-}MNK2^{-/-}$ MEF were seeded at 250 cells/mm^2. On the day of labeling, cells were exposed to the indicated concentrations of rocaglates for 2 hours. During the last 30 minutes of incubation, [^{35}S]-methionine/cysteine was added (150-200 μCi/ml; 1175 Ci/mmole) (Perkin Elmer, Waltham, MA). Levels of [^{35}S]-methionine/cysteine incorporation into protein were determined by TCA precipitation and quantitated by scintillation counting (Beckman Coulter). Radioactive counts were standardized to total protein content as determined by DC protein assay (Bio-Rad).

2.6.3 RNA Binding assay.

Body-labelled [^{32}P]-labeled RNA was produced by *in vitro* transcription of pSP/CAT (linearized with *Pvu*II) using SP6 RNA polymerase. Recombinant eIF4A was purified as previously reported (Cencic et al., 2012). Binding assays were performed by incubating [^{32}P]-labeled RNA (35000 cpm) with recombinant eIF4AI in binding buffer (25 mM $Tris_{7.5}$ 1 mM DTT, 100 mM KCl, 1 mM ATP, 5 mM $MgCl_2$) for 10 minutes at 37 °C. Reactions were terminated by the addition of 1 mL stop buffer (25 mM $Tris_{7.5}$, 100 mM KCl, 3 mM $MgCl_2$) and then passed through a nitrocellulose filter (45 μM HA Millipore) (preblocked with 0.1% sodium pyrophosphate). Filters were washed 3 times with 1

mL stop buffer, dried, and the amount of retained [^{32}P]-labeled RNA quantitated by liquid scintillation counting.

2.7 Acknowledgments

This work was supported by grants from the Canadian Institutes of Health Research to JP (MOP-106530) and the National Institutes of Health (R01 GM073855 to J.A.P., Jr.). Research at the Center for Chemical Methodology and Library Development at Boston University (CMLD-BU) was supported by NIH grant GM-067041.

2.8 References

1. Ebada SS, Lajkiewicz N, Porco JA, Jr., Li-Weber M, Proksch P. Chemistry and biology of rocaglamides (= flavaglines) and related derivatives from aglaia species (meliaceae). Prog Chem Org Nat Prod 2011; 94:1-58.
2. Cencic R, Carrier M, Galicia-Vazquez G, Bordeleau ME, Sukarieh R, Bourdeau A, Brem B, Teodoro JG, Greger H, Tremblay ML, et al. Antitumor activity and mechanism of action of the cyclopenta[b]benzofuran, silvestrol. PLoS One 2009; 4:e5223.
3. Lucas DM, Edwards RB, Lozanski G, West DA, Shin JD, Vargo MA, Davis ME, Rozewski DM, Johnson AJ, Su BN, et al. The novel plant-derived agent silvestrol has B-cell selective activity in chronic lymphocytic leukemia and acute lymphoblastic leukemia in vitro and in vivo. Blood 2009; 113:4656-66.
4. Alachkar H, Santhanam R, Harb JG, Lucas DM, Oaks JJ, Hickey CJ, Pan L, Kinghorn AD, Caligiuri MA, Perrotti D, et al. Silvestrol exhibits significant in vivo and in vitro antileukemic activities and inhibits FLT3 and miR-155 expressions in acute myeloid leukemia. Journal of hematology & oncology 2013; 6:21.
5. Bordeleau ME, Robert F, Gerard B, Lindqvist L, Chen SM, Wendel HG, Brem B, Greger H, Lowe SW, Porco JA, Jr., et al. Therapeutic suppression of translation initiation modulates chemosensitivity in a mouse lymphoma model. J Clin Invest 2008; 118:2651-60.
6. Robert F, Roman W, Bramoulle A, Fellmann C, Roulston A, Shustik C, Porco JA, Jr., Shore GC, Sebag M, Pelletier J. Translation initiation factor eIF4F modifies the dexamethasone response in multiple myeloma. Proc Natl Acad Sci U S A 2014; 111:13421-6.
7. Giaisi M, Kohler R, Fulda S, Krammer PH, Li-Weber M. Rocaglamide and a XIAP inhibitor cooperatively sensitize TRAIL-mediated apoptosis in Hodgkin's lymphomas. Int J Cancer 2012; 131:1003-8.

8. Chu J, Pelletier J. Targeting the eIF4A RNA helicase as an anti-neoplastic approach. Biochim Biophys Acta 2014.
9. Rodrigo CM, Cencic R, Roche SP, Pelletier J, Porco JA. Synthesis of rocaglamide hydroxamates and related compounds as eukaryotic translation inhibitors: synthetic and biological studies. J Med Chem 2012; 55:558-62.
10. Duncan R, Hershey JW. Identification and quantitation of levels of protein synthesis initiation factors in crude HeLa cell lysates by two-dimensional polyacrylamide gel electrophoresis. J Biol Chem 1983; 258:7228-35.
11. Galicia-Vazquez G, Cencic R, Robert F, Agenor AQ, Pelletier J. A cellular response linking eIF4AI activity to eIF4AII transcription. RNA 2012; 18:1373-84.
12. Wolfe AL, Singh K, Zhong Y, Drewe P, Rajasekhar VK, Sanghvi VR, Mavrakis KJ, Jiang M, Roderick JE, Van der Meulen J, et al. RNA G-quadruplexes cause eIF4A-dependent oncogene translation in cancer. Nature 2014; 513:65-70.
13. Rubio CA, Weisburd B, Holderfield M, Arias C, Fang E, DeRisi JL, Fanidi A. Transcriptome-wide characterization of the eIF4A signature highlights plasticity in translation regulation. Genome Biol 2014; 15:476.
14. Liu T, Nair SJ, Lescarbeau A, Belani J, Peluso S, Conley J, Tillotson B, O'Hearn P, Smith S, Slocum K, et al. Synthetic silvestrol analogues as potent and selective protein synthesis inhibitors. J Med Chem 2012; 55:8859-78.
15. Chambers JM, Lindqvist LM, Webb A, Huang DC, Savage GP, Rizzacasa MA. Synthesis of biotinylated episilvestrol: highly selective targeting of the translation factors eIF4AI/II. Org Lett 2013; 15:1406-9.
16. Sadlish H, Galicia-Vazquez G, Paris CG, Aust T, Bhullar B, Chang L, Helliwell SB, Hoepfner D, Knapp B, Riedl R, et al. Evidence for a functionally relevant rocaglamide binding site on the eIF4A-RNA complex. ACS Chem Biol 2013; 8:1519-27.
17. Polier G, Neumann J, Thuaud F, Ribeiro N, Gelhaus C, Schmidt H, Giaisi M, Kohler R, Muller WW, Proksch P, et al. The natural anticancer compounds rocaglamides inhibit the Raf-MEK-ERK pathway by targeting prohibitin 1 and 2. Chemistry & biology 2012; 19:1093-104.
18. Rajalingam K, Wunder C, Brinkmann V, Churin Y, Hekman M, Sievers C, Rapp UR, Rudel T. Prohibitin is required for Ras-induced Raf-MEK-ERK activation and epithelial cell migration. Nat Cell Biol 2005; 7:837-43.
19. Topisirovic I, Ruiz-Gutierrez M, Borden KL. Phosphorylation of the eukaryotic translation initiation factor eIF4E contributes to its transformation and mRNA transport activities. Cancer Res 2004; 64:8639-42.
20. Wendel HG, Silva RL, Malina A, Mills JR, Zhu H, Ueda T, Watanabe-Fukunaga R, Fukunaga R, Teruya-Feldstein J, Pelletier J, et al. Dissecting eIF4E action in tumorigenesis. Genes Dev 2007; 21:3232-7.
21. Pestova TV, Shatsky IN, Hellen CU. Functional dissection of eukaryotic initiation factor 4F: the 4A subunit and the central domain of the 4G subunit are sufficient to mediate internal entry of 43S preinitiation complexes. Mol Cell Biol 1996; 16:6870-8.
22. Furic L, Rong L, Larsson O, Koumakpayi IH, Yoshida K, Brueschke A, Petroulakis E, Robichaud N, Pollak M, Gaboury LA, et al. eIF4E phosphorylation promotes tumorigenesis and is associated with prostate cancer progression. Proc Natl Acad Sci U S A 2010; 107:14134-9.

23. Robichaud N, Del Rincon SV, Huor B, Alain T, Petruccelli LA, Hearnden J, Goncalves C, Grotegut S, Spruck CH, Furic L, et al. Phosphorylation of eIF4E promotes EMT and metastasis via translational control of SNAIL and MMP-3. Oncogene 2014.
24. Ueda T, Sasaki M, Elia AJ, Chio, II, Hamada K, Fukunaga R, Mak TW. Combined deficiency for MAP kinase-interacting kinase 1 and 2 (Mnk1 and Mnk2) delays tumor development. Proc Natl Acad Sci U S A 2010; 107:13984-90.
25. Ueda T, Watanabe-Fukunaga R, Fukuyama H, Nagata S, Fukunaga R. Mnk2 and Mnk1 Are Essential for Constitutive and Inducible Phosphorylation of Eukaryotic Initiation Factor 4E but Not for Cell Growth or Development. Mol Cell Biol 2004; 24:6539-49.
26. Wang X, Flynn A, Waskiewicz AJ, Webb BL, Vries RG, Baines IA, Cooper JA, Proud CG. The phosphorylation of eukaryotic initiation factor eIF4E in response to phorbol esters, cell stresses, and cytokines is mediated by distinct MAP kinase pathways. J Biol Chem 1998; 273:9373-7.
27. Lee KH, Nishimura S, Matsunaga S, Fusetani N, Horinouchi S, Yoshida M. Inhibition of protein synthesis and activation of stress-activated protein kinases by onnamide A and theopederin B, antitumor marine natural products. Cancer Sci 2005; 96:357-64.
28. Bleumink M, Kohler R, Giaisi M, Proksch P, Krammer PH, Li-Weber M. Rocaglamide breaks TRAIL resistance in HTLV-1-associated adult T-cell leukemia/lymphoma by translational suppression of c-FLIP expression. Cell Death Differ 2011; 18:362-70.
29. Stone SD, Lajkiewicz NJ, Whitesell L, Hilmy A, Porco JA, Jr. Biomimetic kinetic resolution: highly enantio- and diastereoselective transfer hydrogenation of aglain ketones to access flavagline natural products. J Am Chem Soc 2015; 137:525-30.
30. Gerard B, Sangji S, O'Leary DJ, Porco JA, Jr. Enantioselective photocycloaddition mediated by chiral Bronsted acids: asymmetric synthesis of the rocaglamides. J Am Chem Soc 2006; 128:7754-5.
31. Gerard B, Cencic R, Pelletier J, Porco JA, Jr. Enantioselective synthesis of the complex rocaglate (-)-silvestrol. Angew Chem Int Ed Engl 2007; 46:7831-4.
32. Cencic R, Galicia-Vazquez G, Pelletier J. Inhibitors of 511:437-61. translation targeting eukaryotic translation initiation factor 4A. Methods Enzymol 2012;

CHAPTER 3 CRISPR-MEDIATED DRUG-TARGET VALIDATION REVEALS SELECTIVE PHARMACOLOGICAL INHIBITION OF THE RNA HELICASE EIF4A

Published in:

Chu J., Galicia-Vázquez G., Cencic R., Mills J. R., Katigbak A., Porco J. A. Jr., and Pelletier J. (2016). CRISPR-Mediated Drug-Target-Validation Reveals Selective Pharmacological Inhibition of the RNA helicase eIF4A. *Cell Rep.* **15(11):** 2340-2347

3.1 Preface to Chapter 3

In Chapter 2, we demonstrate that rocaglate mechanism of action does not depend on perturbation of eIF4E phosphorylation, but the question of its cellular target remains. Having ruled out the MAPK signalling pathway, we next wanted to evaluate contribution of eIF4A to rocaglate-mediated cytotoxicity. Previously, a collaborative investigation conducted by our lab and Novartis identified mutations in the yeast homologs of eIF4A (TIF1 and TIF2) that were capable of conferring resistance to rocaglates (Sadlish et al., 2013). However, it remains to be seen whether these results also hold true within the mammalian setting. In this chapter, we address this question by first generating the equivalent mammalian eIF4A mutants and evaluating their activity in response to the rocaglate, silvestrol. The effects of these mutants on rocaglate-mediated cytotoxicity *in vivo* was then assessed by introducing these mutants into cells ectopically via retroviral transduction, or endogenously through CRISPR/Cas9 gene editing. Finally, using the CRISPR-modified cell lines harboring the rocaglate-resistant eIF4A mutant, we evaluated whether the diminished translation of the proto-oncogene c-Myc by rocaglates is indeed eIF4A dependent.

3.2 Abstract

Targeting translation initiation is an emerging anti-neoplastic strategy that capitalizes on de-regulated upstream MAPK and PI3K-mTOR signaling pathways in cancers. A key regulator of translation that controls ribosome recruitment flux is eukaryotic initiation factor (eIF) 4F, a hetero-trimeric complex composed of the cap binding protein, eIF4E; the scaffolding protein, eIF4G; and the RNA helicase, eIF4A. Small molecule inhibitors targeting eIF4F display promising anti-neoplastic activity in preclinical settings, among which are some rocaglate family members which are well-tolerated *in vivo*, deplete eIF4F of its eIF4A helicase subunit, have shown activity as single agents in several xenograft models, and can reverse acquired resistance to MAPK and PI3K-mTOR targeted therapies. Herein, we highlight the power of using genetic complementation approaches and CRISPR/Cas9-mediated editing for drug-target validation *ex vivo* and *in vivo* - linking the anti-tumor properties of rocaglates to eIF4A inhibition.

3.3 Introduction

Protein synthesis is a tightly controlled process that is deregulated in many human cancers and is required to sustain several cancer hallmarks (Bhat et al., 2015). In part, this is attributed to hyper-activation of the MAPK and PI3K-mTOR pathways, both of which impact on the activity of eukaryotic initiation factor (eIF) 4F. As well, resistance to targeted therapies aimed at inhibiting the PI3K-mTOR and MAPK signaling pathways in various cancers has been linked to elevated eIF4F activity (Bhat et al., 2015). Therefore, there is significant interest in developing eIF4F inhibitors as anti-neoplastic compounds (Bhat et al., 2015).

The eIF4F heterotrimeric complex binds to m^7GpppN mRNA cap structures through its eIF4E subunit, remodels proximal secondary structure via its eIF4A RNA helicase subunit, and recruits 40S ribosomes (with associated initiation factors) through its eIF4G subunit. The mammalian genome encodes two highly related (>90% identity) eIF4A isoforms, eIF4A1 and eIF4A2. These two isoforms were initially thought to be functionally redundant, but there is evidence suggesting they may also possess distinct biological properties (Galicia-Vazquez et al., 2012).

Strategies aimed at inhibiting eIF4F include blocking eIF4E:eIF4G and eIF4E-cap interaction, interfering with eIF4A1/2 activity, and suppressing eIF4E expression with antisense oligonucleotides (ASO) (Bhat et al., 2015). The development of eIF4E ASOs has provided proof-of-concept validation for targeting eIF4F in xenograft models, as well as generating safety data profiling from Phase I clinical trials (Graff et al., 2007; Hong et al., 2011). Transient inhibition of eIF4E (and hence eIF4F) is tolerated at the organismal level (Lin et al., 2012), despite its essential nature (Truitt et al., 2015). The most potent small molecule inhibitors of the eIF4F complex derive from a family of compounds referred to as rocaglates, which are characterized by a common cyclopenta[*b*]benzofuran skeleton. Extensive structure-activity relationship into the biological activity of these compounds has been obtained (Pan et al., 2014), with a few compounds capable of potently inhibiting translation (Bordeleau et al., 2008; Rodrigo et al., 2012).

Rocaglates decrease eIF4A1/2 levels present in the eIF4F complex (Bordeleau et al., 2008), exhibit anti-tumor activity in a number of pre-clinical models (Bordeleau et al., 2008; Cencic et al., 2009; Wolfe et al., 2014), and are thought to exert their effects by preferentially inhibiting the translation of key oncogenic mRNAs (e.g. MYC) (Cencic et al., 2009; Rubio et al., 2014; Wolfe et al., 2014). Chemogenomic profiling in yeast have identified the eIF4A orthologs, TIF1 and TIF2, as

targets of rocaglates (Sadlish et al., 2013). However, prohibitins (PHB) 1 and 2 have also been proposed as potential rocaglate targets in mammals (Polier et al., 2012). PHB1/2 are involved in a variety of processes, including activation of MAPK signaling (Rajalingam et al., 2005). Given the possibility of alternative targets (PHB1/2 or others), it is critical to validate the rocaglate - eIF4A1/2 drug target relationship *in vivo* since poor drug-target characterization is a frequent cause of drug development failures (Smurnyy et al., 2014). Here, we validate the rocaglate - eIF4A1 drug target relationship by identifying a drug-resistant and functional mammalian eIF4A1 allele that is capable of rescuing rocaglate anti-neoplastic activity upon introduction into cells either by genetic complementation or genome editing.

3.4 Results

3.4.1 eIF4A1 F163L is Unresponsive to Rocaglates in Vitro

We previously identified mutations in the yeast eIF4A orthologs, TIF1 and TIF2, that conferred resistance to rocaglates which mapped to the TIF-RNA interface (P147Q, F151L, and Q183E) (Sadlish et al., 2013). We sought to determine if analogous mutations in the mammalian setting (P159Q and F163L) could inform on the eIF4A:rocaglate relationship. P159Q and F163L map within, or adjacent of, the conserved TPGR Ib motif, which along with the PTRELA motif, is implicated in RNA binding (Figure 3.1A). Following purification of recombinant proteins (Figure 3.1B), we performed ATPase assays and noted that eIF4A1(F163L), but not eIF4A1(P159Q), retained robust ATPase activity (Figure 3.1C). The kinetics of ATP hydrolysis by eIF4A1(F163L) were similar to wild-type (wt) eIF4A and to published values (Figure 3.1D) (Lorsch and Herschlag, 1998). Since rocaglates increase the RNA binding of eIF4A and lead to its depletion from the eIF4F complex

(Bordeleau et al., 2008; Rodrigo et al., 2012), we monitored binding of eIF4A1 to ^{32}P-labelled RNA *in vitro.* Whereas silvestrol stimulated wt eIF4A1:RNA binding, eIF4A1(F163L):RNA complex formation was unaffected (Figure 3.1E). As well, eIF4A1(F163L) helicase activity was comparable to wt eIF4A1 but remained unaffected by silvestrol (Figure 3.1F).

Rocaglate resistance of eIF4A1(F163L) was also demonstrated using differential scanning fluorimetry (DSF) (Figure 3.1G). This approach monitors temperature-dependent protein unfolding with an increase in fluorescence arising from dye binding to newly exposed hydrophobic domains. Protein/ligand interactions are expected to promote protein stability, leading to a shift (increase) in denaturation temperature (Niesen et al., 2007). As this approach consumes large quantities of compounds, we used the related synthetic rocaglate (-)-SDS-1-021 instead of the scarcer natural product silvestrol (Figure S3.1a). In our hands, (-)-SDS-1-021 is more active than silvestrol with respect to stimulating eIF4A RNA binding activity (Chu et al., 2016a), inhibiting translation (Chu et al., 2016a), and affecting cell viability (Figure S3.1b). Only wt eIF4A1 showed a transition midpoint temperature shift of ~ +2-3 °C (Figure 3.1g), which is consistent with the ability of rocaglates to interact with eIF4A1, but not as robustly (if at all) with eIF4A1(F163L). Taken together, these experiments indicate that eIF4A1(F163L) ATPase activity and RNA binding are resistant to rocaglates *in vitro* while displaying V_{max} and K_m values for ATP hydrolysis that are similar to wt eIF4A1.

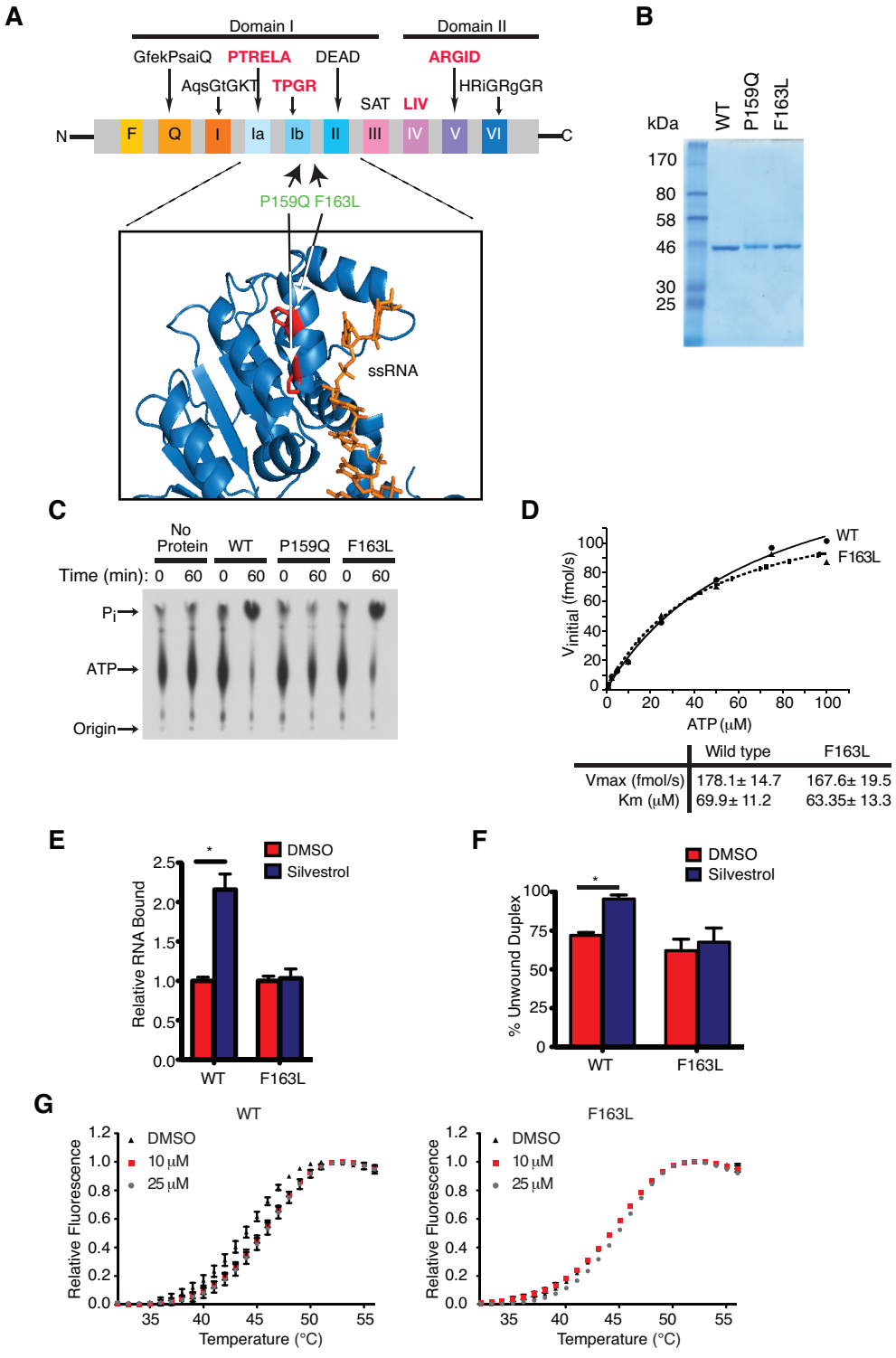

Figure 3.1 Response of eIF4A1(163L) to Silvestrol *In Vitro*

(A) Schematic illustrating conserved motifs of the DEAD-box helicase family. Sequences of the conserved motifs are denoted with motifs involved in RNA binding highlighted in bold red. The structure of eIF4A indicates it to be dumbbell in shape with two domains (I and II) linked via a flexible linker sequence. The inset shows a ribbon diagram of eIF4A1 (PDB 2ZU6) aligned to eIF4A3 (not

shown; PDB 2HYI). The residues targeted for mutagenesis are highlighted and the single-stranded RNA substrate (positioned relative to the eIF4A3 crystal structure) is shown in orange.
(B) Coomassie stain of purified recombinant eIF4A1 proteins.
(C) Assessment of ATP hydrolysis by recombinant proteins via thin layer chromatography.
(D) Kinetics of ATP hydrolysis by eIF4A1 and eIF4A1(F163L). ATPase assays were performed with 1 μg protein and varying ATP concentrations. Graph represents the Michaelis-Menten fit from two independent experiments.
(E) RNA binding activity of eIF4A1 and eIF4A1(F163L) using [32P]-labeled RNA generated from pSP/CAT (see Supplemental Experimental Procedures). Assays were performed in the presence of 0.5% DMSO or 1 μM silvestrol and the retained eIF4A:RNA complexes are set relative to DMSO controls. n = 3 biological replicates performed in triplicate ±SEM; $*p < 0.001$.
(F) Quantitation of eIF4A1 and eIF4A1(F163L) helicase activity performed with 0.5 μg recombinant eIF4A1 and an 11-nt radiolabeled RNA duplex in the presence of DMSO or 50 μM silvestrol. n = 3 biological replicates ±SEM; $*p < 0.05$.
(G) DSF analysis of eIF4A1 or eIF4A1(F163L) in the presence of DMSO or (–)-SDS-1-021

3.4.2 Introduction of eIF4A1(F163L) Confers Cellular Resistance to Silvestrol

To determine if eIF4A1(F163L) could complement for loss of wt eIF4A1 *in cellulo,* we engineered a retroviral complementation vector (RCV) that affords simultaneous shRNA-mediated suppression of endogenous eIF4A1 while co-expressing exogenous His-tagged eIF4A1 (Figure 3.2A). As previously reported, knockdown of eIF4A1 led to increased expression of eIF4A2 (Figure 3.2B) (Galicia-Vazquez et al., 2012). Ectopic expression of wt eIF4A1 or eIF4A1(F163L), but not the inactive eIF4A1(P159Q) mutant, rescued this response (Figure 3.2B). Cells expressing eIF4A1(F163L) showed resistance to silvestrol as assessed by monitoring cell viability (Figure 3.2C), growth competition assays (Figure 3.2D), ^{35}S-methionine metabolic labeling (Figure 3.2E), and polysome profiling (Figure 3.2F). The resistance phenotype observed upon ectopic expression of the eIF4A1(F163L) allele was not pleiotropic since these cells were still sensitive to the structurally unrelated eIF4A inhibitor, hippuristanol (Figs. S3.1A and S3.1C). Taken together, these results demonstrate that the eIF4A1(F163L) allele can functionally compensate for suppression of eIF4A1 and is sufficient to confer cellular resistance to silvestrol.

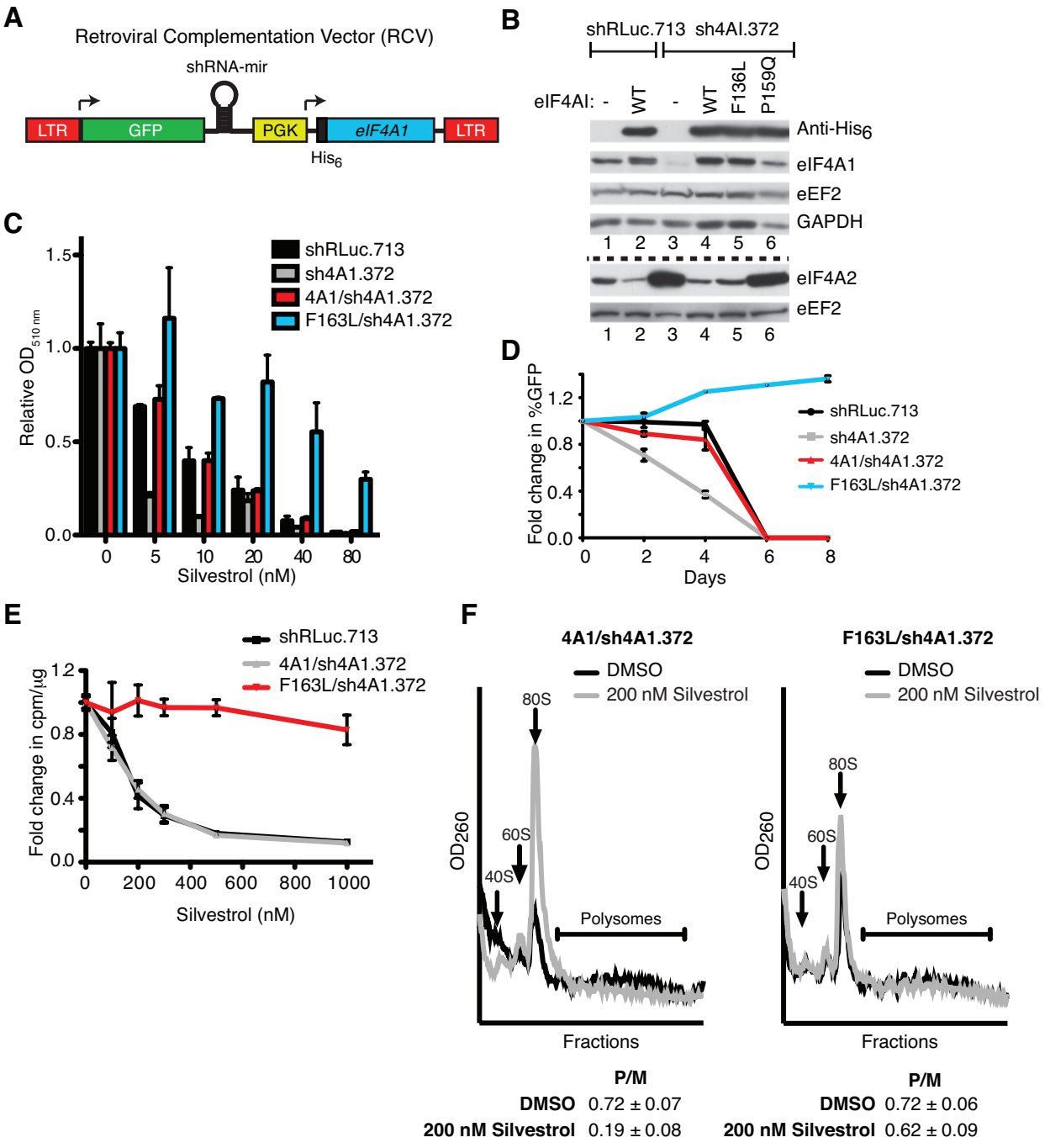

Figure 3.2 Ectopic Expression of eIF4A1(F163L) Confers Resistance to Rocaglates in Mammalian Cells

(A) Schematic diagram of RCV designed to simultaneously express an shRNA-resistant His_6-eIF4A1 allele while suppressing endogenous eIF4A1.

(B) Representative western blot NIH/3T3 cells transduced with RCVs. The dashed line separates the two sets of western blots.

(C) Viability assay of RCV-transduced NIH/3T3 cells. Cells were exposed to the indicated concentrations of silvestrol and relative viability was assessed 6 days later by Sulforhodamine B (SRB). n = 2 biological replicates performed in duplicates ±SEM.
(D) Competition assay of transduced NIH/3T3 cells. Transduced cells (GFP^+) were mixed with parental cells (GFP^-) and cultured in the presence of 20 nM silvestrol. The percentage of GFP^+ cells was determined on the indicated days. n = 2 biological replicates performed in triplicate ±SEM.
(E) Cells expressing eIF4A1(F163L) are resistant to translation inhibition by silvestrol. Transduced cells were incubated with the indicated concentrations of silvestrol for 1 hr and labeled with [^{35}S]-methionine/cysteine during the last 15 min. n = 4 biological replicates ±SEM.
(F) Polysome profiles of transduced NIH/3T3 cells following exposure to 200 nM silvestrol for 30 min. P/M represents the polysome/monosome ratio. n = 3 biological replicates ±SEM.
See also Figure S3.1

3.4.3 Cas9-Mediated Editing of the *Eif4a1* Locus Rescues Cells from the Inhibitory Effects of Rocaglates

To strengthen these results, we utilized CRISPR/Cas9 gene editing to introduce the F163L mutation into the endogenous *Eif4a1* locus. To this end, two sgRNAs were designed to target *Eif4a1* exon 5 and co-transfected with a single-stranded oligonucleotide (ssODN) donor template (Figure 3.3A). In addition to harboring the desired F163L change, two silent mutations were present in the ssODN that altered the PAMs to prevent re-cleavage (Figure 3.3A, indicated in red). Control cells received Cas9 and sgRNAs targeting the neutral Rosa26 locus (*Rosa26*^{em1JP}). Two cell populations, *eIF4A1*^{em1JP} and *eIF4A1*^{em2JP}, derived from sgRNA2 and sgRNA1 respectively, were characterized by sequencing exon 5 PCR products (Figure 3.3B). The results indicate that the *eIF4A1*^{em1JP} population contains *Eif4a1* alleles that harbor CTT or CTC codons encoding for leucine at position 163, whereas the *eIF4A1*^{em2JP} population also has *Eif4a1* alleles with deletions within exon 5 (Figs. 3.3B and S3.2A). No silvestrol-resistant colonies arose from *Rosa26* targeted cells and we did not detect mutant *Eif4a1* alleles in *Rosa26*^{em1JP} cells. The growth of *eIF4A1*^{em1JP} cells showed increased resistance (~10-fold) to silvestrol and (-)-SDS-1-021 (Figure S3.2B). To ensure that the observed resistance was not due to

off-target alterations by CRISPR/Cas9, we suppressed the mutated *Eif4a1* alleles in *eIF4A1*^{em1JP} and *eIF4A1*^{em2JP} using the RCV system (Figure 3.3C, D). Resensitization was monitored using ^{35}S-methionine/cysteine protein labeling. As expected *eIF4A1*^{em1JP} showed increased resistant (~10-20 fold) to silvestrol compared to control *Rosa26*^{em1JP} cells (Figure 3.3C). Importantly, suppressing endogenous eIF4A1(F163L) using sh4A1.372 and co-expressing wt eIF4A1 resensitized *eIF4A1*^{em1JP} cells to silvestrol (Figure 3.3C). Similar results were also obtained with *eIF4A1*^{em2JP} cells (Figure 3.3 C).

To assess whether eIF4A1(F163L) showed altered rocaglate binding *in cellulo*, we implemented a cellular thermal shift assay (CETSA) by measuring the thermal stability of wt eIF4A1 or eIF4A1(F163L) from *Rosa26*^{em1JP} and *eIF4A1*^{em1JP} cells, respectively that had been exposed to vehicle or (-)-SDS-1-021 (Figure 3.3E). In this assay, thermal stability is assessed by heating cells over a range of temperatures, followed by separation of insoluble (i.e., denatured/aggregated) from soluble proteins (Jafari et al., 2014). Levels of the protein of interest remaining in the soluble fractions are then determined by immunoblotting. Similar to DSF, CETSA is based on the principle that thermal stability of a protein is increased upon binding to a ligand (Jafari et al., 2014). For *Rosa26*^{em1JP} cells, wt eIF4A1 displayed a 2 °C increase in thermal stability when cells were exposed to (-)-SDS-1-021 (Figure 3.3E). For *eIF4A1*^{em1JP} cells, we observed no differences in the denaturation profile of eIF4A1(F163L), suggesting reduced target engagement for eIF4A1(F163L) (Figure 3.3E).

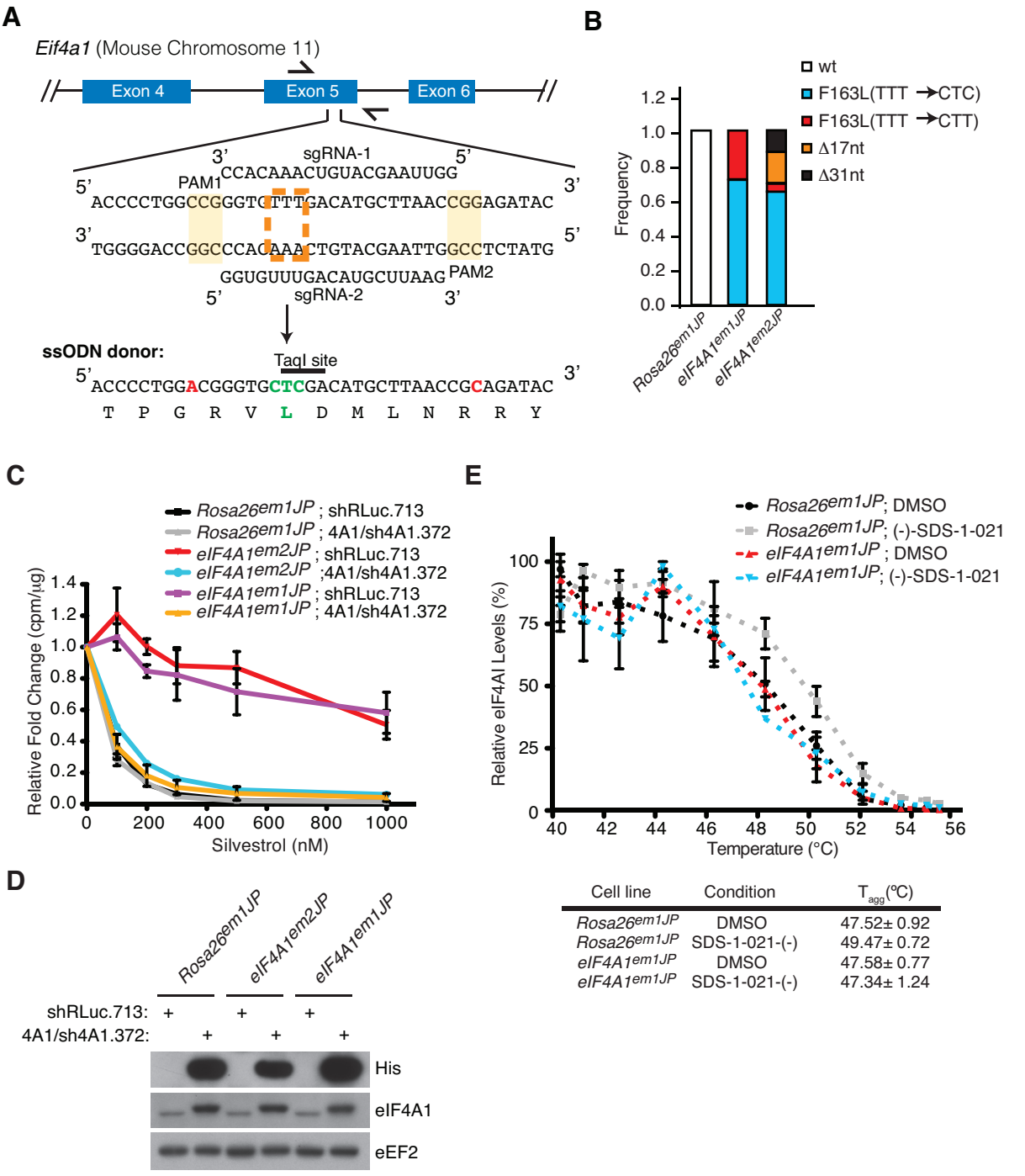

Cell line	Condition	T_{agg}(ºC)
Rosa26^{em1JP}	DMSO	47.52± 0.92
Rosa26^{em1JP}	SDS-1-021-(-)	49.47± 0.72
eIF4A1^{em1JP}	DMSO	47.58± 0.77
eIF4A1^{em1JP}	SDS-1-021-(-)	47.34± 1.24

Figure 3.3 Cas9-Mediated Editing of *Eif4a1*

(A) Strategy for introducing the *Eif4a1(F163L)* mutant allele. The sequence of two sgRNAs targeting exon 5 and the partial sequence of the ssODN donor are shown. The PAMs are shaded, and the nucleotide changes in the ssODN donor that abolishes their presence are indicated in red. The targeted TTT (F) codon is indicated by a dashed orange box, and engineered CTC (L) change in the ssODN donor is indicated in green.

(B) Sequence analysis the PCR products from *eIF4A1*^{em1JP} and *eIF4A1*^{em2JP} cells indicating loss of the wild-type *Eif4a1* allele and composition of mutant alleles.
(C) Relative translation rates in *Rosa26*^{em1JP}, *eIF4A1*^{em1JP}, *eIF4A1*^{em2JP} cells transduced with the indicated retroviruses.
(D) Western blot assessing His_6-eIF4A1 and total eIF4A1 in the cell lines used in (C).
(E) CETSA of *Rosa26*^{em1JP} and *eIF4A1*^{em1JP} cells. Cells were incubated with 1 μM (–)-SDS-1-021 or DMSO for 1 hr at 37°C and heated at the indicated temperatures for 3 min. Soluble lysates were prepared and used for western blotting. n = 4 biological replicates ±SEM. See also Figure S3.2

We next investigated the relationship between eIF4A1 status and the *in vivo* anti-neoplastic activity of rocaglates. To this end, *Rosa26*^{em1JP} and *eIF4A1*^{em1JP} cells were transduced with a retrovirus expressing Myr-Akt and single clones from these populations were isolated (referred to as *Rosa26*^{em1JP}(Myr-Akt), *eIF4A1*^{em1JP}(Myr-Akt#1), and *eIF4A1*^{em1JP}(Myr-Akt#2)). The relative distribution of the different *Eif4a1* alleles in *eIF4A1*^{em1JP}(Myr-Akt#1) was assessed by cloning and sequencing exon 5 PCR products and revealed the presence of 4 different *Eif4a1(F163L)* alleles in approximately equimolar ratios, with no intragenic deletions (Figs. S3.3A and S3.3B). These results are consistent with NIH/3T3 cells being tetraploid for chromosome 11 (the location of murine *Eif4a1*) (Leibiger et al., 2013). Direct sequencing of the exon 5 PCR products independently demonstrated that a mixture of CTC and CTT alleles were present (Figure S3.3B). Colony formation assays demonstrated that *eIF4A1*^{em1JP}(Myr-Akt#1) cells were resistant to rocaglates *ex vivo* (Figure 3.4A). *In vivo*, *eIF4A1*^{em1JP}(Myr-Akt#1) cells formed tumors faster than *Rosa26*^{em1JP}(Myr-Akt) cells (Figure 3.4B), despite displaying similar doubling rates *ex vivo* (Figure S3.3C). Nevertheless, an eight-day treatment course with silvestrol significantly curtailed tumor outgrowth in mice transplanted with *Rosa26*^{em1JP}(Myr-Akt) cells while having no effect on *eIF4A1*^{em1JP}(Myr-Akt#1) tumors (Figure 3.4B). Independently generated tumors from the second cell line, *eIF4A1*^{em1JP}(Myr-Akt#2), formed tumors slower than *eIF4A1*^{em1JP}(Myr-Akt#1) in mice, but nonetheless remained unresponsive to silvestrol

(Figure 3.4B). The failure to respond to silvestrol *in vivo* was associated with a ~3-fold reduction in apoptosis (Figure 3.4C). Previous studies have identified several rocaglate-responsive mRNAs, of which c-Myc is a representative anti-cancer target (Robert et al., 2014; Wolfe et al., 2014). Polysome analysis revealed that c-Myc mRNA distribution shifts from heavy polysome fractions to light polysome fractions when *Rosa26*^{em1JP}(Myr-Akt) cells were exposed to silvestrol but remains unaffected in *eIF4A1*^{em1JP}(Myr-Akt#1) cells (Figs. 3.4D and 3.4E). Translation of ATP5o, a prototypical mRNA harboring a TISU element which confers eIF4A independence (Elfakess et al., 2011), was unaffected when either cell line was exposed to silvestrol (Figure 3.4E). Immunoblotting and immunoprecipitation of metabolically labeled proteins were consistent with the ability of silvestrol to inhibit MYC protein production in *Rosa26*^{em1JP}(Myr-Akt), but not *eIF4A1*^{em1JP}(Myr-Akt#1), cells (Figure S3.4). These results indicate that the anti-neoplastic activity of silvestrol is a consequence of eIF4A1 suppression, which subsequently is associated with diminished expression of c-Myc, a quintessential oncogene.

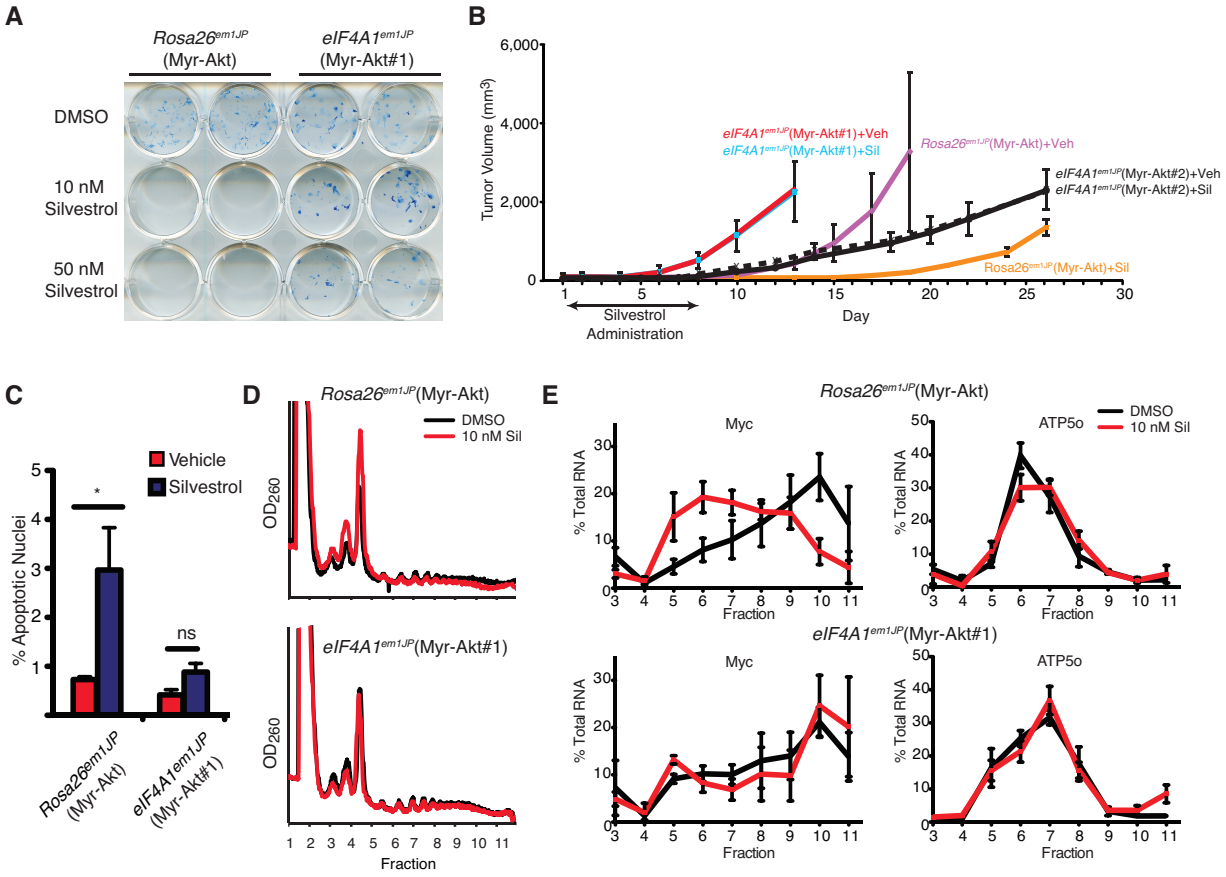

Figure 3.4 Cas9-Mediated Editing of the *Eif4a1* Locus Confirms the Drug-Target Hypothesis

(A) Colony formation assay of Myr-Akt-transformed *Rosa26*^{em1JP} or *eIF4A1*^{em1JP} cells in the presence of silvestrol.

(B) Response of Myr-Akt-transformed *Rosa26*^{em1JP} or *eIF4A1*^{em1JP} xenografts *in vivo* to silvestrol. On the indicated days, mice were treated with silvestrol (0.2 mg/kg) following tumor appearance. n = 6–7 mice/cohort ±SEM.

(C) Bar graph of the percentage of apoptotic nuclei from tumor sections. Three hours before harvesting of tumors, mice were treated with vehicle or 0.2 mg/kg silvestrol. n = 2 biological replicates (with ~7,000 nuclei analyzed per tumor) ±SD; *$p < 0.05$; ns, not significant.

(D) Polysome profiles of Myr-Akt-transformed *Rosa26*^{em1JP} or *eIF4A1*^{em1JP} cells exposed to 10 nM silvestrol for 1 hr.

(E) Distribution of mRNAs in polysome fractions shown in (D).

See also Figures S3.3 and S3.4

3.5 Discussion

Using genetic complementation and CRISPR/Cas9-mediated gene editing, we validate eIF4A1 as the primary molecular target of rocaglates in mammalian cells responsible for the inhibition

of translation observed with this class of compounds. These results significantly strengthen the drug-target link between rocaglates and eIF4A1 *in vivo* and were critical to undertake since rocaglates have also been reported to bind to prohibitins (PHB) 1 and 2 and block their interaction with cRaf (Polier et al., 2012). Our results indicate that this is not the mechanism by which rocaglates inhibit translation (Chu et al., 2016a) and in our hands cannot be responsible for the *ex vivo* or *in vivo* activity of rocaglates. However, rocaglates may have other unsuspected biological targets. Although both eIF4A1 and eIF4A2 can cycle through the eIF4F complex *in vitro* (Yoder-Hill et al., 1993), there is emerging evidence suggesting that their activities are not interchangeable (Galicia-Vazquez et al., 2012). Whether eIF4A2 plays a significant role in response to rocaglate-mediated inhibition and could be responsible for the partial sensitivity of *eIF4A1*^{em1JP} to high rocaglate concentration (Figure S3.2B) remains to be elucidated. Nevertheless, these results consolidate the position of eIF4A1 as an anti-cancer target.

We were surprised to find several alleles of *Eif4a1*(F136L) in our silvestrol-resistant population, both at the codon encoding leucine and at the PAM motifs (Figs. 3.3B, S3.3A, and S3.3B). This may be a consequence of strand-switching during HDR occurring before incorporation of the second mutation present on the ODN. This has previously been documented when simultaneously introducing two mutations at a given locus, with as much as a 17% drop in efficiency occurring with mutations positioned 8-10 base pairs apart (Elliott et al., 1998; Yang et al., 2013b). These results highlight the importance of thorough characterization of cell lines generated by CRISPR/Cas9.

In silico analysis of the yeast TIF1/2 proteins predicted a rocaglate-binding pocket at the TIF1-RNA interface (Sadlish et al., 2013). Our results from DSF and CETSA assays are consistent with

rocaglates directly interacting with eIF4A *in vitro* and *in cellulo*. Although structural studies of eIF4A1-rocaglate interaction are necessary to unequivocally identify the rocaglate binding site and understand how the F163L mutation affects rocaglate binding, our results suggest that eIF4A1(F136L) is likely resistant to rocaglates due to reduced compound engagement (Figs. 3.1G and 3.3E).

Precise genome editing of change-of-function alleles coupled with drug selection has been shown to be a powerful approach to generate tailored cell lines and validate drug:target interactions (Smurnyy et al., 2014). Our results extend this paradigm to gain-of-function alleles coupled with activity screening to validate drug-target relationships *in vivo*. Although our previous work had identified several TIF1 alleles as capable of conferring rocaglate-resistance in yeast (Sadlish et al., 2013), we found that not all corresponding *Eif4a1* alleles encoded for functional proteins in the mammalian setting. This highlights the importance of undertaking detailed biochemical studies coupled with an approach, such as the RCV system (Figure3.2), to demonstrate complementation before undertaking the more labor- and time-intensive task of engineering the alleles into the cellular genome. Our genetic complementation and genome editing approaches, in combination with *in cellulo* and *in vivo* data converge to position eIF4A1 as a critical anti-neoplastic target.

3.6 Materials and Methods

3.6.1 Cell Lines and Retrovirus Generation.

All cell lines were cultured in DMEM supplemented with 10% FBS, 100 U/ml penicillin/streptomycin, and 2 mM L-glutamine at 37°C and 5% CO_2. For retroviral transductions, 25 μg of plasmid was transfected into ecotropic Phoenix cells using calcium phosphate in the presence of 25 μM chloroquine and the media changed the following day. Starting 48 h after transfection, viral

supernatant was filtered and added to NIH/3T3 cells in the presence of 4 μg/ml polybrene. Cells were spinoculated at 1000x g for 1 h at 30°C. Infections were performed every 8 h, for a total of six infections. Cas9-modified cell lines are named as suggested (http://www.informatics.jax.org/mgihome/nomen/gene.shtml#endim) - for example, *eIF4A1*^{em1JP} indicates the first endonuclease-induced mutation (em1) of the *Eif4a1* gene produced in the JP lab).

3.6.2 Xenograft Models.

Four million cells were injected with matrigel sub-cutaneously into 4–6 weeks old female Balb/c-nu/nu mice. Tumor growth was monitored every second day using calipers. Treatments began when tumors had reached 25–50 mm^3 with silvestrol (0.2 mg/kg) delivered by intraperitoneal (IP) injection daily for 8 consecutive days. Tumor growth was monitored for the remainder of the experiment and no further drug treatments were performed. For tumor analysis, mice were treated with compound or vehicle three hours prior to harvesting of the tumors. Tumors were collected into 10% formalin, embedded in paraffin, and sectioned. TUNEL staining was performed using the DeadEnd™ Fluorometric TUNEL System (Promega) according to the manufacturer's instructions. The percentage of cells undergoing apoptosis was determined by counting the number of TUNEL positive nuclei on Fiji (ImageJ, National Institutes of Health) and dividing it by the total number of nuclei in the field.

Additional details regarding methodology are presented in the Supplemental Experimental Procedures

3.7 Author Contributions

J.C. and J.P. conceived and designed the study. J.C. performed all experiments with the following exceptions: GG-V generated the CRISPR modified cell lines and performed experiments in Figs

3.3Bb, S3.2 and S3.3. RC performed experiments in Figs. 3.4B, JRM generated the RCV constructs, AK undertook analysis of tumors derived from *Rosa26*^{em1JP}(Myr-Akt) and *eIF4A1*^{em1JP}(Myr-Akt#1) cells. J.A.P. Jr. provided unique rocaglate derivatives. J.P. supervised the study. J.C. and J.P. wrote the manuscript and all authors contributed to editing the manuscript.

3.8 Acknowledgments

We thank Mr. Steven Stone and Dr. Neil Lajkiewicz (Boston University) for the synthesis of (-)-SDS-1-021. This work was supported by grants from the Canadian Institutes of Health Research to JP (MOP-106530 and MOP-115126) and the National Institutes of Health (R01 GM073855 to J.A.P., Jr.). Research in the BU-CMD is supported by NIH grant GM111625.

3.9 References

Bhat, M., Robichaud, N., Hulea, L., Sonenberg, N., Pelletier, J., and Topisirovic, I. (2015). Targeting the translation machinery in cancer. Nat Rev Drug Discov 14, 261-278.

Bordeleau, M.E., Robert, F., Gerard, B., Lindqvist, L., Chen, S.M., Wendel, H.G., Brem, B., Greger, H., Lowe, S.W., Porco, J.A., Jr., et al. (2008). Therapeutic suppression of translation initiation modulates chemosensitivity in a mouse lymphoma model. J Clin Invest 118, 2651-2660.

Cencic, R., Carrier, M., Galicia-Vazquez, G., Bordeleau, M.E., Sukarieh, R., Bourdeau, A., Brem, B., Teodoro, J.G., Greger, H., Tremblay, M.L., et al. (2009). Antitumor activity and mechanism of action of the cyclopenta[b]benzofuran, silvestrol. PLoS One 4, e5223.

Cencic, R., Galicia-Vazquez, G., and Pelletier, J. (2012). Inhibitors of translation targeting eukaryotic translation initiation factor 4A. Methods Enzymol 511, 437-461.

Chu, J., Cencic, R., Wang, W., Porco, J.A.J., and Pelletier, J. (2016). Translation Inhibition by Rocaglates is Independent of eIF4E Phosphorylation Status. Mol Cancer Ther 15, 136-141.

Elfakess, R., Sinvani, H., Haimov, O., Svitkin, Y., Sonenberg, N., and Dikstein, R. (2011). Unique translation initiation of mRNAs-containing TISU element. Nucleic Acids Res 39, 7598-7609.

Elliott, B., Richardson, C., Winderbaum, J., Nickoloff, J.A., and Jasin, M. (1998). Gene conversion tracts from double-strand break repair in mammalian cells. Mol Cell Biol 18, 93-101.

Galicia-Vazquez, G., Cencic, R., Robert, F., Agenor, A.Q., and Pelletier, J. (2012). A cellular response linking eIF4AI activity to eIF4AII transcription. RNA 18, 1373-1384.

Graff, J.R., Konicek, B.W., Vincent, T.M., Lynch, R.L., Monteith, D., Weir, S.N., Schwier, P., Capen, A., Goode, R.L., Dowless, M.S., et al. (2007). Therapeutic suppression of translation initiation factor eIF4E expression reduces tumor growth without toxicity. J Clin Invest 117, 2638-2648.
Hong, D.S., Kurzrock, R., Oh, Y., Wheler, J., Naing, A., Brail, L., Callies, S., Andre, V., Kadam, S.K., Nasir, A., et al. (2011). A phase 1 dose escalation, pharmacokinetic, and pharmacodynamic evaluation of eIF-4E antisense oligonucleotide LY2275796 in patients with advanced cancer. Clin Cancer Res 17, 6582-6591.
Jafari, R., Almqvist, H., Axelsson, H., Ignatushchenko, M., Lundback, T., Nordlund, P., and Martinez Molina, D. (2014). The cellular thermal shift assay for evaluating drug target interactions in cells. Nature protocols 9, 2100-2122.
Leibiger, C., Kosyakova, N., Mkrtchyan, H., Glei, M., Trifonov, V., and Liehr, T. (2013). First molecular cytogenetic high-resolution characterization of the NIH 3T3 cell line by murine multicolor banding. J Histochem Cytochem 61, 306-312.
Lin, C.J., Nasr, Z., Premsrirut, P.K., Porco, J.A., Jr., Hippo, Y., Lowe, S.W., and Pelletier, J. (2012). Targeting Synthetic Lethal Interactions between Myc and the eIF4F Complex Impedes Tumorigenesis. Cell Reports 1, 325-333.
Lorsch, J.R., and Herschlag, D. (1998). The DEAD box protein eIF4A. 1. A minimal kinetic and thermodynamic framework reveals coupled binding of RNA and nucleotide. Biochemistry 37, 2180-2193.
Niesen, F.H., Berglund, H., and Vedadi, M. (2007). The use of differential scanning fluorimetry to detect ligand interactions that promote protein stability. Nature protocols 2, 2212-2221.
Pan, L., Woodard, J.L., Lucas, D.M., Fuchs, J.R., and Kinghorn, A.D. (2014). Rocaglamide, silvestrol and structurally related bioactive compounds from Aglaia species. Nat Prod Rep 31, 924-939.
Polier, G., Neumann, J., Thuaud, F., Ribeiro, N., Gelhaus, C., Schmidt, H., Giaisi, M., Kohler, R., Muller, W.W., Proksch, P., et al. (2012). The natural anticancer compounds rocaglamides inhibit the Raf-MEK-ERK pathway by targeting prohibitin 1 and 2. Chemistry & biology 19, 1093-1104.
Rajalingam, K., Wunder, C., Brinkmann, V., Churin, Y., Hekman, M., Sievers, C., Rapp, U.R., and Rudel, T. (2005). Prohibitin is required for Ras-induced Raf-MEK-ERK activation and epithelial cell migration. Nat Cell Biol 7, 837-843.
Robert, F., Roman, W., Bramoulle, A., Fellmann, C., Roulston, A., Shustik, C., Porco, J.A., Jr., Shore, G.C., Sebag, M., and Pelletier, J. (2014). Translation initiation factor eIF4F modifies the dexamethasone response in multiple myeloma. Proc Natl Acad Sci U S A 111, 13421-13426.
Rodrigo, C.M., Cencic, R., Roche, S.P., Pelletier, J., and Porco, J.A. (2012). Synthesis of rocaglamide hydroxamates and related compounds as eukaryotic translation inhibitors: synthetic and biological studies. J Med Chem 55, 558-562.
Rubio, C.A., Weisburd, B., Holderfield, M., Arias, C., Fang, E., DeRisi, J.L., and Fanidi, A. (2014). Transcriptome-wide characterization of the eIF4A signature highlights plasticity in translation regulation. Genome Biol 15, 476.
Sadlish, H., Galicia-Vazquez, G., Paris, C.G., Aust, T., Bhullar, B., Chang, L., Helliwell, S.B., Hoepfner, D., Knapp, B., Riedl, R., et al. (2013). Evidence for a functionally relevant rocaglamide binding site on the eIF4A-RNA complex. ACS Chem Biol 8, 1519-1527.
Smurnyy, Y., Cai, M., Wu, H., McWhinnie, E., Tallarico, J.A., Yang, Y., and Feng, Y. (2014). DNA sequencing and CRISPR-Cas9 gene editing for target validation in mammalian cells. Nat Chem Biol 10, 623-625.

Truitt, M.L., Conn, C.S., Shi, Z., Pang, X., Tokuyasu, T., Coady, A.M., Seo, Y., Barna, M., and Ruggero, D. (2015). Differential Requirements for eIF4E Dose in Normal Development and Cancer. Cell 162, 59-71.
Wolfe, A.L., Singh, K., Zhong, Y., Drewe, P., Rajasekhar, V.K., Sanghvi, V.R., Mavrakis, K.J., Jiang, M., Roderick, J.E., Van der Meulen, J., et al. (2014). RNA G-quadruplexes cause eIF4A-dependent oncogene translation in cancer. Nature 513, 65-70.
Yang, L., Guell, M., Byrne, S., Yang, J.L., De Los Angeles, A., Mali, P., Aach, J., Kim-Kiselak, C., Briggs, A.W., Rios, X., et al. (2013). Optimization of scarless human stem cell genome editing. Nucleic Acids Res 41, 9049-9061.
Yoder-Hill, J., Pause, A., Sonenberg, N., and Merrick, W.C. (1993). The p46 subunit of eukaryotic initiation factor (eIF)-4F exchanges with eIF-4A. J Biol Chem 268, 5566-5573.

3.10 Supplemental Figures

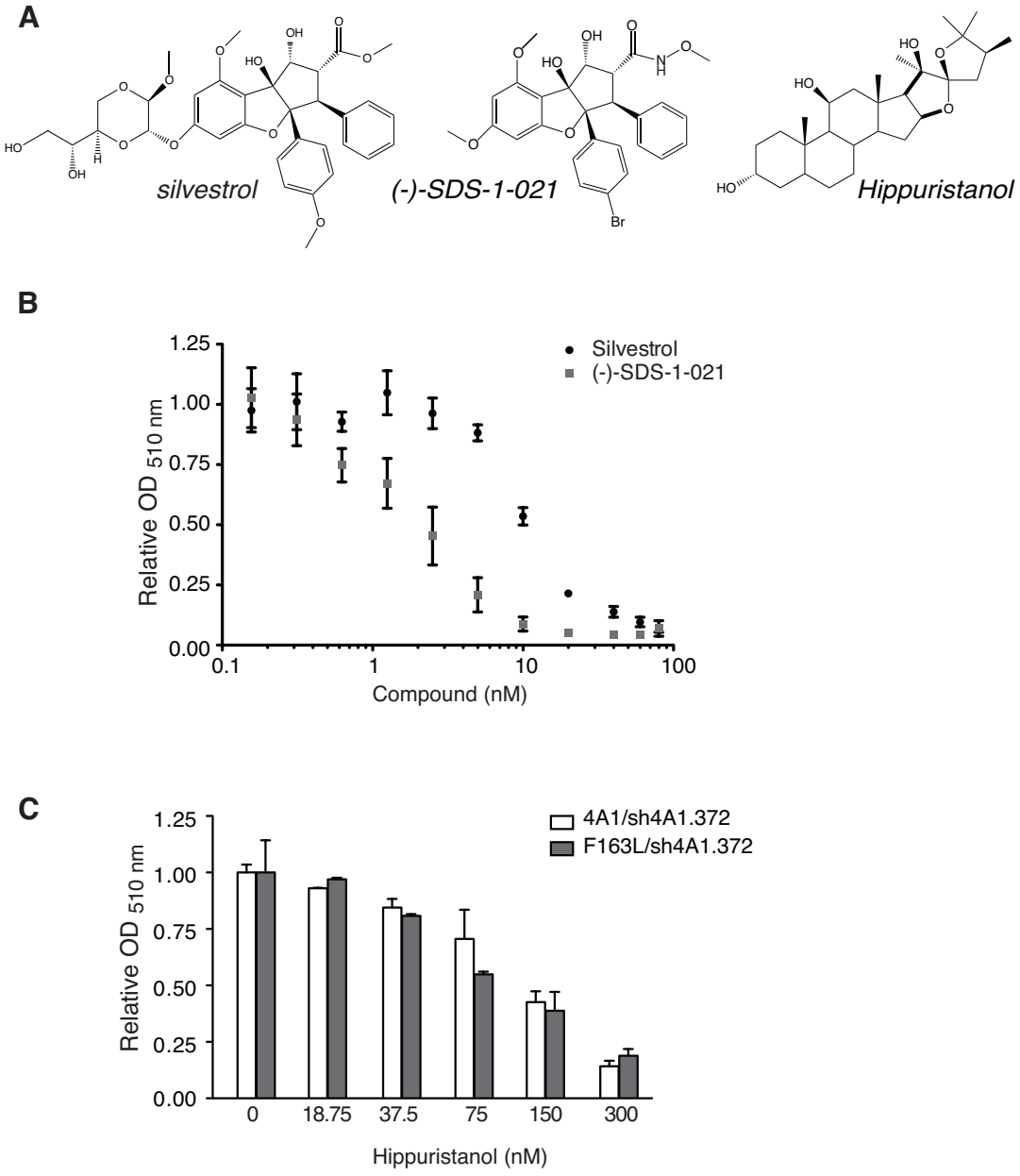

Figure S3.1 The Eif4a1(F163L) Allele Does Not Confer Cross-Resistance to Hippuristanol.
(A) Chemical structure of compounds used in this study.
(B) Cell viability following exposure of NIH/3T3 cells to the indicated concentrations of silvestrol or (-)-SDS-1-021. Cells were exposed to the indicated concentrations of compound for 4 days and viability assessed by the SRB assay. N= 3 biological replicates performed in duplicates ± SEM.
(C) Cell viability following exposure of NIH/3T3 cells transduced with the indicated retroviruses. Cells were cultured for 4 days in the presence of the indicated concentrations of hippuristanol and relative growth assessed using the SRB assay. N=2 technical replicates ± SD.

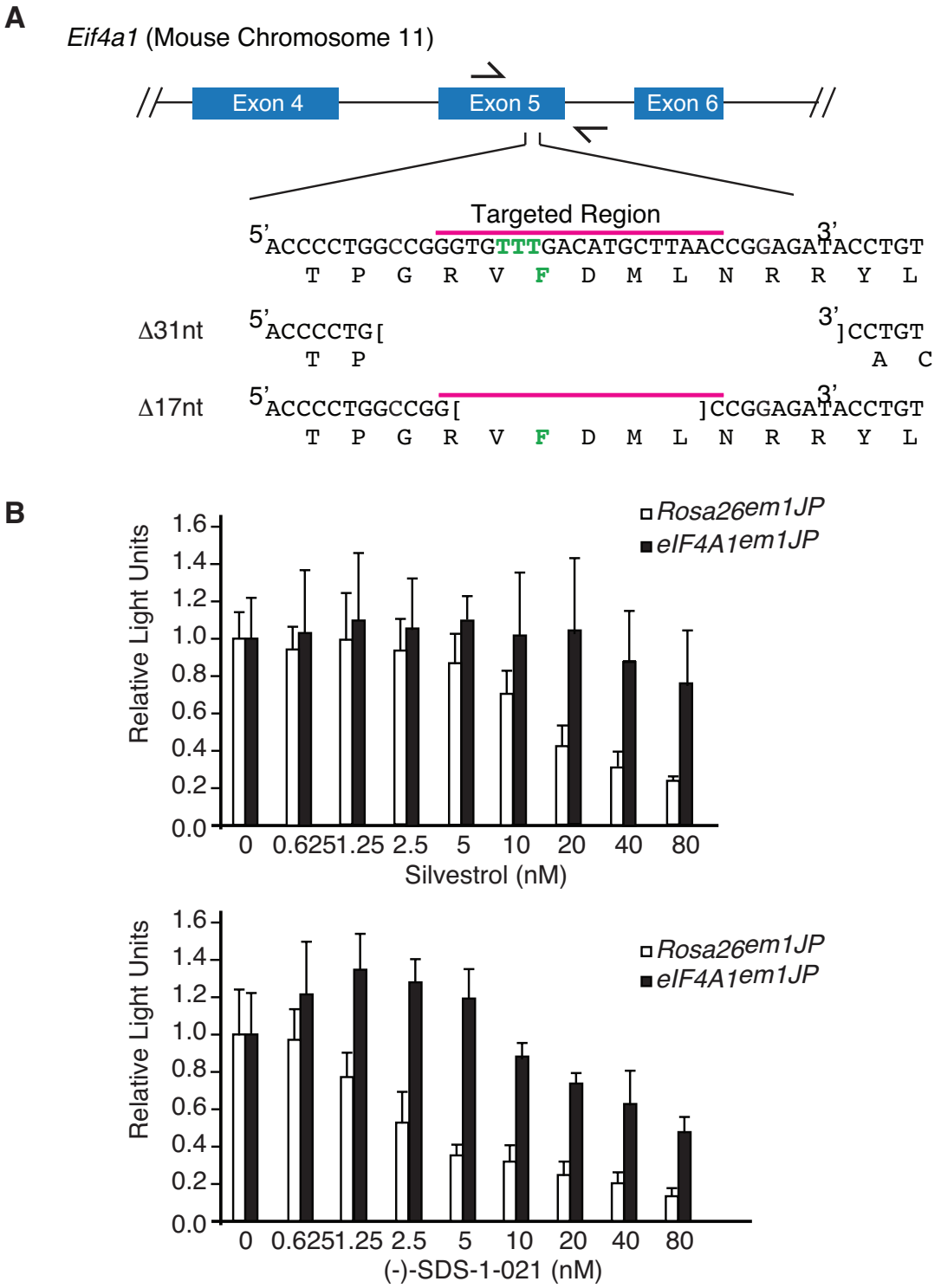

Figure S3.2 Related to Figure 3.3 eIF4A1(F163L) Confers Resistance to Rocaglates

(A) Sequence of *Eif4a1* alleles containing exon 5 deletions in the *eIF4A1*^{em2JP} cell population.

(B) Cell viability following exposure of *Rosa26*^{em1JP} and *eIF4A1*^{em1JP} cells to the indicated concentrations of silvestrol or (-)-SDS-1-021 for 48 h. Viability was assessed using the Cell Titer Glo assay. N=5 biological replicates ± SD.

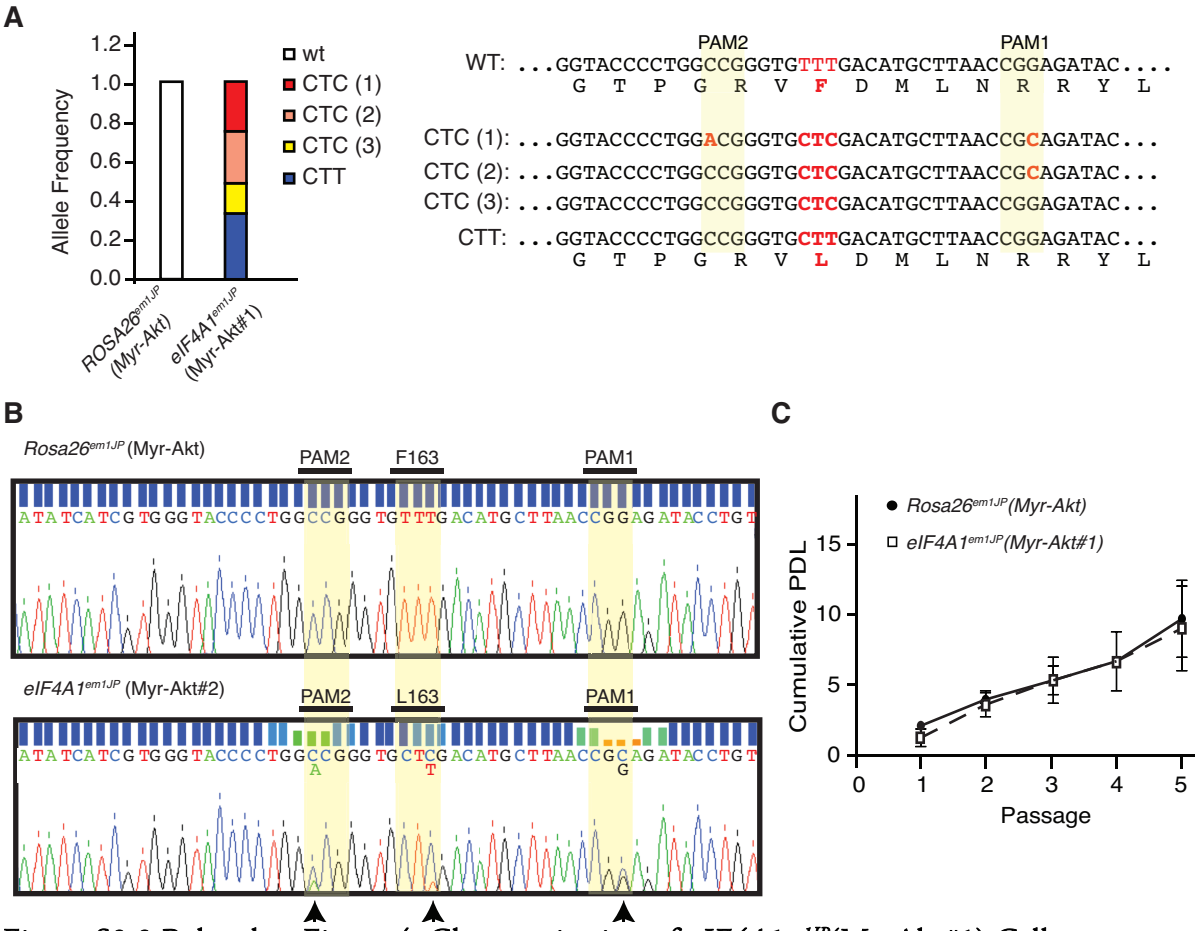

Figure S3.3 Related to Figure 4. Characterization of *eIF4A1*^{em1JP}(MyrAkt#1) Cells.

(A) Sequence analysis of cloned PCR products from *eIF4A1*^{em1JP}(MyrAkt#1) cells. Data is compiled from 49 and 42 sequence reads from *Rosa26*^{em1JP}(Myr-Akt) and *eIF4A1*^{em1JP}(Myr-Akt#1) cells, respectively.

(B) Chromatograms of PCR products specific to *Eif4a1* exon 5 of *Rosa26*^{em1JP}(Myr-Akt) and *eIF4A1*^{em1JP} (Myr-Akt#2) cells

(C) Cell doubling rates of Myr-Akt transformed *Rosa26*^{em1JP} or *eIF4A1*^{em1JP} cells.

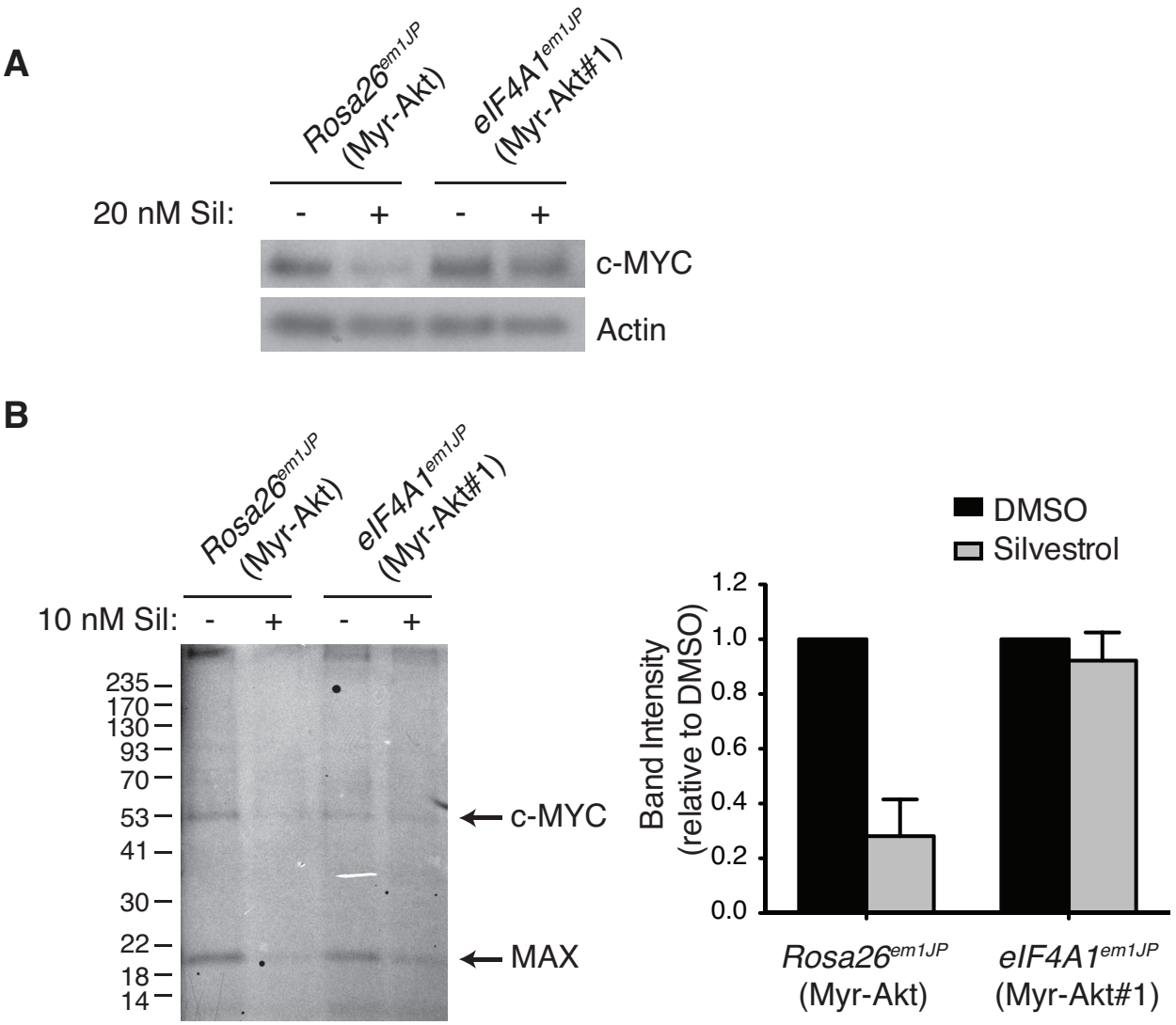

Figure S3.4, Related to Figure 4. Effect of Rocaglates on c-MYC Expression

(A) Western blot of c-MYC in *Rosa26*^{em1JP} (Myr-Akt) or *eIF4A1*^{em1JP}(Myr-Akt#1) cells treated with 20 nM silvestrol for 5 hours. Nuclear extracts were prepared and analyzed by Western blotting.

(B) Metabolic labeling and immunoprecipitation (IP) of de novo synthesized c-MYC. *Rosa26*^{em1JP} (Myr-Akt) or *eIF4A1*^{em1JP}(Myr-Akt#1) cells were labeled with 35SMet/Cys for 5 hours in the presence of 10 nM silvestrol. IPs were performed using equal amounts of protein (500 μg). Following IPs, samples were resolved by SDS-PAGE, and the gels were treated with EN^{3}HANCE (Perkin Elmer, MA), dried and exposed to X-ray film. A representative autoradiograph of the resulting immunoprecipitated proteins with the position of migration of c-MYC and the c-MYC interacting protein, MAX, indicated. The relative c-MYC band intensities are shown to the right. N=2 biological replicates ± SD.

3.11 Supplemental Experimental Procedures

3.11.1 Compounds.

Silvestrol was synthesized as previously reported (Gerard et al., 2007; Rodrigo et al., 2012). The rocaglate hydroxamate (-)-SDS-1-021 was generated using biomimetic kinetic resolution of chiral, racemic aglain ketone precursors (Stone et al., 2015) followed by amide formation (Gerard et al., 2006). Hippuristanol was synthesized as previously described (Somaiah et al., 2014).

3.11.2 Purification of Recombinant eIF4A1 Protein.

Recombinant eIF4A1 protein was purified as previously described (Cencic et al., 2012). Briefly, BL21 (DE3) codon+ *E. coli* cells were transformed with pET15b-His_6-eIF4A1, cultured at 37°C until the OD600 reached 0.6, and induced with 1 mM IPTG for 3 h. Recombinant His_6-eIF4A1 was enriched on a Ni^{2+}-NTA agarose column and then further purified on a Q-Sepharose fast flow matrix and eluted with a linear salt gradient (100-500 mM KCl). Fractions containing recombinant His_6-eIF4A1 were pooled and dialyzed against Buffer A (20 mM Tris-Cl [pH 7.5], 10% glycerol, 0.1 mM EDTA) overnight at 4°C.

3.11.3 Competition Assay.

Transduced NIH/3T3 cells were mixed with an equal number of untransduced cells and cultured in 12 well plates in the presence of the indicated concentrations of compound. Every two days, cells were trypsinized and the relative population of GFP positive cells determined by flow cytometry (Guava EasyCyte, Millipore).

3.11.4 Sulforhodamine B (SRB) Assay.

One thousand cells were seeded per well in a 96-well plate and cultured in various concentrations of compound or vehicle (DMSO) for 6 days. To assay for relative viability, cells were washed with PBS,

fixed with 50% TCA for 1 h, then stained with 0.4% SRB for 10 minutes. Plates were washed 4 times with 1% acetic acid, dried, and the remaining dye was resuspended in 200 µl of 10 mM Tris base [pH 10.5] per well. The OD_{510nm} was measured using a microplate reader (SpectraMax M5, Molecular Devices) and relative viability was calculated by normalizing to the DMSO control.

3.11.5 Cell Doubling Assay.

Ten thousand cells were seeded in 12 well plates at the beginning of each passage. Two days later, cells were trypsinized, counted by flow cytometry (GUAVA EasyCyte Plus; Millipore), and reseeded. Population doubling levels for each passage was calculated as follows: Cumulative PDL= [Log(Final cell number/Initial cell number)/Log(2)]+Starting PDL) (Faraonio et al., 2012; Hayflick, 1973).

3.11.6 Colony Formation Assay.

Five hundred cells were seeded per well in a 12 well plate and 48 h post-seeding the indicated amounts of silvestrol or DMSO was added to the cells. Cells were cultured under these conditions for another 14 days, with the media being changed every 3 days. Wells were washed with PBS and colonies fixed for 10 min with ice-cold methanol. The colonies were stained with 0.4% methylene blue solution (in 50% methanol). Wells were washed five times with water and then dried at room temperature.

3.11.7 Western Blots.

Cells were lysed in RIPA buffer (20 mM Tris [pH 7.6], 100 mM NaCl, 1 mM EDTA, 1 mM EGTA, 1% NP40, 0.5% Sodium Deoxycholate, 0.1% SDS, 1 mM PMSF, 4 µg/ml aprotinin, 2 µg/ml leupeptin, 2 µg/ml pepstatin), resolved on a 10% Nu-PAGE gel, and transferred to a PVDF membrane (Bio-Rad). For Western blots probing for c-MYC, nuclear extracts were prepared by resuspending pelleted cells into cytoplasmic lysis buffer (50 mM Tris at pH 7.4, 150 mM NaCl, 1 mM EDTA, 0.1% Triton X-100), followed by centrifugation at 14000 rpm for 10 minutes to isolate the nuclei.

The pelleted nuclei were then lysed using RIPA buffer and equal protein was loaded onto 10% Nu-PAGE gels. Antibodies used in this study were directed against the following: His6-tag (27-4710- 01, GE Healthcare Life Sciences), eIF4A1 (ab31217, Abcam), eIF4A2 (ab31218, Abcam), eEF2 (#9742, Cell Signaling), GAPDH (ab8245, Abcam), c-Myc (N262, Santa Cruz), and actin (A5316, Sigma-Aldrich).

3.11.8 [^{35}S]-Methionine/Cysteine Metabolic Labeling.

Cells were incubated in methionine/cysteine-free DMEM supplemented with 10% dialyzed FBS, 100 U/ml penicillin/streptomycin and 2 mM L-Glutamine in the presence of the indicated concentration of compound or vehicle (DMSO) for 45 min prior to the addition of [^{35}S]-methionine/cysteine (150-200 μCi/ml) (Perkin Elmer, Waltham, MA). The incubations were continued for an additional 15 min and extracts were prepared by lysing the cells in RIPA buffer. Radiolabeled proteins were precipitated onto 3 MM Whatman paper using trichloroacetic acid and quantitated by scintillation counting. CPMs were normalized to total protein as determined by the DC assay (Bio-Rad) and plotted relative to the values obtained from the DMSO controls.

3.11.9 eIF4A1 Functional Assays.

ATPase assays were performed as previously described using Condition B (Lorsch and Herschlag, 1998). In essence, 1 μM [γ ^{32}P]-ATP (10 Ci/mmol) (unless indicated otherwise) was added to a buffer containing 1 μg of purified recombinant protein, 2.5 mM $MgCl_2$, 1 mM DTT, 1% glycerol, 20 mM MES-KOH [pH 6.0], 10 mM KOAc, 2.5 μM poly (U) RNA, and 50 μM silvestrol or DMSO. Reactions were incubated at 25°C for 60 min (unless indicated otherwise) and quenched by adding EDTA to a final concentration of 2.5 mM. Reactions were then resolved on PEI-cellulose TLC plates using 1 M LiCl/0.3 M NaH_2PO_4 as the developing solvent. The extent of ATP hydrolysis was

quantitated using a Typhoon Trio Imager (GE Healthcare). Experiments used to determine kinetic parameters of eIF4A1 ATP hydrolysis were performed under the conditions described above with varying concentrations of ATP (each reaction contained 1 μM [γ ^{32}P]-ATP mixed with the appropriate amount of unlabeled ATP) and 2 μl of the reaction was removed and quenched at 0, 2.5, 7.5, 12.5, and 17.5 min after addition of ATP. ATP hydrolysis of each time point was quantitated and plotted with respect to time in order to determine the $V_{initial}$ for each ATP concentration. $V_{initial}$ values were then plotted with respect to ATP concentration and the K_m and V_{max} values determined by fitting the curves to the Michaelis-Menten model on GraphPad Prism (v5.0a).

For RNA binding assays, body-labeled [^{32}P]- RNA was generated from pSP/CAT linearized with PvuII. Following *in vitro* transcription with SP6 RNA Polymerase, an RNA of 157 nucleotides is produced

[$^{5'}$pppGAATACAAGCTTGGCGAGATTTTCAGGAGCTAAGGAAGCTAAAATGGAGA
AAAAAATCACTGGATATACCACCGTTGATATATCCCAATGGCATCGTAAAGAACATTT
TGAGGCATTTCAGTCAGTTGCTCAATGTACCTATAACCAGACCGTTCAG$^{3'}$] (Cencic et al., 2007; Gorman, 1985).

RNA binding assays were performed by incubating 3 μg recombinant protein with body labeled [^{32}P]-RNA (35000 cpm) in binding buffer (25 mM Tris [pH 7.5], 1 mM DTT, 100 mM KCl, 1 mM ATP, 5 mM $MgCl_2$) in the presence of DMSO or 1 μM silvestrol at 37°C for 10 min. Binding reactions were stopped by the addition of ice-cold wash buffer (25 mM Tris [pH 7.5], 100 mM KCl, 3 mM $MgCl_2$) and then applied onto a nitrocellulose filter (45 μM HA Millipore) (preblocked with 0.1% sodium pyrophosphate). Filters were washed 3 times with wash buffer and dried prior to scintillation counting in order to assess the amount of [^{32}P]-labeled RNA retained on the filter.

Helicase assays were performed as previously published (Rogers et al., 1999). Briefly 0.5 μg of recombinant protein was added to a 20 μl reaction buffer containing DMSO or 50 μM silvestrol, 2 nM of [^{32}P]- RNA-11 duplex (Rogers et al., 1999), 20 mM HEPES-KOH [pH 7.5], 70 mM KCl, 20 mM DTT, 10 mM $Mg(OAc)_2$, 1 mg/ml acetylated BSA, and 1 mM ATP. Reactions were incubated at 35°C for 15 min and terminated by adding 5 μl of a solution containing 50% glycerol, 2% SDS, 20 mM EDTA, and Bromophenol Blue and Xylene Cyanol dyes. The products of the helicase assays were resolved on a 12% polyacrylamide gel, dried and quantitated using a Typhoon Trio Imager (GE Healthcare).

3.11.10 Differential Scanning Fluorimetry (DSF).

Experiments were performed as previously reported (Niesen et al., 2007) with slight modifications to the buffer conditions. Briefly, 2.1 μM of recombinant eIF4A1 (wild type or F163L) was incubated with compound or DMSO in DSF buffer (20 mM HEPES-KOH [pH 7.5], 70 mM KCl, 2 mM DTT, 1 mM $Mg(OAc)_2$, 1 mM ATP, 7.5X Sypro Orange (S-6650, Thermo Fisher), and 0.7 μM RNA-1 (Rogers et al., 1999). The samples were heated and read from 25°C to 70°C at 1 °C/min ramp rate using the CFX96 Touch™ Real-Time PCR Detection System (Bio-Rad). Data analysis was performed as previously described (Niesen et al., 2007).

3.11.11 Cas9-mediated Editing of *Eif4a1*.

Targeting of the *Eif4a1* locus was undertaken using a previously described pQCX-based vector system (Malina et al., 2013) expressing human codon-optimized Cas9, GFP, and an sgRNA targeting *Eif4a1* exon 5. A single stranded oligonucleotide (ssODN) harboring the desired F136L change, a novel TaqI site, and mutated PAMs was used as template. DNA was introduced into NIH/3T3 cells by nucleofection of 2.5 μg of plasmid and 0.3 ng of ssODN (Amaxa Cell Line Nucleofector Kit R for

NIH/3T3, VCA-1001, Lonza). After 48h, cells were placed in media containing 80 nM silvestrol. Two days later, individual colonies were isolated and characterized by restriction digest analysis. Characterization of the *Eif4a1* locus was determined via PCR amplification of the targeted locus using the following primers: *Eif4a1ex5*-1 fwd 5'-AACTTGCATCCAAGAAAATGACA-3', *Eif4a1ex5*-1 rev 5'- AGAAGCTGCAGATGGAAGCTC-3'. To determine allele frequencies, the PCR product was then cloned into pBluescript KS II, transformed into DH10β cells, and single colonies were picked for mini-prepping and sequencing. Direct sequencing of the *Eif4a1* locus was also performed on PCR products amplified by the following primers: *Eif4a1ex5*-2 fwd 5'-ATGTGGTAGTAGGGTGGAGAGT-3', *Eif4a1ex5*-2 rev 5'GCATCCAAGAAAATGACATGTGGG-3'

3.11.12 Cellular Thermal Shift Assay (CETSA).

Experiments were performed essentially as described (Jafari et al., 2014). Briefly, 5 x 10^6 cells were seeded into a 15 cm dish and on the following day were exposed to 1 μM (-)-SDS-1-021 or DMSO for 1 h. Cells were pelleted, washed twice with PBS (containing 1 μM (-)-SDS-1-021 or DMSO), resuspended in PBS (containing 1 μM (-)-SDS-1-021 or DMSO) and distributed into a 96 well PCR plate (Axygen). Cells were heated to the indicated temperatures for 3 min using a PCR machine (Mastercycler Pro, Eppendorf) and then cooled to RT for 3 min. Cells were lysed by 3 freeze/thaw cycles and the insoluble fraction pelleted by centrifugation at 14000 rpm for 10 min. Equivalent volumes of the soluble fraction was resolved on a 10% Nu-PAGE gel and transferred to a PVDF membrane for Western blotting. Quantitations were performed using the Li-COR Odyssey Imaging System (v3.0). Relative soluble eIF4A1 levels were determined by normalizing band intensities to the highest intensity value obtained in the set. The aggregation temperatures (as defined by the

temperature where 50% of the protein is denatured) were determined by fitting the curves to the Boltzmann Sigmoidal function.

3.11.13 Polysome Analysis and RT-qPCR analysis of mRNA.

Cells were incubated with the indicated concentration of compound for 1 h and washed twice with ice-cold PBS supplemented with 100 μg/ml cycloheximide. Cells were pelleted and lysed with hypotonic lysis buffer (5 mM Tris-HCl [pH 7.5], 2.5 mM $MgCl_2$, 1.5 mM KCl, 2 mM DTT, 1% Triton X-100, 0.5% sodium deoxycholate, 100 μg/ml cycloheximide) and the subsequent extract was loaded onto a 10-50% sucrose gradient. Samples were centrifuged at 35000 rpm for 2:15 hours at 4°C and the gradients were then fractionated while reading the UV_{254} absorbance. RNA was extracted from each fraction using TRIzol (Life Technologies) according to the manufacturer's instructions. SuperScript III reverse transcriptase (Invitrogen) and oligo$(dT)_{20}$ primers were used generate cDNAs and qPCRs were performed with SsoFast Evagreen Supermix (Bio-Rad) using the CFX96 PCR system. The following primers were used: *myc* fwd 5'- ATTTCCTTTGGGCGTTGGA-3', *myc* rev 5'-TCCTGTTGGTGAAGTTCACGTT-3', *Atp5o* fwd 5'- TCTCGACAGGTTCGGAGCTT-3', *Atp5o* rev 5'-AGAGTACAGGGCGGTTGCATA-3'.

3.11.14 Metabolic Labeling with ^{35}S-methionine/cysteine.

For immunoprecipitations, cells were incubated in methionine/cysteine-free DMEM supplemented with 10% dialyzed FBS, 100 U/ml penicillin/streptomycin, and 2 mM L-Glutamine for 45 min prior to the addition of [^{35}S]-methionine/cysteine (final concentration 50 μCi/ml) (Perkin Elmer, Waltham, MA) and 10 nM silvestrol or DMSO. After 5 hours of S^{35} metabolic labeling, cells were washed with ice cold PBS, pelleted, and resuspended with IP lysis buffer (0.1% SDS, 0.5% Triton X-100, 20 mM Tris-HCl [pH 8], 150 mM NaCl). Lysates were cleared by centrifugation at 14,000 rpm

for 5 minutes before protein quantitation using DC assay (Bio-Rad). For each immunoprecipitation, 500 μg of lysate was incubated with 25 ul dynabeads protein G and 1 μg c-Myc antibody (N262, Santa Cruz) overnight at 4°C. Beads were washed 5 times in wash buffer and eluted by boiling in SDS sample buffer.

References

Cencic, R., Robert, F., and Pelletier, J. (2007). Identifying small molecule inhibitors of eukaryotic translation initiation. Methods Enzymol 431, 269-302.

Faraonio, R., Salerno, P., Passaro, F., Sedia, C., Iaccio, A., Bellelli, R., Nappi, T.C., Comegna, M., Romano, S., Salvatore, G., et al. (2012). A set of miRNAs participates in the cellular senescence program in human diploid fibroblasts. Cell death and differentiation 19, 713-721.

Gerard, B., Cencic, R., Pelletier, J., and Porco, J.A., Jr. (2007). Enantioselective synthesis of the complex rocaglate (-)-silvestrol. Angew Chem Int Ed Engl 46, 7831-7834.

Gerard, B., Sangji, S., O'Leary, D.J., and Porco, J.A., Jr. (2006). Enantioselective photocycloaddition mediated by chiral Bronsted acids: asymmetric synthesis of the rocaglamides. J Am Chem Soc 128, 7754-7755.

Gorman, C. (1985). High efficiency gene transfer into mammalian cells. DNA cloning II A practical approach IRL Press Ltd., Oxford, England, 143-190.

Hayflick, L. (1973). Subculturing human diploid fibroblast cultures (New York: Academic Press).

Jafari, R., Almqvist, H., Axelsson, H., Ignatushchenko, M., Lundback, T., Nordlund, P., and Martinez Molina, D. (2014). The cellular thermal shift assay for evaluating drug target interactions in cells. Nature protocols 9, 2100-2122.

Lorsch, J.R., and Herschlag, D. (1998). The DEAD box protein eIF4A. 1. A minimal kinetic and thermodynamic framework reveals coupled binding of RNA and nucleotide. Biochemistry 37, 2180-2193.

Malina, A., Mills, J.R., Cencic, R., Yan, Y., Fraser, J., Schippers, L.M., Paquet, M., Dostie, J., and Pelletier, J. (2013). Repurposing CRISPR/Cas9 for in situ functional assays. Genes Dev 27, 2602-2614.

Niesen, F.H., Berglund, H., and Vedadi, M. (2007). The use of differential scanning fluorimetry to detect ligand interactions that promote protein stability. Nature protocols 2, 2212-2221.

Rodrigo, C.M., Cencic, R., Roche, S.P., Pelletier, J., and Porco, J.A. (2012). Synthesis of rocaglamide hydroxamates and related compounds as eukaryotic translation inhibitors: synthetic and biological studies. J Med Chem 55, 558-562.

Rogers, G.W., Jr., Richter, N.J., and Merrick, W.C. (1999). Biochemical and kinetic characterization of the RNA helicase activity of eukaryotic initiation factor 4A. J Biol Chem 274, 12236-12244.

Somaiah, R., Ravindar, K., Cencic, R., Pelletier, J., and Deslongchamps, P. (2014). Synthesis of the antiproliferative agent hippuristanol and its analogues from hydrocortisone via Hg(II)-catalyzed spiroketalization: structure-activity relationship. J Med Chem 57, 2511-2523.

Stone, S.D., Lajkiewicz, N.J., Whitesell, L., Hilmy, A., and Porco, J.A., Jr. (2015). Biomimetic kinetic resolution: highly enantio- and diastereoselective transfer hydrogenation of aglain ketones to access flavagline natural products. J Am Chem Soc 137, 525-530.

CHAPTER 4 AMIDINO-ROCAGLATES– A POTENT NEW CLASS OF EIF4A INHIBITORS

Published in:

Chu J., Zhang W., Cencic R., Devine W. G., Beglov D., Henkel T., Brown L. E., Vajda S., Porco J. A. Jr., and Pelletier J. (2016). Translation Inhibition by Rocaglates is Independent of eIF4E Phosphorylation Status. *Cell Chem. Biol.* **In Press**

4.1 Preface to Chapter 4

The work presented in Chapters 2 and 3 utilized both natural (Roc-A, silvestrol) and synthetically derived (CR-1-31-B, SDS-1-0-21) rocaglates, but these compounds represent only a small subset of the entire rocaglate family. Over 100 naturally occurring rocaglates have been isolated and efforts made towards the generation of synthetic analogs have expanded this family significantly. To better understand how rocaglate structure influences compound potency, we compared the activities of >200 unique rocaglate derivatives. From this work, we discovered a new synthetic subclass of rocaglates with promising properties called amidino-rocaglates (ADRs). This work has also guided us in the design of the ADR, CMLD012612, which was found to possess improved potency compared to previous lead compounds.

4.2 Abstract

Rocaglates share a common cyclopenta[*b*]benzofuran core that inhibits eukaryotic translation initiation by modifying the behavior of the RNA helicase, eIF4A. Working as interfacial inhibitors, rocaglates stabilize the association between eIF4A and RNA, which can lead to the formation of steric barriers that block initiating ribosomes. There is significant interest in the development and expansion of rocaglate derivatives, as several members of this family have been shown to possess potent anti-neoplastic activity *in vitro* and *in vivo*. To further our understanding of rocaglate diversity and drug design, herein we explore the RNA clamping activity of >200 unique rocaglate derivatives. Through this, we report on the identification and characterization of a potent class of synthetic rocaglates called amidino-rocaglates. These compounds are among the most potent rocaglates documented to date and, taken together, this work offers important information that will guide the future design of rocaglates with improved biological properties.

4.3 Introduction

Small molecules targeting the translation machinery show considerable promise in the treatment of a variety of human maladies including cancer, viral infection, and neurodegeneration. In particular, there is significant interest towards the development of a family of compounds collectively known as rocaglates (Bhat et al., 2015), a class of translation inhibitors that possess potent cytotoxic activity against tumor cells (Bhat et al., 2015). This family of small molecules shares a common cyclopenta[*b*]benzofuran core and were originally isolated from extracts of the *Aglaia* species of angiosperms (King et al., 1982a). To date, numerous rocaglate analogs have been synthesized with the goals of improving potency and bioavailability (Ebada et al., 2011; Pan et al., 2014; Ribeiro et al.,

2012). Studies using silvestrol, a natural product isolated from *Aglaia foveolata*, indicate that rocaglates enhance the RNA binding affinity of the DEAD-box RNA helicase, eukaryotic initiation factor (eIF) 4A (Bordeleau et al., 2008; Iwasaki et al., 2016).

Cap-dependent translation is regulated by the rate-limiting eIF4F complex which recognizes mRNA cap structures *via* its eIF4E subunit, remodels adjacent mRNA structure via eIF4A, and recruits 43S pre-initiation complexes (40S subunit and associated factors) through its eIF4G subunit (Pelletier and Sonenberg, 2019). The dependency on eIF4F for ribosome recruitment by different mRNAs varies and scales with the degree of 5' leader secondary structure (Svitkin et al., 2001). Only ~5% of eIF4A is present in the eIF4F complex, suggesting that multiple eIF4A molecules may be used per initiation round and/or eIF4A may have non-eIF4F related activities in translation (Sokabe and Fraser, 2017). Assembly of the eIF4F complex is under mTOR regulation, ensuring that rheostatic and selective regulation of mRNA translation is linked to extra- and intra-cellular cues (Pelletier and Sonenberg, 2019).

Structural elucidation of the RocA:eIF4A1:polypurine RNA complex revealed that rocaglates function as interfacial inhibitors and make critical contacts with eIF4A1 (F163L, Q195) and two adjacent RNA purine bases (Iwasaki et al., 2019). When present within 5' mRNA leader regions, polypurine sequences serve as nucleation sites for rocaglate:eIF4A1 complexes, leading to the formation of steric barriers that impede 43S PIC scanning (Iwasaki et al., 2016). A rocaglate-resistant eIF4A1 mutant (F163L) has been characterized and introduction of this allele into cells using CRISPR/Cas9-mediated gene editing confers resistance to rocaglate cytotoxicity (Chu et al., 2016b; Iwasaki et al., 2019), further demonstrating that the mechanism of action of these compounds is dependent on their ability to interfere with eIF4A1 activity. Mammalian cells also express a second

eIF4A paralog (known as eIF4A2) that shares 90% amino acid identity with eIF4A1 and has been shown to participate in translation initiation (Rogers et al., 2002; Yoder-Hill et al., 1993). However, the effects of rocaglates on eIF4A2 have been largely unexplored as eIF4A1 is the predominant paralog in most cell types (Galicia-Vazquez et al., 2012; Nielsen and Trachsel, 1988).

Herein, we characterized the activities >200 rocaglates from an in-house library (the BU-CMD collection) to with respect to stimulation of RNA clamping of eIF4A1 and eIF4A2, inhibition of cap-dependent translation, and attenuating cellular proliferation. During the course of these studies, we uncovered and characterized a novel class of rocaglates, amidino-rocaglates (ADRs), that rank among the most potent synthetic derivatives identified to date.

4.4 Results and Discussion

4.4.1 Rocaglates Similarly Enhance RNA Binding of eIF4A1 and eIF4A2

In order to rapidly evaluate the ability of rocaglates to stimulate binding of eIF4A to RNA, we took advantage of a fluorescence polarization (FP) assay using a FAM (fluorescein amidite)-labelled RNA probe (Figure 4.1A) (Iwasaki et al., 2016). The ATPase activity of eIF4A1 is stimulated by the presence of RNA; previous studies have documented that the homoribopolymers poly r(A) and poly r(U) are more potent than poly r(C), poly r(I), poly r(G), globin mRNA, tRNA, poly r(I-C), or poly r(A)•poly r(U) substrates, suggesting that eIF4A has an inherent nucleotide bias for RNA binding (Abramson et al., 1987). Using the FP assay, we revisited the RNA sequence specificity of eIF4A1, and took the opportunity to characterize the RNA binding activity of its paralog, eIF4A2. Studies focusing on the pharmacological targeting of eIF4A2 has been comparatively limited due to the fact that it is the less abundant eIF4A variant in many cell types. However, this remains an area of interest

to explore as there is evidence suggesting that eIF4A2 may have tumor promoting effects (Chen et al., 2019) and in certain cancers, eIF4A2 is the predominant paralog (Wolfe et al., 2014). The ability to target eIF4A2 is also important within the context of eIF4A1 inhibition as it has been demonstrated that suppression of eIF4A1 leads to increased eIF4A2 expression (Galicia-Vazquez et al., 2012). We found that both proteins have a preference for mixed polypurine (poly r$(AG)_8$ or poly rA$(GAA)_5$) sequences versus poly r$(A)_{16}$, poly r$(C)_{16}$ or mixed polypyrimidine (poly r$(UC)_8$) (Figs 4.1B, C). In the presence of the synthetic rocaglate, CR-1-31-B, the binding activities of eIF4A1 and eIF4A2 to poly r$(AG)_8$ were enhanced to similar extents, indicating that the compound targets both paralogs equally (Figure 4.1D, E).

The rocaglate CR-1-31-B also preferentially stimulated binding of eIF4A1 to poly rA$(GAA)_5$ and to a lesser extent poly $(A)_{16}$, but had no effect when a polypyrimidine-containing RNA (poly r$(C)_{16}$ or poly r$(UC)_8$) was used (Figure 4.1F). To better understand the requirements for rocaglate-mediated stimulation of RNA binding, we next performed this experiment using RNA probes with varying (AG) repeat length. A single r(AG) dinucleotide embedded within a polypyrimidine track was sufficient for CR-1-31-B to stimulate eIF4A1-RNA binding and the extent of binding increased with higher AG content (Figure 4.1G). The location of an AG dinucleotide within a 16 nt RNA probe harboring otherwise poly r(U) sequences influenced stimulation of RNA binding, with the optimal preference being seven nucleotides downstream from the RNA 5' end (Figure S1). Taken together, these results indicate that: (i) eIF4A1 and eIF4A2 show similar RNA sequence binding specificity and have a distinct preference towards polypurine bases, (ii) the RNA binding activity of both eIF4A1 and eIF4A2 is similarly stimulated by CR-1-31-B, and (iii) the stimulation of RNA binding of eIF4A1 to RNA by CR-1-31-B scales with polypurine content.

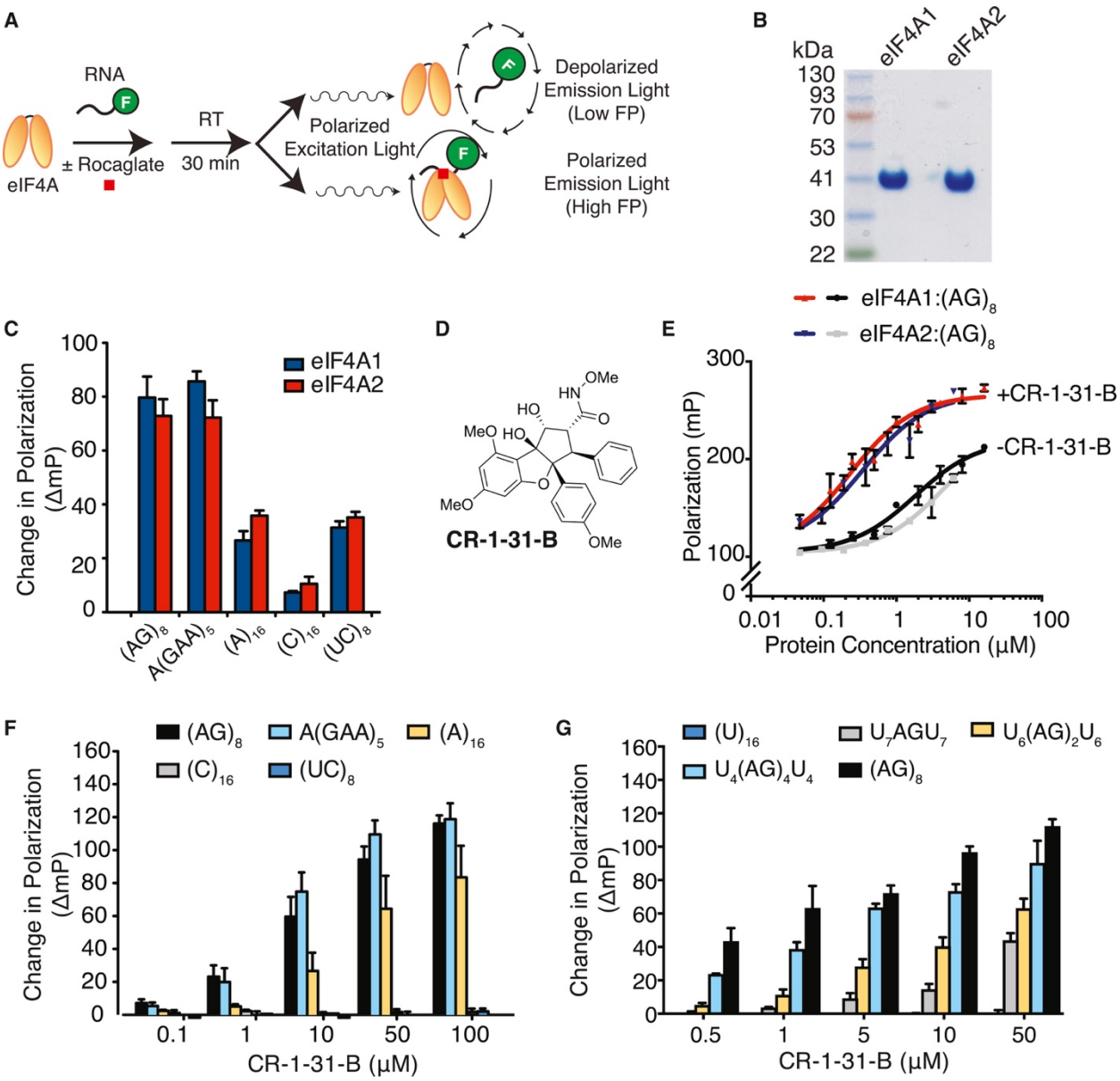

Figure 4.1 Rocaglates Similarly Enhance RNA Binding of eIF4A1 and eIF4A2

(A) Schematic diagram of FP assay used to measure eIF4A:RNA association. FAM-labeled RNA probes are excited by plane-polarized light in the presence of eIF4A ± rocaglate. In the absence of eIF4A binding, the RNA probe rapidly tumbles, and the emitted light becomes depolarized. Binding of eIF4A to RNA hinders probe rotation and results in polarized light emission.

(B) Coomassie blue staining of SDS-PAGE showing eIF4A1 and eIF4A2 preparations used herein.

(C) eIF4A1 and eIF4A2 possess similar RNA binding specificities. eIF4A1 or eIF4A2 (500 nM) were incubated in the presence of FAM-labeled RNA (10 nM) having the indicated sequence composition for 30 min, after which FP measurements were taken. The change in FP obtained relative to the DMSO control (which represents the eIF4A1:RNA association in the absence of compound) is presented. n = 3 ± SEM.

(D) Chemical structure of CR-1-31-B.

(E) Binding of eIF4A1 and eIF4A2 to RNA is equally responsive to CR-1-31-B. FAM-labeled poly r(AG)$_8$ (10 nM) was mixed with the indicated concentrations of eIF4A1 or eIF4A2 in the presence of either vehicle (DMSO) or 10 μM CR-1-31-B. Reactions were equilibrated at room temperature for 30 min prior to measuring light polarization. n = 3 ± SEM.
(F) Stimulation of eIF4A1:RNA binding by CR-1-31-B shows preference for polypurine-enriched sequences. FAM-labeled RNA was incubated in the presence of 500 nM eIF4A1 and the indicated concentration of CR-1-31-B for 30 min, after which time FP measurements were obtained. The change in FP relative to vehicle controls is presented. n = 3 ± SEM.
(G) The extent of eIF4A1:RNA binding stimulated by CR-1-31-B scales with polypurine content. FAM-labeled RNA was incubated with 500 nM eIF4A1 and the indicated concentration of CR-1-31-B for 30 min, after which time FP measurements were obtained. The change in FP obtained relative to vehicle controls is presented. n = 3 ± SEM.

4.4.2 Comparative Assessment of Rocaglate-Induced eIF4A:RNA Binding

The interest towards rocaglates as potential anti-neoplastic agents and the significant efforts made towards the development of synthetic strategies have greatly expanded the number of members in this family (Qian et al., 2016). However, it has also meant that various laboratories are employing different rocaglates in biological studies. These include the natural products, silvestrol and RocA, as well as the synthetic derivatives CR-1-31-B, SDS-1-021, RHT, and FL3 (Figs. 4.1D, 4.2A). The *X*-ray crystal structure of eIF4A1 complexed with RocA and poly r(AG)$_5$ RNA revealed that aryl rings A and B (Figure 4.2A) stack with adjacent adenine and guanine bases, respectively (Iwasaki et al., 2019). In addition, the C8b-OH hydrogen bonds to the N7 of the same guanine stacked to aryl ring B. One outstanding question is whether structural differences among rocaglates can influence polypurine sequence preference. To address this, we took advantage of an in-house curated library of >200 rocaglates (which are part of the BU-CMD collection) to rank compounds for their ability to stimulate eIF4A1:RNA binding (Figure 4.2B). We were also interested to see if there were any rocaglate capable of imparting a polypyrimidine [poly r(UC)$_8$] specificity to eIF4A1 but found that none of the compounds in our collection possessed this property (Figure 4.2B). We also did not identify any

rocaglate that significantly stimulated RNA binding to eIF4A1 over eIF4A2 or vice versa (Figure 4.2C, Suppl Table S4.1). This is perhaps not surprising since the two amino acids involved in rocaglate binding (F163 [F164 in eIF4A2] and Q195 [Q196 in eIF4A2]) are conserved between the two proteins. A significant proportion of compounds stimulated binding of poly r(AG)$_8$ RNA to both eIF4A1 and eIF4A2 (Figure 4.2C, Suppl Table S4.1).

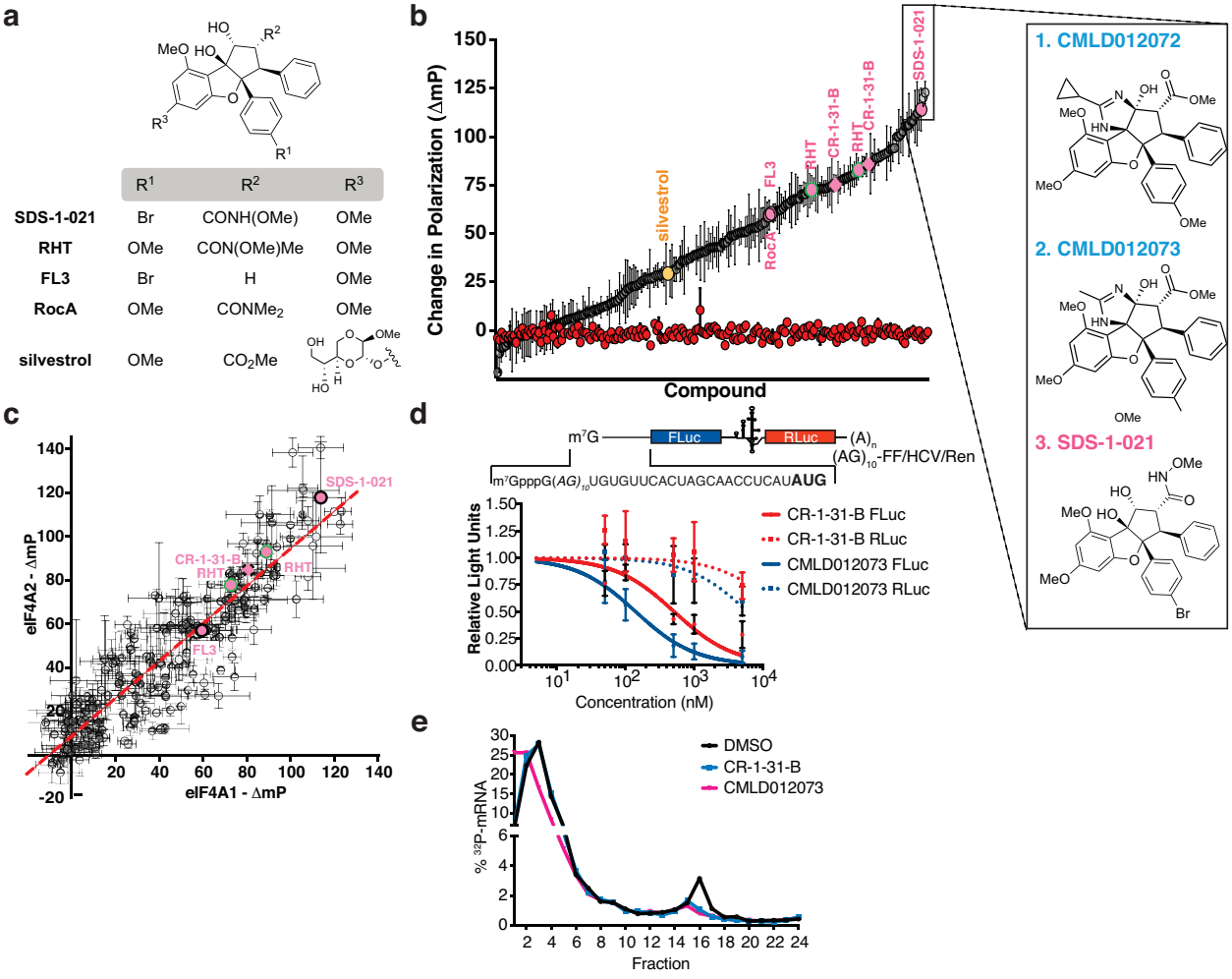

Figure 4.2 Rocaglate Activity Profiling

(A) Chemical structure of the most commonly used rocaglates in biological studies.

(B) Assessing eIF4A1:poly r(AG)$_8$ (gray circles) or eIF4A1:poly r(UC)$_8$ (red circles) RNA binding by FP in the presence of 10 μM rocaglate. Values are expressed relative to the DMSO control (containing RNA and protein in the absence of compound) and data is rank ordered. n = 3 ± SEM. Expanded view to the right shows the structures of the top three rocaglate hits. The duplication of RHT and CR-1-31-B represent independent compound preparations of different enantiomeric composition (see Table S4.1, column I for more details).

(C) Change in polarization obtained with eIF4A1:poly r(AG)$_8$ and eIF4A2:poly r(AG)$_8$ RNA. Pearson's r = 0.814; p < 0.0001.
(D) Inhibition of cap-dependent and independent translation (as reflected by firefly and renilla relative light units, respectively) measured in response to compound in Krebs-2 extracts programmed with mRNA. n = 3 ± SEM.
(E) ^{32}P-labeled (AG)$_{10}$-FF/HCV/Ren mRNA was incubated with 100 nM eIF4A1 in the presence of 500 nM compound for 10 min at room temperature, then added to RRL in the presence of 600 μM cycloheximide. Complexes were resolved by sedimentation through a 10%–30% glycerol gradient.

4.4.3 ADRs Represent a Class of Potent Rocaglates

Among the most potent inhibitors of translation uncovered by our screen were two ADRs, CMLD012072 and CMLD012073 (Figure 4.2B). These arose as a consequence of a recently described intercepted retro-Nazarov reaction that was harnessed to generate novel rocaglates (Zhang et al., 2019). The ADRs are distinguished from other rocaglates by the presence of an additional heterocyclic ring (imidazoline) which is fused to the cyclopenta[*b*]benzofuran core (Figure 4.2B). In *in vitro* translation assays, CMLD012073 was ~3-fold more potent at inhibiting cap-dependent translation (FF) than CR-1-31-B (Figure 4.2D). In ribosome recruitment experiments, CMLD012073 (and CR-1-31-B) diminished assembly of the 80S ribosome on the mRNA, thus further supporting the notion that this compound acts as an inhibitor of initiation (Figure 4.2E).

To characterize this novel chemical series, we synthesized 21 additional congeners and determined their relative potency towards inhibiting translation *in vitro* and cellular cytotoxicity (Figure 4.3A and Suppl. Table S4.2). Among these was CMLD012612, an ADR containing an hydroxamate group, which we found to be the most potent analogue (Figure 4.3A, B). We have previously demonstrated that the addition of the hydroxamate moiety improves rocaglate potency (Roche et al., 2010; Rodrigo et al., 2012). Compounds containing this moiety (e/.g. CR-1-31-B, RHT, and SDS-1-0-21) ranked highly among all rocaglates in our collection with respect to enhancing eIF4A1:RNA binding (Figure 4.2B). To understand how the imidazoline modification present in the

amidino-rocaglates impacts binding in the context of available structural data, we computationally modeled CMLD012612 into the 5ZC9 structure (Figure 4.3C). The modeled pose shows stacking of aryl rings A and B with RNA bases A7 and G8, respectively. Interactions with eIF4A1 F163 is mediated by ring C and with Q195 by the C1-OH and C2 carbonyl. We observed a potential hydrogen bond interaction (2.4 Å) between the imidazoline N-H (shown in white) and N7 of G8. This interaction is reminiscent of the hydrogen bond between N7 of G8 and the 8b-OH of RocA, previously attributed as the main driver of purine-selectivity (Iwasaki et al., 2019).

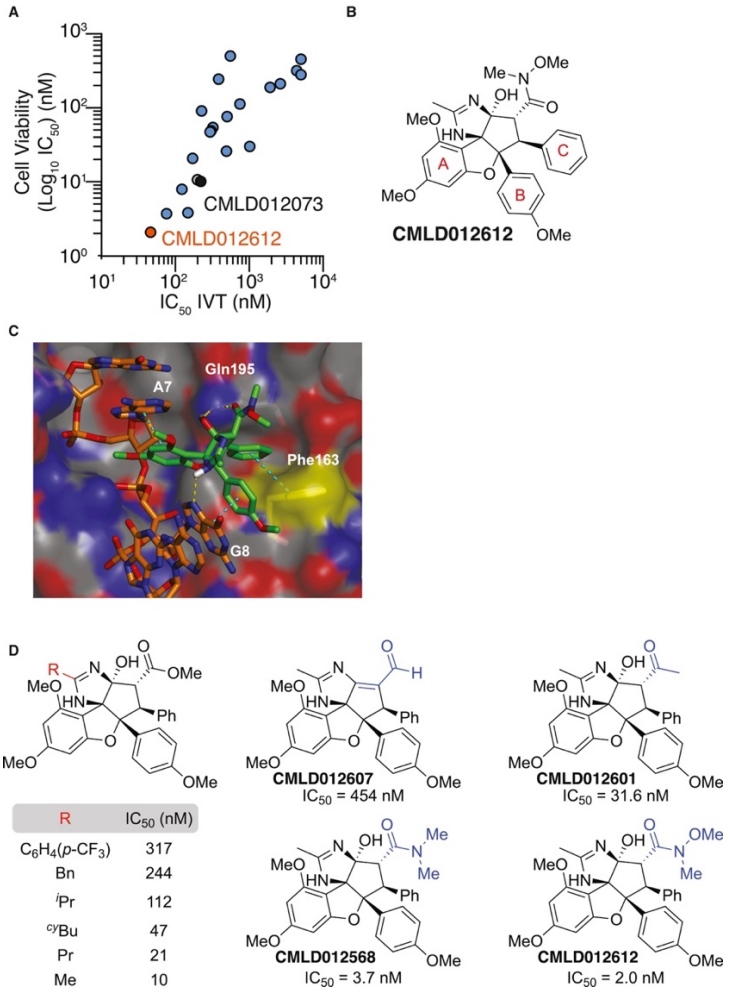

R	IC_{50} (nM)
$C_6H_4(p\text{-}CF_3)$	317
Bn	244
^{i}Pr	112
^{cy}Bu	47
Pr	21
Me	10

Figure 4.3 ADRs Represent a Potent Class of Rocaglates

(A) The IC_{50} for cytotoxicity against NIH/3T3 cells versus inhibition of *in vitro* translation is plotted for the ADR subfamily. Translation reactions were performed in RRL programmed with 10 ng/mL m^7GpppG-$(AG)_{10}$-FF/HCV/Ren. n = 3. See Table S4.2 for SEM values. Pearson's r = 0.69, $p < 0.001$.

(B) Structure of CMLD012612.
(C) Modeling of ADR CMLD012612 into the published X-ray structure of RocA in complex with eIF4A1 and poly-$(AG)_5$ RNA (PDB: 5ZC9). Hydrogen bonds are represented by a yellow line and π-stacking interactions are shown in cyan.
(D) SAR analysis of ADRs.

To establish initial structure activity relationships (SAR) for amidino rocaglates (ADRs), we compared IC_{50}'s of compounds against NIH/3T3 cells (Figure 4.3A). We noticed increased cytotoxicity with the decrease of the rigidity and size of the imidazoline substituent (Figure 4.3D, red). In particular, an ADR bearing a methyl (Me) group exhibited an IC_{50} of 10 nM. Subsequently, we evaluated substitution of the ADR carbonyl moiety (blue) where we found increased cytotoxicity of the electron-rich carbonyls (Figure 4.3D, NMe(OMe) > NMe_2 > OMe > Me > H). Of note, the stereochemistry of ADRs is also critical to biological activity, where we found minimal cytotoxicity (IC_{50} = 454 nM) for the unsaturated aldehyde CMLD012607. The latter trends appear to correlate with the strong ability of the hydroxamate CMLD012612 as a hydrogen bond acceptor to the Q195 residue of eIF4A selectivity (Iwasaki et al., 2019; Rodrigo et al., 2012; Tecle et al., 2009).

The activity of CMLD012612 surpasses those of our previous lead compounds, CR-1-31-B and CMLD012073, with respect to inhibition of cellular translation (Figure 4.4A), and cytotoxicity towards NIH/3T3 cells (Figure 4.4B; IC_{50} ~ 2 nM). This cytotoxicity was significantly blunted in $eIF4A1^{em1JP}$ cells, a CRISPR-engineered NIH/3T3 line harboring rocaglate-resistant eIF4A1(F163L) alleles (Figure 4.4B, Suppl Table S4.2), demonstrating that the mechanism of action of CMLD012612 is eIF4A1 dependent.

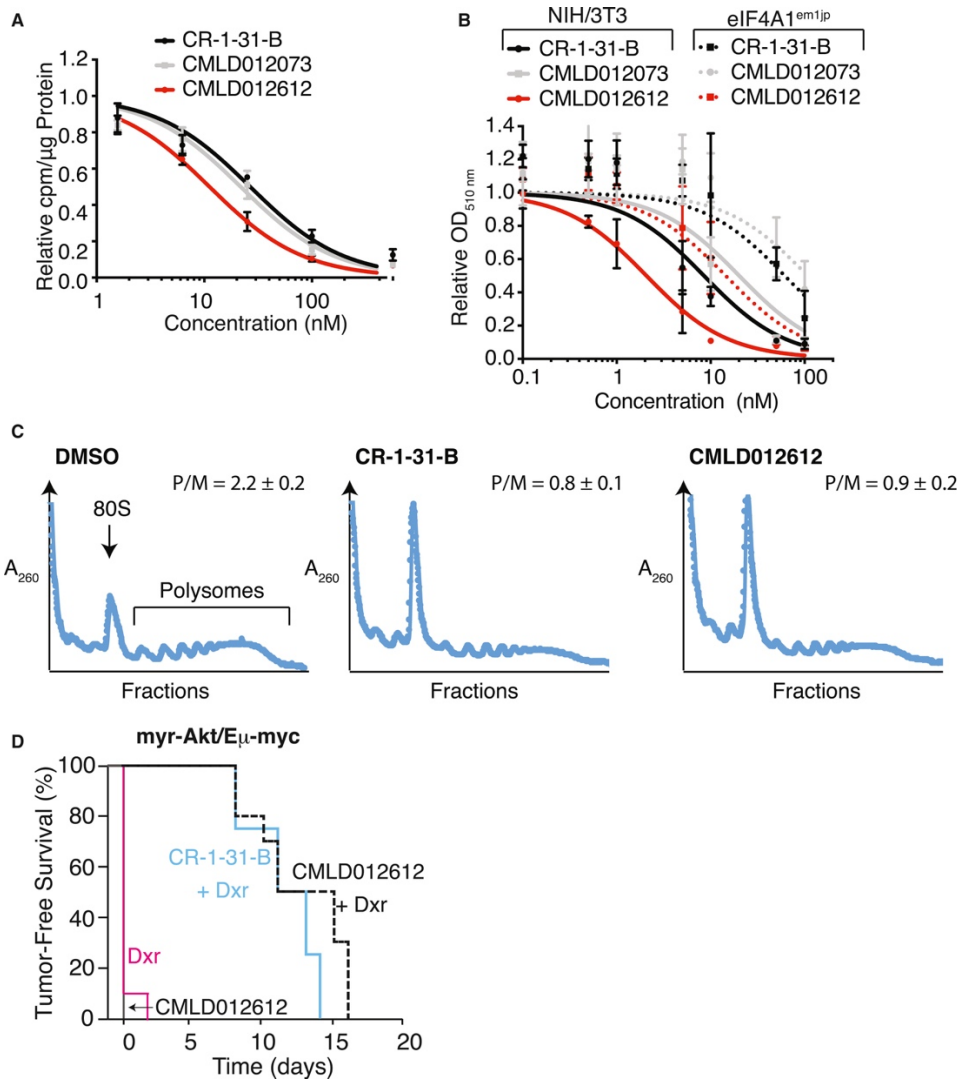

Figure 4.4 CMLD012612 Inhibits Tumor Cell Survival

(A) Inhibition of [^{35}S]-methionine incorporation in HEK293 cells following 1 h of compound exposure. n = 3 ± SEM.

(B) Cytotoxicity of CMLD012612 toward NIH/3T3 and eIF4A1^{em1JP} cells following 4 days of compound exposure. n = 3 ± SEM.

(C) CMLD012612 inhibits translation *in vivo* in the liver. Mice were injected with vehicle or CMLD012612 (0.5 mg/kg). Cytoplasmic extracts were prepared from livers 3 h later and resolved on 10%–50% sucrose gradients by centrifugation in an SW40 rotor at 150,000 × *g* for 2 h. Plotted are results of one representative experiment of two that showed similar results. The positions of 80S ribosomes and polysomes in the gradient are labeled, and the polysome/monosome (P/M) ratios indicated.

(D) CMLD012612 sensitizes Myr-Akt/*E*μ-*Myc* tumors to doxorubicin *in vivo*. Kaplan-Meier plot showing tumor-free survival of mice bearing Myr-Akt/*E*μ-*Myc* tumors following treatment with doxorubicin (Dox, red line; n = 10), CMLD012612 (solid black line; n = 10), CR-1-31-B + Dox (blue line; n = 4), or CMLD012612 + Dox (dashed black line; n = 10). $p < 0.003$ for CR-1-31-B + Dox versus Dox, and $p < 0.00001$ for CMLD012612 + Dox versus Dox.

Rocaglates are capable of chemo-sensitizing drug resistant tumors, as first reported using engrafted Pten$^{+/-}$Eμ-*myc* and Eμ-*myc*/eIF4E tumors in syngeneic mice (Bordeleau et al., 2008). The Eμ-Myc model is an *in vivo* tumor model that is capable of recapitulating many pathological features observed in Non-Hodgkin lymphomas. Dysregulation of mTOR signaling (such as through inactivation of Pten or sustained Akt activity) in this model accelerates tumor onset, suppresses apoptosis, and confers resistance towards conventional chemotherapies such as cyclophosphamide and doxorubicin. However, suppression of eIF4F has been shown to restore chemosensitivity. To characterize the *in vivo* activity of CMLD012612, we first assessed the ability of the compound to inhibit translation following intraperitoneal delivery. CMLD012612, like CR-1-31-B, effectively suppressed liver polysomes 3 h after injection indicating inhibitory activity towards protein synthesis (Figure 4.4C). When administered to mice bearing Myr-Akt/*E*μ-*Myc* lymphomas, CMLD012612 effectively synergized with doxorubicin leading to complete tumor loss that extended to 15-16 days (Figure 4.4D).

Our large-scale screen has identified a novel, potent class of rocaglates – the ADRs. This screen has also guided us in the design of an ADR derivative, CMLD012612, which was found to be more potent than previous lead compounds. Whereas the IC_{50} of CR-1-31-B towards NIH/3T3 cells is ~8.5 nM, CMLD012612 displays an IC_{50} of ~2 nM (Figure 4.4B). The primary mechanism of action of CMLD012612 is dependent on eIF4A1, since eIF4A^{em1jp} cells are at least 10-fold more resistant than parental NIH/3T3 cells. The sensitivity of eIF4A^{em1jp} cells to CMLD012612 observed at higher concentrations may be due to the presence of wild-type eIF4A2 in the cells. Our results highlight the value of further exploring modification of the rocaglate core including the C8b position for improving and extending the potency of rocaglates, while retaining *in vivo* activity. Taken together, these results

identify ADRs as a potent subclass of inhibitors capable of targeting eIF4A-mediated initiation *in vitro* and *in vivo*.

4.5 Significance

The ability of rocaglates to function as interfacial inhibitors offers an opportunity by which to identify new functional family members. Given the keen interest in this class of compounds as well as their target, we characterized the RNA binding specificity of eIF4A1 and eIF4A2 and found that both are quite similar in sequence preference and in their response to rocaglates. A screen of >200 rocaglates identified amidino-rocaglates – a novel, potent chemical series extending knowledge on the structure-activity relationship of these compounds.

4.6 STAR ★ Methods

4.6.1 Key Resources Table

REAGENT or RESOURCE	SOURCE	IDENTIFIER
Bacterial and Virus Strains		
E.coli BL21(DE3)pLys	Promega	Cat#: L1195
E.coli DH10B	New England Biolabs	Cat#: C3019I
Chemicals, Peptides, and Recombinant Proteins		
UTP, [α-32P]- 3000Ci/mmol	Perkin Elmer	Cat#: BLU507H250UC
Cycloheximide	Sigma-Aldrich	Cat#: C7698-5G
EasyTag™ EXPRESS 35S Protein Labeling Mix	Perkin Elmer	Cat#: NEG772007MC
Sulforhodamine B sodium salt	Sigma-Aldrich	Cat#: S1402-5G
T3 RNA polymerase	New England Biolabs	Cat#: M0378S

REAGENT or RESOURCE	SOURCE	IDENTIFIER
$m^7G(5')ppp(5')G$ RNA cap structure analog	New England Biolabs	Cat#: S1404S
AMP-PNP	Sigma-Aldrich	Cat#: 10102547001
L-methionine	Sigma-Aldrich	Cat#: M9625
Sephadex G-25	GE Life Sciences	Cat#: 17003101
His_6-eIF4A1	This Paper	N/A
His_6-eIF4A2	This Paper	N/A
Critical Commercial Assays		
DC Protein Assay	Bio-Rad	Cat#: 5000112
Experimental Models: Cell Lines		
Mouse: NIH/3T3	ATCC	RRID: CVCL_0594
Mouse: $eIF4A1^{em1JP}$	NIH/3T3 cell line generated through CRISPR/Cas9 editing (Chu et al., 2016)	
Human: HEK293T	ATCC	RRID: CVCL0063
Mouse: Eμ-Myc/Myr-Akt lymphoma cells	Wendel et al., 2004	
Experimental Models: Organisms/Strains		
Mouse: C57BL/6J Mice	Jackson Laboratories	Cat#: 000664
Oligonucleotides		
5' 6-FAM (Fluorescein)	Integrated DNA Technologies	N/A
Recombinant DNA		
pET15b-His_6-eIF4A	Bordeleau et al., 2005	N/A
pKS-FF-HCV-Ren	Novac et al., 2004	N/A
Software and Algorithms		
Prism 7.0c	Graphpad	https://www.graphpad.com/

4.6.2 Lead Contact and Materials Availability

Further information and requests for resources and reagents should be directed to and will be fulfilled by Jerry Pelletier (Lead Contact) (jerry.pelletier@mcgill.ca) or John A. Porco, Jr. (porco@bu.edu).

4.6.3 Experimental Model and Subject Detail

All cell lines used in this study were maintained in DMEM supplemented with 10% FBS (Wisent), 100 U/mL penicillin/streptomycin, and 2 mM L-glutamine at 37°C and 5% CO_2. Animal studies were approved by the McGill University Faculty of Medicine Animal Care Committee. All mice used in this study were female C57BL/6 mice, aged 6-8 weeks.

4.6.4 Compounds

Rocaglate derivatives provided from the BU-CMD collection were synthesized using ESIPT photocycloaddition of 3-hydroxyflavones with cinnamates as previously published followed by further functionalizations (Rodrigo et al., 2012; Stone et al., 2015; Yueh et al., 2017). Note that there are duplicate values for some compounds in this collection from different synthesis batches or containing two enantiomers (see Supp Table S4.1). Compounds were resuspended to 10 mM in neat DMSO and stored at -80° C.

4.6.5 Purification of Recombinant Proteins

BL21 (DE3) *E. coli* cells were transformed with pET15b-His_6-eIF4A1 or pET15b-His_6-eIF4A2 plasmids. Single colonies were picked and grown in an overnight starter culture at 37°C in LB media supplemented with 100 mg/L ampicillin. On the following day, the starter culture was used to inoculate at a 1:50 dilution, and the cultures continued growing at 37°C. When the OD_{600} reached 0.6-0.8, 1 mM IPTG was added to induce protein production and the cultures were grown for an additional 3 h. Cells were pelleted, resuspended in a buffer containing 20 mM Tris (pH 7.5), 10%

glycerol, 0.1 mM EDTA, 200 mM KCl, 0.1% Triton X-100, 3.4 mM β-mercaptoethanol, and sonicated. The lysates were cleared via centrifugation and supplemented with 20 mM imidazole prior to loading onto a Ni-NTA agarose column (Qiagen). The column was washed 3 times with 4 column volumes of wash buffer 1 (20 mM Tris (pH 7.5), 10% glycerol, 0.1 mM EDTA, 800 mM KCl, 20 mM imidazole), and then washed 3 more times with 4 column volumes of wash buffer 2 (Wash buffer 1 containing 300 mM KCl). Elution was achieved using Wash buffer 2 supplemented with 200 mM imidazole and dialyzed overnight in a buffer containing 20 mM Tris (pH 7.5), 10% glycerol, 0.1 mM EDTA, 100 mM KCl, and 2 mM DTT. The resulting samples were further purified using a Q-Sepharose Fast Flow (Amersham) column and eluted with a 100 - 500 mM KCl gradient in 20 mM Tris (pH 7.5,) 10% glycerol and 0.1 mM EDTA. Eluted fractions of high protein yield and purity (as assessed by Coomassie blue staining) were combined and dialyzed against 20 mM Tris (pH 7.5), 10% glycerol, 0.1 mM EDTA and 2 mM DTT.

4.6.6 *In Vitro* Translation Assays

In vitro translation assays performed in Krebs-2 cell extracts supplemented with 5 mM $MgCl_2$, 30 mM Tris-HCl (pH 7.5), 1.5 mM ATP, 0.1 mM GTP, 0.6 mM CTP, 10 mM διποτασσιυμ creatine phosphate, 80 μg/mL creatine kinase, and 0.04 mM amino acids. The specified mRNA reporters were added to each reaction at a final concentration of 10 ng/mL. Translation reactions were performed in the presence or absence of compound for 60 minutes at 30°C prior to the measurement of luciferase activities.

4.6.7 Fluorescence Polarization Assays

Unless otherwise specified, eIF4A (500 nM) was incubated with 10 nM FAM-labelled RNA for 30 min in FP buffer (14.4 mM HEPES-NaOH (pH 8), 108 mM NaCl, 1 mM $MgCl_2$, 14.4%

glycerol, 0.1% DMSO, 2 mM DTT, 1 mM AMPPNP) at room temperature in black, low volume 384 well plates (Corning 3820). FP readings were performed on a Pherastar FS microplate reader (BMG Labtech). In Table S1, compounds were tested at a final concentration of 10 μM.

4.6.8 Sulforhodamine B (SRB) Assay

NIH/3T3 cells were seeded at a density of 1000 cells/well in a 96 well format and incubated in presence of 40 nM compound. After 4 days of culture, cells were washed with PBS, fixed with 50% trichloroacetic (TCA) acid for 1 hour, and stained with 0.5% Sulforhodamine B in 1% acetic acid for 15 min. Plates were then washed 5 times with 1% acetic acid, dried, and the stained wells were resuspended with 10 mM Tris (pH 9) prior to measuring the absorbance at 510 nm on a SpectraMax M5 (Molecular Devices).

4.6.9 [^{35}S]-Methionine Labeling

293T cells were seeded at a density of 40 000 cells per well in a 24 well plate and on the following day incubated in the presence of the indicated concentration of compound in methionine/cysteine-free media supplemented with 10% dialyzed FBS for 1 hour. *De novo* protein synthesis was monitored through the addition of S^{35}methionine/cysteine labelling mix (1175 Ci/mmol) and incubating the cells for an additional 15 min. The labeling reaction was terminated by washing the cells twice with ice cold PBS and lysing with RIPA buffer. Half of the lysate was then spotted onto 3 MM Whatman paper that had been pre-blocked with amino acids and precipitated using 10% trichloroacetic acid (TCA) at 4°C for 20 min. The spotted samples were boiled in 5% TCA for 15 min, washed twice with 5% TCA, followed by one wash with 75% EtOH, dried, and quantitated using scintillation counting. Protein concentration was determined with the DC Protein assay (BioRad) and used for normalization.

4.6.10 Ribosome Binding Assays

^{32}P-labeled $(AG)_{10}$-FF/HCV/Ren mRNA was incubated with 100 nM eIF4A1 in the presence of 500 nM compound for 10 min at RT, then added to rabbit reticulocyte lysates in the presence of 600 μM cycloheximide. Incubations were performed at 30°C for 10 min after which time, the lysate was applied onto a 10-30% glycerol gradient. Centrifugation was for 3.5 h at 39,000 rpm at 4°C in an SW40 rotor. Fractions were collected using a Brandel Tube Piercer connected to an ISCO fraction collector and radioactivity was determined by scintillation counting.

4.6.11 Liver Polysomes

For polysome profiling analysis on liver extracts, female C57BL/6 mice were treated at a single dose of either vehicle (5.2% PEG400/5.2% Tween-80), 0.2 mg/kg CR-1-31-B or 0.5 mg/kg CMLD012612 and animals sacrificed 3 h after injection. Livers were excised, washed in cold PBS containing 100 μg/mL cycloheximide and homogenized in 3 volumes of lysis buffer (40 mM HEPES (pH 7.5), 100 mM KCl, 5 mM $MgCl_2$, 100 μg/mL cycloheximide) in a Eurostar Power-b homogenizer (IKA Liver Labortechnik, Staufen, Germany). After homogenization, samples were centrifuged for 10 min at 1200 x g and 4°C and the supernatant transferred to a new tube.

Three hundred microliter of detergent mix (0.5% Triton X-100 and 0.5% sodium deoxycholate) were added to 150 μl of supernatant and the sample spun briefly (10,000 x g for 10 min) before loading onto 10-50% sucrose gradients and centrifuged in an SW40 rotor at 35 000 rpm for 135 min. Gradients were analyzed by piercing the tube with a Brandel tube piercer and passing 60% sucrose through the bottom of the tube. Recording of the data was performed using InstaCal Version 5.70 and TracerDaq Version 1.9.0.0 (Measurement Computing Corporation, Norton, MA).

4.6.12 Lymphoma Studies

A total of 2×10^6 Eμ-Myc/Myr-Akt lymphoma cells were injected into the tail vein of 6 - 8 week-old female C57BL/6 mice. Upon development of well-palpable tumors (auxiliary and inguinal lymph nodes), mice were injected intraperitoneal (IP) with doxorubicin (once at 10 mg/kg) or CMLD012612 (0.2 mg/kg daily for 5 days). In combination studies, CMLD012612 was administered once daily for 5 consecutive days, while doxorubicin was administered on day 2. Tumor-free survival is defined as the time between disappearance and reappearance of a palpable lymphoma following treatment.

4.6.13 Quantification and Statistical Analysis

All values reported in this study represent the mean ± SEM of at least 3 biological replicates. The IC_{50} values for *in vitro* translation in Krebs extracts and cell viability were determined from 3-5 independent experiments using 6 concentration points and were fitted using nonlinear regression on Graphpad Prism 7.0c.

4.7 Acknowledgments

This work was supported by a Canadian Institutes of Health Research (CIHR) Foundation grant (FDN-148366) to JP, and research grants from the NIH to JAP, Jr. (R35 GM118173, R24 GM-111625, R01 GM-067041).

4.8 Author Contributions

J.C., W.Z., J.A.P. Jr, and J.P. conceived and designed this study. J.C., W.Z., R.C., W.G.D., and L.E.B. acquired, analyzed, and interpreted data. T.H. provided essential reagents. J.C. and J.P. wrote the manuscript. All authors commented on, edited and approved the manuscript.

4.9 Declaration of Interests

J.C., W.Z., J.A.P. Jr, and J.P. have filed a US provisional patent application on the use of amidino- and amino-rocaglates as novel translation inhibitors and anticancer agents.

4.10 Supplemental Figures

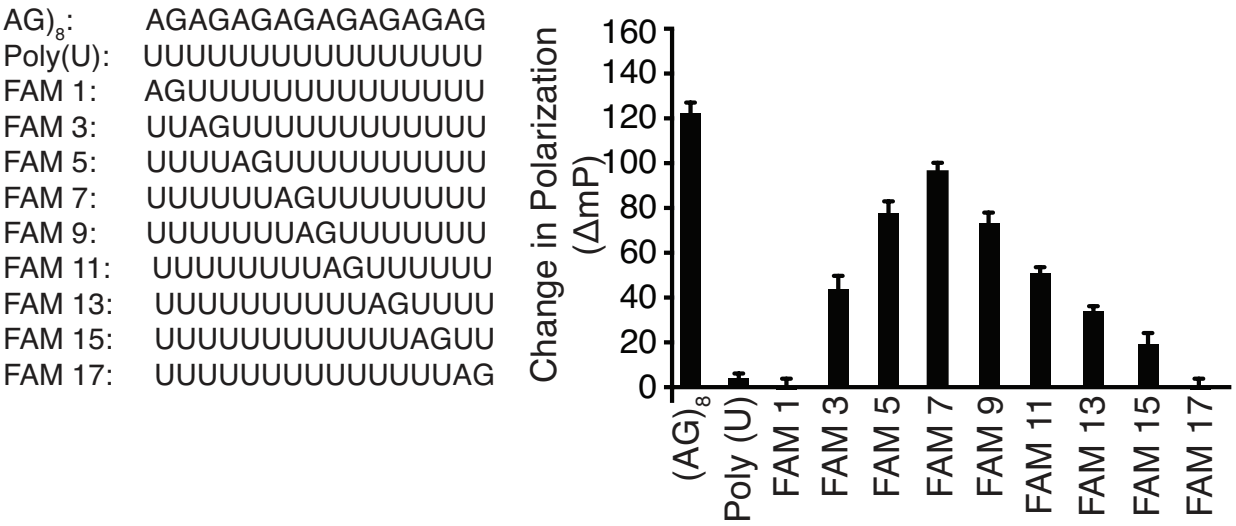

Figure S4.1 Related to Figure 4.1. Effect of AG Position on Rocaglate-Stimulated eIF4A1:RNA Binding

The location of a single AG dinucleotide within a poly r(U) track promotes rocaglate-stimulated eIF4A1:RNA binding. The RNA sequences used in this experiment are indicated to the left and the FP results obtained with these are plotted to the right. eIF4A1:RNA binding assays were performed in the presence of vehicle or 50 μM CR-1-31-B. n = 4 ± SEM.

4.11 References

Abramson, R.D., Dever, T.E., Lawson, T.G., Ray, B.K., Thach, R.E., and Merrick, W.C. (1987). The ATP-dependent interaction of eukaryotic initiation factors with mRNA. J Biol Chem 262, 3826-3832.

Bhat, M., Robichaud, N., Hulea, L., Sonenberg, N., Pelletier, J., and Topisirovic, I. (2015). Targeting the translation machinery in cancer. Nat Rev Drug Discov 14, 261-278.

Bordeleau, M.E., Matthews, J., Wojnar, J.M., Lindqvist, L., Novac, O., Jankowsky, E., Sonenberg, N., Northcote, P., Teesdale-Spittle, P., and Pelletier, J. (2005). Stimulation of mammalian translation initiation factor eIF4A activity by a small molecule inhibitor of eukaryotic translation. Proc Natl Acad Sci U S A 102, 10460-10465.

Bordeleau, M.E., Robert, F., Gerard, B., Lindqvist, L., Chen, S.M., Wendel, H.G., Brem, B., Greger, H., Lowe, S.W., Porco, J.A., Jr., et al. (2008). Therapeutic suppression of translation initiation modulates chemosensitivity in a mouse lymphoma model. J Clin Invest 118, 2651-2660.

Chen, Z.H., Qi, J.J., Wu, Q.N., Lu, J.H., Liu, Z.X., Wang, Y., Hu, P.S., Li, T., Lin, J.F., Wu, X.Y., et al. (2019). Eukaryotic initiation factor 4A2 promotes experimental metastasis and oxaliplatin resistance in colorectal cancer. Journal of experimental & clinical cancer research : CR 38, 196.

Chu, J., Galicia-Vazquez, G., Cencic, R., Mills, J.R., Katigbak, A., Porco, J.A., Jr., and Pelletier, J. (2016). CRISPR-Mediated Drug-Target Validation Reveals Selective Pharmacological Inhibition of the RNA Helicase, eIF4A. Cell Rep 15, 2340-2347.

Ebada, S.S., Lajkiewicz, N., Porco, J.A., Jr., Li-Weber, M., and Proksch, P. (2011). Chemistry and biology of rocaglamides (= flavaglines) and related derivatives from aglaia species (meliaceae). Prog Chem Org Nat Prod 94, 1-58.

Galicia-Vazquez, G., Cencic, R., Robert, F., Agenor, A.Q., and Pelletier, J. (2012). A cellular response linking eIF4AI activity to eIF4AII transcription. RNA 18, 1373-1384.

Iwasaki, S., Floor, S.N., and Ingolia, N.T. (2016). Rocaglates convert DEAD-box protein eIF4A into a sequence-selective translational repressor. Nature 534, 558-561.

Iwasaki, S., Iwasaki, W., Takahashi, M., Sakamoto, A., Watanabe, C., Shichino, Y., Floor, S.N., Fujiwara, K., Mito, M., Dodo, K., et al. (2019). The Translation Inhibitor Rocaglamide Targets a Bimolecular Cavity between eIF4A and Polypurine RNA. Mol Cell 73, 738-748 e739.

King, M.L., Chiang, C.-C., Limng, H.-C., Fujita, E., Ochiai, M., and McPhail, A.T. (1982). X-Ray Crystal Structure of Rocaglamide, a Novel Antileukemic I H-Cyclopenta[b] benzofuran from Aglaia elliptifolia. J Chem Sco Chem Commun 20, 1150-1151.

Nielsen, P.J., and Trachsel, H. (1988). The mouse protein synthesis initiation factor 4A gene family includes two related functional genes which are differentially expressed. EMBO J 7, 2097-2105.

Novac, O., Guenier, A.S., and Pelletier, J. (2004). Inhibitors of protein synthesis identified by a high throughput multiplexed translation screen. Nucleic Acids Res 32, 902-915.

Pan, L., Woodard, J.L., Lucas, D.M., Fuchs, J.R., and Kinghorn, A.D. (2014). Rocaglamide, silvestrol and structurally related bioactive compounds from Aglaia species. Nat Prod Rep 31, 924-939.

Pelletier, J., and Sonenberg, N. (2019). The Organizing Principles of Eukaryotic Ribosome Recruitment. Annu Rev Biochem 88, 307-335.

Qian, Z., Hussein, A.-H., and Laurent, D. (2016). Recent Advances in the Synthesis of Flavaglines, a Family of Potent Bioactive Natural Compounds Originating from Traditional Chinese Medicine. Eur J Org Chem 2016, 5908 - 5916.

Ribeiro, N., Thuaud, F., Nebigil, C., and Desaubry, L. (2012). Recent advances in the biology and chemistry of the flavaglines. Bioorg Med Chem 20, 1857-1864.
Roche, S.P., Cencic, R., Pelletier, J., and Porco, J.A., Jr. (2010). Biomimetic photocycloaddition of 3-hydroxyflavones: synthesis and evaluation of rocaglate derivatives as inhibitors of eukaryotic translation. Angew Chem Int Ed Engl 49, 6533-6538.
Rodrigo, C.M., Cencic, R., Roche, S.P., Pelletier, J., and Porco, J.A. (2012). Synthesis of rocaglamide hydroxamates and related compounds as eukaryotic translation inhibitors: synthetic and biological studies. J Med Chem 55, 558-562.
Rogers, G.W., Jr., Komar, A.A., and Merrick, W.C. (2002). eIF4A: the godfather of the DEAD box helicases. Prog Nucleic Acid Res Mol Biol 72, 307-331.
Sokabe, M., and Fraser, C.S. (2017). A helicase-independent activity of eIF4A in promoting mRNA recruitment to the human ribosome. Proc Natl Acad Sci U S A 114, 6304-6309.
Svitkin, Y.V., Pause, A., Haghighat, A., Pyronnet, S., Witherell, G., Belsham, G.J., and Sonenberg, N. (2001). The requirement for eukaryotic initiation factor 4A (elF4A) in translation is in direct proportion to the degree of mRNA 5' secondary structure. RNA 7, 382-394.
Tecle, H., Shao, J., Li, Y., Kothe, M., Kazmirski, S., Penzotti, J., Ding, Y.H., Ohren, J., Moshinsky, D., Coli, R., et al. (2009). Beyond the MEK-pocket: can current MEK kinase inhibitors be utilized to synthesize novel type III NCKIs? Does the MEK-pocket exist in kinases other than MEK? Bioorg Med Chem Lett 19, 226-229.
Wolfe, A.L., Singh, K., Zhong, Y., Drewe, P., Rajasekhar, V.K., Sanghvi, V.R., Mavrakis, K.J., Jiang, M., Roderick, J.E., Van der Meulen, J., et al. (2014). RNA G-quadruplexes cause eIF4A-dependent oncogene translation in cancer. Nature 513, 65-70.
Yoder-Hill, J., Pause, A., Sonenberg, N., and Merrick, W.C. (1993). The p46 subunit of eukaryotic initiation factor (eIF)-4F exchanges with eIF-4A. J Biol Chem 268, 5566-5573.
Zhang, W., Chu, J., Cyr, A.M., Yueh, H., Brown, L.E., Wang, T.T., Pelletier, J., and Porco, J.A. (2019). Intercepted Retro-Nazarov Reaction: Syntheses of Amidino-Rocaglate Derivatives and Their Biological Evaluation as eIF4A Inhibitors. J Am Chem Soc. https://doi.org/10.1021/jacs.9b06446.

CHAPTER 5 ROCAGLATES CAUSE GAIN-OF-FUNCTION ALTERATIONS TO EIF4A AND EIF4F

Manuscript Under Revision:

Chu J., Zhang W., Cencic R., O'Connor P. B. F., Robert F., Devine W. G., Selznick A., Henkel T., Merrick W. C., Brown L. E., Porco J. A. Jr., and Pelletier J. (2019). Rocaglates Cause Gain-of-Function Alterations to eIF4A and eIF4F, *Cell Rep.* **Under Revision**

5.1 Preface to Chapter 5

As shown in the chapter 4, the presence of different chemical moieties can influence compound bioactivity. However, it also conceivable that structural differences can modify compound mechanism of action. A recent study published by Iwasaki and colleagues identified that rocaglamide A causes preferential inhibition of translation of mRNAs with enriched with polypurine repeats (Iwasaki et al., 2016). However, purine richness was not identified as a sensitizing element in ribosome profiling studies performed using silvestrol (Rubio et al., 2014; Wolfe et al., 2014). It is possible that this discrepancy stems from differences in mechanism between silvestrol and RocA. To address whether different rocaglates analogs possess non-identical mechanisms of action, we tested the rocaglate library introduced in chapter 4 with respect to their ability to stimulate eIF4A:RNA association, inhibit translation *in vitro*, and impede cell growth.

5.2 Abstract

Rocaglates are a diverse family of biologically active molecules that have gained tremendous interest in recent years due to their promising activities in pre-clinical cancer studies. As a result, this has led to the significant expansion of this family of compounds through the development of efficient synthetic schemes. However, it is unknown whether all members of the rocaglate family act through similar mechanisms of action. Here, we present a comprehensive study comparing the biological activities of >200 rocaglates to better understand how the presence of different chemical entities influence their biological activities. Through this, we find that most rocaglates preferentially repress translation of mRNAs containing purine rich 5' leaders but intriguingly, certain rocaglates lack this bias in translation repression. We also uncover a novel aspect of rocaglate mechanism of action in which the pool translationally active eIF4F is diminished due to sequestration of the complex onto RNA.

5.3 Introduction

Translation is an essential process that enables cells to make rapid and spatiotemporal alterations to the proteome. Regulation of translation is critical to a wide variety of biological processes, including growth, differentiation, and development. Accordingly, aberrant translational control is associated with several pathological disorders. Much of translation regulation is imposed at the initiation phase, which is an intricate process involving the coordination of multiple essential factors. In the canonical mechanism of translation initiation, eukaryotic initiation factor (eIF) 4F complex (comprised of eIF4A, 4E, and 4G) binds to the mRNA 5' m^7GpppN cap to facilitate recruitment of 43S pre-initiation complexes (PIC: 40S ribosomal subunit and associated factors). The 43S PIC then scans the mRNA 5' leader in search of an appropriate initiation codon. Structural barriers within the

5' leader can affect an mRNA's dependency on eIF4F and consequently influence its ability to recruit a 43S PIC or alter the scanning efficacy of the 43S PIC (Pelletier and Sonenberg, 2019).

There is great interest in targeting translation initiation as it is a regulatory step that is frequently usurped in disease, and manipulation of this process can achieve selective changes in gene expression (Pelletier and Sonenberg, 2019). Of particular interest are small molecule inhibitors of eIF4A which differentially affect its activity. In the presence of hippuristanol, a poly-oxygenated steroid isolated from *Isis hippuris*, eIF4A loses its ability to bind to RNA (Bordeleau et al., 2006b). In contrast, a family of compounds collectively known as rocaglates stabilize eIF4A:RNA interactions. Rocaglamide A (RocA) causes eIF4A1 to preferentially clamp onto purine-rich regions of RNA and when this occurs within 5' leader regions, the stabilized eIF4A:RNA complex acts as a barrier for the scanning 43S PIC (Iwasaki et al., 2016; Iwasaki et al., 2019). However, this clamping barrier model does not fully explain the mechanism of inhibition by RocA. Moreover, purine content was not identified as a sensitizing element in ribosome profiling studies using silvestrol, which is a related member of the rocaglate family (Rubio et al., 2014; Wolfe et al., 2014). In these studies, 5' leader regions with long, structured sequences, the presence of G-quadruplexes, and low overall GC content were identified to be most significant. Whether this discrepancy can be attributed to the fact that different rocaglate entities were used in these studies is unknown and if so, this raises the question of whether every member of the rocaglate family operate through a shared common mechanism of action.

Over 100 rocaglates have been either isolated from natural sources or synthetically derived, and limitations in accessing specific structural entities have led to laboratories employing different molecules for their biological studies. In addition to RocA and silvestrol, commonly used include CR-1-31-B, FL3, RHT, and SDS-1-0-21 (Figure S1a). In this study, we address the question of whether

universal conclusions can be drawn across the rocaglate family. To this end, we characterize the biological activity of >200 rocaglates. In general, we found a strong correlation between the ability of a rocaglate to stimulate binding of eIF4A1 to RNA and their ability to inhibit translation. However, there were clear outliers suggesting that the presence of specific chemical groups within rocaglates can differentially modulate eIF4A activity and caution must be taken when formulating global generalizations across all rocaglate family members. We also expand our understanding of the mechanism of action of rocaglates and show that they can stabilize the eIF4F complex at the cap structure, exerting two previously unappreciated consequences on the initiation process: i) direct inhibition of translation of the target mRNA and ii) a bystander effect on mRNAs whose sequences are not directly targeted by rocaglates.

5.4 Results

5.4.1 Rocaglate-induced eIF4A1:RNA clamping is not a universal predictor of translation inhibition potency.

We have amassed a collection of >200 rocaglates and used this unique resource to quantitate their behaviour *in vitro* in Krebs-2 translation extracts and assess their ability to induced eIF4AI:RNA complexes using a fluorescence polarization (FP) assay with FAM labelled r$(AG)_8$ RNA. Overall, the ability of a rocaglate to stimulate eIF4A:RNA association correlates with inhibition of cap dependent translation *in vitro* (Figure 5.1A). However, silvestrol and two synthetic silvestrol derivatives (WGD-57-590 and WGD-57-591) deviate from this trend as these compounds exhibited relatively weak activity in the FP assay yet strongly inhibited cap-dependent translation (Figs 5.1A, S5.1B). We also noted compounds that were potent at inducing eIF4A1:RNA association, yet showed no or weak

activity towards cap-dependent translation *in vitro* (Figs 5.1A pink box, S5.1C). Among these were two cis-diol-containing rocaglaols (CMLD011166 and CMLD011167). This analysis also uncovered a new potent class of rocaglates, amidino-rocaglates (Figure 5.1A, yellow oval) whose characterization are reported elsewhere (Chu et al., 2019).

All rocaglates tested had a bias for polypurine containing RNAs over polypyrimidine substrates (Figs S5.1B, S5.1D, Table S5.1). In contrast, pateamine A, a structurally unrelated eIF4A inhibitor, potently induced eIF4A binding to all RNA substrates tested (Figure S5.1D). All rocaglate-induced eIF4A1:poly r$(AG)_8$ complexes were significantly more stable in the presence of the non-hydrolyzable ATP analog, AMP-PNP than in the presence of ATP (Figure S5.1E), as previously reported for eIF4A1:RocA:poly r$(AG)_8$. Therefore, a distinct change in RNA sequence specificity cannot explain the unusual behaviour of WGD-57-591 or CMLD011167.

5.4.2 Rocaglates show differing mRNA targeting spectra in translation assays.

The *in vitro* translation experiments described above were performed at a fixed rocaglate concentration (2 μM) using a generic bicistronic mRNA reporter (Novac et al., 2004). To better evaluate the consequences of eIF4A:polypurine clamping, we designed a series of reporters harboring cap-proximal polypurine tracks of varying lengths in their 5' leader region (Figure 5.1C). Translation reactions using mRNA reporters containing no AG dinucleotide, $(AG)_2$, $(AG)_5$, or $(AG)_{16}$ indicated that 5x (AG) was sufficient to elicit maximum inhibition of cap-dependent FF luciferase production by CR-1-31-B, while the HCV IRES remained recalcitrant to inhibition (Figure 5.1C).

We next tested the translational response of mRNA reporters with cap-proximal $(AG)_{10}$ or $(UC)_{10}$ sequences in the presence of select rocaglates (Figure 5.1D). CR-1-31-B and Roc A inhibited

cap-dependent translation from only the $(AG)_{10}$-containing mRNA, while exerting little effect on the $(UC)_{10}$ reporter (Figure 5.1D). Unexpectedly, silvestrol and WGD-57-591 equally inhibited both mRNA reporters (Figure 5.1D), even though they do not stimulate binding of recombinant eIF4A1 to polypyrimidine RNA (Figs 5.1B, S5.1D). The rocaglaol derivative, CMLD011167 failed to inhibit either reporter (Figure S5.2A), consistent with its apparent lack of *in vitro* activity in the previous experiments. The non-rocaglate eIF4A inhibitors, hippuristanol and pateamine A, equally repressed cap-dependent translation from both reporters, demonstrating that purine selectivity in translation inhibition is not shared among all eIF4A-targeting molecules (Figure S5.2a).

The difference in mRNA targeting spectrum observed between CR-1-31-B and silvestrol was not restricted to cap-proximal polypurine tracks, but also observed with reporters where the polypurine/polypyrimidine tracks were situated 15 nt downstream from the cap, although here the $(AG)_{10}$-reporter appeared more responsive to silvestrol than the $(UC)_{10}$-reporter (Figure S5.2B). Positioning a polypurine track within the 3' UTR did not sensitize translation of the mRNA to CR-1-31-B indicating that the influence of purine-richness is 5' leader-dependent (Figure S5.2C).

To complement the results described using the FP experiments, which looked at the binding activity of recombinant eIF4A in isolation, we performed biotinylated RNA pulldowns (RPDs) to evaluate whether rocaglates induced preferential association of eIF4A1 to polypurine templates in the presence of other initiation factors and competing RNA binding proteins. In these experiments, 30 nt biotinylated RNA baits were added to translation extracts in the presence or absence of rocaglate followed by purification using streptavidin beads. RPDs performed with CR-1-31-B or Roc A showed that eIF4A1 was recruited to the purine-rich template in a cap-independent manner (Figure S5.3A). Unlike the results obtained in the FP experiments, silvestrol stabilized eIF4A1 to both the polypurine and polypyrimidine baits (Figure S5.3A, right panels). When the RPDs were performed using with

purified eIF4A1 or eIF4F rather than translation extracts, no increase in eIF4A1:polypyrimidine RNA association was observed with silvestrol (Figure S5.3B). These results indicate that an additional co-factor present in translation lysates is required to stimulate eIF4A1 binding to pyrimidine sequences in the presence of silvestrol.

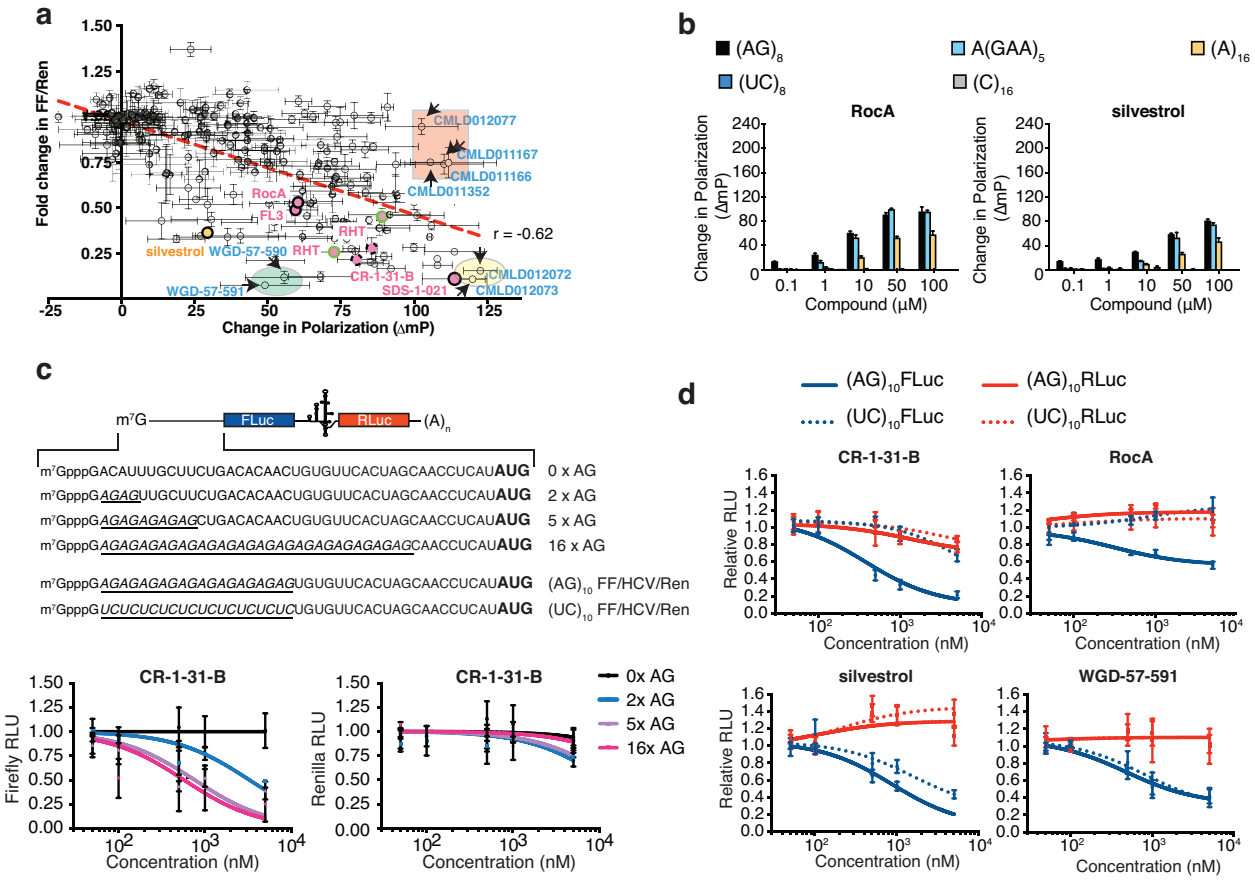

Figure 5.1 Different Rocaglates Exhibit Distinct Biological Activities. Related to Figures S5.1, S5.2, S5.3, and Table S5.1

(A) Polypurine clamping is a strongly correlative, but not universal, predictor cap dependent inhibition. The change in polarization obtained with eIF4A1:poly r(AG)$_8$ RNA was measured for each compound (10 μM) and is plotted against the fold inhibition for cap-dependent translation (2 μM) obtained in Krebs-2 extracts programmed with FF/HCV/Ren. Note the duplicate values for RHT (open circles) are due to two preparations of different enantiomeric purity, and for CR-1-31-B (dotted circles) are due to two different compound batches (see Table S5.1). Pearson r = -0.62; $p < 0.0001$.
(B) Rocaglates preferentially stimulate eIF4A binding onto purine rich RNAs. Different RNA probes were incubated in the presence of 500 nM eIF4A1 and compound for 30 min prior to measurement. The change in FP in the presence of compound relative to vehicle control is presented. n=3 ± SD.

(C) mRNA sensitivity toward CR-1-31-B is correlated to purine content in the mRNA 5' leader region. Inhibition of cap-dependent and independent translation (as reflected by firefly and renilla RLU, respectively) were measured in response CR-1-31-B in Krebs-2 extracts. n = 3 ± SD.
(D) Dose response of the indicated rocaglates in Krebs-2 extracts programmed with the indicated reporter mRNAs.

5.4.3 *In Cellula* Activity of Rocaglates.

All rocaglates were evaluated for cytotoxic activity towards NIH/3T3 cells. To assess whether there were any compound our collection that could act through an eIF4A-independent mechanism, cytotoxicity was also measured in the CRISPR-modified NIH/3T3 cell line, eIF4A1^{em1JP}, which harbors an F163L mutation in eIF4A1 (Chu et al., 2016b). We identified 13 compounds that induced >70% cell death relative to vehicle-treated cells when tested at 40 nM (Figs 5.2A and S5.4, Table S5.1). Among these were rocaglates that have been reported to possess potent biological activity (SDS-1-021, RHT, CR-1-31-B, and RocA), as well as novel structures that have not been previously described (CMLD010853, CMLD010503, CMLD010512, CMLD010426). Surprisingly, CMLD011166 and CMLD011167, which were inactive *in vitro* (Figure 5.1A) ranked very highly among all rocaglates tested with in terms of cytotoxic activity (rank 17 and 1, respectively) (Figure 5.2A, Table S5.1). In contrast, WGD-57-590 and WGD-57-591, which were highly active in the *in vitro* translation experiments were found to be weakly cytotoxic. All cytotoxic rocaglates showed little or significantly diminished activity towards the eIF4A1^{em1JP} cell line, indicating that eIF4A1 on-target engagement is critical to the observed phenotypic response (Figure 5.2a, Table S5.1).

To address if differences in behavior among rocaglates towards the $(AG)_{10}$- and $(UC)_{10}$-reporters observed *in vitro* extended *in cellula*, we transfected the mRNA reporters into 293 cells and measured the relative production of luciferase in the presence of compound (Figure 5.2B). CR-1-31-B showed preference for inhibiting translation of $(AG)_{10}$-FF/HCV/Ren over $(UC)_{10}$-FF/HCV/Ren

mRNA (Figure 5.2B), although the differences were not as pronounced as what was observed *in vitro* (Figure 5.1D). On the other hand, silvestrol and WGD-57-591 inhibited both reporters equally (Figure 5.2B). CMLD011167, while inactive in *in vitro* extracts, showed a behavior that mirrored CR-1-31-B with a clear preference for inhibiting $(AG)_{10}$-FF/HCV/Ren mRNA (Figure 5.2B). The unrelated eIF4A inhibitors, pateamine A and hippuristanol, inhibited both reporters equally (Figure 5.2C).

Upon reanalyzing published ribosome profiling data (Iwasaki et al., 2016; Rubio et al., 2014), we found that it indeed is possible to discriminate between RocA (3 μM in HEK 293 cells) and silvestrol (25 nM in MDA-MB-231 cells) treatments based on the occurrence of polypurines ($\overline{\Delta Z}$ = -0.29, p = 2.1 x 10^{-25}, Mann Whitney U-test), but not polypyrimidine ($\overline{\Delta Z}$ = 0.09, p = 0.083, Mann Whitney U-test) stretches at the beginning of coding regions (Figure 5.2D, first 300 nt). Surprisingly, there were substantial similarities between the gene expression responses upon RocA and silvestrol treatments, despite the use of different rocaglate concentrations and cell lines (Figure 5.2E, Pearson correlation coefficient 0.55). In addition to establishing that the mRNA targeting differences observed among rocaglates *in vitro* extend *in cellula*, our re-analysis suggest that other mechanisms are at play to inhibit expression of common, overlapping gene sets.

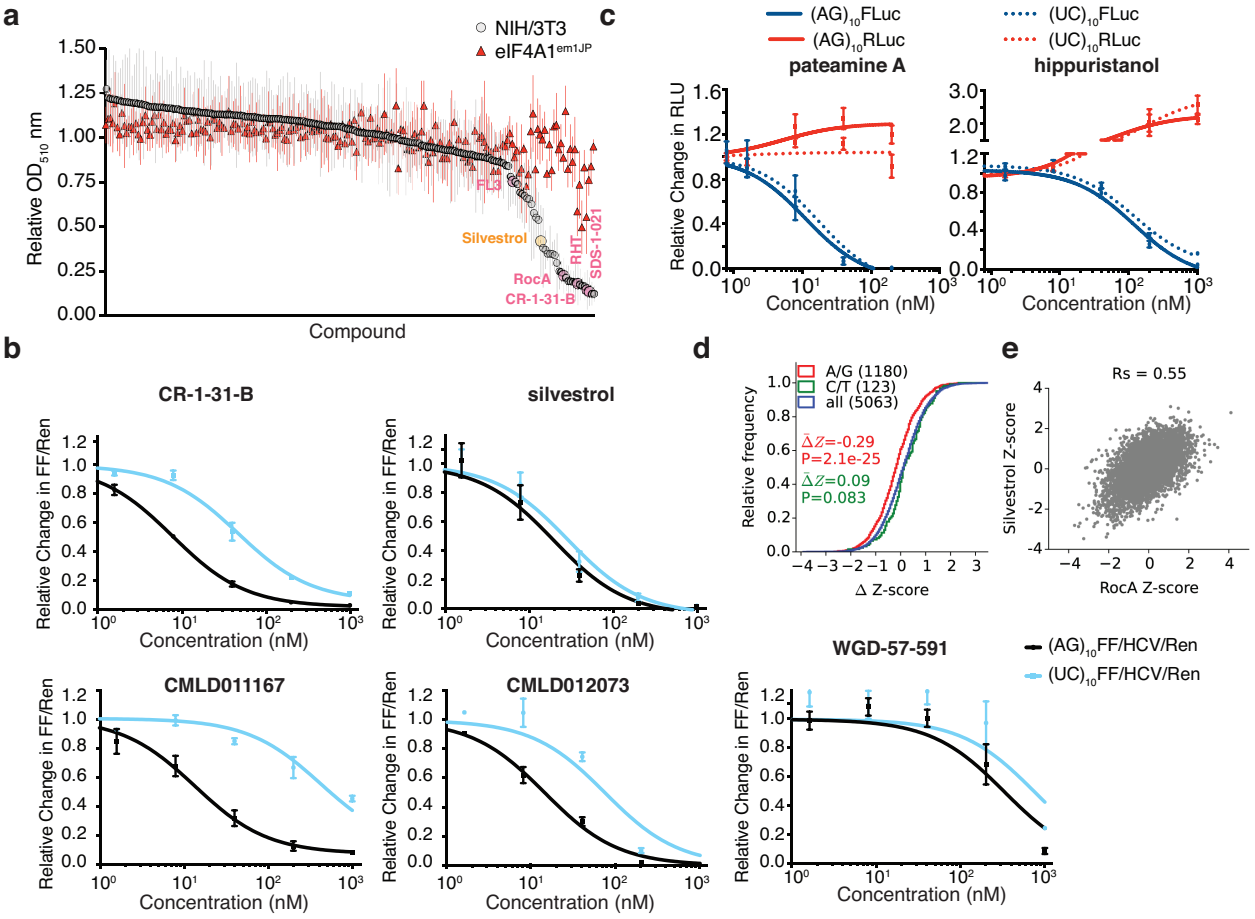

Figure 5.2. *In Cellula* Activity of Rocaglates. See Also Figure S5.4, and Table S5.1

(A) Cytotoxicity of rocaglates towards NIH/3T3 (grey circle) and eIF4A1^{em1JP} (red triangle) cells. Cells were exposed to 40 nM compound for 4 days and viability was measured using the SRB assay. n = 3 ± SEM.

(B) Rocaglates show different sequence preferences for inhibiting cap-dependent translation *in cellula*. HEK 293 cells were transfected with *in vitro* synthesized capped $(AG)_{10}$-FF/HCV/Ren or $(UC)_{10}$-FF/HCV/Ren mRNA and compounds were added 1 h later. Cells were cultured for an additional 6 h before measuring luciferase activity. n = 3 ± SEM.

(C) Dose-response of $(AG)_{10}$- and $(UC)_{10}$-FF/HCV/Ren mRNAs to hippuristanol and pateamine in HEK 293 cells. Experiments were performed as described in panel 5.2B. n = 3 ± SEM.

(D) Cumulative plot of the distribution of the difference in gene expression (TE ΔZ-score, Silvestrol - RocA) for genes classified as having more than 12 polypurine or polypyrimidine tracts (each having 5 consecutive pyrimidines or purines) within the first 100 codons of their CDS.

(E) Scatter plot of gene expression changes (TE Z-scores) obtained with RocA (X axis) and silvestrol (Y axis)

5.4.4 Rocaglates sequester eIF4F onto RNA.

Since eIF4A is a critical component of the eIF4F complex, we asked whether rocaglates affected eIF4F association towards RNA. To this end, we performed RPDs with m^7G-capped polypurine RNA and purified eIF4F (Figure 5.3A). Here, we observed an increase in eIF4E, eIF4A, and eIF4G association with capped polypurine RNA in the presence of a selected subset of rocaglates (Figure 5.3A). We then measured how stable the rocaglate-induced recruitment of eIF4F on RNA was in the presence of competitor RNA (Figure 5.3B). In the absence of compound, the eIF4F complex is not efficiently retained on the target RNA template ($t_{1/2}$ < 2 min), but in the presence of CR-1-31-B, a significant proportion eIF4E and eIF4A are still associated with the bait RNA 10 mins following the addition of excess competitor RNA (Figure 5.3B, compare lanes 6 and 5 to 4). The increased eIF4F resident time on the polypurine RNA in the presence of rocaglate is much longer than the rates of translation initiation (median < 1 min) (Shah et al., 2013; Yan et al., 2016). Thus, we assessed if rocaglate-induced trapping of eIF4F was sufficient to inhibit translation. To do this, we pre-formed eIF4F/CR-1-31-B/m^7GpppG$(AG)_{10}$-FF/HCV/Ren complexes and added these to RRL translation extracts. Indeed, upon doing so, we found that mRNAs associated with a rocaglate-stabilized eIF4F complex were less efficiently translated (Figure 5.3C).

We hypothesized that prolonged retention of eIF4F onto mRNA may deplete the limiting eIF4F pool available for ribosome recruitment and consequently exert a *trans*-inhibitory (bystander) effect towards mRNAs that are not directly affected by clamping. To test this, we programmed *in vitro* translation reactions with the $(UC)_{10}$-reporter, which is not responsive to CR-1-31-B or RocA (Figure 5.1D), followed by addition of 25-fold molar excess of m^7GpppG-$(AG)_{10}$ or ApppG-$(AG)_{10}$ competitor RNA (Figure 5.3D). The addition of m^7GpppG-$(AG)_{10}$ competitor sensitized

$m^7GpppG(UC)_{10}$-FF/HCV/Ren mRNA to inhibition by CR-1-31-B and RocA (Figure 5.3D). In contrast, addition of uncapped $ApppG\text{-}(AG)_{10}$ and CR-1-31-B or RocA had little impact on translation of $m^7GpppG(UC)_{10}$-FF/HCV/Ren mRNA, demonstrating this to be a cap-dependent phenomenon (Figure 5.3D). Consistent with this, we found that addition of eIF4F partially rescued cap-dependent inhibition induced by CR-1-31-B or silvestrol (Figure 5.3E).

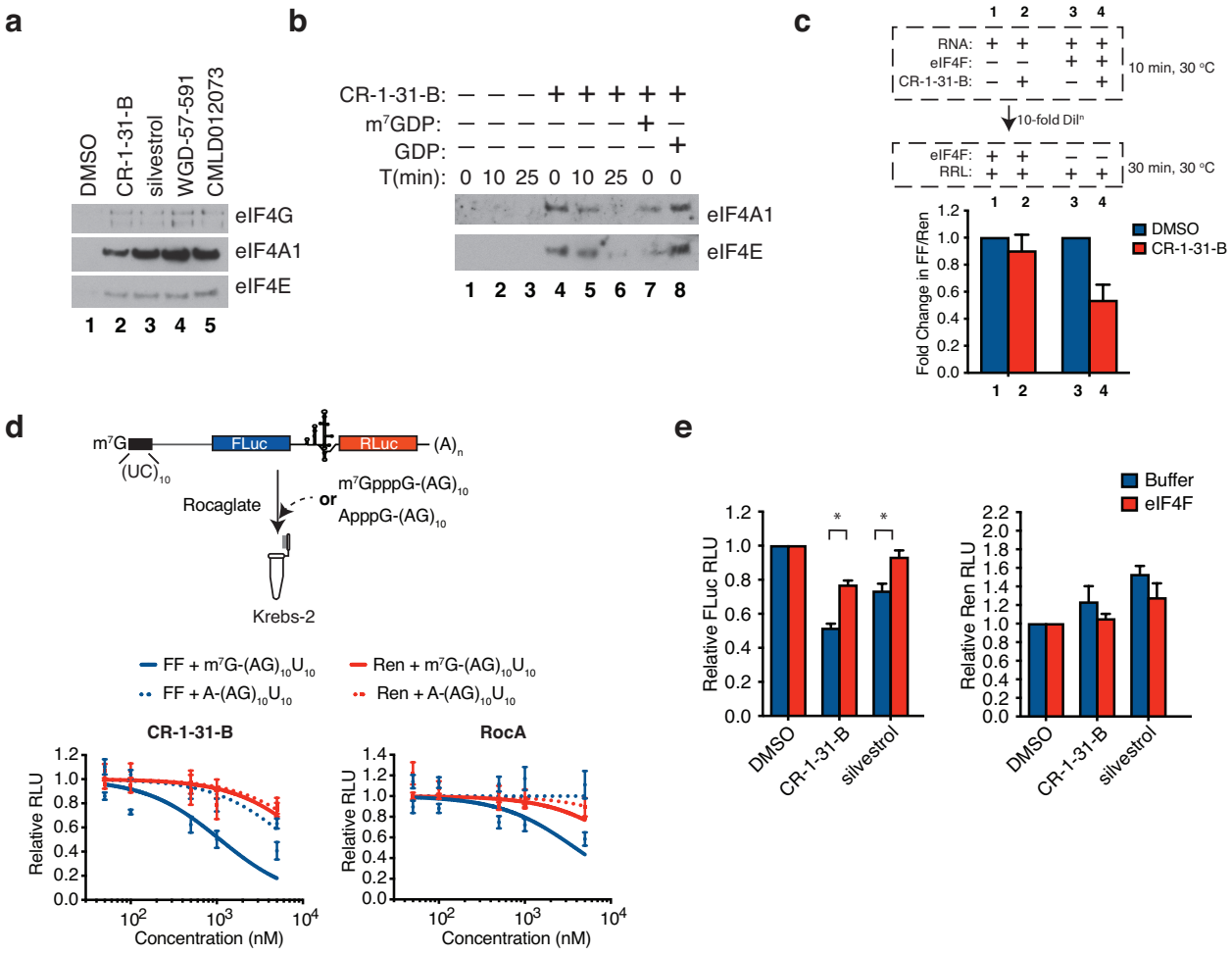

Figure 5.3. Increased eIF4F Retention Time on mRNA by Rocaglates Inhibit Protein Synthesis
(A) RPDs performed with m^7GpppG-capped RNA in RRL with DMSO or 500 nM rocaglate. (B) eIF4F:RNA complexes are stabilized by rocaglates. m^7GpppG-capped polypurine RNA (1 μM) was incubated in the presence of purified eIF4F (4 nM) in the presence or absence of CR-1-31-B (500 nM). Ten-fold molar excess of non-biotinylated RNA was then added to the reaction for the indicated periods of time.

(C) eIF4F pre-stabilized onto $m^7GpppG(AG)_{10}$-FF-HCV-Ren by CR-1-31-B repress cap-dependent translation in RRL. RNA (100 nM), eIF4F (100 nM), and CR-1-31-B (50 nM) were incubated at 30°C for 10 min to generate pre-formed complexes, and then added to RRL translation extracts.
(D) The presence of m^7GpppG-capped, but not ApppG-capped, purine-rich RNAs sensitizes the RocA/CR-1-31-B-unresponsive $m^7GpppG(UC)_{10}$-FF/HCV/Ren mRNA reporter. Translation reactions were performed in Krebs-2 extracts with 10 nM of $m^7GpppG(UC)_{10}$-FF/HCV/Ren reporter and 250 nM of competitor RNA. n=3 ± SEM.
(E) Addition of purified eIF4F rescues rocaglate-mediated translation inhibition. The $m^7GpppG(AG)_{10}$-FF/HCV/Ren reporter was added to Krebs-2 translation extracts in the presence eIF4F (10 nM) and 100 nM of the indicated compound. n≥ 3 ± SEM.

To further evaluate the significance of rocaglate-induced gain of function activity of eIF4F in cells, we reasoned that expression of wt eIF4A1 in $eIF4A1^{em1JP}$ cells should re-sensitize these cells to rocaglates. To test this, NIH/3T3 and $eIF4A1^{em1JP}$ cells were transduced with an empty MSCV cassette, MSCV/His_6-eIF4A1, or MSCV/His_6-eIF4A1(F163L) (Figure 5.4A). NIH/3T3 cells overexpressing wt eIF4A1 or eIF4A1(F163L) were similarly sensitive to rocaglates and there were little differences noted among them (Figure 5.4B, compare grey and red to black lines, respectively). Introduction of eIF4A1(F163L) into $eIF4A1^{em1JP}$ cells had little effect on rocaglate-responsiveness (Figure 5.4B, compare light blue to dark blue lines). However, expression of wt eIF4A1 in $eIF4A1^{em1JP}$ cells significantly sensitized these to all tested rocaglates (Figure 5.4B, compare orange to dark blue lines). Overall, these results are consistent with the notion that rocaglates exert their effects by imparting a gain-of-function activity to eIF4A1.

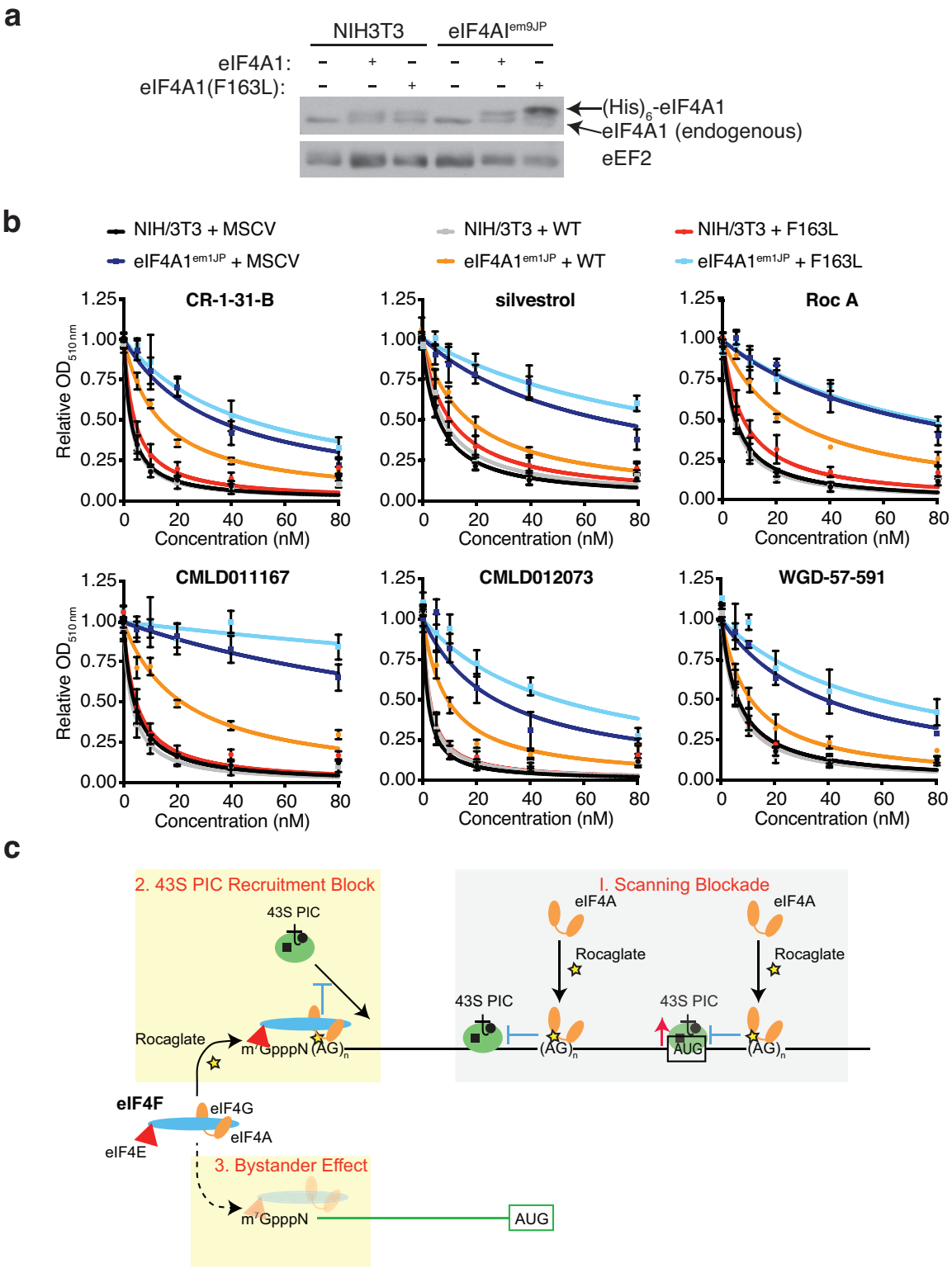

Figure 5.4. Rocaglates Function Through a Conditional Gain-of-Function Mechanism
(A) Western blot documenting endogenous and ectopic eIF4A1 levels.

(B). Ectopic expression of wt eIF4A1 sensitizes rocaglate-resistant cells to cell death. NIH/3T3 or eIF4A1^{em1JP} cells were infected with an empty MSCV cassette or expressing either wt eIF4A1 or the eIF4A1(F163L) rocaglate-resistant mutant. Viability was assessed following a 4-day exposure to 40 nM of compound. n = 3 ± SEM.
(C) Schematic diagram highlighting the different ways by which rocaglates inhibit translation (I) Rocaglates can induce binding of eIF4A to polypurine-rich sequences present in mRNA 5' leader regions to induce a scanning blockade. (Iwasaki et al., 2016). (II) Rocaglates can stimulate recruitment and retention of eIF4F to mRNAs with cap-proximal polypurines, which can lead to a by-stander effect (III) through a decreasing the pool of translationally active eIF4F complexes.

5.5 Discussion

A surprising revelation of this study is that rocaglates can exert different effects on gene expression. While the degree of eIF4A1 stabilization onto RNA was generally a good predictor of the extent of translation inhibition, there were clear outliers to this trend. Moreover, we also found differences between rocaglates in their mRNA targeting preference. For example, CR-1-31-B and RocA preferentially inhibited purine-rich mRNAs whereas this bias was lost with compounds like silvestrol (Figs 5.1D, 5.2B). Silvestrol, WGD-57-590 and WGD-57-591 are the only molecules within the collection containing a 1,4-dioxanyloxy moiety and that inhibited translation *in vitro* far more potently than what one may have predicted based on their relatively weak ability to stimulate eIF4A1:RNA association (Figure 5.1A, Table S5.1). RNA pulldown assays using recombinant eIF4A1 or purified eIF4F in the presence of silvestrol showed these to be incapable of associating with poly r(UC)$_{10}$. However, when the RPDs were performed from cell-free translation systems using poly r(UC)$_{10}$, silvestrol was able to stimulate eIF4A1 association (Figure S5.3B). Identifying the underlying molecular basis for silvestrol's different mRNA targeting range is currently under investigation.

Another class of outliers include CMLD011166 and CMLD011167, which are the only compounds in our collection having a *cis*-1,2 cyclopentadiol, rather than a *trans*-1,2 cyclopentadiol core. In spite of their potent ability to stimulate eIF4A1:RNA association, the *cis*-diol rocaglaols did

not inhibit translation in *in vitro* cell-free translation systems. Nevertheless, these compounds are able to block translation in cells and are highly cytotoxic (Figure 5.5A, B and Supplementary Table S5.1). The mechanism of action the *cis*-diol rocaglaols is also eIF4A1 dependent since cells harboring the eIF4A1 F163L mutation were resistant. Taken together, our results caution against generalizations attributing specific mRNA responsive features to all biologically active rocaglates.

Additionally, the observations made in this report can address some discrepancies in the literature regarding rocaglate mechanism of action. It has been reported that RocA does not inhibit translation but instead targets the MAPK signalling pathway (Bleumink et al., 2011). The absence of translation inhibition by RocA in the aforementioned study could be attributed to the absence of purine repeats within the 5' leader region of the reporter under study. Indeed, we have found that the mRNA reporter provided in commercial rabbit reticulocyte lysates (RRL) kits (Promega) is not inhibited by RocA when tested at concentrations as high as 10 μM (JC, data not shown).

The additional mechanisms of action by rocaglates found in this work complement the recently proposed clamped-barrier model (Figure 5.4C). As reported, rocaglates can stabilize eIF4A to 5' leader regions and block 43S scanning (Figure 5.4C, Step I) (Iwasaki et al., 2016). Consistent with this, we find that introduction of wild-type eIF4A1 is able to re-sensitize eIF4A1^{em1JP} cells to the cytotoxicity of these compounds. However, this mechanism is does not fully encapsulate the global changes in mRNA translation induced by rocaglates. Our data provides a more complete mechanism of action, as we found that rocaglates can trap eIF4F complexes at the cap (Figure 5.3). This is associated with reduced translation presumably due to diminished 43S PIC recruitment to the targeted mRNA (Figure 5.4C, Step 2). By extending the resident time of eIF4F at the cap (Figure 5.3B), rocaglates exert a bystander effect that leads to *trans*-inhibition of translation on otherwise normally unresponsive

mRNAs (Figure 5.4C, Step 3). As this effect is rescued by addition of eIF4F, we surmise it results from a decrease in levels of free eIF4F. In providing a better understanding into the mechanism of translation repression by rocaglates, we have begun to define the nuances and complexities that this class of compounds exert on gene expression.

5.6 Acknowledgments

This work was supported by a HRB-SFI-Wellcome Trust Biomedical Research Partnership Investigator Award in Science (210692/Z/18/) to PBFO'C and PVB) a Canadian Institutes of Health Research (CIHR) Foundation grant (FDN-148366) to JP, and research grants from the NIH to JAP, Jr. (R35 GM118173, R24 GM-111625, R01 GM-067041).

5.7 Author Contributions

J.C., W.Z., J.A.P. Jr, and J.P. conceived and designed this study. J.C., W.Z., R.C., W.G.D., A.S., and L.E.B. acquired, analyzed, and interpreted data. T.H. provided essential reagents. J.C. and J.P. wrote the manuscript. All authors commented on, edited and approved the manuscript.

5.8 STAR ★ Methods

5.8.1 Compounds

Rocaglates were synthesized using ESIPT photocycloaddition of 3-hydroxyflavones with cinnamates as previously reported, followed by further functionalization (Rodrigo et al., 2012; Stone et al., 2015; Yueh et al., 2017). A few compounds are present more than once in the collection and arose from

different synthesis batches or the preparations contain two enantiomers (see Supp Table S5.1). Compounds were resuspended in DMSO to a final concentration of 10 mM and stored at -80°C.

5.8.2 Recombinant DNA Constructs

Plasmids expressing the $(AG)_{10}$- and $(UC)_{10}$-reporters were constructed through modification of pKS/FF/HCV/Ren vector (Novac et al., 2004). To facilitate the replacement of 5' leader sequences, an MluI and NdeI restriction sites were introduced upstream of the T3 promoter and of the FF AUG start codon, respectively. These sites were added as part of G blocks and cloned into the pKS/FF/HCV/Ren vector using PciI and NarI restriction sites. Different 5' leader sequences were then introduced to the reporters by annealing two overlapping phosphorylated oligonucleotides with the desired sequences, and directionally cloned into the vector using the MluI and NdeI restriction sites.

5.8.3 Cell Culture and Retroviral Transduction

All cell lines used in this study were maintained in DMEM supplemented with 10% FBS (Wisent), 100 U/mL penicillin/streptomycin, and 2 mM L-glutamine at 37 °C and 5% CO_2. For over-expression studies with eIF4A1 in NIH/3T3 or eIF4A1^{em1jp} cells, ecotropic Phoenix cells were first transfected with retroviral vectors expressing codon optimized His_6-tagged eIF4A1 (WT or F163L). Forty-eight hours post-transfection, the viral supernatant was harvested, filtered, and added to NIH/3T3 or eIF4A1^{em1jp} cells in the presence of 4 μg/mL polybrene once every 12 h for a total of 4 infections. Two days after the final infection, cells were seeded for SRB assays (described above) and western blotting.

5.8.4 Purification of Recombinant Proteins

pET15b-His_6-eIF4A1 or pET15b-His_6-eIF4A2 plasmids were transformed into BL21 (DE3) bacteria, plated onto LB-Agar plates, and single colonies were used to inoculate an overnight starter culture in

LB containing 100 mg/L ampicillin. This culture was expanded the following day at a 1:50 dilution, and the bacterial was further cultured at 37°C until the OD_{600} reached 0.6-0.8. At this point, the cultures were induced with 1 mM IPTG and grown for an additional 3 h. The bacteria was pelleted and the pellet resuspended in a buffer containing 20 mM Tris (pH 7.5), 10% glycerol, 0.1 mM EDTA, 200 mM KCl, 0.1% Triton X-100, 3.4 mM β-mercaptoethanol. Cells were lysed via sonication and cellular debris were cleared via centrifugation. The clear lysates were supplemented with 20 mM imidazole and then subjected to purification through a Ni-NTA agarose column (Qiagen). The column was washed 3 times with 4 column volumes of wash buffer 1 (20 mM Tris (pH 7.5), 10% glycerol, 0.1 mM EDTA, 800 mM KCl, 20 mM imidazole), followed by 3 washes using 4 column volumes of wash buffer 2 (Wash buffer 1, but with 300 mM KCl). Purified proteins were eluted with wash buffer 2 containing with 200 mM imidazole. The eluate was dialyzed overnight in a buffer containing 20 mM Tris (pH 7.5), 10% glycerol, 0.1 mM EDTA, 100 mM KCl, and 2 mM DTT. The next day, the dialyzed samples were subjected to further purification through a Q-Sepharose Fast Flow (Amersham) column, and with a 100 mM-500 mM KCl gradient in 20 mM Tris (pH 7.5,) 10% glycerol and 0.1 mM EDTA. The final dialysis was performed in a buffer containing 20 mM Tris (pH 7.5), 10% glycerol, 0.1 mM EDTA and 2 mM DTT.

5.8.5 *In Vitro* Translation Assays

In vitro translation assays performed in Krebs-2 cell extracts with the addition of 5 mM $MgCl_2$, 30 mM Tris-HCl (pH 7.5), 1.5 mM ATP, 0.1 mM GTP, 0.6 mM CTP, 10 mM dipotassium creatine phosphate, 80 μg/mL creatine kinase, and 0.04 mM amino acids. The *in vitro* transcribed mRNA reporters were added to the Krebs-2 extracts to a final concentration of 10 ng/μl and incubated for 60 minutes at 30 °C prior to the measurement of luciferase activities.

5.8.6 Fluorescence Polarization Assay

Unless otherwise specified, 500 nM recombinant eIF4A1 was added to 10 nM FAM-labelled RNA in a buffer containing 14.4 mM HEPES-NaOH (pH 8), 108 mM NaCl, 1 mM $MgCl_2$, 14.4% glycerol, 0.1% DMSO, 2 mM DTT and 1 mM AMPPNP in black, low volume 384 well plates (Corning 3820). Binding reactions were allowed to equilibrate for 30 min at 22 ºC away from light prior to measuring polarization values on a Pherastar FS microplate reader (BMG Labtech). For the dissociation experiments, the eIF4A:FAM-$(AG)_8$ complexes were pre-formed in the presence of 50 μM compound, incubated at 22 ºC for 30 min in presence of either 1 mM ATP or AMP-PNP, at which point 100 μM unlabelled $(AG)_8$ RNA was added and measurements were performed. For conditions involving ATP and DMSO, 50 μM eIF4A was used instead of 1 μM because of the low affinity of 4A for RNA.

5.8.7 RNA Transfections

HEK 293 cells were transfected in a 24 well plate with 0.25 μg/well of *in vitro* synthesized capped $m^7GpppG(AG)_{10}$FF/HCV/Ren or $m^7GpppG(UC)_{10}$FF/HCV/Ren mRNA and 1 h later were exposed to the indicated concentrations of compounds for an additional 6 h. Following this, extracts were prepared using passive lysis buffer (PLB, Promega) and luciferase activity measured on a Berthold Lumat LB 9507 luminometer.

5.8.8 Sulforhodamine B (SRB) Assay

One thousand cells were seeded per well in a 96 well format and then cultured in the presence of 40 nM compound (unless indicated otherwise). Cells were grown for 4 days before processing. Plates were washed with PBS, fixed with 50% cold trichloroacetic (TCA) acid for 1 hour, and stained with 0.5% Sulforhodamine B (dissolved in 1% acetic acid) for 15 min. The unbound dye was removed by

washing the plates 5 times with 1% acetic acid. The plates were then dried, and the remaining dye was recovered in 10 mM Tris (pH 9) before measuring OD510 nm values on a SpectraMax M5 (Molecular Devices).

5.8.9 RNA Pulldown Experiments

Rabbit reticulocyte lysates (Promega) were pre-incubated with 500 nM of the indicated compound for 15 min at 30 °C prior to the addition of m^7GpppG- or ApppG-capped biotinylated RNAs (added to a final concentration of 1 μM biotinylated RNA bait). Reactions were incubated for an additional 15 min at 30 °C and then diluted 10x with ice cold wash buffer (0.5% v/v NP-40, 50 mM HEPES (pH 7.3), 150 mM KCl, 2 mM EDTA, 2 mM $MgCl_2$,). Magnetic streptavidin beads (NEB) were used to capture the biotinylated RNA baits and the reactions were incubated end over end for 1 hour at 4 °C. The beads were then washed three times with ice cold wash buffer (10 minutes per wash) and the RNA bound proteins were eluted by digesting with 50 U of RNaseI (Ambion, AM2294) for 15 minutes at 37 °C. Eluted proteins were analyzed by Western blotting.

5.8.10 Western Blotting

Cells were pelleted, washed with PBS and lysed with NP40 lysis buffer (150 mM NaCl, 2 mM EDTA, 0.5% NP40, 20 mM Tris (pH 7.3), supplemented with 1 mM PMSF, 4 μg/mL aprotinin, 2 μg/mL leupeptin, 2 μg/mL pepstatin). The cellular debris was pelleted by centrifugation at 16000 x *g* for 5 minutes and the protein concentration of the lysates was quantitated using DC assay (BioRad) according to manufacturer's instructions. The prepared lysates were then resolved on a 10% NuPAGE gel. The antibodies used for protein expression analysis were directed against eIF4A1 (Abcam, ab31217), eIF4E (Cell Signaling, #9742), eIF4G (Cell Signaling, #2498), and eEF2 (Cell Signaling, #2332).

5.8.11 Ribosome Profiling Data Analysis

The RNA-seq and ribosome profiling raw data for the silvestrol study (GSE61375) and RocA study (GSE70211) were obtained from Gene Expression Omnibus (Clough and Barrett, 2016). The analysis was carried out only on RocA treatment at the highest concentration (3 μM). The non-rRNA reads aligned to the human RefSeq transcriptome (downloaded on 09/08/2018) using Bowtie with parameters (-a -m 100) (Langmead et al., 2009). The gene expression analysis was locus-based, that is footprints aligning to all transcripts derived from the same locus ('gene') were aggregated. Genes with less than 10 mapped footprints in either condition were discarded. The differential gene expression analysis was carried using Z-score transformation as described earlier (Andreev et al., 2015). Polypurine and polypyrimidine tracts were defined as 5 consecutive pyrimidines or purines, respectively. To compare sequence dependence of gene expression response upon two treatments, genes were classified based on occurrence of 12 or more non-overlapping tracts within first 300 nt of the coding sequence (CDS). Transcripts with CDS shorter than 300 nt were discarded. The difference in gene expression response was calculated as an average difference between translation efficiency (TE) Z-scores in two treatments (Silvestrol – RocA).

5.8.12 Statistics

All indicated replicates represent biological replicates. The Mann Whitney U-test was used to assess differences between ΔZ-scores for different treatments and genes containing either polypurine or polypyrimidine tracts. The eIF4A:FAM-$(AG)_8$ dissociation half-life ($t_{1/2}$) calculations were performed using the non-linear regression function in Prism.

5.9 Declaration of Interests

J.C., W.Z., J.A.P. Jr, and J.P. have filed a US provisional patent application on the use of amidino- and amino-rocaglates as novel translation inhibitors and anticancer agents.

5.10 Supplemental Figures

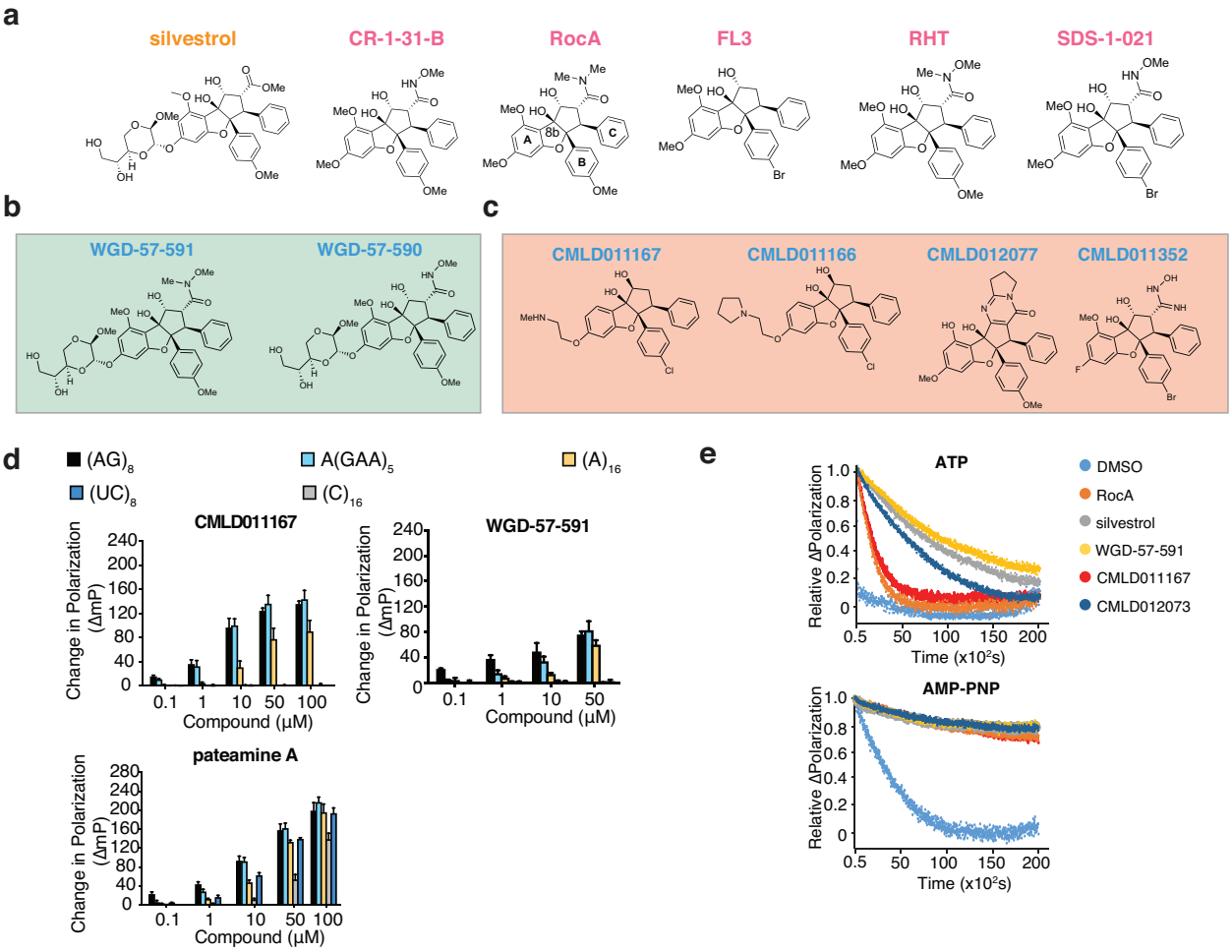

Figure S5.1. Different Rocaglates Exhibit Distinct Biological Activities. Related to Figure 5.1
(A) Chemical structures of commonly used rocaglates in biological studies.
(B) Structures of two rocaglates that potently inhibit cap-dependent translation, but modestly stimulate eIF4A1:RNA binding.
(C) Structures of four rocaglates that potently stimulate eIF4A1:RNA binding but are inactive or show weak activity as protein synthesis inhibitors *in vitro*.

(D) Rocaglates induce preferential association between eIF4A1 and purine-rich RNA. Experiments were performed as described in Figure 1b. Limitations in WGD-57-591 availability prevented us from extending the titrations to 100 μM. The change in FP obtained relative to vehicle controls is presented. n = 3 ± SEM.

(E) Relative dissociation of pre-formed eIF4A1:rocaglate:FAM-poly r(AG)$_{10}$ complexes were measured by the addition of 1000-fold molar excess of poly r(AG)$_{10}$ and ATP (DMSO, $t_{1/2}$ < 1 min; RocA, $t_{1/2}$ ~ 16 min; CMLD011167, $t_{1/2}$ ~ 24 min; CMLD012073, $t_{1/2}$ ~ 70 min; silvestrol, $t_{1/2}$ ~ 110 min; WGD-57-591, $t_{1/2}$ ~ 143 min) or AMP-PNP (DMSO, $t_{1/2}$ ~ 33 min; RocA, $t_{1/2}$ ~ 580 min; CMLD011167, $t_{1/2}$ ~ 591 min; CMLD012073, $t_{1/2}$ ~ 832 min; silvestrol, $t_{1/2}$ ~ 924 min; WGD-57-591, $t_{1/2}$ ~ 928 min). Relative dissociation was measured as a function of time. n = 3 ± SEM

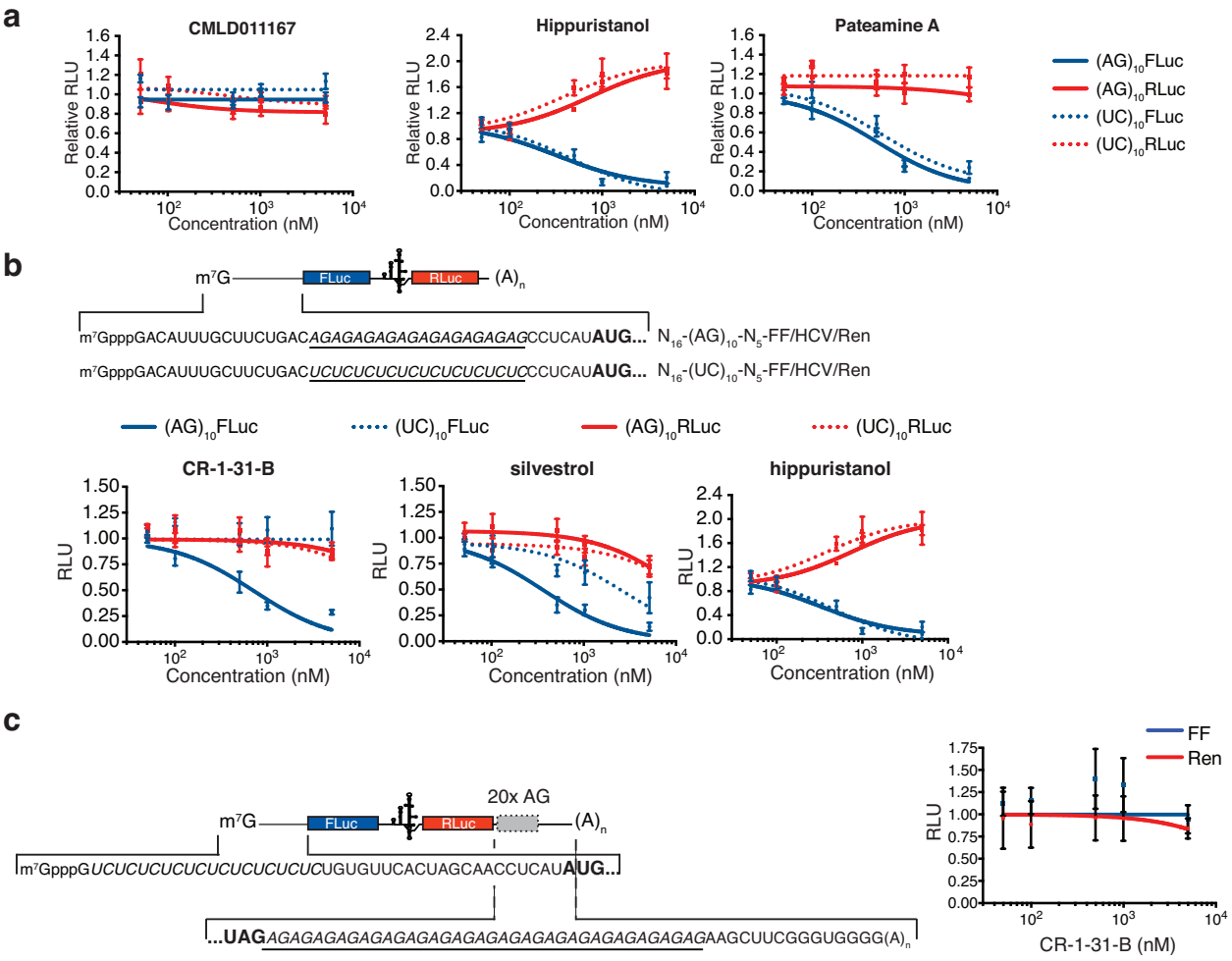

Figure S5.2 Preferential Inhibition of Purine-Rich 5' Leaders is Not a Shared Property Found Between Small Molecules Targeting eIF4A1. Related to Figure 5.1

(A-C). Dose response of the indicated compounds in Krebs-2 extracts programmed with the indicated mRNAs. n = 3 ± SEM.

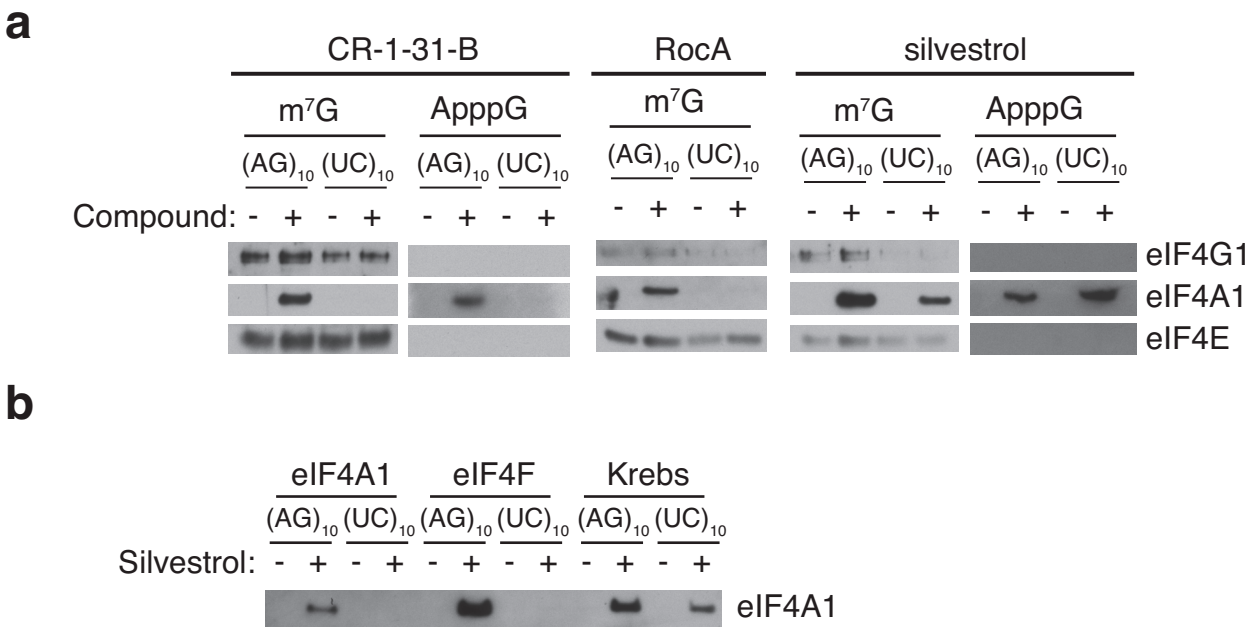

Figure S5.3. Cap-Independent Clamping of eIF4A Cannot Account for the Inhibitory Effects of Rocaglates. Related to Figure 5.1

(A) RPDs performed with the indicated m^{7}GpppG- or ApppG-capped RNA species incubated with retic lysate and either vehicle or 500 nM rocaglate.

(B) RPDs performed with m^{7}GpppG-capped RNA species incubated in the presence of recombinant eIF4A (125 nM) eIF4F (10 nM), or Krebs-2 extracts and either vehicle or 500 nM silvestrol.

Rank Order	Compound	Structure
1	CMLD011167	see Fig S1c
2	CMLD010853	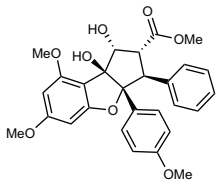
3	SDS-1-021	see Fig S1a
4	CMLD010513 (CR-1-31-B) (Enantioenriched)	see Fig S1a
5	CMLD010503	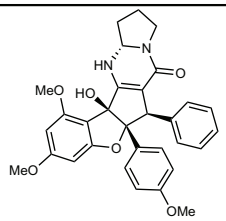
6	CMLD010512	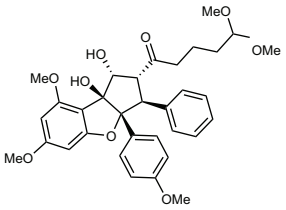
7	CMLD011610 (RHT) (Racemic)	see Fig S1a
8	CMLD010515 ((-)-RHT)	see Fig S1a
9	CR-1-31-B	see Fig S1a
10	CMLD012073	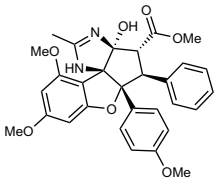
11	CMLD011881 (SDS-1-021) (Enantioenriched)	see Fig S1a

Rank Order	Compound	Structure
12	CMLD005522 (CR-1-31-B) (Racemic)	see Fig S1a
13	CMLD010426	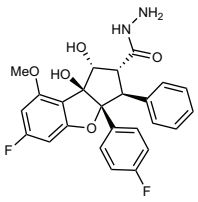
14	Roc A	see Fig S1a
15	CMLD012072	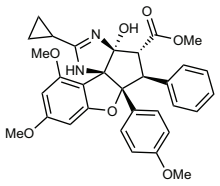
16	CMLD010536	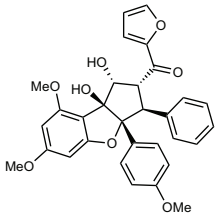
17	CMLD011166	see Fig S1c

Figure S5.4. Structures of the Most Potent Cytotoxic Rocaglates Exhibiting Activity Towards NIH/3T3 Cells Identified From the BU-CMD Library. Related to Figure 5.2.

Chemical structures of 13 most cytotoxic rocaglates in the BU-CMD collection.

Table S5.1 Activities of BU-CMD Rocaglates

Supplementary Table 5.1. Activity results of BU-CMD rocaglates.

	FF/HCV/Ren		eIF4A1 FP - Poly(AG)8		eIF4A1 FP Poly(UC)8		eIF4A2 FP - Poly(AG)8		SRB (NIH3T3)		SRB (NIH3T3-F163L)		
Compound	Avg - FF/Ren	SEM - FF/Ren	Avg	SEM	Avg	SEM	Avg	SEM	AVG	SEM	Avg	SEM	SMILES
BUCMD00001	0.9367319	0.03262066	14.02663	4.926966	-0.5331981	1.33456924	11.7885371	5.24607972	0.85977	0.1574	0.87862	0.16255615	COC1=CC=C(C=C1)[C@]12OC3=C(C(OC)=CC(OC)=C3)[C@@]1(O)C1=C([C@@H]2C2=CC=CC=C2)C(=O)N2CCC[C@H]2N1
BUCMD00003	0.3755094	0.01312235	90.56272	1.42793	-1.8100406	1.69389964	109.583394	2.74508529	0.98024	0.30241	0.99102	0.100923604	CONC(=O)[C@H]1[C@@H](O)[C@@]2(O)C3=C(O[C@]2([C@@H]1C1=CC=CC=C1)C1=CC=C(Br)C=C1)C=C(O)C=C3OC
BUCMD00209	0.1918971	0.013685	86.44875	4.978528	-1.5814998	1.48944377	83.4016749	2.59814357	0.78215	0.16752	1.02519	0.095675518	COC1=CC2=C(C(OC)=C1)[C@]1(O)C3=C([C@@H](C4=CC=CC=C4)[C@@]1(O2)C1=CC=C(Br)C=C1)C(=O)N1CCC[C@H]1N3
BUCMD00210	0.3908459	0.01749583	73.24647	6.190203	-3.4103399	1.43994954	53.8035978	4.97935213	1.04798	0.22559	1.08445	0.107344367	COC1=CC2=C(C(OC)=C1)[C@]1(O)C3=C([C@@H](C4=CC=CC=C4)[C@@]1(O2)C1=CC=C(Br)C=C1)C(=O)N1CCC[C@@H]1N3
BUCMD00211	0.2007755	0.00952394	85.12878	4.318938	-5.2032727	1.66297614	98.3126638	17.5546334	1.06551	0.23412	1.00509	0.042974366	COC1=CC2=C(C(OC)=C1)[C@]1(O)C3=C([C@@H](C4=CC=CC=C4)[C@@]1(O2)C1=CC=C(Br)C=C1)C(=O)N1CCC[C@H]1O3
BUCMD00254	0.56000127	0.01525394	89.2573785	4.21558606	-0.6344755	1.2528191	96.5078309	12.3278805	0.88468	0.1941	0.94701	0.18810809	COC1=CC=C(C=C1)[C@@]12OC3=CC(OC)=CC(OC)=C3[C@]1(O)C1=C([C@H]2C2=CC=CC=C2)C(=O)N=C(C)N1
BUCMD00258	0.9714687	0.02138328	12.09034	2.393128	-3.3442493	1.12303949	15.1584911	4.09520376	1.13244	0.15436	1.05497	0.081784395	COCCOCOC(=C(F)F)C1=CC=C(C=C1)[C@@H]1[C@H]([C@@H](O)[C@@]2(O)C3=C(O[C@@]12C1=CC=C(OC)C=C1)C=C(OC)C=C3OC)C(=O)N(C)OC
BUCMD00268	1.00204	0.0146707	7.405706	3.349498	-5.5676499	0.73462231	11.0577542	2.80591897	0.93796	0.18028	0.94279	0.143330292	COC1=CC=C(C=C1)[C@@]12OC3=CC(OCCC4(CCC#C)N=N4)=CC(OC)=C3[C@]1(O)[C@H](O)[C@@H]([C@H]2C1=CC=CC=C1)C(=O)C1=CC=CO1
BUCMD00269	0.9622904	0.02334091	-1.393162	2.932511	-0.5083065	1.72944038	2.27269024	2.7161236	0.86575	0.16551	0.81382	0.151745206	COC1=CC=C(C=C1)[C@@]12OC3=CC(OC)=CC(OC)=C3[C@]1(O)[C@H](O)[C@@H]([C@H]2C1=CC=C(OCCC2(CCC#C)N=N2)C=C1)C(=O)C1=CC=CO1
BUCMD00270	0.8670405	0.02330647	-0.5387915	1.522138	-0.7185267	1.7641354	1.79620365	1.68439124	1.06465	0.17918	0.95454	0.074762636	CON(C)C(=O)[C@H]1[C@@H](O)[C@@]2(O)C3=C(O[C@]2([C@@H]1C1=CC=C(OCCC2(CCC#C)N=N2)C=C1)C1=CC=C(OC)C=C1)C=C(OC)C=C3OC
CMLD005522	0.34587346	0.00777843	26.9853851	2.64597123	-1.835719	0.8958012	55.6572941	2.17096953	0.19509	0.0866	0.82489	0.102194258	COC1=C2C(O[C@]3(C4=CC=C(OC)C=C4)[C@@]2(O)[C@H](O)[C@H](C(NOC)=O)[C@H]3C5=CC=CC=C5)=CC(OC)=C1
CMLD008820	1.01626528	0.03047633	0.19835781	9.54356078	3.362045	0.9016185	27.3536067	6.02805688	0.84404	0.09301	0.95213	0.103749447	COc1ccc(cc1)[C@@]12Oc3cc(OC)cc(OC)c3[C@@](O)([C@@H]1O)[C@@H]([C@H]2c1ccccc1)C(=O)OCc1ccccc1
CMLD008821	0.87176995	0.06273807	7.10943466	6.771977	2.833095	0.5104879	26.8832567	2.11312541	1.18252	0.21657	1.12605	0.160134219	COC(=O)[C@@H]1[C@@H](c2ccccc2)[C@@]2(Oc3cc(OC)cc(OC)c3[C@@]1(O)[C@@H]2O)c1ccc(OC)cc1
CMLD009401	1.015793	0.01102144	38.78492	2.578983	-4.0382672	2.11444145	19.455642	1.25901205	1.0417	0.22741	1.09966	0.049898078	COC1=CC=C(C=C1)[C@@]12OC3=CC(OC)=CC(OC)=C3[C@]1(O)C1=NNC(=O)C1=C2C1=CC=CC=C1
CMLD009433	0.42732857	0.0054342	52.8791647	6.44334323	-3.663511	0.2172463	69.8421559	7.40737477	0.95352	0.25037	1.18039	0.139079597	COC1=C2C(O[C@]3(C4=CC=C(OC)C=C4)[C@@]2(O)C5=C(C(O)=NN5)[C@H]3C6=CC=CC=C6)=CC(OC)=C1
CMLD009731	0.54580778	0.0095113	25.4093202	5.60466593	-1.89392	0.5356829	59.7590604	3.79209662	0.9464	0.09812	0.86529	0.179520556	COC1=C2C(O[C@]3(C4=CC=C(OC)C=C4)[C@@]2(O)[C@H]5[C@H](C(O5)=O)[C@H]3C6=CC=CC=C6)=CC(OC)=C1
CMLD010332	0.66275729	0.04537313	72.9044759	12.2982006	3.707204	0.9218051	67.2756079	6.48010444	1.02842	0.27927	1.14227	0.049339224	COC1=CC=C(C=C1)[C@@]12OC3=CC(OC)=CC(OC)=C3[C@]1(O)[C@H](O)[C@H](CO)[C@H]2C1=CC=CC=C1
CMLD010335	0.33118917	0.02439123	76.9491342	6.47824152	1.638009	0.430233	82.7057582	5.1515145	0.37156	0.10732	1.04458	0.1010153	CONC(=O)[C@H]1[C@@H](O)[C@@]2(O)C3=C(O[C@]2([C@@H]1C1=CC=CC=C1)C1=CC=C(Br)C=C1)C=C(F)C=C3OC
CMLD010336	0.44640276	0.08151852	50.400453	5.77258066	1.283119	0.8344854	59.6120245	3.67119649	0.94456	0.14052	1.0704	0.078805095	COC1=C2C(O[C@]3([C@@H]([C@H]([C@@H](O)[C@@]23O)C2=NC(C)=NO2)C2=CC=CC=C2)C2=CC=C(Br)C=C2)=CC(F)=C1
CMLD010337	0.72299648	0.05322447	41.0574756	5.00779676	-1.437349	0.5882999	41.6606639	2.66311371	1.22306	0.27002	1.10591	0.140118696	COC(=O)[C@H]1[C@@H](O)[C@@]2(O)C3=C(OC)C=C(F)C=C3O[C@]2([C@@H]1C1=CC=CC=C1)C1=CC=C(Br)C=C1
CMLD010338	0.39554102	0.0376347	67.6697452	12.9708637	1.524809	1.161628	54.0660788	4.43594593	0.62778	0.31677	1.03661	0.153622396	COC1=C2C(O[C@]3([C@@H]([C@H]([C@@H](O)[C@@]23O)C2=NOC(C)=N2)C2=CC=CC=C2)C2=CC=C(Br)C=C2)=CC(F)=C1
CMLD010343	0.75319506	0.0526414	55.430322	7.95533507	-5.881813	0.4619792	37.2227629	3.94017743	1.01342	0.08999	1.13261	0.227884169	COC1=C2C(O[C@]3([C@@H]([C@@H](C#N)[C@@H](O)[C@@]23O)C2=CC=CC=C2)C2=CC=C(Br)C=C2)=CC(F)=C1
CMLD010423	0.87978895	0.11141718	51.0453201	7.82938785	2.936022	1.278922	72.5081082	8.10677706	0.97483	0.22695	0.93468	0.153126449	CONC(=O)[C@H]1[C@@H](O)[C@@]2(O)C3=C(OC)C=C(F)C=C3O[C@]2([C@@H]1C1=CC=CC=C1)C1=CC=C(F)C=C1
CMLD010425	0.81387825	0.04067819	48.8450273	10.4668113	2.692035	0.4915644	70.2136741	10.9275464	1.18564	0.30436	1.08707	0.11314217	COC1=C2C(O[C@]3([C@@H]([C@H]([C@@H](O)[C@@]23O)C2=NC(C)=NO2)C2=CC=CC=C2)C2=CC=C(F)C=C2)=CC(F)=C1
CMLD010426	0.73810503	0.06427807	93.7806036	6.64464909	1.409209	0.8380465	95.2125	15.217455	0.21439	0.07191	1.1492	0.142432307	COC1=C2C(O[C@]3([C@@H]([C@H]([C@@H](O)[C@@]23O)C(=O)NN)C2=CC=CC=C2)C2=CC=C(F)C=C2)=CC(F)=C1
CMLD010428	0.61926715	0.05038145	71.8818949	13.0570681	2.098732	0.4351928	83.0212235	8.31469667	0.99624	0.30749	1.18094	0.208246192	CONC(=O)[C@H]1[C@@H](O)[C@@]2(O)C3=C(OC)C=C(F)C=C3O[C@]2([C@@H]1C1=CC=CC=C1)C1=CC=C(Cl)C=C1
CMLD010429	0.91695356	0.06613062	18.0268153	5.3568617	-3.624021	0.923263	45.5948145	7.30386919	0.66055	0.05493	0.72838	0.204643867	COC1=C2C(O[C@]3(C4=CC=C(OC)C=C4)[C@@]2(O)[C@H](O)[C@@H](C(OC)=O)[C@@H]3C5=CC=CC=C5)=CC(OC)=C1
CMLD010430	0.81660573	0.09943091	42.2133292	10.4247912	1.925208	0.4327831	58.2104087	7.09147745	1.19513	0.15208	1.06228	0.101084546	COC(=O)[C@@H]1[C@@H](O)[C@@]2(O)C3=C(OC)C=C(F)C=C3O[C@]2([C@H]1C1=CC=CC=C1)C1=CC=C(Br)C=C1
CMLD010441	0.98401486	0.10954087	21.7137658	10.8599748	-1.585113	0.6009488	36.4439909	4.47530996	1.27384	0.16221	1.07169	0.101284851	CON(C)C(=O)[C@@H]1[C@@H](O)[C@@]2(O)C3=C(OC)C=C(OC)C=C3O[C@]2([C@H]1C1=CC=CC=C1)C1=CC=C(OC)C=C1
CMLD010442	0.95984681	0.08914673	36.1918535	10.0763716	-0.3754824	0.7510926	45.4984116	8.77620805	1.12968	0.14459	1.1346	0.089528924	CONC(=O)[C@@H]1[C@@H](O)[C@@]2(O)C3=C(OC)C=C(OC)C=C3O[C@]2([C@H]1C1=CC=CC=C1)C1=CC=C(OC)C=C1
CMLD010482	0.2818446	0.02292892	99.97409	3.779472	-0.500681	2.7999143	99.0551911	3.05111498	0.91629	0.19148	0.99151	0.065137858	COC1=CC(F)=CC2=C1[C@]1(O)C3=C([C@@H](C4=CC=CC=C4)[C@@]1(O2)C1=CC=C(Br)C=C1)C(=O)N1CCC[C@@]1(C)N3
CMLD010493	0.73730573	0.11042572	9.48240906	12.5022156	-4.120084	1.340639	25.2454193	4.87005385	1.10744	0.15948	1.08614	0.018359603	[H]O[C@@]1([H])[C@@]2(O[H])[C@@H]([C@@H](C3=CC=CC=C3)[C@@]1(OC1=C2C(OC)=CC(OC)=C1)C1=CC=C(OC)C=C1)C(=O)N([H])CCCC(OC)OC
CMLD010498	0.79738853	0.11135894	9.597849	3.12702009	2.463012	0.6977322	22.6087656	5.04956437	1.02059	0.15266	0.99911	0.133380356	[H]O[C@@]1([H])[C@@]2(O[H])[C@@H]([C@@H](C3=CC=CC=C3)[C@@]1(OC1=C2C(OC)=CC(OC)=C1)C1=CC=C(OC)C=C1)C(=O)OC
CMLD010500	0.42811467	0.09996396	13.6249074	12.1938382	-3.64787	0.9230193	29.803851	11.6835495	0.89575	0.20179	0.89259	0.145871309	COC1=C2C(O[C@]3(C4=CC=C(Br)C=C4)[C@@]2(O)[C@H]5[C@H](C(O5)=O)[C@H]3C6=CC=CC=C6)=CC(OC)=C1
CMLD010502	0.5641682	0.03179508	94.11703	1.031429	-2.029097	1.36312294	86.0146624	3.08472379	0.34102	0.08636	1.06364	0.09530609	COC1=CC=C(C=C1)[C@@]12OC3=CC(OC)=CC(OC)=C3[C@]1(O)C1=C([C@H]2C2=CC=CC=C2)C(=O)N2CCC[C@H]2N1
CMLD010503	0.3396338	0.01280483	105.4035	0.698939	-1.7347659	1.32706585	109.97098	6.49814036	0.16708	0.0779	0.83408	0.096143339	COC1=CC=C(C=C1)[C@@]12OC3=CC(OC)=CC(OC)=C3[C@]1(O)C1=C([C@H]2C2=CC=CC=C2)C(=O)N2CCC[C@H]2N1
CMLD010506	0.53527548	0.03663426	65.6366613	9.97857246	0.6791258*	0.3834146	57.3304881	2.37684482	0.57806	0.25488	1.13609	0.213986405	[H]O[C@@]12C3=C([C@@H](C4=CC=CC=C4)[C@@]1(OC1=CC(OC)=CC(OC)=C21)C1=CC=C(OC)C=C1)C(=O)N1CCCC1=N3
CMLD010507	1.00773791	0.07288961	79.5260375	9.82253585	2.428694	1.739458	72.3045951	3.97963391	1.1295	0.21335	1.15161	0.194594587	[H]O[C@@H]1[C@@H]([C@@H](C2=CC=CC=C2)[C@@]2(OC3=CC(F)=CC(F)=C3[C@]12O[H])C1=CC=C(OC)C=C1)C(=O)OC
CMLD010510	0.12099019	0.02700382	68.0881003	10.9721629	-2.743349	0.4225305	70.4070864	12.1191882	0.13709	0.07886	0.76356	0.087536622	COC1=C2C(O[C@]3(C4=CC=C(Br)C=C4)[C@@]2(O)[C@H](O)[C@H](C(N(C)OC)=O)[C@H]3C5=CC=CC=C5)=CC(OC)=C1
CMLD010511	0.21050304	0.02296101	52.5442722	9.93521359	-4.026495	0.3509034	47.0629848	10.9047032	0.34941	0.15607	0.96261	0.091082735	COC1=C2C(O[C@]3(C4=CC=C(Br)C=C4)[C@@]2(O)[C@H](O)[C@H](C(OC)=O)[C@H]3C5=CC=CC=C5)=CC(OC)=C1
CMLD010512	0.3887323	0.0396196	88.0674782	10.5167866	1.081513	1.716872	71.0410098	2.2775049	0.16974	0.04509	0.49812	0.149303671	[H]O[C@@H]1[C@@H]([C@@H](C2=CC=CC=C2)[C@@]2(OC3=CC(OC)=CC(OC)=C3[C@]12O[H])C1=CC=C(OC)C=C1)C(=O)N([H])CCCC(OC)OC
CMLD010513	0.21519065	0.01337487	80.3744307	6.51060068	-2.649312	0.3693925	84.8609845	9.26611927	0.14683	0.10985	0.5557	0.20573544	COC1=C2C(O[C@]3(C4=CC=C(OC)C=C4)[C@@]2(O)[C@H](O)[C@H](C(NOC)=O)[C@H]3C5=CC=CC=C5)=CC(OC)=C1
CMLD010514	0.26023036	0.01788445	79.8803209	5.56523124	-0.4890109	0.1614399	64.7784224	4.16095523	1.10823	0.26744	0.99644	0.059533728	[H]O[C@@H]1[C@@H]([C@@H](C2=CC=CC=C2)[C@@]2(OC3=CC(OC)=CC(OC)=C3[C@]12O[H])C1=CC=C(OC)C=C1)C(=O)N([H])OCCOCCOCCN=[N+]=[N-]
RHT	0.25631623	0.02711298	72.6139237	7.30069837	1.271928	1.369169	77.7342779	9.12801993	0.18242	0.12003	0.58692	0.137241904	COC1=C2C(O[C@]3(C4=CC=C(OC)C=C4)[C@@]2(O)[C@H](O)[C@H](C(N(C)OC)=O)[C@H]3C5=CC=CC=C5)=CC(OC)=C1
CMLD010516	0.80072192	0.07530378	31.4864538	6.06543147	2.689019	0.6476151	32.8308578	1.69606577	1.17271	0.31273	1.12598	0.129254652	[H]O[C@@H]1[C@@H]([C@@H](C2=CC=CC=C2)[C@@]2(OC3=CC(OCC4=CC=CC=C4)=CC(OC)=C3[C@]12O[H])C1=CC=C(OC)C=C1)C(=O)OC
FL3	0.48796457	0.02220478	59.4778022	7.61437753	1.296228	0.7676818	57.2084381	3.36399443	0.75489	0.12554	0.96587	0.103803295	COC1=CC2=C(C(OC)=C1)[C@]1(O)[C@H](O)C[C@@H](C3=CC=CC=C3)[C@@]1(O2)C1=CC=C(Br)C=C1
CMLD010518	0.57193231	0.1007542	72.0923198	8.83768538	-5.83752	1.021717	71.587275	6.95394445	0.73925	0.18759	0.92775	0.157240528	[H]O[C@@H]1C[C@@H](C2=CC=CC=C2)[C@@]2(OC3=CC(OC)=CC(OC)=C3[C@]12O[H])C1=CC=C(OC)C=C1
CMLD010519	0.9008305	0.05463891	6.33158841	9.07069598	2.26267	1.472994	20.1351525	7.10173982	1.19456	0.21623	1.04774	0.144133444	[H]O[C@]1([H])[C@@]2(O[H])[C@@H]([C@@H](C3=CC=CC=C3)[C@@]1(OC1=C2C(OC)=CC(OC)=C1)C1=CC=C(OC)C=C1)C(=O)NCCCC(OC)OC
CMLD010520	1.01042484	0.10650951	-3.72228312	13.1829162	1.380309	0.368301	1.43355703	6.64742599	1.00082	0.15022	0.99349	0.090256337	[H]O[C@]1([H])[C@@]2(O[H])[C@@H]([C@@H](C3=CC=CC=C3)[C@@]1(OC1=C2C=CC=C1)C1=CC=CC=C1)C(=O)OC
CMLD010522	1.01221843	0.11947554	2.90880993	7.04556595	-4.0309655	1.07348091	16.3062967	3.50398598	1.16881	0.15569	1.08526	0.122352472	[H]O[C@]1([H])[C@]2(O[H])[C@H]([C@H](C3=CC=CC=C3)[C@]1(OC1=C2C(OC)=CC(OC)=C1)C1=CC=C(Br)C=C1)C(=O)OC
CMLD010523	0.9806373	0.04539216	-1.64586269	4.4399406	-0.7462003	0.7704719	14.8573103	4.28869233	1.1716	0.18855	1.04865	0.082591823	[H]O[C@]1([H])[C@]2(O[H])[C@H]([C@H](C3=CC=CC=C3)[C@]1(OC1=C2C(OC)=CC(OC)=C1)C1=CC=C(OC)C=C1)C(=O)OC
CMLD010524	1.095199	0.03586324	-8.676203	1.897372	-0.9143578	1.088717	-3.1155117	4.62983754	0.93772	0.16448	0.97474	0.112164436	COC1=CC=C(C=C1)[C@]12OC3=CC(OC)=CC(OC)=C3[C@@]3(O[C@@H]4CCCN4C(=O)[C@@H]3[C@H]1C1=CC=CC=C1)[C@@H]2O
CMLD010527	0.95525236	0.06423697	7.99148705	9.62326032	3.849882	0.3789664	21.8696014	5.62193535	1.15152	0.18411	1.12547	0.154950214	[H]O[C@]12[C@H]3OC(=O)[C@H]3[C@H](C3=CC=CC=C3)[C@]1(OC1=CC(OC)=CC(OC)=C21)C1=CC=C(OC)C=C1
CMLD010528	0.84018618	0.0865204	54.3731598	8.67602742	-4.316917*	0.3394552	61.9125168	7.53225813	1.2155	0.24628	1.08143	0.162191656	[H]O[C@]12[C@H]3OC(=O)[C@H]3[C@H](C3=CC=CC=C3)[C@]1(OC1=CC=CC=C21)C1=CC=CC=C1
CMLD010533	0.95036493	0.06560003	27.257072	5.03374842	0.8018929	0.3645906	30.6178689	2.19753843	1.11798	0.19555	1.05917	0.094491394	[H]OC1[C@@]2(O[H])[C@H]([C@H](C3=CC=CC=C3)[C@@]1(OC1=C2C(OC)=CC(OC)=C1)C1=CC=C(OC)C=C1)C(=O)OC
CMLD010535	0.33161115	0.02941333	72.8533329	11.2532366	2.696207*	0.3036869	62.8542585	7.97624124	0.85699	0.19727	0.9621	0.058528548	[H]OC12C3=C([C@@H](C4=CC=CC=C4)[C@@]1(OC1=CC(OC)=CC(OC)=C21)C1=CC=C(OC)C=C1)C(=O)N1CCC[C@@]1([H])O3
CMLD010536	0.3400498	0.03442256	61.9001781	11.8220609	1.447808	0.5524768	57.153566	14.9994307	0.25058	0.10024	0.93519	0.119342266	COC1=CC=C(C=C1)[C@@]12OC3=CC(OC)=CC(OC)=C3[C@]1(O)[C@H](O)[C@@H]([C@H]2C1=CC=CC=C1)C(=O)C1=CC=CO1
CMLD010582	0.65794686	0.10402101	26.5953911	4.98487384	0.7415915	1.194304	49.5156126	10.1642094	0.87223	0.17301	0.81255	0.118482857	COC1=CC=C(C=C1)[C@@]12OC3=CC(OC)=CC(OC)=C3[C@]1(O)C1=C([C@H]2C2=CC=CC=C2)C(=O)N2CCC[C@@]2(C)N1
CMLD010583	0.86786925	0.05392335	34.3544871	9.14725608	0.4834529	0.7353068	45.4729631	17.3937827	1.1092	0.17625	1.05303	0.079705838	COC1=C2C(O[C@]3([C@H]([C@H](C#N)[C@@H](O)[C@@]23O)C2=CC=CC=C2)C2=CC=C(Br)C=C2)=CC(F)=C1
CMLD010584	0.90000168	0.08455037	39.0037745	10.0699153	0.4390115*	1.17898	58.2780435	17.822752	1.1552	0.24232	1.06719	0.112758192	COC(=O)[C@@H]1[C@@H](O)[C@@]2(O)C3=C(OC)C=C(F)C=C3O[C@]2([C@H]1C1=CC=CC=C1)C1=CC=C(Cl)C=C1
CMLD010585	0.90378199	0.05961661	22.7197285	9.04458013	-2.850581	0.2659218	34.0674247	7.09338662	1.15019	0.19833	1.10121	0.064001415	COC1=CC=C(C=C1)[C@]12OC3=CC(OC)=CC(OC)=C3[C@@]1(O)[C@@H](O)C[C@@H]2C1=CC=CC=C1
CMLD010833	0.95727004	0.08335614	5.0541019	7.53309921	-0.5482016	1.622837	14.0284595	7.57911514	1.16527	0.20738	1.04533	0.077535467	COC1=CC=C(C=C1)[C@]12OC3=C(C(OC)=CC(OC)=C3)[C@]1(O)C1=C([C@H]2C2=CC=CC=C2)C(=O)N2CCCC2=N1
CMLD010850	1.0060205	0.11867311	-1.21199122	11.2995119	-1.539754	0.9984611	11.3221529	8.54675946	1.11698	0.22098	1.08841	0.163026367	O[C@@H]1[C@H](C(C2=CC=CS2)=O)[C@@H](C3=CC=CC=C3)[C@]4(C5=CC=C(OC)C=C5)OC6=CC(OC)=CC(OC)=C6[C@@]41O
CMLD010852	0.61598116	0.08378342	53.0145342	9.88004191	-0.6664854	1.183897	58.9967391	10.3626451	0.84123	0.24795	0.98667	0.082254334	COC1=C2C(O[C@]3(C4=CC=C(OC)C=C4)[C@@]2(O)[C@H](O)[C@H](C(OC)=O)[C@H]3C5=CC=CC=C5)=CC(OC)=C1
CMLD010853	0.5787596	0.10362857	93.6160445	11.255953	1.730001	1.284643	82.4433079	4.95449797	0.12579	0.06504	0.8395	0.099162575	COC1=C2C(O[C@]3(C4=CC=C(OC)C=C4)[C@@]2(O)[C@H](O)[C@H](C(OC)=O)[C@H]3C5=CC=CC=C5)=CC(OC)=C1
CMLD010854	0.52300207	0.05225316	57.4953317	4.83863658	-0.2954528	0.7992162	59.3167408	5.74188012	0.8664	0.14044	0.94196	0.089362035	COC1=C2C(O[C@]3(C4=CC=C(OC)C=C4)[C@@]2(O)C5=C(C(O)=NN5)[C@H]3C6=CC=CC=C6)=CC(OC)=C1
CMLD010855	0.73192852	0.08525018	50.7197657	7.56563379	2.318718	0.4191505	57.9783982	23.056851	0.88428	0.1846	0.9323	0.186136128	COC1=C2C(O[C@]([C@H](C3=CC=CC=C3)[C@H]4C(OC)=O)(C5=CC=C(OC)C=C5)[C@@]2(O)C4=O)=CC(OC)=C1
CMLD010856	0.87328494	0.05995275	6.16717934	9.88204458	-1.88942	0.2632706	16.5198683	8.2299163	1.106	0.2212	1.04295	0.135181307	COC1=C2C(O[C@]([C@H](C3=CC=CC=C3)[C@H]4C(OC)=O)(C5=CC=C(OC)C=C5)[C@@]2(O)C4=O)=CC(OC)=C1
CMLD010857	0.99181445	0.06485753	3.68393459	6.51835802	-0.9584947	0.8315646	24.4120959	6.50385361	1.00166	0.15428	1.02855	0.075652079	COC1=C2C(O[C@]3(C4=CC=C(Br)C=C4)[C@@]2(O)[C@H](O)[C@@H](C(OC)=O)[C@@H]3C5=CC=CC=C5)=CC(OS(C6=CC=C(C)C=C6)(=O)=O)=C1
CMLD010858	0.96392971	0.05176019	-3.19859659	6.14143541	-0.8902757	1.167668	10.7352736	5.7064113	1.09338	0.16082	1.06822	0.087451858	COC(=O)[C@@H]1[C@@H](C2=CC=CC=C2)[C@@]2(OC3=CC(OC)=CC(OC)=C3[C@@]1(O)C2(O)O)C1=CC=C(OC)C=C1
CMLD010865	0.99628144	0.08248553	4.27679578	10.2206578	-1.776095	0.8054614	15.600789	11.9155876	1.19767	0.31059	1.06181	0.06151208	O[C@@]12[C@@]([C@H](C3=CC=CC=C3)[C@@H](C(OC)=O)[C@H]2O)(C4=CC=C(OC)C=C4)N(C)C5=C1C(F)=CC=C5
CMLD010866	1.01401481	0.09939999	8.55333531	6.27484663	-4.19926	0.5693113	15.9833693	11.4554777	1.20202	0.23499	1.13924	0.103435096	O[C@@]12[C@@]([C@H](C3=CC=CC=C3)C[C@H]2O)(C4=CC=C(OC)C=C4)N(C)C5=C1C(F)=CC=C5
CMLD010867	0.99596325	0.10840644	5.7457192	8.17083394	1.46791	1.297958	10.6372386	10.3310825	1.10978	0.17546	1.03743	0.031027692	O[C@@]12[C@@]([C@H](C3=CC=CC=C3)[C@@H](C(OC)=O)[C@H]2O)(C4=CC=C(OC)C=C4)N(C)C5=C1C(OC)=CC=C5
CMLD010868	0.94259833	0.09337445	1.14743271	11.1765436	8.211238	0.9021693	8.39803656	7.04391653	1.01813	0.13364	0.97247	0.140412364	O[C@@]12[C@@]([C@H](C3=CC=CC=C3)C[C@H]2O)(C4=CC=C(OC)C=C4)N(C)C5=C1C(OC)=CC=C5
CMLD010869	0.7677447	0.12023991	-2.99425595	11.0927747	-0.5448524	2.217923	12.6063765	11.0312431	0.90623	0.1893	0.87751	0.094808501	COC(=O)[C@H]1[C@@H](O)[C@@]2(O)C3=C(C=CC=C3OC)N(C)[C@]2([C@@H]1C1=CC=CC=C1)C1=CC=C(Br)C=C1
CMLD010870	0.94082931	0.02486746	1.92986771	11.7685684	-0.8090127	0.8683751	34.2533913	27.8011459	1.10299	0.242	1.06143	0.13588913	O[C@@]12[C@@]([C@H](C3=CC=CC=C3)[C@@H](C(OC)=O)[C@H]2O)(C4=CC=C(Br)C=C4)N(C)C5=C1C(OC)=CC(OC)=C5
CMLD011157	0.96798222	0.09677523	-1.79493511	11.9479122	0.01640815	0.7229729	4.59204816	17.3043231	1.13796	0.20231	1.09074	0.088534592	COC1=CC(OC)=C([C@@](O)(C2O)[C@H]([C@@H]3C4=CC=CC=C4)C(OC)=O)C(O[C@@]32C5=CC=C(OC)C=C5)=C1
CMLD011166	0.74036235	0.0545077	110.330688	13.4163531	0.3809214	0.4825381	95.7938023	24.5079222	0.29739	0.16592	1.07329	0.176891239	O[C@@]12[C@@]([C@H](C3=CC=CC=C3)C[C@@H]2O)(C4=CC=C(Cl)C=C4)OC5=CC(OCCN6CCCC6)=CC=C51
CMLD011167	0.74711425	0.08333281	111.816985	16.488323	0.4139448	0.1988816	99.9479137	16.5161755	0.12534	0.04425	0.95113	0.038973043	O[C@@]12[C@@]([C@H](C3=CC=CC=C3)C[C@@H]2O)(C4=CC=C(Cl)C=C4)OC5=CC(OCCNC)=CC=C51

CMLD011244	0.79872774	0.11082818	-1.84243108	11.6317248	-1.389151	1.059521	15.8350296	8.47239333	0.99474	0.14297	0.82889	0.14759674	COC1=C2C(OC(C3=CC=C(Br)C=C3)C2=O)=CC(OC)=C1
CMLD011294	0.98523275	0.09307134	0.35822819	12.6226586	-2.27159	1.12022	15.7031209	10.4703968	1.11369	0.19048	1.03139	0.166491252	O[C@@]12[C@@]([C@H](C3=CC=CC=C3)C[C@H]2O)(C4=CC=C(Br)C=C4)N(C)C5=C1C(OC)=CC(OC)=C5
CMLD011295	0.98437554	0.0618921	-2.33168488	13.6313472	-2.815487	0.3809276	19.2247374	11.607718	1.09982	0.21232	1.03899	0.188098637	O[C@@]12[C@@]([C@H](C3=CC=CC=C3)[C@@H](C(OC)=O)[C@H]2O)(C4=CC=C(OC)C=C4)N(CC=C)C5=C1C(OC)=CC(OC)=C5
CMLD011296	1.07706267	0.0773044	20.0524077	16.3408958	-3.440863	0.6377589	42.9334327	13.3635963	1.12458	0.21958	1.05203	0.127368304	O[C@@]12[C@@]([C@H](C3=CC=CC=C3)[C@@H](C(OC)=O)[C@H]2O)(C4=CC=C(OC)C=C4)NC5=C1C(OC)=CC(OC)=C5
CMLD011297	1.01986648	0.06763829	2.0276151	13.8041201	-0.5956184	0.58861778	23.2111466	12.2895526	1.11792	0.20285	1.02427	0.160864868	O[C@@]12[C@@]([C@H](C3=CC=CC=C3)[C@@H](C(OC)=O)[C@H]2O)(C4=CC=C(OC)C=C4)N(C/C=C/C(OC)=O)C5=C1C(OC)=CC(OC)=C5
CMLD011298	0.84591401	0.1177504	-5.03238302	16.1905722	1.551605*	1.996418*	20.5067609	6.65241943	0.9772	0.22579	0.93741	0.130605593	O[C@@]12[C@@]([C@H](C3=CC=CC=C3)[C@@H](C(NOC)=O)[C@H]2O)(C4=CC=C(Br)C=C4)N(C)C5=C1C(OC)=CC(OC)=C5
CMLD011352	0.75071626	0.00696449	105.610587	6.8453521	0.03874517	1.382807	122.115276	14.8326636	1.14357	0.19169	1.10093	0.17526851	COC1=CC(F)=CC2=C1[C@]1(O)C(O)[C@@H]([C@@H](C3=CC=CC=C3)[C@@]1(O2)C1=CC=C(Br)C=C1)C(=N)NO
CMLD011353	0.41968552	0.04702381	52.185556	18.0606141	-0.926564	0.08316994	59.8892164	14.7676653	0.65653	0.18405	0.79431	0.081843107	[H][C@@]12CCCN1C(=O)C1=C(N2)[C@@]2(O)C3=C(C[C@]2([C@@H]1C1=CC=CC=C1)C1=CC=C(Br)C=C1)C=C(F)C=C3OC
CMLD011403	0.68263432	0.10906221	16.5287284	13.2344261	-2.617286	0.8337824	27.4644058	11.1535126	1.13773	0.29127	1.00177	0.179672454	O[C@@]12[C@@]([C@H](C3=CC=CC=C3)[C@@H](C(C4=CC(C=CC=C5)=C5N4C)=O)[C@H]2O)(C6=CC=C(OC)C=C6)OC7=CC(OC)=CC(OC)=C71
CMLD011404	0.34482591	0.03889917	40.5836589	15.4634269	-2.659949	0.6492308	42.7793377	10.7643886	0.38236	0.22191	0.99031	0.117069588	O[C@@]12[C@@]([C@H](C3=CC=CC=C3)[C@@H](C(C4=CC=C(C)O4)=O)[C@H]2O)(C5=CC=C(OC)C=C5)OC6=CC(OC)=CC(OC)=C61
CMLD011405	0.60882315	0.11527056	22.784132	10.974664	-2.072262	0.7072069	27.3342006	6.22935238	1.05908	0.22409	1.07571	0.074584732	O[C@@]12[C@@]([C@H](C3=CC=CC=C3)[C@@H](C(C4=CC(C)=C(C)O4)=O)[C@H]2O)(C5=CC=C(OC)C=C5)OC6=CC(OC)=CC(OC)=C61
CMLD011406	0.43560312	0.03954525	30.6282096	13.7504761	-5.63624	0.5829946	36.4443216	8.73682819	1.01984	0.28037	1.0548	0.125922954	O[C@@]12[C@@]([C@H](C3=CC=CC=C3)[C@@H](C(C4=CC=C(CCC)O4)=O)[C@H]2O)(C5=CC=C(OC)C=C5)OC6=CC(OC)=CC(OC)=C61
CMLD011407	0.51716232	0.08865985	29.3383796	11.9153468	-1.506765	1.58605	27.2830726	9.37595329	1.14712	0.1845	1.02717	0.132262206	O[C@@]12[C@@]([C@H](C3=CC=CC=C3)[C@@H](C(C4=NC=CN4C)=O)[C@H]2O)(C5=CC=C(OC)C=C5)OC6=CC(OC)=CC(OC)=C61
CMLD011408	0.33887552	0.04824211	36.2390406	17.4259012	-0.7136276	0.5327247	42.976078	16.2508654	0.98491	0.17975	1.04903	0.101295771	O[C@@]12[C@@]([C@H](C3=CC=CC=C3)[C@@H](C(C4=CC5=C(C=CC=C5)O4)=O)[C@H]2O)(C6=CC=C(OC)C=C6)OC7=CC(OC)=CC(OC)=C71
CMLD011409	0.85362275	0.14039658	-0.40673028	10.2051131	-0.2170284	1.297125	12.3891677	7.16193089	0.96903	0.14196	0.94512	0.097427689	O[C@@]12[C@@]([C@H](C3=CC=CC=C3)[C@@H](C(C4=CC=CC=C4)=O)[C@H]2O)(C5=CC=C(OC)C=C5)OC6=CC(OC)=CC(OC)=C61
CMLD011410	0.32773954	0.0195094	18.6823391	9.79676834	-0.7393329	1.995334	41.9267999	6.99925186	0.69375	0.1466	0.80354	0.146018189	O[C@@]12[C@@]([C@H](C3=CC=CC=C3)[C@@H](C(C4=C(OC)C=CC=C4)=O)[C@H]2O)(C5=CC=C(OC)C=C5)OC6=CC(OC)=CC(OC)=C61
CMLD011411	0.90416116	0.07726463	-9.01952554	7.23922356	-2.595303	0.9239766	-4.2286252	8.18644434	1.10148	0.26402	0.98907	0.14106716	O[C@]1([C@@]2([H])O)[C@@H](C3=CC=CC=C3)[C@@H](C(NCCCCNC(C4=CC=CC=C4)=O)=O)C2(C5=CC=C(OC)C=C5)OC6=CC(OC)=CC(OC)=C61
CMLD011452	1.02389937	0.10376527	-3.42222762	8.08528273	-2.2104	1.465814	3.28746819	4.38714957	1.14022	0.29467	1.04466	0.184880712	FC(F)(F)COC1=C2C(C(C3=CC=C(Br)C=C3)OC2=O)=CC(F)=C1
CMLD011453	0.8961851	0.06790874	21.5487939	14.5295343	-1.430788	0.5588655	32.7618093	8.90193646	1.09791	0.24048	1.04527	0.201510989	FC1=C2C(O[C@]([C@H](C3=CC=CC=C3)C4)(C5=CC=C(Br)C=C5)[C@@]2(O)C4=O)=CC(F)=C1
CMLD011454	0.91341858	0.05716433	29.1198812	15.5949413	3.72106662	2.6668815	37.4495312	4.40754344	1.12671	0.29412	1.07523	0.14319542	FC1=C2C(O[C@]3(C4=CC=C(Br)C=C4)[C@@]2(O)[C@H](O)C[C@H]3C5=CC=CC=C5)=CC(F)=C1
CMLD011455	0.85869783	0.0642371	-2.13138252	11.2378663	-3.425611	1.434806	2.8959895	3.87540544	1.01416	0.26509	0.99767	0.140509327	O[C@]1(C2=O)[C@@H](C(OC)=O)[C@@H](C3=CC=CC=C3)C2(C4=CC=C(Br)C=C4)N(C)C5=CC(OC)=CC(OC)=C51
CMLD011472	0.69656587	0.04913792	45.5996599	8.33101738	-2.406668	1.110581	40.5625827	7.63698071	1.01202	0.30724	1.03028	0.116032542	OC1=CC(OC)=C2C(O[C@]3(C4=CC=C(Br)C=C4)[C@@]2(O)[C@H](O)C[C@H]3C5=CC=CC=C5)=C1
CMLD011610 (RHT)	0.449755	0.0455216	89.02657	1.894295	-4.406315	1.747159	92.7863274	5.81908173	0.17724	0.08768	0.737	0.188931101	CON(C)C(=O)[C@H]1[C@@H](O)[C@@]2(O)C3=C(O[C@]2([C@@H]1C1=CC=CC=C1)C1=CC=C(OC)C=C1)C=C(OC)C=C3OC
CMLD011615	1.00200294	0.03188893	-21.6090773	8.77328145	-5.920433	2.332845	1.68712241	4.6454086	0.75371	0.13362	0.89023	0.081034461	COC1=C2C(O[C@@]3(C4=CC=C(Br)C=C4)[C@H](C5=CC=CC=C5)[C@@H](C(OC)=O)[C@@]2(C3(O)O)O)=CC(OC)=C1
CMLD011683	0.9509794	0.03756003	-7.99655616	5.50516489	4.95442283	1.58028941	9.66865078	6.6185144	1.09531	0.11462	1.08918	0.103863541	COC1=C2C(O[C@@]3(C4=CC=C(OC)C=C4)[C@H](C5=CC=CC=C5)[C@@H](C(OC)=O)[C@@]2([C@]3([H])O)O)=CC(OC)=C1
CMLD011684	0.93089507	0.02112922	-11.792303	9.79455464	-1.3611247	0.64127385	15.0609321	2.86853688	1.15185	0.18285	1.03923	0.108528041	COC1=C2C(O[C@@]3(C4=CC=C(OC)C=C4)[C@H](C5=CC=CC=C5)[C@@H](C(OC)=O)[C@@]2([C@]3(O)[H])O)=CC(OC)=C1
CMLD011685	1.01284161	0.02587493	3.45567621	4.42220423	0.04613006	1.84219257	-1.9641325	7.35511588	1.10754	0.2261	1.08701	0.172408647	CCOCCOCCN(OC)C(=O)[C@H]1[C@@H](O)[C@@]2(O)C3=C(O[C@]2([C@@H]1C1=CC=CC=C1)C1=CC=C(OC)C=C1)C=C(OC)C=C3OC
CMLD011702	0.6684463	0.02521869	83.93735	2.194825	10.9	11.3084776	76.8050973	3.81442456	0.55187	0.16564	0.82325	0.185223578	COC1=CC=C(C=C1)[C@@]12OC3=CC(OC)=CC(OC)=C3[C@]1(O)C1=C([C@H]2C2=CC=CC=C2)C(=O)N2CCCC2=N1
CMLD011831	0.8448681	0.02260498	37.2142643	1.60108616	-2.4056175	1.08874187	41.079215	8.91934986	1.11667	0.21448	1.04315	0.100195748	COC1=CC=C(C=C1)[C@@]12OC3=CC(OC)=CC(OC)=C3[C@]1(O)C1=C([C@H]2C2=CC=CC=C2)C(=O)N=CN1
CMLD011832	0.77835524	0.03764207	22.7869275	9.74590846	-6.2310012	1.10962137	44.4453619	12.3817247	1.1482	0.2191	1.1413	0.115607728	COC1=CC=C(C=C1)[C@@]12OC3=CC(OC)=CC(OC)=C3[C@]1(O)C1=C([C@H]2C2=CC=CC=C2)C(=O)N=C(N1)C1=CC=C(F)C=C1
CMLD011833	0.76478472	0.05588362	39.9499986	14.0805122	-2.1442224	0.84471578	71.8381812	25.4055653	1.08648	0.17556	1.08326	0.161057518	COC1=CC=C(C=C1)C1=NC(=O)C2=C(N1)[C@@]1(O)C3=C(OC)C=C(OC)C=C3O[C@]1([C@@H]2C1=CC=CC=C1)C1=CC=C(OC)C=C1
CMLD011839	0.68420881	0.02907922	60.9603062	4.38637434	-1.181407	0.33639852	27.9342042	2.37293396	1.10663	0.18686	1.02668	0.210899364	COC1=CC=C(C=C1)[C@@]12OC3=CC(OC)=CC(OC)=C3[C@]1(O)C1=C([C@H]2C2=CC=CC=C2)C(=O)N2CCCCC2=N1
CMLD011840	0.59205723	0.04984937	61.87533	9.47806299	-3.4741876	0.83384617	71.6342599	15.3162507	1.06475	0.09157	1.00776	0.075703869	COC1=CC=C(C=C1)[C@@]12OC3=CC(OC)=CC(OC)=C3[C@]1(O)C1=C([C@H]2C2=CC=CC=C2)C(=O)N=C(N1)C1CC1
CMLD011841	0.98037623	0.03813327	9.63246789	5.27086838	1.29902536	2.85836996	21.7709323	10.8207924	0.9284	0.1054	0.88554	0.154931692	CCOC(=O)[C@H]1[C@@H](O)[C@@]2(O)C3=C(O[C@]2([C@@H]1C1=CC=C(Br)C=C1)C1=CC=C(OC)C=C1)C=C(OC)C=C3OC
CMLD011842	0.91094557	0.0233439	43.0860255	12.8859872	4.58181749	0.17814528	56.2907999	10.4704595	1.12429	0.10987	1.13094	0.160361461	CON(C)C(=O)[C@H]1[C@@H](O)[C@@]2(O)C3=C(O[C@]2([C@@H]1C1=CC=C(Br)C=C1)C1=CC=C(OC)C=C1)C=C(OC)C=C3OC
CMLD011845	1.067848	0.02446569	-6.431582	1.820242	-0.4343927	3.50932418	-2.0014331	3.50921382	1.2004	0.24879	1.02613	0.076210574	CON(C)C(=O)[C@H]1[C@@H](O)[C@@]2(OC)C3=C(O[C@]2([C@@H]1C1=CC=C(C=C1)C(=O)C(F)F)C1=CC=C(OC)C=C1)C=C(OC)C=C3OC
CMLD011849	0.87313154	0.00690643	54.1301046	18.5025298	-3.1483543	1.00500979	57.0937671	14.84525	1.13246	0.16635	1.10136	0.12917052	COC1=CC=C(C=C1)[C@@]12OC3=CC(OC)=CC(OC)=C3[C@]1(O)C1=C([C@H]2C2=CC=CC=C2)C(=O)N=C(N1)C1=CC=CC=C1
CMLD011850	0.9993636	0.03027844	65.4392	1.939111	-2.7317772	0.63768519	52.8916002	6.6407691	0.92631	0.10782	0.95511	0.310192245	COC1=CC=C(C=C1)[C@@]12OC3=CC(OC)=CC(OC)=C3[C@]1(O)C1=C([C@@H]2C2=CC=CC=C2)C(=O)N2CCCC2=N1
CMLD011853	1.167744	0.03705836	10.97934	3.341654	-1.0250314	1.23715323	7.72079659	4.45724951	0.94558	0.11973	0.91737	0.278529934	COC(=O)C1=C(OS(=O)(=O)C2=CC=C(C)C=C2)[C@@]2(O)C3=C(O[C@]2([C@@H]1C1=CC=CC=C1)C1=CC=C(OC)C=C1)C=C(OC)C=C3OC
CMLD011865	0.71228491	0.081945	76.3971051	10.6494093	-5.0591527	1.6587702	87.9215213	7.5280165	1.21468	0.21556	1.19171	0.175846096	COC1=CC=C(C=C1)[C@@]12OC3=CC(OC)=CC(OC)=C3[C@]1(O)C1=C([C@H]2C2=CC=CC=C2)C(=O)N=C(N1)C(C)C
CMLD011866	0.53028266	0.03942738	99.9916393	13.9510265	-7.1206156	1.53626824	105.321033	7.86833595	1.06556	0.24927	1.07921	0.096936231	COC1=CC=C(C=C1)[C@@]12OC3=CC(OC)=CC(OC)=C3[C@]1(O)C1=C([C@H]2C2=CC=CC=C2)C(=O)N2CCCC2=N1
CMLD011871	0.97087676	0.08115433	74.7107829	13.861114	0.55258763	0.35876577	70.6914987	10.8256834	1.16128	0.12623	1.08222	0.087871046	COC1=CC=C(C=C1)[C@@]12OC3=CC(OC)=CC(OC)=C3[C@]1(O)[C@H](O)[C@@H]([C@H]2C1=CC=C(O)C=C1)C(=O)C1=CC=CO1
CMLD011872	0.72945346	0.01813274	67.1512094	14.2314308	-0.7054736	0.835926	27.1937192	5.54179301	1.21695	0.11742	1.11016	0.156431203	COC1=CC=C(C=C1)[C@@]12OC3=CC(O)=CC(OC)=C3[C@]1(O)[C@H](O)[C@@H]([C@H]2C1=CC=CC=C1)C(=O)C1=CC=CO1
CMLD011876	0.99182939	0.03787021	45.1553296	3.46883124	-1.7333279	1.27028	59.3738407	13.4522667	1.2012	0.2658	1.06674	0.234703068	COC(=O)[C@@H]1[C@@H](O)[C@@]2(O)C3=C(O[C@]2([C@H]1C1=CC=CC=C1)C1=CC=C(Br)C=C1)C=C(OC)C=C3OC
CMLD011877	0.9412632	0.0164692	47.4248006	14.5963408	-4.0341582	1.27295559	64.962911	11.0485688	0.90792	0.13374	0.983	0.17291653	CONC(=O)[C@@H]1[C@@H](O)[C@@]2(O)C3=C(O[C@]2([C@H]1C1=CC=CC=C1)C1=CC=C(Br)C=C1)C=C(OC)C=C3OC
CMLD011878	0.89046801	0.03450831	73.6880431	10.2377069	-3.0976953	1.42972677	76.4909734	1.12165217	1.17144	0.17761	1.12979	0.184132852	CON(C)C(=O)[C@H]1[C@@H](O)[C@@]2(O)C3=C(O[C@]2([C@@H]1C1=CC=C(O)C=C1)C1=CC=C(OC)C=C1)C=C(OC)C=C3OC
CMLD011879	0.62397557	0.02895109	78.3470197	6.95619068	-2.2004137	4.95497103	96.8226223	4.82725475	1.133	0.18938	1.10369	0.108079543	CON(C)C(=O)[C@H]1[C@@H](O)[C@@]2(O)C3=C(O[C@]2([C@@H]1C1=CC=CC=C1)C1=CC=C(OC)C=C1)C=C(O)C=C3OC
SDS-1-0-21	0.10916397	0.01231618	113.925554	11.084326	-0.359621	1.49581057	117.853139	25.3546409	0.19458	0.06069	0.93695	0.13722854	CONC(=O)[C@H]1[C@@H](O)[C@@]2(O)C3=C(O[C@]2([C@@H]1C1=CC=CC=C1)C1=CC=C(Br)C=C1)C=C(OC)C=C3OC
CMLD011882	0.68068006	0.15658541	15.0593937	5.46476987	2.78958405	4.35836243	43.9673915	19.949857	1.12705	0.15979	1.07682	0.127530762	COC(=O)[C@H]1[C@@H](O)[C@@]2(O)C3=C(O[C@]2([C@@H]1C1=CC=CC=C1)C1=CC=C(Br)C=C1)C=C(OS(=O)(=O)C1=CC=C(C)C=C1)C=C3OC
CMLD011883	0.69260885	0.15479755	15.4341822	5.566712	-3.6565748	0.34748615	39.075	22.625	1.13956	0.1343	1.03577	0.134158287	COC(=O)[C@H]1[C@@H](O)[C@@]2(O)C3=C(O[C@]2([C@@H]1C1=CC=CC=C1)C1=CC=C(Br)C=C1)C=C(OS(=O)(=O)C1=CC=C(C)C=C1)C=C3OC
CMLD011884	0.91443978	0.03804642	-5.18228086	9.91508336	-3.1522712	1.05873209	-7.7354613	5.18147276	1.08879	0.21067	1.01022	0.111513407	COC(=O)[C@@H]1[C@@H](O)[C@@]2(O)C3=C(O[C@]2([C@H]1C1=CC=CC=C1)C1=CC=C(OC)C=C1)C=C(OS(=O)(=O)C1=CC=C(C)C=C1)C=C3OC
CMLD011885	0.46149763	0.01154696	91.5705398	13.9338784	-4.0303473	0.73979916	106.362632	16.9442768	0.95442	0.10174	1.03574	0.28271396	COC1=CC=C(C=C1)[C@@]12OC3=CC(OC)=CC(OC)=C3[C@]1(O)[C@H](O)[C@@H]([C@H]2C1=CC=CC=C1)C(O)=O
CMLD011886	0.40187429	0.02313879	105.998487	16.2167491	-4.7037126	1.43776442	121.088489	2.99003681	1.1659	0.18924	1.04605	0.125226605	COC1=CC=C(C=C1)[C@@]12OC3=CC(OC)=CC(OC)=C3[C@]1(O)[C@H](O)[C@@H]([C@H]2C1=CC=CC=C1)C(O)=O
CMLD011887	0.69957776	0.13724811	28.5217791	6.22282835	-7.2491951	1.60061412	53.2003855	3.94120999	1.18935	0.09463	0.99347	0.143815188	COC(=O)[C@H]1[C@@H](O)[C@@]2(O)C3=C(O[C@]2([C@@H]1C1=CC=CC=C1)C1=CC=C(OC)C=C1)C=C(OS(=O)(=O)C1=CC=C(C)C=C1)C=C3OC
CMLD011888	0.83517447	0.02202886	86.0362233	15.468077	-0.2886638	2.92577218	110.011472	8.60081531	1.21008	0.15462	1.05875	0.132366933	COC1=CC=C(C=C1)[C@@]12OC3=CC(OC)=CC(OC)=C3[C@]1(O)C(=O)[C@@H]([C@H]2C1=CC=CC=C1)C(=O)NCCCC1(C)OCCO1
CMLD011889	0.57239528	0.05510613	38.1696782	3.00195949	-1.6784903	2.61526436	73.0924873	1.07587594	1.20822	0.18138	1.0189	0.120052226	CON(C)C(=O)[C@H]1[C@@H](O)[C@@]2(O)C3=C(O[C@]2([C@@H]1C1=CC=CC=C1)C1=CC=C(Br)C=C1)C=C(O)C=C3OC
CMLD011891	0.45845257	0.02979331	101.049418	9.25323413	-2.2546725	1.07395491	138.406056	6.60950374	1.17333	0.15027	1.09001	0.145710191	COC(=O)[C@H]1[C@@H](O)[C@@]2(O)C3=C(O[C@]2([C@@H]1C1=CC=CC=C1)C1=CC=C(Br)C=C1)C=C(O)C=C3OC
CMLD011892	0.99653092	0.11069134	26.9173571	14.8023741	-4.0521168	1.96030458	48.1645365	4.89442989	1.06622	0.097	0.996	0.188218186	COC(=O)[C@H]1[C@@H](O)[C@@]2(O)C3=C(O[C@]2([C@@H]1C1=CC=CC=C1)C1=CC=C(OC)C=C1)C=C(O)C=C3OC
CMLD011929	0.7459486	0.0549469	67.38379	2.823519	1.18160316	1.97634751	54.0399051	6.14449546	0.97365	0.13991	0.929	0.220906566	COC1=CC=C(C=C1)[C@@]12OC3=CC(OC)=CC(OC)=C3[C@]1(O)C=C([C@H]2C1=CC=CC=C1)C(=O)C1=CC=CO1
CMLD012038	0.92057054	0.01460259	26.560533	3.1685271	0.32696971	2.01554567	13.1535689	4.06385209	0.94804	0.10655	0.90846	0.125051058	COC1=CC=C(C=C1)[C@@]12OC3=CC(OC)=CC(OC)=C3[C@]1(O)C1=C([C@H]2C2=CC=CC=C2)C(=O)N(C(NC2=CC=CC=C2)=N1)C1=CC=CC=C1
CMLD012039	1.37075028	0.03791484	23.5766997	6.98271496	1.0553732	2.17823853	18.7833333	7.63469784	1.10699	0.13139	1.05324	0.107068209	COC1=CC=C(C=C1)[C@@]12OC3=CC(OC)=CC(OC)=C3[C@]1(O)C(=O)C(CC1=CC=CC=C1)=C2C1=CC=CC=C1
CMLD012040	0.64440305	0.01594133	74.3550851	9.72608353	0.54719711	2.91164086	35.9953178	6.26483478	1.02349	0.08531	0.9965	0.126416709	COC1=CC=C(C=C1)[C@@]12OC3=CC(OC)=CC(OC)=C3[C@]1(O)C1=C([C@H]2C2=CC=CC=C2)C(=O)N=C(N1)N1CCOCC1
CMLD012041	0.83086424	0.01303802	48.8480518	4.2718841	1.38387311	1.43108571	40.3094172	5.78280092	0.98277	0.08229	1.04169	0.160470748	COC1=CC=C(C=C1)[C@@]12OC3=CC(OC)=CC(OC)=C3[C@]1(O)C1=C([C@H]2C2=CC=CC=C2)C(=O)N=C(N1)C1=CC=NC=C1
CMLD012042	1.05750062	0.03027909	70.28901	6.353523	-0.8530895	0.76600897	61.5022536	4.11285708	1.04483	0.10509	0.97842	0.084474421	COC1=CC=C(C=C1)[C@@]12OC3=CC(OC)=CC(OC)=C3[C@]1(O)C1=C([C@H]2C2=CC=CC=C2)C(=O)N=C(N1)C1=CC=CN=C1
CMLD012043	1.03424128	0.06214603	25.8154447	3.60643596	-2.8786661	1.06285261	5.26822192	1.88819715	1.13141	0.09659	1.06865	0.16920042	COC1=CC=C(C=C1)[C@@]12OC3=CC(OC)=CC(OC)=C3[C@]1(O)C1=C([C@H]2C2=CC=CC=C2)C(=O)N=C(N1)C1=CC=C(C)C=C1
CMLD012044	0.99170394	0.01808085	39.6001015	3.77724714	-3.3892444	1.48368019	31.1474842	3.00933433	1.14898	0.0941	1.02445	0.067179179	COC1=CC=C(C=C1)[C@@]12OC3=CC(OC)=CC(OC)=C3[C@]1(O)C1=C([C@H]2C2=CC=CC=C2)C(=O)N=C(N1)C1=CC=CC(OC)=C1
CMLD012045	0.7532857	0.01907534	72.7864756	5.90680955	1.43806522	1.79838929	79.3627781	6.39440177	1.02757	0.12761	1.03567	0.141871354	COC(=O)CC1=NC(=O)C2=C(N1)[C@@]1(O)C3=C(O[C@]1([C@@H]2C1=CC=CC=C1)C1=CC=C(OC)C=C1)C=C(OC)C=C3OC
CMLD012046	0.83762658	0.03562225	78.9484016	5.95835387	0.40394778	1.75987674	67.8871925	7.013308	1.0624	0.12162	0.98089	0.079955563	CCOC(=O)CC1=NC(=O)C2=C(N1)[C@@]1(O)C3=C(O[C@]1([C@@H]2C1=CC=CC=C1)C1=CC=C(OC)C=C1)C=C(OC)C=C3OC
CMLD012047	0.81058079	0.0348677	70.1992046	4.65878279	0.6801614	2.31362522	63.6148702	6.48397329	1.11131	0.128	1.11268	0.100287578	COC1=CC=C(C=C1)[C@@]12OC3=CC(OC)=CC(OC)=C3[C@]1(O)C1=C([C@H]2C2=CC=CC=C2)C(=O)N=C(N1)C1=CSC(C)=N1
CMLD012048	1.08581152	0.02980706	60.4884975	4.5737372	0.29849657	2.69492773	33.1629825	3.97354658	1.11819	0.11154	1.0292	0.092621453	COC1=CC=C(C=C1)[C@@]12OC3=CC(OC)=CC(OC)=C3[C@]1(O)C1=C([C@@H]2C2=CC=CC=C2)C(=O)N=C(N1)C1=CC=CC=C1
CMLD012049	0.4159262	0.01177647	77.1569	2.10734	-0.350365	1.69988009	77.0885936	8.94972024	0.97124	0.13065	1.02257	0.1769151	COC1=CC=C(C=C1)[C@@]12OC3=CC(OC)=CC(OC)=C3[C@]1(O)[C@@H](O)[C@@H]([C@H]2C1=CC=CC=C1)C(=O)C1=CC=CO1
CMLD012050	1.05343	0.07699442	90.91727	2.114875	-1.6550007	1.48150513	85.7259218	6.39137788	0.87388	0.1934	0.92169	0.163570335	COC1=CC=C(C=C1)[C@@]12OC3=CC(OC)=CC(OC)=C3[C@]1(O)C(=O)C[C@H]2C1=CC=CC=C1
CMLD012051	0.99512417	0.03025512	85.2993248	5.85982551	-3.9435455	0.71712328	83.563281	7.72102409	1.17694	0.11404	1.04568	0.117479822	COC1=CC=C(C=C1)[C@@]12OC3=CC(OC)=CC(OC)=C3[C@]1(O)[C@@H](O)C[C@H]2C1=CC=CC=C1
CMLD012070	0.58473266	0.02445646	83.4056796	5.77993365	-5.4	1.95959179	66.9331603	5.49666833	1.14037	0.18507	1.04801	0.081199469	COC(=O)[C@@H]1[C@@H](C2=CC=CC=C2)[C@@]2(OC3=CC(OC)=CC(OC)=C3[C@@]22N=C3CCCN3[C@@]12O)C1=CC=C(OC)C=C1
CMLD012071	0.96409557	0.04061756	42.761822	7.24370916	-4.5592043	1.1709686	27.5971368	1.58583464	1.13022	0.13043	1.05571	0.053374686	COC1=CC=C(C=C1)[C@@]12OC3=CC(OC)=CC(OC)=C3[C@]1(O)C(=O)[C@@H]([C@H]2C1=CC=CC=C1)C(=O)NC1=CC=CC=N1
CMLD012072	0.153684	0.00801142	122.728499	5.71450922	-6.041068	1.47559998	105.771671	4.65343771	0.24545	0.06242	0.96919	0.105967792	COC(=O)[C@@H]1[C@@H](C2=CC=CC=C2)[C@@]2(OC3=CC(OC)=CC(OC)=C3[C@@]22NC(=N[C@@]12O)C1CC1)C1=CC=C(OC)C=C1
CMLD012073	0.10724119	0.00759297	120.040844	4.33107651	1.97490425	0.57779601	111.384142	2.4701127	0.19234	0.06018	0.86497	0.141578772	COC(=O)[C@@H]1[C@@H](C2=CC=CC=C2)[C@@]2(OC3=CC(OC)=CC(OC)=C3[C@@]22NC(C)=N[C@@]12O)C1=CC=C(OC)C=C1
CMLD012074	1.124544	0.02341884	14.6837	2.589497	-0.4762857	1.23767469	8.23022291	3.8644917	1.13184	0.214	1.08731	0.110882279	COC1=CC=C(C=C1)[C@@]12OC3=CC(OC)=CC(OC)=C3[C@]1(O)C(OS(=O)(=O)C1=CC=C(C)C=C1)=C([C@H]2C1=CC=CC=C1)C(=O)NC1=CC=CC=N1
CMLD012075	0.40237632	0.03519451	76.0120336	4.10491442	-0.2512608	1.54981494	66.3951062	5.3155478	0.91396	0.12105	0.9231	0.118616567	COC(=O)[C@@H]1[C@@H](C2=CC=CC=C2)[C@@]2(OC3=CC(OC)=CC(OC)=C3[C@@]22NC(=N[C@@]12O)C1=CC=CC=C1)C1=CC=C(OC)C=C1
CMLD012076	0.74994116	0.08047144	49.8893629	2.37504717	1.02816516	2.99744358	22.3833333	7.9400007	1.06837	0.19763	1.04265	0.191485864	CCCC[C@@]12CCCN1C(=O)C1=C(N2)[C@@]2(O)C3=C(O[C@]2([C@@H]1C1=CC=CC=C1)C1=CC=C(OC)C=C1)C=C(OC)C=C3OC
CMLD012077	0.94596268	0.0443055	102.639699	12.4217889	-1.2887808	1.75510261	71.4166667	8.34727168	1.00425	0.33177	0.98891	0.127527379	COC1=CC=C(C=C1)[C@@]12OC3=CC(OC)=CC(O)=C3[C@]1(O)C1=C([C@H]2C2=CC=CC=C2)C(=O)N2CCCC2=N1
CMLD012098	1.14642121	0.04588767	42.7670422	10.7769481	-2.9527653	0.62384437	12.3339934	2.16788883	1.02564	0.14592	0.99911	0.116244613	COC(=O)[C@H]1[C@H](C2=CC=CC=C2)[C@@]2(OC3=CC(OC)=CC(OC)=C3[C@@]22OC(=N[C@@]12O)C1=CC=CC=C1)C1=CC=C(OC)C=C1

CMLD012099	1.07450222	0.03564861	40.519258	2.82481836	-4.5140602	0.57521898	12.1052958	2.1853967	1.16076	0.14282	1.02813	0.080311727	COC(=O)[C@@H]1[C@@H](C2=CC=CC=C2)[C@@]2(OC3=CC(OC)=CC(OC)=C3[C@@]22OC(=N[C@@]12O)C1=CC=CN=C1)C1=CC=C(OC)C=C1
CMLD012100	0.81869628	0.04419692	83.215089	8.02219434	-2.7742242	1.1930139	57.4672153	6.81510028	1.12908	0.1887	1.03721	0.062929891	COC1=CC=C(C=C1)[C@@]12OC3=CC(OC)=CC(OC)=C3[C@]1(O)C1=C([C@H]2C2=CC=CC=C2)C(=O)N=C(N1)C1=CC=CC=N1
CMLD012101	1.04099196	0.04734182	24.232531	3.19381851	2.2844061	1.95133558	6.55454314	0.92505259	1.10216	0.12218	0.99476	0.087210603	COC1=CC=C(C=C1)[C@@]12OC3=CC(OC)=CC(OC)=C3[C@]1(O)C1=C([C@H]2C2=CC=CC=C2)C(=O)N=C(N1)C1=CC=C(Br)C=C1
CMLD012102	1.04171249	0.04683126	11.0406415	2.62969888	-1.0988709	2.53663511	0.60905501	1.93651355	1.09626	0.09894	1.05936	0.048069229	COC(=O)[C@@H]1[C@@H](C2=CC=CC=C2)[C@@]2(OC3=CC(OC)=CC(OC)=C3[C@@]22OC(=N[C@@]12O)C1=CC=CC=C1)C1=CC=C(OC)C=C1
CMLD012103	1.06028068	0.02481624	33.8105772	1.69985761	0.3295535	2.33479909	20.4077681	4.31632675	1.05197	0.14506	0.96904	0.085725015	COC(=O)[C@@H]1[C@@H](C2=CC=CC=C2)[C@@]2(OC3=CC(OC)=CC(OC)=C3[C@@]22OC(C)=N[C@@]12O)C1=CC=C(OC)C=C1
CMLD012104	1.12221786	0.0315421	36.9050233	5.8300166	0.56286716	2.18289738	11.2165654	4.02165651	1.17378	0.18154	1.01731	0.089818817	COC(=O)[C@@H]1[C@@H](C2=CC=CC=C2)[C@@]2(OC3=CC(OC)=CC(OC)=C3[C@@]22OC(=N[C@@]12O)C1=CC=C(OC)C=C1)C1=CC=C(OC)C=C1
CMLD012105	1.00329698	0.09933623	10.7286533	1.83883662	-1.6302443	0.96234166	3.66743875	2.2914156	1.07086	0.152	1.05163	0.21923272	COC(=O)[C@@H]1[C@@H](C2=CC=CC=C2)[C@@]2(OC3=CC(OC)=CC(OC)=C3[C@@]22OC(=N[C@@]12O)C1=CC=C(F)C=C1)C1=CC=C(OC)C=C1
CMLD012106	1.002555	0.08312796	42.91242	4.992269	-6.6315818	1.40941247	35.7717349	1.01558204	0.90635	0.19505	0.86522	0.162036668	COC1=CC=C(C=C1)[C@@]12OC3=CC(OC)=CC(OC)=C3[C@]1(O)[C@H](OC(=O)CCC#C)[C@@H]([C@H]2C1=CC=CC=C1)C(=O)C1=CC=CO1
CMLD012107	0.43065843	0.02198934	84.5276791	5.2440942	-2.4183759	0.79010728	92.2809564	5.17060488	0.89254	0.24194	0.99974	0.11989066	COC1=CC=C(C=C1)[C@@]12OC3=CC(OC)=CC(OC)=C3[C@]1(O)C1=C([C@H]2C2=CC=CC=C2)C(=O)N2CCC[C@H]2N1C
CMLD012108	0.2190598	0.00846552	107.978129	5.91755683	-3.8220488	1.33577238	81.6812925	6.17460712	0.67544	0.18325	0.93834	0.02801819	COC1=CC=C(C=C1)[C@@]12OC3=CC(OC)=CC(OC)=C3[C@]1(O)C1=C([C@H]2C2=CC=CC=C2)C(=O)N2CCC[C@H]2N1CCN(C)C
CMLD012110	0.81059338	0.06848355	53.0462816	4.35334606	-0.2461882	1.42099746	29.6741324	3.49884636	1.10668	0.136	1.01749	0.07969175	COC1=CC=C(C=C1)[C@@]12OC3=CC(OC)=CC(OC)=C3[C@]1(O)C1=C([C@H]2C2=CC=CC=C2)C(=O)N2CCC[C@H]2N1CC1=CC=CN=C1
CMLD012111	0.75487875	0.06870216	43.112815	4.41625391	-0.2664915	1.35458257	32.2062243	2.73243945	1.08185	0.13791	1.03589	0.039690859	COC1=CC=C(C=C1)[C@@]12OC3=CC(OC)=CC(OC)=C3[C@]1(O)C1=C([C@H]2C2=CC=CC=C2)C(=O)N2CCC[C@H]2N1CC1=CC=NC=C1
CMLD012117	1.11901948	0.04559769	12.5659076	1.06079871	0.528403	1.14161873	9.11666667	5.73296995	0.68526	0.1602	0.82656	0.248243226	O[C@@]([C@H](C(OC)=O)[C@H]1C2=CC=CC=C2)(N=C(C3=CN=C(Cl)C=C3)O4)[C@]54[C@@]1(C6=CC=C(OC)C=C6)OC7=CC(OC)=CC(OC)=C75
CMLD012118	0.18372958	0.00874379	108.057116	5.01029277	0.70382605	3.35990811	107.263298	6.52069704	0.34871	0.06688	0.81798	0.114204083	COC(=O)[C@@H]1[C@@H](C2=CC=CC=C2)[C@@]2(OC3=CC(OC)=CC(OC)=C3[C@@]22NC(=N[C@@]12O)N1CCOCC1)C1=CC=C(OC)C=C1
CMLD012146	1.049795	0.06039666	28.6447	4.002837	-1.1838336	0.66679162	17.7126369	7.0940825	0.97098	0.19826	0.99997	0.185708798	COC1=CC=C(C=C1)[C@@]12OC3=CC(OC)=CC(OC)=C3[C@]1(O)C1=C([C@H]2C2=CC=CC=C2)C(=O)N=C(N1)C1=CC=C(Cl)C=C1
CMLD012147	0.6722091	0.05473981	73.3103	3.990591	-2.1132381	2.10661181	45.1165785	2.91071916	0.93035	0.16899	0.88555	0.118680039	COC1=CC=C(C=C1)[C@@]12OC3=CC(OC)=CC(OC)=C3[C@]1(O)C1=C([C@H]2C2=CC=CC=C2)C(=O)N=C(N1)C1=CC=C(Cl)N=C1
CMLD012148	1.025345	0.03527673	7.854098	0.3083146	-2.2673531	1.14013106	4.53051591	2.95052821	1.16113	0.28977	0.98613	0.12181175	COC(=O)[C@@H]1[C@@H](C2=CC=CC=C2)[C@@]2(OC3=CC(OC)=CC(OC)=C3[C@@]22OC(=N[C@@]12O)C1=CC=C(Cl)C=C1)C1=CC=C(OC)C=C1
CMLD012149	1.016863	0.06533861	28.33881	5.170015	-3.8406072	0.59590475	15.9669922	2.5278892	1.03051	0.16095	1.05617	0.139562286	COC(=O)[C@@H]1[C@@H](C2=CC=CC=C2)[C@@]2(OC3=CC(OC)=CC(OC)=C3[C@@]22OC(=N[C@@]12O)C1=CC=C(Cl)N=C1)C1=CC=C(OC)C=C1
CMLD012150	0.1651173	0.01775844	92.19633	4.811044	1.25363261	1.78702966	82.0919128	6.07861445	0.89096	0.31774	1.01023	0.218111053	COC(=O)[C@@H]1[C@@H](C2=CC=CC=C2)[C@@]2(OC3=CC(OC)=CC(OC)=C3[C@@]22NC(=N[C@@]12O)C1=CSC(C)=N1)C1=CC=C(OC)C=C1
CMLD012151	0.2324373	0.02323408	89.69595	2.719674	-0.2777388	2.24785982	76.5148306	4.56954514	1.07591	0.29294	1.06627	0.063664871	COC(=O)[C@@H]1[C@@H](C2=CC=CC=C2)[C@@]2(OC3=CC(OC)=CC(OC)=C3[C@@]22NC(=N[C@@]12O)C1=CC=C(OC)C=C1)C1=CC=C(OC)C=C1
CMLD012152	0.2742425	0.01789587	78.55846	2.87589	0.74121467	2.41248242	70.8224238	7.3207564	0.89745	0.31641	1.03973	0.075714037	COC(=O)[C@@H]1[C@@H](C2=CC=CC=C2)[C@@]2(OC3=CC(OC)=CC(OC)=C3[C@@]22NC(=N[C@@]12O)C1=CC=CN=C1)C1=CC=C(OC)C=C1
CMLD012172	0.7177975	0.04368851	70.33348	5.740157	-3.3909837	3.55634566	70.8533186	5.81844459	1.05124	0.13316	1.01844	0.072585087	CO\N=C(\[C@H]1[C@@H](O)[C@@]2(O)C3=C(O[C@]2([C@@H]1C1=CC=CC=C1)C1=CC=C(OC)C=C1)C=C(OC)C=C3OC)C1=CC=CO1
CMLD012176	0.882477	0.06438942	28.99981	6.013402	0.75942407	1.59992821	33.6247178	15.3687236	1.02531	0.1371	0.97952	0.136085427	COC1=CC=C(C=C1)[C@@]12OC3=CC(OC)=CC(OC)=C3[C@]1(O)[C@H](O)[C@@H]([C@H]2C1=CC=CC=C1)C(=O)C1=C(C)C2=CC=CC=C2O1
CMLD012177	0.8707864	0.08318061	43.00469	10.27315	-2.0721702	2.00758065	26.805357	5.31217418	0.90303	0.17232	0.8364	0.092277866	COC1=CC=C(C=C1)[C@@]12OC3=CC(OC)=CC(OC)=C3[C@]1(O)[C@H](O)[C@@H]([C@H]2C1=CC=CC=C1)C(=O)C1=CC2=CC=CC(OC)=C2O1
CMLD012184	0.968167	0.03359017	73.24907	3.967191	-2.9303244	1.46410524	82.4995008	5.51141087	1.06623	0.19041	1.00078	0.111533401	CON(C)C(=O)[C@H]1[C@@H](O)[C@@]2(O)C3=C(O[C@]2([C@@H]1C1=CC=CC(OC)=C1)C1=CC=C(OC)C=C1)C=C(OC)C=C3OC
CMLD012185	1.019503	0.02356702	62.59066	7.734404	-4.5713472	0.65207691	59.8257205	4.55553571	1.09338	0.20628	1.0026	0.136538691	COC1=CC=C(C=C1)[C@@]12OC3=CC(OC)=CC(OC)=C3[C@]1(O)[C@H](O)[C@@H]([C@H]2C1=CC=CC(OC)=C1)C(=O)C1=CC=CO1
CMLD012186	0.4387542	0.02044192	73.0496	3.217728	-0.9662942	1.45330814	80.006437	4.93420959	0.53951	0.15436	1.05	0.169940643	CON(C)C(=O)[C@H]1[C@@H](O)[C@@]2(O)C3=C(O[C@]2([C@@H]1C1=CC=CC=C1OC)C1=CC=C(OC)C=C1)C=C(OC)C=C3OC
CMLD012187	0.4240072	0.01273776	75.81915	4.446432	-1.391112	1.48708108	75.9960277	6.42734372	0.92809	0.2943	0.97077	0.112481339	COC1=CC=C(C=C1)[C@@]12OC3=CC(OC)=CC(OC)=C3[C@]1(O)[C@H](O)[C@@H]([C@H]2C1=CC=CC=C1OC)C(=O)C1=CC=CO1
CMLD012220	0.9854261	0.02156706	58.18531	8.043281	-0.9328887	1.96021935	56.6815703	5.36662988	1.16619	0.21492	1.02221	0.107274494	COC1=CC=C(C=C1)[C@@]12OC3=CC(OC)=CC(OC)=C3[C@]1(O)[C@@H](O)[C@@H]([C@H]2C1=CC=CC(OC)=C1)C(=O)C1=CC=CO1
CMLD012304	1.153212	0.04124948	9.437269	3.244408	-2.01695	2.0839451	4.98923171	5.12201218	1.18943	0.31422	1.01836	0.08718809	COC(=O)[C@@H]1[C@@H](C2=CC=CC=C2)[C@@]2(OC3=CC(OC)=CC(OC)=C3[C@]2(NCC#C)C1=O)C1=CC=C(OC)C=C1
CMLD012305	1.128099	0.02029029	3.970015	2.685575	-0.5502739	0.90388446	4.00132995	3.45954569	0.91755	0.23571	0.93712	0.097429393	CCCCN[C@@]12C(=O)[C@@H]([C@@H](C3=CC=CC=C3)[C@@]1(OC1=CC(OC)=CC(OC)=C21)C1=CC=C(OC)C=C1)C(=O)OC
CMLD012306	1.106864	0.05809462	5.563013	2.346258	-3.3936028	2.67785028	4.81325944	3.55202984	0.93278	0.17081	0.88577	0.140675656	CCCN(CCC)[C@@]12C(=O)[C@@H]([C@@H](C3=CC=CC=C3)[C@@]1(OC1=CC(OC)=CC(OC)=C21)C1=CC=C(OC)C=C1)C(=O)OC
CMLD012307	1.022793	0.02672583	6.386514	0.6068553	-2.3950072	0.15445888	4.90480417	1.63079495	1.08419	0.13843	1.04915	0.144134499	COC(=O)[C@@H]1[C@@H](C2=CC=CC=C2)[C@@]2(OC3=CC(OC)=CC(OC)=C3[C@]2(NCC2=CC=CC=C2)C1=O)C1=CC=C(OC)C=C1
CMLD012308	1.005053	0.0257293	31.5221	6.295606	-3.6593851	0.94238516	23.9005168	3.84984206	1.09845	0.14677	1.06092	0.094050342	COC(=O)[C@@H]1[C@@H](C2=CC=CC=C2)[C@@]2(OC3=CC(OC)=CC(OC)=C3[C@]2(NCCN(C)C)C1=O)C1=CC=C(OC)C=C1
CMLD012309	0.952038	0.02626452	36.25178	3.282104	-1.9185529	1.68760739	30.5083313	4.52034137	1.12333	0.1846	1.08141	0.06433786	COC(=O)[C@@H]1[C@@H](C2=CC=CC=C2)[C@@]2(OC3=CC(OC)=CC(OC)=C3[C@]2(NN(C)C)C1=O)C1=CC=C(OC)C=C1
CMLD012310	0.9472269	0.1657435	1.659367	1.167565	-1.3621527	2.16535426	3.23199521	2.52666289	1.08058	0.18241	1.06629	0.098554185	COC(=O)[C@@H]1[C@@H](C2=CC=CC=C2)[C@@]2(OC3=CC(OC)=CC(OC)=C3[C@]2(NC2=CC=CC=C2)C1=O)C1=CC=C(OC)C=C1
CMLD012311	1.050354	0.02538623	28.5899	3.025368	-2.2445857	1.48118173	15.5345876	2.73654997	1.19453	0.27957	1.08117	0.066263022	COC(=O)[C@@H]1[C@@H](C2=CC=CC=C2)[C@@]2(OC3=CC(OC)=CC(OC)=C3[C@]2(NCCN2CCOCC2)C1=O)C1=CC=C(OC)C=C1
CMLD012312	1.104423	0.04023865	-4.14132	2.220604	0.7776549	0.3272495	-1.8087192	3.11120219	1.15047	0.22488	1.09417	0.019813255	COC1=CC=C(C=C1)[C@@]12OC3=CC(OC)=CC(OC)=C3[C@]1(NCC1=CC=CC=C1)C(=O)C[C@H]2C1=CC=CC=C1
CMLD012318	0.936811	0.06800327	50.7046	2.602063	-4.160376	1.110783	41.9700842	5.1720064	0.94621	0.21454	0.98827	0.14899678	COC1=CC=C(C=C1)[C@@]12OC3=CC(OC)=CC(OC)=C3[C@]1(O)C1=C([C@H]2C2=CC=CC=C2)C(=O)N=C(N1)C1=CC=CC=C1Cl
CMLD012319	0.9963753	0.03410985	45.09385	4.847905	-1.981889	1.566829	20.7353099	2.89128668	0.91175	0.18781	0.89035	0.106423421	COC1=CC=C(C=C1)[C@@]12OC3=CC(OC)=CC(OC)=C3[C@]1(O)C1=C([C@H]2C2=CC=CC=C2)C(=O)N=C(N1)C1=CC=CC(C)=C1
CMLD012320	0.8452986	0.03672372	68.12268	6.683224	-2.819895	3.58722	39.0947401	1.99153916	1.07598	0.13768	1.04047	0.11246501	COC1=CC=C(C=C1)[C@@]12OC3=CC(OC)=CC(OC)=C3[C@]1(O)C1=C([C@H]2C2=CC=CC=C2)C(=O)N=C(CC2=CC=CC=C2)N1
CMLD012321	1.000697	0.02807021	12.72949	4.699019	-0.3892669	0.23629461	7.67899726	3.6092594	1.17122	0.28335	1.04672	0.099893013	COC(=O)[C@@H]1[C@@H](C2=CC=CC=C2)[C@@]2(OC3=CC(OC)=CC(OC)=C3[C@@]22OC(=N[C@@]12O)C1=CC=CC=C1Cl)C1=CC=C(OC)C=C1
CR-1-31-b	0.2772761	0.05849462	85.54308	1.833662	-2.0577543	0.30813035	74.8075481	12.5089296	0.18904	0.10547	0.93533	0.181105929	CONC(=O)[C@H]1[C@@H](O)[C@@]2(O)C3=C(O[C@]2([C@@H]1C1=CC=CC=C1)C1=CC=C(OC)C=C1)C=C(OC)C=C3OC
RocA-(-)	0.5292261	0.03583449	60.35647	3.033703	-0.4284737	2.104868	87.3184052	14.3815948	0.22531	0.09897	0.88878	0.07782009	COC1=CC=C(C=C1)[C@@]12OC3=CC(OC)=CC(OC)=C3[C@]1(O)[C@H](O)[C@@H]([C@H]2C1=CC=CC=C1)C(=O)N(C)C
Silvestrol	0.3631712	0.02659531	29.31148	0.8591651	-2.3278434	1.69714288	47.5987811	7.24287947	0.42038	0.20086	1.01806	0.165327012	CO[C@@H]1OC[C@@H](O[C@@H]1OC1=CC2=C(C(OC)=C1)[C@]1(O)[C@H](O)[C@@H]([C@@H](C3=CC=CC=C3)[C@@]1(O2)C1=CC=C(OC)C=C1)C(=O)OC)[C
WDG57-590	0.11723617	0.03400571	55.580691	13.2136349	-3.3347634	0.46613137	52.6166667	3.28460212	0.88919	0.13605	0.97606	0.342313092	COC1=C2C(O[C@]3(C4=CC=C(OC)C=C4)[C@@]2(O)[C@H](O)[C@H](C(NOC)=O)[C@H]3C5=CC=CC=C5)=CC(OC6O[C@@H]([C@@H](CO)O)CO[C@H]6OC)=C1
WDG57-591	0.07349902	0.01699897	49.0111785	15.1570087	-3.3347634	0.46613137	43.95	9.76119016	1.0332	0.19267	0.9217	0.158116993	COC1=C2C(O[C@]3(C4=CC=C(OC)C=C4)[C@@]2(O)[C@H](O)[C@H](C(N(C)OC)=O)[C@H]3C5=CC=CC=C5)=CC(OC6O[C@@H]([C@@H](CO)O)CO[C@H]6OC)=C

5.11 References

Bleumink, M., Kohler, R., Giaisi, M., Proksch, P., Krammer, P.H., and Li-Weber, M. (2011). Rocaglamide breaks TRAIL resistance in HTLV-1-associated adult T-cell leukemia/lymphoma by translational suppression of c-FLIP expression. Cell Death Differ *18*, 362-370.

Bordeleau, M.E., Mori, A., Oberer, M., Lindqvist, L., Chard, L.S., Higa, T., Belsham, G.J., Wagner, G., Tanaka, J., and Pelletier, J. (2006). Functional characterization of IRESes by an inhibitor of the RNA helicase eIF4A. Nat Chem Biol *2*, 213-220.

Chu, J., Galicia-Vazquez, G., Cencic, R., Mills, J.R., Katigbak, A., Porco, J.A., Jr., and Pelletier, J. (2016). CRISPR-Mediated Drug-Target Validation Reveals Selective Pharmacological Inhibition of the RNA Helicase, eIF4A. Cell Rep *15*, 2340-2347.

Iwasaki, S., Floor, S.N., and Ingolia, N.T. (2016). Rocaglates convert DEAD-box protein eIF4A into a sequence-selective translational repressor. Nature *534*, 558-561.

Iwasaki, S., Iwasaki, W., Takahashi, M., Sakamoto, A., Watanabe, C., Shichino, Y., Floor, S.N., Fujiwara, K., Mito, M., Dodo, K.*, et al.* (2019). The Translation Inhibitor Rocaglamide Targets a Bimolecular Cavity between eIF4A and Polypurine RNA. Mol Cell *73*, 738-748 e739.

Novac, O., Guenier, A.S., and Pelletier, J. (2004). Inhibitors of protein synthesis identified by a high throughput multiplexed translation screen. Nucleic Acids Res *32*, 902-915.

Pelletier, J., and Sonenberg, N. (2019). The Organizing Principles of Eukaryotic Ribosome Recruitment. Annu Rev Biochem *88*, 307-335.

Rubio, C.A., Weisburd, B., Holderfield, M., Arias, C., Fang, E., DeRisi, J.L., and Fanidi, A. (2014). Transcriptome-wide characterization of the eIF4A signature highlights plasticity in translation regulation. Genome Biol *15*, 476.

Shah, P., Ding, Y., Niemczyk, M., Kudla, G., and Plotkin, J.B. (2013). Rate-limiting steps in yeast protein translation. Cell *153*, 1589-1601.

Wolfe, A.L., Singh, K., Zhong, Y., Drewe, P., Rajasekhar, V.K., Sanghvi, V.R., Mavrakis, K.J., Jiang, M., Roderick, J.E., Van der Meulen, J.*, et al.* (2014). RNA G-quadruplexes cause eIF4A-dependent oncogene translation in cancer. Nature *513*, 65-70.

Yan, X., Hoek, T.A., Vale, R.D., and Tanenbaum, M.E. (2016). Dynamics of Translation of Single mRNA Molecules In Vivo. Cell *165*, 976-989.

CHAPTER 6 GENERAL DISCUSSION

Selected Sections Published in:

Chu, J., and Pelletier, J. (2015). Targeting the eIF4A RNA helicase as an anti-neoplastic approach. *Biochimica et biophysica acta* **1849**, 781-791.

With copyright permission from Elsevier

Chu, J., Cargnello, M., Topisirovic, I., and Pelletier, J. (2016). Translation Initiation Factors: Reprogramming Protein Synthesis in Cancer. *Trends in cell biology* **26**, 918-933.

With copyright permission from Elsevier

Chu, J., and Pelletier, J. (2018). Chemical and CRISPR/Cas9 Tools for Functional Characterization of RNA Helicases. *Applied RNA Bioscience*, S. Masuda, and Izawa S., ed. (Springer), pp. 221-245.

With copyright permision from Springer Nature

6.1 Pharmacological Inhibition of DEAD-Box Helicases

6.1.1 Pharmacological Strategies to Inhibit DEAD-Box Helicases

RNA helicases can potentially be targeted by small molecules through a wide variety of mechanisms. These include preventing ATP and RNA binding, blocking cofactor interaction, and inhibition of ATP hydrolysis and RNA unwinding. Since each conformation change undertaken by the helicase during these events represents a different pose, there are potentially multiple druggable opportunities (Figure 6.1, labelled a-f)

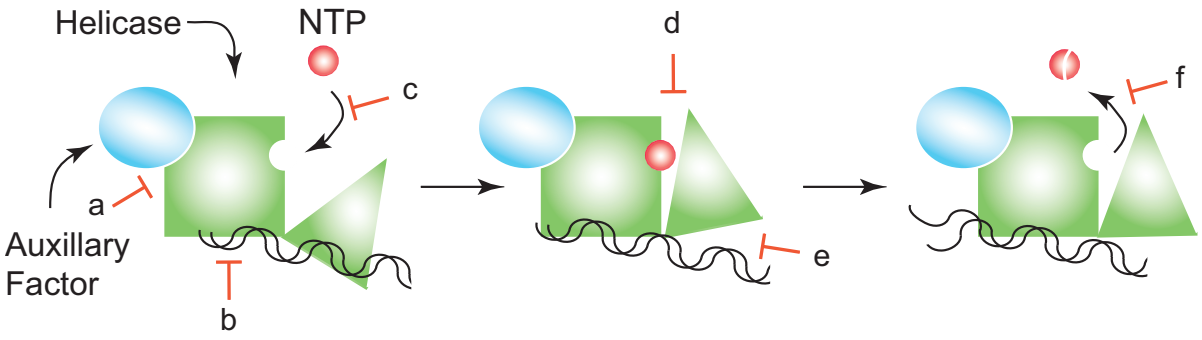

Figure 6.1 Points of Interdiction Available to Block RNA Helicase Activity.
The RNA helicase is represented as two domains (square and triangular) that undergo conformational changes as a consequence of NTP hydrolysis. An auxiliary protein is depicted as a blue shaded circle and could function to anchor or modulate helicase activity. Small molecule inhibitors could inhibit (a) ancillary factor:helicase interaction, (b) helicase:RNA binding, (c) NTP binding, (d) conformational changes during helicase domain movement, (e) helicase activity, and (f) NTP hydrolysis or release.

RNA helicases are implicated in nearly all aspects of RNA biology and because dysregulated helicase activity has been linked to many diseases, targeting these may provide therapeutic benefit. For example, several RNA helicases have been reported to promote tumor onset and progression, and suppression of these using RNAi have demonstrated anti-tumor effects (Fuller-Pace, 2013). These

results bode well for the discovery of small molecules to block RNA helicases as having significant potential to the field of cancer therapeutics. However, there are certain challenges towards identifying such inhibitors. For one, many compounds found in chemical libraries possess inherent affinity towards nucleic acids or are contaminated with low levels of RNAses—both of which can lead to artefacts in screens that utilize RNA binding or unwinding as a read-out (Shadrick et al., 2013). The development ATP competitive inhibitors of RNA helicases face the obstacle that the ATP binding pocket is highly conserved between RNA helicases, thus making it challenging to identify a selective inhibitor.

Not only do selective inhibitors of RNA helicases hold value has potential therapeutic agents, but they can act as highly beneficial tools for furthering our current understanding of the biological functions of different RNA helicases. While approaches like CRISPR knockouts and RNAi-based strategies are capable of mimicking (to some extent) an inhibited RNA helicase activity, there is a significant delay in kinetics of onset (relative to a small molecule inhibitor). This makes interpretation of subsequent downstream phenotypes complicated due to the potential for secondary effects to confound resulting analyses. As well, small molecule inhibitors do not necessarily lead to target depletion, which is quite distinct than what is achieved by CRISPR or RNAi and may thus have a different impact on helicase-dependent ancillary factors. An example central to this thesis is observed with the rocaglate family of eIF4A inhibitors, in which a gain-of-function activity is conferred.

One strategy by which some of these issues can be addressed is to borrow the concept of "gatekeeper' residue mutations in kinases that enabled the design of analog-sensitive proteins (Lopez et al., 2014). Applying this to helicases by engineering the ATP binding site with an appropriately designed novel space or cavity that can accommodate a small molecule, the activity of the altered

helicase can be placed under regulation of a unique small molecule inhibitor. Indeed, this approach has been implemented by Floor *et al.* (2016) for DDX3 (Floor et al., 2016). Here, an F182A change placed DDX3^{F182A} under regulation of ATP (GXJ1-76) and aniloquinazoline analogues *in vitro* (Floor et al., 2016). However, it should be noted that the introduction of mutations to the ATP binding pocket may result in loss of enzymatic function. When we attempted this strategy with eIF4A by mutating F34 to an alanine, cysteine or glycine, we found that resulting mutants were not capable of hydrolysing ATP *in vitro* (Figure 6.2). Therefore, this strategy may not be applicable for all DEAD-box helicases.

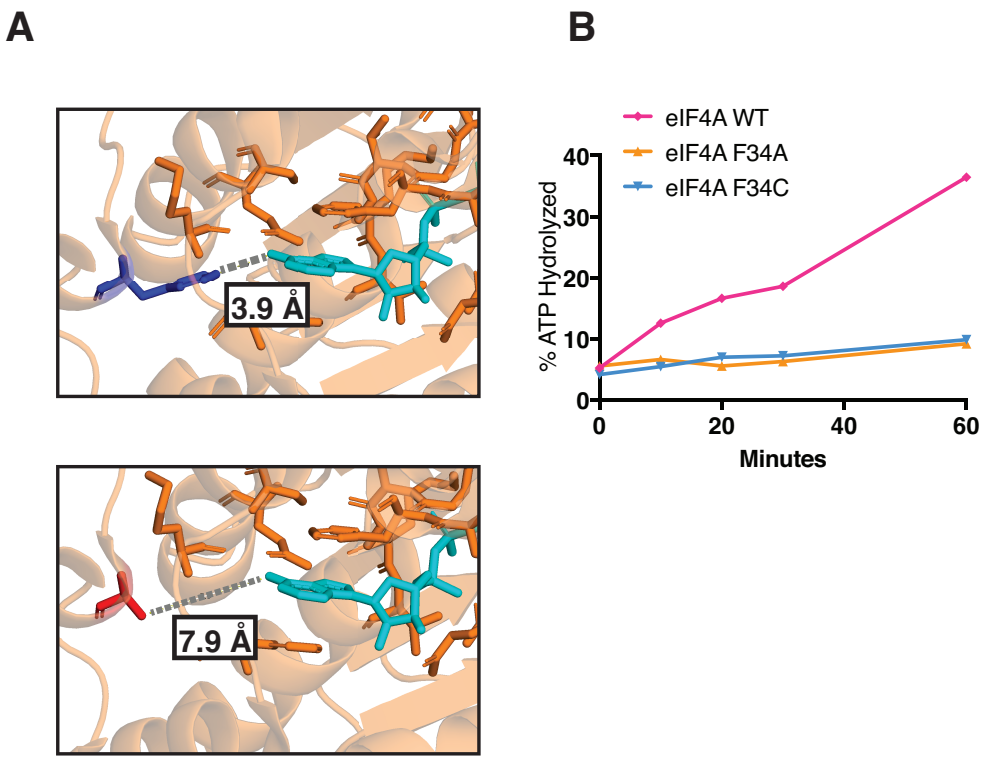

Figure 6.2 Expansion of the eIF4A ATP Binding Pocket Inactivates ATP Hydrolysis Activity
(A) Structural consequence of mutating the F34 "gatekeeper" residue (navy blue, top panel) to alanine (red, bottom panel) on the size of the eIF4A ATP binding pocket (orange, PDB 5zc9). AMPPNP is colored in cyan.
(B) Mutations to F34 in eIF4A cause loss of function. ATPase activity was evaluated following a protocol developed by Lorsch and Herschlag (1998). Briefly, 2 µg of wild type eIF4A1, eIF4A1 (F34A), or eIF4A1 (F34C) protein was incubated with 1µM γ-32P-ATP (20 Ci/mmol) at 25°C in the presence or absence of 2.5 µM poly U RNA. At the indicated time points, aliquots of the reaction

were removed and stopped with 12.5 mM EDTA. γ-32P-ATP and inorganic phosphate were separated using thin layer chromatography and the extent of ATP hydrolysis was quantitated using phosphorimaging (Typhoon Trio Imager, GE Healthcare.

6.1.2 Targeting eIF4A for Therapeutic Purposes

Numerous investigations conducted by our lab as well as others have demonstrated that targeting eIF4A is a highly promising anti-neoplastic strategy and decreased eIF4A levels have been identified as a predictive indicator of improved prognosis (Liang et al., 2014). As an essential member of the eIF4F complex, small molecules that target eIF4A act as surrogate eIF4F inhibitors and could be a promising therapeutic avenue for treating tumors that overexpress eIF4E or exhibit overactive mTOR signaling (Joyce et al., 2017).

Inhibitors of eIF4A have also been shown to be effective in combination strategies (Table 6.1). Chemotherapies such as oxaliplatin and ABT-737 inhibit cancer cell growth through the induction of apoptosis but overexpression of anti-apoptotic proteins such as Mcl-1, Bcl-$_{XL}$, Bcl-2, c-FLIP, and XIAP can cause resistance to these treatments. Consequently, inhibitors of eIF4A have been reported to restore sensitivity by repressing the synthesis of all of these proteins. Similarly, long term exposure to CDK4/6 inhibitors such as palbociclib can lead to acquired resistance through the upregulation of factors involved in cell cycle progression such as cyclin D1 and cyclin E1 but because the translation these cell cycle regulators are highly sensitive to changes in eIF4A activity, small molecules that target eIF4A are effective in resensitizing the tumor cells. (Kong et al., 2019). Furthermore, inhibition of eIF4F may serve as a viable strategy to overcome drug insensitivity stemming from intra-tumor heterogeneity as numerous commonly deregulated signalling pathways converge to the regulation of this complex. However, that is not to say that eIF4A inhibitors could be utilized in *every* combination strategy. For instance, it has been observed that the combination of silvestrol and bortezomib, a

proteasome inhibitor, is antagonistic when tested on multiple myeloma cell lines (Robert and Pelletier, unpublished data).

Recently, the pharmaceutical company, eFFECTOR, performed a CRISPR/Cas9 screen in search of novel synthetic lethal interactions with the rocaglate, eFT226, (also known as zotatifin) against a KRAS/p53 driven NSCLC cell line (Young et al., 2019). From this, perturbation of NRF2 regulation through mutations of the KEAP1-CUL3 complex was found to be synthetic lethal with eFT226 (Young et al., 2019). NRF2 is a transcription factor that is activated by oxidative stress and directs an antioxidant transcriptional program (Sporn and Liby, 2012). Under basal conditions, NRF2 expression levels are suppressed by the cytoplasmic adaptor protein, KEAP1, bound to the ubiquitin ligase, CUL3 (Sporn and Liby, 2012). The role of NRF2 in tumorigenesis is context dependent; while NRF2 can act as a tumor suppressor by downregulating the levels of reactive oxygen species, it can also promote cancer cell survival in the presence of stress (Sporn and Liby, 2012). Accordingly, KEAP1 loss-of-function mutations or increased NRF2 levels have been identified to confer chemoresistance in NSCLCs (Mine et al., 2014; Tao et al., 2014; Tung et al., 2015). Therefore, it is rather intriguing that genetic ablation of the KEAP1/CUL3 complex forms a synthetic lethal interaction with eFT226 and, perhaps, this may suggest eFT226 could be an effective agent against chemoresistant NSCLCs driven by upregulated NRF2.

Table 6.1 Select Studies Reporting on the Synergistic Properties of Rocaglates

Rocaglate	Chemotherapy	Model tested	Reference
Silvestrol	Oxaliplatin (DNA intercalator)	PDX and CDX models of colorectal cancer	(Chen et al., 2019)
Silvestrol	ABT-737 (Bcl-XL and Bcl-2 inhibitor)	AML cell culture	(Cencic et al., 2010)
Silvestrol	Cisplatin (DNA intercalator)	Cell culture model of nasopharyngeal carcinoma	(Daker et al., 2016)

RocA	Tumor necrosis factor apoptosis inducing ligand	Xenograft models of multiple myeloma, hepatocellular carcinoma, T-cell lymphoma	(Bleumink et al., 2011; Luan et al., 2015; Wu et al., 2017)
CR-1-31-B	Palbociclib (CDK4/CDK6 inhibitor)	Xenograft model of ER^+ breast cancer, KRAS mutant NSCLC in cell culture	(Kong et al., 2019)

Most studies evaluating inhibitors of eIF4A have primarily looked at their efficacies within the context of cancer therapy, but these compounds may also be effective in other applications. For example, the translation of many viral mRNAs are dependent on eIF4A activity and rocaglates have been demonstrated to inhibit the replication of a variety of viruses (Elgner et al., 2018; Henss et al., 2018; Todt et al., 2018). Interestingly, the rocaglates, CMLD011166 and CMLD011167 (structures shown in Figure S5.1C), were initially identified to be inhibitors of HIF1α and were positioned as potential treatments for neuro-degenerative diseases like Parkinson's (Fahrig et al., 2005; Thuaud et al., 2013; Wabnitz, 2012). However, our work in chapter 5 demonstrates that the primary target of these two compounds is eIF4A, indicating that their original presumed mechanism of action was inaccurate and the decrease in HIF1α-dependent transcription observed may be an indirect effect caused by decreased synthesis of the HIF1α protein. Nevertheless, these compounds displayed anti-inflammatory activity and reduced neuronal cell death by alleviating oxidative stress (Wabnitz, 2012).

6.1.3 Implications of eIF4A Gain-of-Function Activity

In chapters 4 and 5, we explored whether stimulation of eIF4A:RNA association by rocaglates has a direct influence on translation. From our data, it appears to be at least partially the case as we observed that the degree of inhibition of a mRNA correlates with how likely eIF4A will stably bind to the 5' leader in the presence of rocaglates in *in vitro* assays. By stably clamping eIF4A onto the 5'

leader, rocaglates are thought to create a steric barrier that impedes the scanning ribosome from reaching the start codon. Interestingly, at low concentrations of compound, the presence of the stabilized polypurine:eIF4A:rocagalate complex have also been shown to induce initiation events at weak upstream start codons (Iwasaki et al., 2016).

As shown in figure S5.3A, stabilization of eIF4A onto purine sequences by rocaglates can occur in the absence of a cap structure. Therefore, it is possible that eIF4A could also form clamps at locations beyond the 5' leader including the coding sequence, the 3'UTR, and long non-coding RNAs. For instance, ribosomal RNA (which represents ~85% of total cellular RNA (Hirsch, 1967)) is biased for purine content (Smit et al., 2006) and indeed, we have observed that rocaglates cause increased co-sedimentation of eIF4A with ribosomes in Krebs-2 translation extracts (Figure 6.3). The consequences of increased eIF4A association with the ribosome are currently unclear and it is possible that ribosome function may be affected by this. However, while 1 μM CR-1-31-B elicited an increase in the amount of eIF4A co-sedimenting with the ribosome, the same conditions were unable to inhibit the translation of the mRNA with the polypyrimidine-rich 5' leader (Figure 5.1D). This observation may suggest that CR-1-31-B stabilization of eIF4A onto ribosome do not significantly impact ribosomal function but ultimately, more experimentation (e.g. testing the response of different mRNA transcripts, evaluating ribosome binding efficiency) is required before making any definitive conclusions.

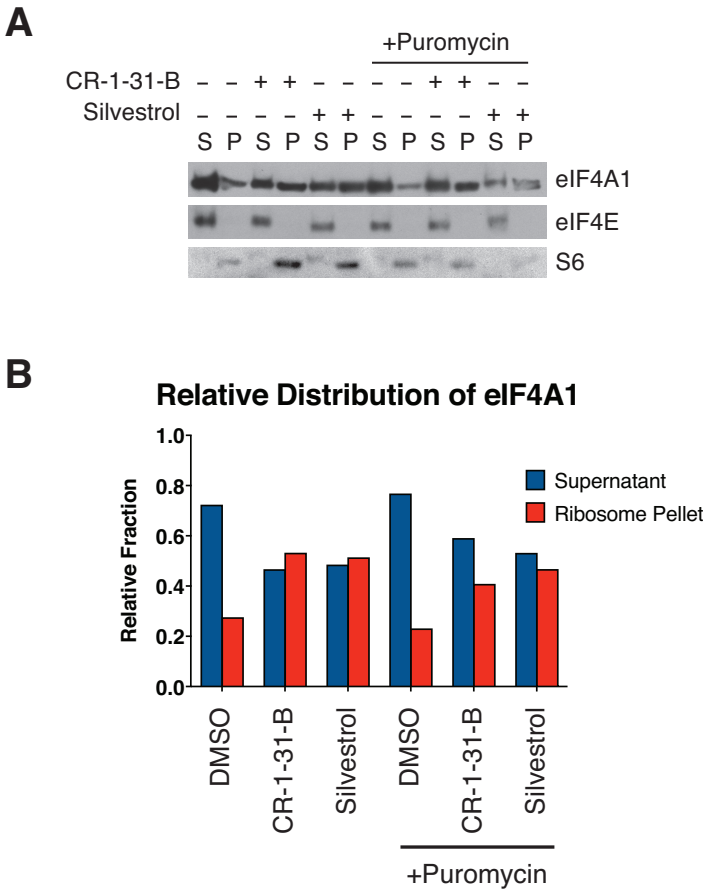

Figure 6.3 Increased eIF4A Association with Ribosomes in the Presence of Rocaglates
Krebs2 extracts were incubated with 0.01% DMSO or 1 μM rocaglate and spun at 100 000 x g for 3 hours to pellet ribosomes. The experiment was also performed in the presence of puromycin to disassemble potential ribosome-mRNA complexes. The supernatant fraction (S) was removed and the ribosomal pellet (P) was washed 3 times with PBS before solubilization in SDS-PAGE sample buffer.
(A) Western blot illustrating the relative distribution of eIF4A in response to rocaglate. eIF4E and ribosomal protein S6 were used as markers for the non-ribosomal and the ribosomal fraction, respectively
(B) Quantitation of the western blot show in (A) using ImageJ. Values are represented as the relative fraction of eIF4A distributed to either the supernatant or to the ribosomal pellet.

Stable eIF4A binding onto regions outside of the 5' leader may also affect other RNA-depending processes apart from translation through perturbing proper RNA folding or interfering with the activities of other RBPs. For instance, LIN28A and LIN28B are RNA binding proteins that preferentially associate with polypurine RNA motifs and are involved in multiple aspects of RNA

biology including enhancing mRNA stability and repressing let-7 miRNA processing, (Hafner et al., 2013; Wilbert et al., 2012). Would rocaglate-induced eIF4A:RNA stabilization interfere with LIN28A/LIN28B function? What about the roles of other RBPs? At this moment, global changes of eIF4A distribution in the presence of rocaglates have not been extensively studied but we are in the process of examining this aspect of rocaglate mechanism more thoroughly using eCLIP.

6.1.4 Why is Silvestrol Different?

Silvestrol, WGD-57-590 and WGD-57-591 were the only compounds within our rocaglate collection that possess a dioxyanyloxy moiety and were pinpointed as outliers when we plotted the results of the FP assay with respect to activity of the compounds that inhibited translation *in vitro* (Figure 5.1A). However, when we measured the dissociation rates of the eIF4A:rocaglate:RNA complexes in the presence of ATP as opposed to AMPPNP using the FP assay, we observe that the complexes formed in the presence of silvestrol and WGD-57-591 dissociated more slowly compared to CMLD012073, CR-1-31-B, Roc-A, and CMLD011167 (Figure S5.1E). The slow dissociation rates of the dioxyanyloxy-containing rocaglates may be the underlying basis for why these compounds possess higher translational inhibitory activities than what was originally predicted from the FP data.

Another difference exhibited by the dioxyanyloxy-containing rocaglates is their ability to stabilize eIF4A binding onto polypyrimidine RNA sequences (Figure S5.3). Because RPDs using recombinant eIF4A or purified eIF4F complexes resulted in eIF4A stabilization onto the polypyrimidine bait, we hypothesize that there is a co-factor that enables eIF4A to stably bind onto polypyrimidine sequences in the presence of silvestrol. While we cannot definitely say what this co-factor is, candidates include the eIF4A accessory proteins, eIF4B and eIF4H. It had been previously

reported that pateamine A promotes the association between eIF4A and eIF4B in the presence of RNA (Low et al., 2005), although there is some debate regarding whether the observed increase in association is actually due to co-association of both proteins onto RNA rather than a direct effect stimulating eIF4A:eIF4B interaction (Bordeleau et al., 2006a). Nevertheless, when we performed the RPD in the presence of recombinant eIF4A1 and eIF4H, we observe that eIF4A1 is retained on the polypyrimidine bait in the presence of silvestrol (Figure 6.4). Currently, we are undertaking further experiments to test this hypothesis more extensively. Among these include RPDs in extracts depleted of eIF4B and eIF4H. If this hypothesis is demonstrated to be true, then it may be interesting to assess whether eIF4B and eIF4H expression levels could affect the changes in the translatome and/or modulate cytotoxic response in the presence of silvestrol.

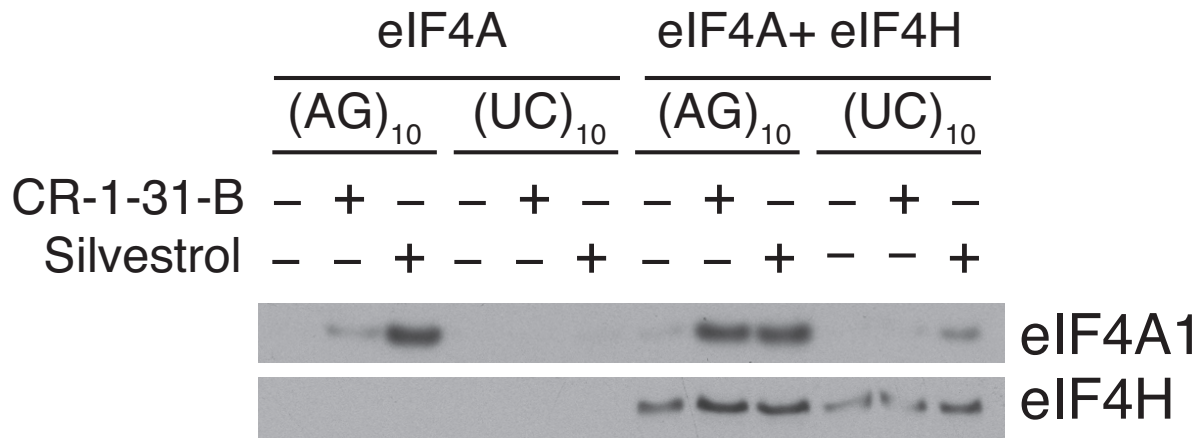

Figure 6.4 Silvestrol Stabilizes eIF4A onto Polypyrimidine Sequences in the Presence of eIF4H
RNA pulldown experiments using biotinylated $(AG)_{10}$ or $(UC)_{10}$ baits in the presence of recombinant eIF4A1 (67 nM) with or without recombinant eIF4H (67 nM). Where indicated, CR-1-31-B or silvestrol was added to the sample at a final concentration of 500 nM.

6.1.5 Possible Mechanisms of Rocaglate Resistance

Intrinsic and/or acquired resistance is a concern that pertains to all therapeutic treatments. While rocaglates have been shown to be effective agents for overcoming chemoresistance through the

depletion of key oncogenes, these compounds are still susceptible to resistance. For example, silvestrol is a known substrate for the ABCB1 (ATP-binding cassette sub-family B member 1, also known as multi-drug resistance 1 (MDR1) and P-glycoprotein-1 (PGP1)), an ATP-dependent efflux pump that is known to cause resistance to many chemotherapeutic agents including doxorubicin, dexamethasone, and imatinib (Gupta et al., 2011; Mahon et al., 2003; Zheng, 2017). ABCB1 regulation is mediated by the MAPK pathway as well as various transcription factors including AP-1 and NF-kB, and upregulation of these factors can indirectly result in silvestrol-resistance (Sui et al., 2012). In addition, several ABCB1 polymorphisms have been identified between different ethnic populations, and many of these variants affect drug response by altering ABCB1 activity and/or modifying ABCB1 mRNA/protein expression (Wolking et al., 2015). However, silvestrol's sensitivity towards ABCB1 is derived from the presence of its dioxyanyloxy moiety and removal of this group reduced cellular efflux and restored compound cytotoxicity in cells overexpressing ABCB1 (Liu et al., 2012). Therefore, it may be preferable to utilize rocaglates lacking the dioxyanyloxy moiety, such as RocA or CR-1-31-B, against tumors with upregulated ABCB1 activity.

Alternatively, ABCB1-mediated tumor resistance can be circumvented by small-molecule inhibitors that target this transporter. One example of such a compound is LY-335979 (also known as zosuquidar), which binds directly to ABCB1 and traps it in a closed conformation that occludes compound binding (Alam et al., 2019; Alam et al., 2018; Dantzig et al., 1996). LY-335979 has been shown to be capable of restoring sensitivity towards many chemotherapies including doxorubicin, vinblastine, taxol, and etoposide (Dantzig et al., 1996). Presently, there are several ABCB-1 inhibitors (among these include LY-335979) being developed in clinical trials but in spite of the highly promising activity of these drugs in preclinical studies, their efficacy within the clinical setting appear to be rather

modest (Dash et al., 2017; Saeki et al., 2007). Nevertheless, efforts are currently being made to better understand the optimal dosing schedule of ABCB-1 inhibitors and to improve compound bioavailability.

Defects in autophagy have also been positioned as a potential mechanism of resistance to rocaglates (Chen et al., 2016). Autophagy describes a collection of processes in which cellular components (such as proteins and organelles) are digested in a lysosome-dependent manner. In nutrient deprived states, AMPK (AMP-activated protein kinase) induces autophagy by activating ULK1(Unc-51 like autophagy activating kinase 1), a kinase integral for the initiation autophagy (Kim et al., 2011). Conversely, under growth-permissive conditions, mTORC1 inhibits ULK1 and prevents it from associating with AMPK (Kim et al., 2011). Suppression of eIF4A has been shown to lead to elevated mTORC1 activity (Galicia-Vazquez et al., 2012; Gandin et al., 2016; Tsokanos et al., 2016), but in spite of this, increased autophagy has been observed in response to various rocaglates (Bhattacharya et al., 2016; Chen et al., 2016; Zhao et al., 2019). In the case of silvestrol, this appears to be attributed to increased transcription of autophagic mRNA such as AMPK, LC3 and p62 (Chen et al., 2016). MEFs lacking Atg7 were also found to be relatively more resistant to silvestrol compared to the wildtype cells in *in vitro* cell culture experiments (Chen et al., 2016). However, in an independent study using RocA, suppression of autophagy using siRNA or pharmacological inhibitors synergized with the cytotoxic effects of RocA (Zhao et al., 2019). Autophagy can be either cytoprotective or can trigger apoptosis and these opposing results highlight the complex relationship between autophagic flux and cell death. Ultimately, further investigation of the effects of autophagy on rocaglate mechanism is warranted.

6.2 Recent Insights on eIF4F Function

6.2.1 Non-overlapping regulation by different initiation factors

It is becoming increasingly evident the regulation of translation initiation is incredibly nuanced and different outcomes can be achieved depending on what initiation factor is targeted. For instance, while eIF4E and eIF4A are both essential components of the eIF4F complex, emerging evidence suggests that these two subunits regulate distinct subsets of mRNAs. The most highly characterized example are transcripts containing an IRES element. IRESes do not depend on eIF4E activity but many, such as the EMCV and the polio IRESes, still require the presence of eIF4G and eIF4A (Hellen and Sarnow, 2001). Additionally, TOP mRNAs are highly sensitive towards eIF4E suppression but are not especially responsive when eIF4A is inhibited (Hsieh et al., 2012; Rubio et al., 2014; Thoreen et al., 2012). A study comparing the global changes in translation upon eIF4E or eIF4A suppression found that although mRNAs harboring long and highly structured 5' leaders were highly sensitive to both factors, transcripts with short 5' leaders containing a TISU element were responsive to eIF4E, but not towards eIF4A inhibition (Gandin et al., 2016). These TISU-containing mRNAs predominantly encoded for proteins involved in mitochondrial function (Gandin et al., 2016). Accordingly, siRNA depletion of eIF4E affected mitochondrial respiration more drastically compared to depletion of eIF4A (Gandin et al., 2016). Similar results were observed when the effects of the mTOR inhibitor torin1 was compared with silvestrol (Gandin et al., 2016).

A separate study employing ribosome profiling to study global changes upon depletion of the yeast homologs of eIF4A (TIF1) and eIF4B (TIF3) found that long and structured 5' leaders to be highly sensitive for these two factors, although this dependency is more pronounced with TIF3 (Sen et al., 2016). Moreover, the length of the entire mRNA body appears to confer sensitivity, with longer

transcripts being more inhibited upon depletion of TIF1 and TIF3 (Sen et al., 2016). However, there were a substantial transcripts that displayed heighted sensitivity towards only one of these two initiation factors (Sen et al., 2016). Depletion of eIF4G (TIF4631), on the other hand, resulted in preferential inhibition of mRNAs with relatively unstructured 5' leaders and short coding regions (Park et al., 2011; Sen et al., 2016). These mRNAs are translated very efficiently in wildtype cells and it is postulated this is because shorter transcripts induce mRNA circularization (driven by the interaction between eIF4G and PABP) more readily (Park et al., 2011). Therefore, although these mRNAs are not particularly dependent on the helicase activity of TIF1 (which is further enhanced by TIF3), their competitive edge in promoting translation initiation is reduced when the ability to circularize the transcript is lost (Sen et al., 2016). It is important to note that there are several differences between the mechanisms of yeast and mammalian translation initiation, and it remains to be seen whether these observations are also seen within the mammalian context.

Overall, it appears that global translation can be differentially modulated depending on which initiation factor is targeted. To further this idea, our data in chapter 5 suggests that structurally and functionally distinct inhibitors targeting the same factor can also exert differing results in the translatome. Our reporter assays indicate that the presence of polypurine sequences within the 5' leader confers high sensitivity towards rocaglates such as RocA, CMLD011167 and CR-1-31-B, but less so when silvestrol or WGD-57-591 is used. Moreover, 5' leader purine content does not influence the translation inhibition exerted by the structurally unrelated eIF4A inhibitor, pateamine A. Although ribosome profiling studies have been performed using RocA and silvestrol, it would be of interest to evaluate other rocaglate derivatives using the same technique. Global changes induced by CMLD011167 would be particularly interesting as it exhibited potent eIF4A-dependent cytotoxic

activity (Figure 5.2A) in spite of its unexpected lack of activity in cell free extracts (Figure 5.1A). Moreover, translation assays in cells using RNA transfected reporters reveal that CMLD011167 show the highest selectivity towards inhibition of polypurine rich 5' leaders (Figure 5.2B). Along with different rocaglate analogues, it would also be intriguing to perform ribosome profiling in the presence of hippuristanol. In doing so, this would allow us to compare changes in translation caused by eIF4A gain of function versus loss of function. Presently, there is one published ribosome profiling dataset illustrating the changes in translation elicited by hippuristanol, but unfortunately, the concentration of hippuristanol (1 μM) used for this experiment was very high, thus making it difficult to determine which transcripts truly exhibited heightened sensitivity to the compound (Iwasaki et al., 2016). Lastly, the non-overlapping changes on gene expression induced by different eIF4A inhibitors also raise the question of whether some compounds are more vulnerable to certain mechanisms of resistance caused by feedback loop activation.

6.2.2 Positioning of eIF4F During 43S PIC Scanning

Even though the discovery of eIF4E was made nearly 40 years ago, our understanding of how eIF4F operates during the initiation process is still in progress. At first glance, our results presented in Figure 5.3 could be a bit perplexing as intuitively, one may predict that increased eIF4F association on the 5'cap would promote efficient translation initiation. Because the opposite was observed instead, our results support a model of initiation in which the association of the eIF4F complex to the mRNA is dynamic in nature. This model is not new (Merrick, 2015). First, the association of eIF4F is not entirely stable and *in vitro* experiments have demonstrated that free eIF4A can displace that eIF4A is present within the complex (Yoder-Hill et al., 1993). Consistent with this point, a eIF4A mutant

(R362Q) exerts dominant negative effects on translation by stably binding to eIF4F, thus preventing this recycling process (Pause et al., 1994). Secondly, it is hypothesized that eIF4E is released at some point during initiation to promote ribosome migration (Scheper et al., 2002). Stable association of eIF4E is also speculated to be incompatible with the threading model of 43S PIC loading as the presence of eIF4E is predicted to hinder the transcript from entering the narrow channel of the 43S PIC (Kumar et al., 2016). In support of this, cap-crosslinking experiments illustrate that 43S PIC binding onto mRNA decreases the levels of eIF4E crosslinked at the cap (Kumar et al., 2016).

6.2.3 Moonlighting Functions of eIF4A

Out of the three eIF4F subunits, eIF4A is by far the most abundant, existing at a ~10-fold excess over eIF4E and a 3-fold excess over the ribosome in mammalian cells (Duncan et al., 1987; Schwanhausser et al., 2011). Similar protein ratios exist in yeast but interestingly, reduction of eIF4A expression by 20% in yeast was sufficient to reduce the rate of global protein synthesis and inhibit cellular proliferation, indicating that high levels of eIF4A is necessary to maintain optimal protein synthesis rates and cellular viability (Firczuk et al., 2013). High concentrations of eIF4A can potentially compensate for its weak RNA binding activity and lack of processivity. However, there are reports suggesting that eIF4A may possess roles outside of translation.

6.2.3.1 eIF4A2 and miRNA-mediated gene repression

It has been proposed that eIF4A2 (but not eIF4A1) plays a critical role in miRNA-mediated gene repression (Meijer et al., 2013). This claim is driven primarily by one study in which miRNA-mediated repression of a luciferase based reporter was alleviated upon eIF4A2 knockdown (Meijer et al., 2013). Immunoprecipitation experiments within this study also show that eIF4A2 associates with

CNOT1, a component of the CCR4-NOT microRNA silencing complex, instead of eIF4G (Meijer et al., 2013). Consequently, rather than functioning as a translation factor, eIF4A2 was suggested to promote miRNA mediated silencing by stably binding onto the 5' leader and blocking the scanning 43S PIC to repress translation. However, this claim is very contentious as many other groups presented results that directly contradict with these findings. In our hands, no defect was observed in miRNA mediated repression in an eIF4A2 knockout NIH/3T3 cell line or through transient suppression of eIF4A2 in HeLa cell using siRNAs (Galicia-Vazquez et al., 2014). In addition pulldown experiments using GFP-eIF4G or GFP-CNOT1 demonstrated that eIF4A2 associates with the former but not the latter (Chen et al., 2014). These results appear to be more reasonable seeing as how the surface that interacts with eIF4G in eIF4A1 is identical in eIF4A2. Moreover, eIF4A2 has been shown to be capable of displacing eIF4A1 within the eIF4F complex (Yoder-Hill et al., 1993) and the addition of a hippuristanol-resistant eIF4A2 mutant to *in vitro* translation extracts is able to rescue the compound inhibition (Lindqvist et al., 2008b).

6.2.3.2 eIF4A as a regulator of mTORC1

Perturbation of eIF4A activity results in feedback regulation of mTORC1 signalling. Upon eIF4A suppression, mTORC1 activity is enhanced (Galicia-Vazquez et al., 2012; Gandin et al., 2016; Tsokanos et al., 2016) and conversely, the opposite is observed when eIF4A is overexpressed (Chu and Pelletier, data not shown). The mechanism of how eIF4A1 regulates mTORC1 is not well defined. One study using Drosophila cells found that knockdown of eIF4A resulted in impaired inactivation of mTORC1 in response to amino acid depletion in a TSC2 dependent manner (Tsokanos et al., 2016). Impaired inactivation of mTORC1 does not appear to be the consequence of general repression in translation as this effect is not phenocopied by the knockdown of other initiation factors (with the

exception of eIF4E and eIF4G) or when cycloheximide was used to inhibit protein synthesis (Tsokanos et al., 2016). Using a series of immunoprecipitation experiments, eIF4A (and eIF4F) was reported to interact with mTORC1 and TSC2, and based on these results, the investigators conducting this study posits that eIF4A directly promotes TSC2 to inactivate mTORC1 during nutrient-compromised states (Tsokanos et al., 2016). Alternatively, while mTORC1 inactivation does not appear to be a consequence of general inhibition of translation, suppression of eIF4F can potentially lead to specific changes in the gene expression. One candidate that may be of interest to look further into is AMPK, as inhibition of eIF4A using silvestrol has been found to increase AMPK transcript levels by ~3000 fold (Chen et al., 2016). Therefore, it is conceivable that the regulation of mTORC1 exerted by eIF4A is not through its direct interaction with TSC2, but instead through indirect stimulation of AMPK.

6.2.3.3 eIF4A and the mediation of RNA granules

When translation initiation is attenuated, the stalled ribonucleoprotein (mRNP) complexes can assemble into phase-separated condensates known as stress granules (SG) (Protter and Parker, 2016). While cellular stressors that lead to the phosphorylation of eIF2 represent a major class of SG inducers, SGs can also form in the absence of eIF2 phosphorylation (Mazroui et al., 2006). Notably, inhibitors of eIF4A are known to cause SG assembly in an eIF2 independent manner (Mazroui et al., 2006). These membrane-less aggregates are composed of mRNAs bound to stalled 43S PICs (but can also include lncRNAs), and are stabilized by numerous intermolecular RNA-protein, RNA-RNA and protein-protein interactions (Protter and Parker, 2016; Van Treeck et al., 2018).

eIF4A is recruited into SGs and was recently observed to be enriched at the SG periphery (Tauber et al., 2019). Due to this preferential partitioning and the fact that eIF4A is much more

abundant that every other initiation factor, it is hypothesized that eIF4A can function outside of its canonical role in translation initiation by unwinding intermolecular RNA-RNA interactions to limit the accumulation of RNAs into SGs (Tauber et al., 2019). In support of this, overexpression of eIF4A prevented the formation of SG in the presence of sodium arsenite without alleviating the inhibition in translation (Tauber et al., 2019). Moreover, inhibition of eIF4A helicase activity using hippuristanol promoted the condensation of RNAs into SGs whereas pateamine A, which causes eIF4A gain-of-function activity, did not (Tauber et al., 2019). Given the recent observations that eIF4A outside of the eIF4F complex preferentially associates with polypurine sequences (Chu et al., 2019; Iwasaki et al., 2016), eIF4A helicase activity may also be biased towards purine substrates. If this holds true, it would be interesting to see if the nucleotide composition of an RNA affects how effectively it gets recruited into SGs.

6.3 Future Directions

eIF4A was discovered approximately 40 years ago, and since then, considerable progress has been made towards understanding its biology. Nevertheless, a number of questions pertaining to eIF4A remain open. First, it is still unclear how exactly eIF4A operates during translation initiation. Although it is evident that the helicase activity of eIF4A is essential for initiation, it is unknown whether it simply unwinds cap-proximal RNA structures to facilitate 43S PIC loading, or if it actually travels with the scanning 43S PIC to unwind structural elements throughout the 5' leader. However, *in vitro* crosslinking experiments do show that eIF4A interacts with nucleotides 52 base pairs from the cap structure (Lindqvist et al., 2008a). If eIF4A does indeed interact with the entire length of the 5' leader, this then leads to the question of whether this is attributed to a processive mechanism or to a

series of multiple binding events. These models remain mostly speculative at this point in time, but hopefully, advances in structural techniques such as cryo-electron microscopy would provide clarity towards the mechanistic details of eIF4A activity in the near future.

Second, the notion that eIF4A functions outside of translation initiation is rather new and have not been examined rigorously. This concept is certainly provocative, but as exemplified by the proposed role of eIF4A2 in miRNA silencing in section 6.2.3.1, further studies performed by independent groups are absolutely essential to evaluate the veracity of such claims. Given that the primary role of eIF4A is to promote translation initiation, the investigation of putative secondary functions could be challenging as one would need to determine if the observed effect is actually direct and not simply an indirect consequence altered protein synthesis. However, the increasing accessibility of high-throughput techniques such as CLIP (to study global RNA binding patterns) and Bio-ID (to establish protein-protein interaction networks) will certainly be of great assistance. As well, utilization of small molecules that promote (i.e. rocaglates and pateamine A) or abrogate (hippuristanol) eIF4A RNA binding can help determine how exactly eIF4A is involved in the process.

Lastly, rocaglates have been shown to possess promising anti-cancer activity in pre-clinical studies and, as highlighted by the work laid out in this thesis, quite a bit is known regarding its mechanism of action. As a result, there is a case to be made in evaluating this class of compounds within the clinical setting. Currently, eFFECTOR Therapeutics is recruiting subjects for a Phase 1-2 clinical investigation of the safety and efficacy of eFT226 against solid tumors exhibiting deregulated activation of ERBB2, ERBB3, FGFR1, FGFR2 or KRAS. However, given the underwhelming results of mTOR-based therapies, it is absolutely pertinent to establish predictive biomarkers to fully optimize rocaglate efficacy within the clinic.

CHAPTER 7 References

Abramson, R.D., Dever, T.E., Lawson, T.G., Ray, B.K., Thach, R.E., and Merrick, W.C. (1987). The ATP-dependent interaction of eukaryotic initiation factors with mRNA. J Biol Chem *262*, 3826-3832.

Alachkar, H., Santhanam, R., Harb, J.G., Lucas, D.M., Oaks, J.J., Hickey, C.J., Pan, L., Kinghorn, A.D., Caligiuri, M.A., Perrotti, D.*, et al.* (2013). Silvestrol exhibits significant in vivo and in vitro antileukemic activities and inhibits FLT3 and miR-155 expressions in acute myeloid leukemia. Journal of hematology & oncology *6*, 21.

Alain, T., Morita, M., Fonseca, B.D., Yanagiya, A., Siddiqui, N., Bhat, M., Zammit, D., Marcus, V., Metrakos, P., Voyer, L.A.*, et al.* (2012). eIF4E/4E-BP ratio predicts the efficacy of mTOR targeted therapies. Cancer research *72*, 6468-6476.

Alam, A., Kowal, J., Broude, E., Roninson, I., and Locher, K.P. (2019). Structural insight into substrate and inhibitor discrimination by human P-glycoprotein. Science (New York, NY) *363*, 753-756.

Alam, A., Kung, R., Kowal, J., McLeod, R.A., Tremp, N., Broude, E.V., Roninson, I.B., Stahlberg, H., and Locher, K.P. (2018). Structure of a zosuquidar and UIC2-bound human-mouse chimeric ABCB1. Proceedings of the National Academy of Sciences of the United States of America *115*, E1973-e1982.

Andreassi, C., and Riccio, A. (2009). To localize or not to localize: mRNA fate is in 3'UTR ends. Trends in cell biology *19*, 465-474.

Andreev, D.E., Dmitriev, S.E., Zinovkin, R., Terenin, I.M., and Shatsky, I.N. (2012). The 5' untranslated region of Apaf-1 mRNA directs translation under apoptosis conditions via a 5' end-dependent scanning mechanism. FEBS letters *586*, 4139-4143.

Andreev, D.E., O'Connor, P.B., Zhdanov, A.V., Dmitriev, R.I., Shatsky, I.N., Papkovsky, D.B., and Baranov, P.V. (2015). Oxygen and glucose deprivation induces widespread alterations in mRNA translation within 20 minutes. Genome Biol *16*, 90.

Asano, K. (2014). Why is start codon selection so precise in eukaryotes? Translation (Austin, Tex) *2*, e28387.

Asano, K., Merrick, W.C., and Hershey, J.W. (1997). The translation initiation factor eIF3-p48 subunit is encoded by int-6, a site of frequent integration by the mouse mammary tumor virus genome. The Journal of biological chemistry *272*, 23477-23480.

Asano, K., Phan, L., Valasek, L., Schoenfeld, L.W., Shalev, A., Clayton, J., Nielsen, K., Donahue, T.F., and Hinnebusch, A.G. (2001). A multifactor complex of eIF1, eIF2, eIF3, eIF5, and tRNA(i)Met promotes initiation complex assembly and couples GTP hydrolysis to AUG recognition. Cold Spring Harbor symposia on quantitative biology *66*, 403-415.

Atkins, C., Liu, Q., Minthorn, E., Zhang, S.Y., Figueroa, D.J., Moss, K., Stanley, T.B., Sanders, B., Goetz, A., Gaul, N.*, et al.* (2013). Characterization of a novel PERK kinase inhibitor with antitumor and antiangiogenic activity. Cancer research *73*, 1993-2002.

Avni, D., Shama, S., Loreni, F., and Meyuhas, O. (1994). Vertebrate mRNAs with a 5'-terminal pyrimidine tract are candidates for translational repression in quiescent cells: characterization of the translational cis-regulatory element. Molecular and cellular biology *14*, 3822-3833.

Badura, M., Braunstein, S., Zavadil, J., and Schneider, R.J. (2012). DNA damage and eIF4G1 in breast cancer cells reprogram translation for survival and DNA repair mRNAs. Proceedings of the National Academy of Sciences of the United States of America *109*, 18767-18772.
Bah, A., Vernon, R.M., Siddiqui, Z., Krzeminski, M., Muhandiram, R., Zhao, C., Sonenberg, N., Kay, L.E., and Forman-Kay, J.D. (2015). Folding of an intrinsically disordered protein by phosphorylation as a regulatory switch. Nature *519*, 106-109.
Baranick, B.T., Lemp, N.A., Nagashima, J., Hiraoka, K., Kasahara, N., and Logg, C.R. (2008). Splicing mediates the activity of four putative cellular internal ribosome entry sites. Proceedings of the National Academy of Sciences of the United States of America *105*, 4733-4738.
Barber, G.N., Wambach, M., Thompson, S., Jagus, R., and Katze, M.G. (1995). Mutants of the RNA-dependent protein kinase (PKR) lacking double-stranded RNA binding domain I can act as transdominant inhibitors and induce malignant transformation. Molecular and cellular biology *15*, 3138-3146.
Bauer, C., Diesinger, I., Brass, N., Steinhart, H., Iro, H., and Meese, E.U. (2001). Translation initiation factor eIF-4G is immunogenic, overexpressed, and amplified in patients with squamous cell lung carcinoma. Cancer *92*, 822-829.
Benjamin, D., Colombi, M., Moroni, C., and Hall, M.N. (2011). Rapamycin passes the torch: a new generation of mTOR inhibitors. Nature reviews Drug discovery *10*, 868-880.
Beroukhim, R., Mermel, C.H., Porter, D., Wei, G., Raychaudhuri, S., Donovan, J., Barretina, J., Boehm, J.S., Dobson, J., Urashima, M.*, et al.* (2010). The landscape of somatic copy-number alteration across human cancers. Nature *463*, 899-905.
Bhat, M., Robichaud, N., Hulea, L., Sonenberg, N., Pelletier, J., and Topisirovic, I. (2015). Targeting the translation machinery in cancer. Nature reviews Drug discovery *14*, 261-278.
Bhattacharya, B., Chatterjee, S., Devine, W.G., Kobzik, L., Beeler, A.B., Porco, J.A., Jr., and Kramnik, I. (2016). Fine-tuning of macrophage activation using synthetic rocaglate derivatives. Scientific reports *6*, 24409.
Bi, M., Naczki, C., Koritzinsky, M., Fels, D., Blais, J., Hu, N., Harding, H., Novoa, I., Varia, M., Raleigh, J.*, et al.* (2005). ER stress-regulated translation increases tolerance to extreme hypoxia and promotes tumor growth. The EMBO journal *24*, 3470-3481.
Bitomsky, N., Bohm, M., and Klempnauer, K.H. (2004). Transformation suppressor protein Pdcd4 interferes with JNK-mediated phosphorylation of c-Jun and recruitment of the coactivator p300 by c-Jun. Oncogene *23*, 7484-7493.
Biyanee, A., Ohnheiser, J., Singh, P., and Klempnauer, K.H. (2014). A novel mechanism for the control of translation of specific mRNAs by tumor suppressor protein Pdcd4: inhibition of translation elongation. Oncogene.
Bleumink, M., Kohler, R., Giaisi, M., Proksch, P., Krammer, P.H., and Li-Weber, M. (2011). Rocaglamide breaks TRAIL resistance in HTLV-1-associated adult T-cell leukemia/lymphoma by translational suppression of c-FLIP expression. Cell death and differentiation *18*, 362-370.
Bohm, M., Sawicka, K., Siebrasse, J.P., Brehmer-Fastnacht, A., Peters, R., and Klempnauer, K.H. (2003). The transformation suppressor protein Pdcd4 shuttles between nucleus and cytoplasm and binds RNA. Oncogene *22*, 4905-4910.
Bordeleau, M.E., Cencic, R., Lindqvist, L., Oberer, M., Northcote, P., Wagner, G., and Pelletier, J. (2006a). RNA-mediated sequestration of the RNA helicase eIF4A by Pateamine A inhibits translation initiation. Chemistry & biology *13*, 1287-1295.

Bordeleau, M.E., Matthews, J., Wojnar, J.M., Lindqvist, L., Novac, O., Jankowsky, E., Sonenberg, N., Northcote, P., Teesdale-Spittle, P., and Pelletier, J. (2005). Stimulation of mammalian translation initiation factor eIF4A activity by a small molecule inhibitor of eukaryotic translation. Proceedings of the National Academy of Sciences of the United States of America *102*, 10460-10465.

Bordeleau, M.E., Mori, A., Oberer, M., Lindqvist, L., Chard, L.S., Higa, T., Belsham, G.J., Wagner, G., Tanaka, J., and Pelletier, J. (2006b). Functional characterization of IRESes by an inhibitor of the RNA helicase eIF4A. Nature chemical biology *2*, 213-220.

Bordeleau, M.E., Robert, F., Gerard, B., Lindqvist, L., Chen, S.M., Wendel, H.G., Brem, B., Greger, H., Lowe, S.W., Porco, J.A., Jr., *et al.* (2008). Therapeutic suppression of translation initiation modulates chemosensitivity in a mouse lymphoma model. The Journal of clinical investigation *118*, 2651-2660.

Boussemart, L., Malka-Mahieu, H., Girault, I., Allard, D., Hemmingsson, O., Tomasic, G., Thomas, M., Basmadjian, C., Ribeiro, N., Thuaud, F., *et al.* (2014). eIF4F is a nexus of resistance to anti-BRAF and anti-MEK cancer therapies. Nature *513*, 105-109.

Braunstein, S., Karpisheva, K., Pola, C., Goldberg, J., Hochman, T., Yee, H., Cangiarella, J., Arju, R., Formenti, S.C., and Schneider, R.J. (2007). A hypoxia-controlled cap-dependent to cap-independent translation switch in breast cancer. Mol Cell *28*, 501-512.

Bulmer, M. (1987). Coevolution of codon usage and transfer RNA abundance. Nature *325*, 728-730.

Buttitta, F., Martella, C., Barassi, F., Felicioni, L., Salvatore, S., Rosini, S., D'Antuono, T., Chella, A., Mucilli, F., Sacco, R., *et al.* (2005). Int6 expression can predict survival in early-stage non-small cell lung cancer patients. Clinical cancer research : an official journal of the American Association for Cancer Research *11*, 3198-3204.

Cai, X., Hagedorn, C.H., and Cullen, B.R. (2004). Human microRNAs are processed from capped, polyadenylated transcripts that can also function as mRNAs. RNA (New York, NY) *10*, 1957-1966.

Castello, A., Alvarez, E., and Carrasco, L. (2006). Differential cleavage of eIF4GI and eIF4GII in mammalian cells. Effects on translation. The Journal of biological chemistry *281*, 33206-33216.

Cencic, R., Carrier, M., Galicia-Vazquez, G., Bordeleau, M.E., Sukarieh, R., Bourdeau, A., Brem, B., Teodoro, J.G., Greger, H., Tremblay, M.L., *et al.* (2009). Antitumor activity and mechanism of action of the cyclopenta[b]benzofuran, silvestrol. PloS one *4*, e5223.

Cencic, R., Carrier, M., Trnkus, A., Porco, J.A., Jr., Minden, M., and Pelletier, J. (2010). Synergistic effect of inhibiting translation initiation in combination with cytotoxic agents in acute myelogenous leukemia cells. Leukemia research *34*, 535-541.

Cencic, R., Galicia-Vazquez, G., and Pelletier, J. (2012). Inhibitors of translation targeting eukaryotic translation initiation factor 4A. Methods Enzymol *511*, 437-461.

Cencic, R., Robert, F., Galicia-Vazquez, G., Malina, A., Ravindar, K., Somaiah, R., Pierre, P., Tanaka, J., Deslongchamps, P., and Pelletier, J. (2013). Modifying chemotherapy response by targeted inhibition of eukaryotic initiation factor 4A. Blood cancer journal *3*, e128.

Cencic, R., Robert, F., and Pelletier, J. (2007). Identifying small molecule inhibitors of eukaryotic translation initiation. Methods Enzymol *431*, 269-302.

Chambers, J.M., Lindqvist, L.M., Webb, A., Huang, D.C., Savage, G.P., and Rizzacasa, M.A. (2013). Synthesis of biotinylated episilvestrol: highly selective targeting of the translation factors eIF4AI/II. Organic letters *15*, 1406-1409.

Chan, C.C., Dostie, J., Diem, M.D., Feng, W., Mann, M., Rappsilber, J., and Dreyfuss, G. (2004). eIF4A3 is a novel component of the exon junction complex. RNA (New York, NY) *10*, 200-209.

Chaney, J.L., and Clark, P.L. (2015). Roles for Synonymous Codon Usage in Protein Biogenesis. Annual review of biophysics *44*, 143-166.
Chen, C.Y., and Shyu, A.B. (1995). AU-rich elements: characterization and importance in mRNA degradation. Trends in biochemical sciences *20*, 465-470.
Chen, C.Y., and Shyu, A.B. (2011). Mechanisms of deadenylation-dependent decay. Wiley interdisciplinary reviews RNA *2*, 167-183.
Chen, G., and Burger, M.M. (2004). p150 overexpression in gastric carcinoma: the association with p53, apoptosis and cell proliferation. International journal of cancer Journal international du cancer *112*, 393-398.
Chen, L., Aktas, B.H., Wang, Y., He, X., Sahoo, R., Zhang, N., Denoyelle, S., Kabha, E., Yang, H., Freedman, R.Y., *et al.* (2012). Tumor suppression by small molecule inhibitors of translation initiation. Oncotarget *3*, 869-881.
Chen, S.L., Lee, W., Hottes, A.K., Shapiro, L., and McAdams, H.H. (2004). Codon usage between genomes is constrained by genome-wide mutational processes. Proceedings of the National Academy of Sciences of the United States of America *101*, 3480-3485.
Chen, W.L., Pan, L., Kinghorn, A.D., Swanson, S.M., and Burdette, J.E. (2016). Silvestrol induces early autophagy and apoptosis in human melanoma cells. BMC cancer *16*, 17.
Chen, Y., Boland, A., Kuzuoglu-Ozturk, D., Bawankar, P., Loh, B., Chang, C.T., Weichenrieder, O., and Izaurralde, E. (2014). A DDX6-CNOT1 complex and W-binding pockets in CNOT9 reveal direct links between miRNA target recognition and silencing. Molecular cell *54*, 737-750.
Chen, Z.H., Qi, J.J., Wu, Q.N., Lu, J.H., Liu, Z.X., Wang, Y., Hu, P.S., Li, T., Lin, J.F., Wu, X.Y., *et al.* (2019). Eukaryotic initiation factor 4A2 promotes experimental metastasis and oxaliplatin resistance in colorectal cancer. Journal of experimental & clinical cancer research : CR *38*, 196.
Cheng, H., Dufu, K., Lee, C.S., Hsu, J.L., Dias, A., and Reed, R. (2006). Human mRNA export machinery recruited to the 5' end of mRNA. Cell *127*, 1389-1400.
Cheung, Y.N., Maag, D., Mitchell, S.F., Fekete, C.A., Algire, M.A., Takacs, J.E., Shirokikh, N., Pestova, T., Lorsch, J.R., and Hinnebusch, A.G. (2007). Dissociation of eIF1 from the 40S ribosomal subunit is a key step in start codon selection in vivo. Genes & development *21*, 1217-1230.
Cho, E.J., Takagi, T., Moore, C.R., and Buratowski, S. (1997). mRNA capping enzyme is recruited to the transcription complex by phosphorylation of the RNA polymerase II carboxy-terminal domain. Genes & development *11*, 3319-3326.
Christensen, A.K., Kahn, L.E., and Bourne, C.M. (1987). Circular polysomes predominate on the rough endoplasmic reticulum of somatotropes and mammotropes in the rat anterior pituitary. The American journal of anatomy *178*, 1-10.
Chu, J., Cencic, R., Wang, W., Porco, J.A.J., and Pelletier, J. (2016a). Translation Inhibition by Rocaglates is Independent of eIF4E Phosphorylation Status. Mol Cancer Ther *15*, 136-141.
Chu, J., Galicia-Vazquez, G., Cencic, R., Mills, J.R., Katigbak, A., Porco, J.A., Jr., and Pelletier, J. (2016b). CRISPR-Mediated Drug-Target Validation Reveals Selective Pharmacological Inhibition of the RNA Helicase, eIF4A. Cell reports *15*, 2340-2347.
Chu, J., and Pelletier, J. (2014). Targeting the eIF4A RNA helicase as an anti-neoplastic approach. Biochim Biophys Acta.
Chu, J., Zhang, W., Cencic, R., Devine, W.G., Beglov, D., Henkel, T., Brown, L.E., Vajda, S., Porco, J.A., Jr., and Pelletier, J. (2019). Amidino-Rocaglates: A Potent Class of eIF4A Inhibitors. Cell chemical biology.

Clough, E., and Barrett, T. (2016). The Gene Expression Omnibus Database. Methods Mol Biol *1418*, 93-110.
Coldwell, M.J., Sack, U., Cowan, J.L., Barrett, R.M., Vlasak, M., Sivakumaran, K., and Morley, S.J. (2012). Multiple isoforms of the translation initiation factor eIF4GII are generated via use of alternative promoters, splice sites and a non-canonical initiation codon. The Biochemical journal *448*, 1-11.
Colgan, D.F., and Manley, J.L. (1997). Mechanism and regulation of mRNA polyadenylation. Genes & development *11*, 2755-2766.
Coller, J., and Parker, R. (2004). Eukaryotic mRNA decapping. Annual review of biochemistry *73*, 861-890.
Conte, M.R., Kelly, G., Babon, J., Sanfelice, D., Youell, J., Smerdon, S.J., and Proud, C.G. (2006). Structure of the eukaryotic initiation factor (eIF) 5 reveals a fold common to several translation factors. Biochemistry *45*, 4550-4558.
Daker, M., Yeo, J.T., Bakar, N., Abdul Rahman, A.S., Ahmad, M., Yeo, T.C., and Khoo, A.S. (2016). Inhibition of nasopharyngeal carcinoma cell proliferation and synergism of cisplatin with silvestrol and episilvestrol isolated from Aglaia stellatopilosa. Experimental and therapeutic medicine *11*, 2117-2126.
Dang, Y., Kedersha, N., Low, W.K., Romo, D., Gorospe, M., Kaufman, R., Anderson, P., and Liu, J.O. (2006). Eukaryotic initiation factor 2alpha-independent pathway of stress granule induction by the natural product pateamine A. The Journal of biological chemistry *281*, 32870-32878.
Dantzig, A.H., Shepard, R.L., Cao, J., Law, K.L., Ehlhardt, W.J., Baughman, T.M., Bumol, T.F., and Starling, J.J. (1996). Reversal of P-glycoprotein-mediated multidrug resistance by a potent cyclopropyldibenzosuberane modulator, LY335979. Cancer research *56*, 4171-4179.
Dash, R.P., Jayachandra Babu, R., and Srinivas, N.R. (2017). Therapeutic Potential and Utility of Elacridar with Respect to P-glycoprotein Inhibition: An Insight from the Published In Vitro, Preclinical and Clinical Studies. European journal of drug metabolism and pharmacokinetics *42*, 915-933.
Dauber, B., Pelletier, J., and Smiley, J.R. (2011). The herpes simplex virus 1 vhs protein enhances translation of viral true late mRNAs and virus production in a cell type-dependent manner. Journal of virology *85*, 5363-5373.
De Benedetti, A., and Graff, J.R. (2004). eIF-4E expression and its role in malignancies and metastases. Oncogene *23*, 3189-3199.
De Benedetti, A., Joshi-Barve, S., Rinker-Schaeffer, C., and Rhoads, R.E. (1991). Expression of antisense RNA against initiation factor eIF-4E mRNA in HeLa cells results in lengthened cell division times, diminished translation rates, and reduced levels of both eIF-4E and the p220 component of eIF-4F. Molecular and cellular biology *11*, 5435-5445.
De Benedetti, A., and Rhoads, R.E. (1990). Overexpression of eukaryotic protein synthesis initiation factor 4E in HeLa cells results in aberrant growth and morphology. Proceedings of the National Academy of Sciences of the United States of America *87*, 8212-8216.
Dhar, M.L., Dhar, M.M., Dhawan, B.N., Mehrotra, B.N., Srimal, R.C., and Tandon, J.S. (1973). Screening of Indian plants for biological activity. IV. Indian journal of experimental biology *11*, 43-54.

Di Marco, S., Cammas, A., Lian, X.J., Kovacs, E.N., Ma, J.F., Hall, D.T., Mazroui, R., Richardson, J., Pelletier, J., and Gallouzi, I.E. (2012). The translation inhibitor pateamine A prevents cachexia-induced muscle wasting in mice. Nature communications *3*, 896.

Dilling, M.B., Germain, G.S., Dudkin, L., Jayaraman, A.L., Zhang, X., Harwood, F.C., and Houghton, P.J. (2002). 4E-binding proteins, the suppressors of eukaryotic initiation factor 4E, are down-regulated in cells with acquired or intrinsic resistance to rapamycin. The Journal of biological chemistry *277*, 13907-13917.

Doldan, A., Chandramouli, A., Shanas, R., Bhattacharyya, A., Cunningham, J.T., Nelson, M.A., and Shi, J. (2008a). Loss of the eukaryotic initiation factor 3f in pancreatic cancer. Molecular carcinogenesis *47*, 235-244.

Doldan, A., Chandramouli, A., Shanas, R., Bhattacharyya, A., Leong, S.P., Nelson, M.A., and Shi, J. (2008b). Loss of the eukaryotic initiation factor 3f in melanoma. Molecular carcinogenesis *47*, 806-813.

Dong, J., Qiu, H., Garcia-Barrio, M., Anderson, J., and Hinnebusch, A.G. (2000). Uncharged tRNA activates GCN2 by displacing the protein kinase moiety from a bipartite tRNA-binding domain. Molecular cell *6*, 269-279.

Donze, O., Deng, J., Curran, J., Sladek, R., Picard, D., and Sonenberg, N. (2004). The protein kinase PKR: a molecular clock that sequentially activates survival and death programs. EMBO J *23*, 564-571.

Donze, O., Jagus, R., Koromilas, A.E., Hershey, J.W., and Sonenberg, N. (1995). Abrogation of translation initiation factor eIF-2 phosphorylation causes malignant transformation of NIH 3T3 cells. The EMBO journal *14*, 3828-3834.

Dorrello, N.V., Peschiaroli, A., Guardavaccaro, D., Colburn, N.H., Sherman, N.E., and Pagano, M. (2006). S6K1- and betaTRCP-mediated degradation of PDCD4 promotes protein translation and cell growth. Science (New York, NY) *314*, 467-471.

Doyle, G.A., Betz, N.A., Leeds, P.F., Fleisig, A.J., Prokipcak, R.D., and Ross, J. (1998). The c-myc coding region determinant-binding protein: a member of a family of KH domain RNA-binding proteins. Nucleic acids research *26*, 5036-5044.

Duncan, R., and Hershey, J.W. (1983). Identification and quantitation of levels of protein synthesis initiation factors in crude HeLa cell lysates by two-dimensional polyacrylamide gel electrophoresis. The Journal of biological chemistry *258*, 7228-7235.

Duncan, R., Milburn, S.C., and Hershey, J.W. (1987). Regulated phosphorylation and low abundance of HeLa cell initiation factor eIF-4F suggest a role in translational control. Heat shock effects on eIF-4F. The Journal of biological chemistry *262*, 380-388.

Duret, L. (2002). Evolution of synonymous codon usage in metazoans. Current opinion in genetics & development *12*, 640-649.

Ebada, S.S., Lajkiewicz, N., Porco, J.A., Jr., Li-Weber, M., and Proksch, P. (2011). Chemistry and biology of rocaglamides (= flavaglines) and related derivatives from aglaia species (meliaceae). Progress in the chemistry of organic natural products *94*, 1-58.

Eckmann, C.R., Rammelt, C., and Wahle, E. (2011). Control of poly(A) tail length. Wiley interdisciplinary reviews RNA *2*, 348-361.

Elfakess, R., and Dikstein, R. (2008). A translation initiation element specific to mRNAs with very short 5'UTR that also regulates transcription. PloS one *3*, e3094.

Elfakess, R., Sinvani, H., Haimov, O., Svitkin, Y., Sonenberg, N., and Dikstein, R. (2011). Unique translation initiation of mRNAs-containing TISU element. Nucleic acids research *39*, 7598-7609.
Elgner, F., Sabino, C., Basic, M., Ploen, D., Grunweller, A., and Hildt, E. (2018). Inhibition of Zika Virus Replication by Silvestrol. Viruses *10*.
Elliott, B., Richardson, C., Winderbaum, J., Nickoloff, J.A., and Jasin, M. (1998). Gene conversion tracts from double-strand break repair in mammalian cells. Mol Cell Biol *18*, 93-101.
Emmanuel, R., Weinstein, S., Landesman-Milo, D., and Peer, D. (2013). eIF3c: a potential therapeutic target for cancer. Cancer letters *336*, 158-166.
Fahrig, T., Gerlach, I., and Horvath, E. (2005). A synthetic derivative of the natural product rocaglaol is a potent inhibitor of cytokine-mediated signaling and shows neuroprotective activity in vitro and in animal models of Parkinson's disease and traumatic brain injury. Molecular pharmacology *67*, 1544-1555.
Fairman-Williams, M.E., Guenther, U.P., and Jankowsky, E. (2010). SF1 and SF2 helicases: family matters. Current opinion in structural biology *20*, 313-324.
Feldman, M.E., Apsel, B., Uotila, A., Loewith, R., Knight, Z.A., Ruggero, D., and Shokat, K.M. (2009). Active-site inhibitors of mTOR target rapamycin-resistant outputs of mTORC1 and mTORC2. PLoS biology *7*, e38.
Feoktistova, K., Tuvshintogs, E., Do, A., and Fraser, C.S. (2013). Human eIF4E promotes mRNA restructuring by stimulating eIF4A helicase activity. Proceedings of the National Academy of Sciences of the United States of America *110*, 13339-13344.
Ferrari, S., Bandi, H.R., Hofsteenge, J., Bussian, B.M., and Thomas, G. (1991). Mitogen-activated 70K S6 kinase. Identification of in vitro 40 S ribosomal S6 phosphorylation sites. The Journal of biological chemistry *266*, 22770-22775.
Firczuk, H., Kannambath, S., Pahle, J., Claydon, A., Beynon, R., Duncan, J., Westerhoff, H., Mendes, P., and McCarthy, J.E. (2013). An in vivo control map for the eukaryotic mRNA translation machinery. Molecular systems biology *9*, 635.
Flaherty, S.M., Fortes, P., Izaurralde, E., Mattaj, I.W., and Gilmartin, G.M. (1997). Participation of the nuclear cap binding complex in pre-mRNA 3' processing. Proceedings of the National Academy of Sciences of the United States of America *94*, 11893-11898.
Floor, S.N., Barkovich, K.J., Condon, K.J., Shokat, K.M., and Doudna, J.A. (2016). Analog sensitive chemical inhibition of the DEAD-box protein DDX3. Protein science : a publication of the Protein Society *25*, 638-649.
Fonseca, B.D., Zakaria, C., Jia, J.J., Graber, T.E., Svitkin, Y., Tahmasebi, S., Healy, D., Hoang, H.D., Jensen, J.M., Diao, I.T., *et al.* (2015). La-related Protein 1 (LARP1) Represses Terminal Oligopyrimidine (TOP) mRNA Translation Downstream of mTOR Complex 1 (mTORC1). The Journal of biological chemistry *290*, 15996-16020.
Fred, R.G., Sandberg, M., Pelletier, J., and Welsh, N. (2011). The human insulin mRNA is partly translated via a cap- and eIF4A-independent mechanism. Biochemical and biophysical research communications *412*, 693-698.
Fringer, J.M., Acker, M.G., Fekete, C.A., Lorsch, J.R., and Dever, T.E. (2007). Coupled release of eukaryotic translation initiation factors 5B and 1A from 80S ribosomes following subunit joining. Molecular and cellular biology *27*, 2384-2397.
Fukao, A., and Fujiwara, T. (2017). The coupled and uncoupled mechanisms by which trans-acting factors regulate mRNA stability and translation. Journal of biochemistry *161*, 309-314.

Fukuchi-Shimogori, T., Ishii, I., Kashiwagi, K., Mashiba, H., Ekimoto, H., and Igarashi, K. (1997). Malignant transformation by overproduction of translation initiation factor eIF4G. Cancer research *57*, 5041-5044.
Fuller-Pace, F.V. (2013). DEAD box RNA helicase functions in cancer. RNA biology *10*, 121-132.
Furic, L., Rong, L., Larsson, O., Koumakpayi, I.H., Yoshida, K., Brueschke, A., Petroulakis, E., Robichaud, N., Pollak, M., Gaboury, L.A., *et al.* (2010). eIF4E phosphorylation promotes tumorigenesis and is associated with prostate cancer progression. Proceedings of the National Academy of Sciences of the United States of America *107*, 14134-14139.
Furuichi, Y. (1974). "Methylation-coupled" transcription by virus-associated transcriptase of cytoplasmic polyhedrosis virus containing double-stranded RNA. Nucleic acids research *1*, 809-822.
Furuichi, Y. (2015). Discovery of m(7)G-cap in eukaryotic mRNAs. Proceedings of the Japan Academy Series B, Physical and biological sciences *91*, 394-409.
Furuichi, Y., and Shatkin, A.J. (2000). Viral and cellular mRNA capping: past and prospects. Advances in virus research *55*, 135-184.
Galicia-Vazquez, G., Cencic, R., Robert, F., Agenor, A.Q., and Pelletier, J. (2012). A cellular response linking eIF4AI activity to eIF4AII transcription. RNA (New York, NY) *18*, 1373-1384.
Galicia-Vazquez, G., Chu, J., and Pelletier, J. (2015). eIF4AII is dispensable for miRNA-mediated gene silencing. RNA *21*, 1826-1833.
Galicia-Vazquez, G., Di Marco, S., Lian, X.J., Ma, J.F., Gallouzi, I.E., and Pelletier, J. (2014). Regulation of eukaryotic initiation factor 4AII by MyoD during murine myogenic cell differentiation. PloS one *9*, e87237.
Gallie, D.R. (1991). The cap and poly(A) tail function synergistically to regulate mRNA translational efficiency. Genes & development *5*, 2108-2116.
Gan, X., Wang, J., Su, B., and Wu, D. (2011). Evidence for direct activation of mTORC2 kinase activity by phosphatidylinositol 3,4,5-trisphosphate. The Journal of biological chemistry *286*, 10998-11002.
Gandin, V., Masvidal, L., Hulea, L., Gravel, S.P., Cargnello, M., McLaughlan, S., Cai, Y., Balanathan, P., Morita, M., Rajakumar, A., *et al.* (2016). nanoCAGE reveals 5' UTR features that define specific modes of translation of functionally related MTOR-sensitive mRNAs. Genome research *26*, 636-648.
Garcia-Garcia, C., Frieda, K.L., Feoktistova, K., Fraser, C.S., and Block, S.M. (2015). RNA BIOCHEMISTRY. Factor-dependent processivity in human eIF4A DEAD-box helicase. Science (New York, NY) *348*, 1486-1488.
Gerard, B., Cencic, R., Pelletier, J., and Porco, J.A., Jr. (2007). Enantioselective synthesis of the complex rocaglate (-)-silvestrol. Angew Chem Int Ed Engl *46*, 7831-7834.
Gerard, B., Sangji, S., O'Leary, D.J., and Porco, J.A., Jr. (2006). Enantioselective photocycloaddition mediated by chiral Bronsted acids: asymmetric synthesis of the rocaglamides. J Am Chem Soc *128*, 7754-7755.
Giaisi, M., Kohler, R., Fulda, S., Krammer, P.H., and Li-Weber, M. (2012). Rocaglamide and a XIAP inhibitor cooperatively sensitize TRAIL-mediated apoptosis in Hodgkin's lymphomas. Int J Cancer *131*, 1003-1008.
Gillis, L.D., and Lewis, S.M. (2013). Decreased eIF3e/Int6 expression causes epithelial-to-mesenchymal transition in breast epithelial cells. Oncogene *32*, 3598-3605.

Gingras, A.C., Gygi, S.P., Raught, B., Polakiewicz, R.D., Abraham, R.T., Hoekstra, M.F., Aebersold, R., and Sonenberg, N. (1999a). Regulation of 4E-BP1 phosphorylation: a novel two-step mechanism. Genes & development *13*, 1422-1437.
Gingras, A.C., Raught, B., Gygi, S.P., Niedzwiecka, A., Miron, M., Burley, S.K., Polakiewicz, R.D., Wyslouch-Cieszynska, A., Aebersold, R., and Sonenberg, N. (2001). Hierarchical phosphorylation of the translation inhibitor 4E-BP1. Genes & development *15*, 2852-2864.
Gingras, A.C., Raught, B., and Sonenberg, N. (1999b). eIF4 initiation factors: effectors of mRNA recruitment to ribosomes and regulators of translation. Annual review of biochemistry *68*, 913-963.
Goh, S.H., Hong, S.H., Hong, S.H., Lee, B.C., Ju, M.H., Jeong, J.S., Cho, Y.R., Kim, I.H., and Lee, Y.S. (2011). eIF3m expression influences the regulation of tumorigenesis-related genes in human colon cancer. Oncogene *30*, 398-409.
Gorlach, M., Burd, C.G., and Dreyfuss, G. (1994). The mRNA poly(A)-binding protein: localization, abundance, and RNA-binding specificity. Experimental cell research *211*, 400-407.
Gorman, C. (1985). High efficiency gene transfer into mammalian cells. DNA cloning II A practical approach *IRL Press Ltd., Oxford, England*, 143-190.
Gradi, A., Imataka, H., Svitkin, Y.V., Rom, E., Raught, B., Morino, S., and Sonenberg, N. (1998). A novel functional human eukaryotic translation initiation factor 4G. Molecular and cellular biology *18*, 334-342.
Graff, J.R., Konicek, B.W., Vincent, T.M., Lynch, R.L., Monteith, D., Weir, S.N., Schwier, P., Capen, A., Goode, R.L., Dowless, M.S.*, et al.* (2007). Therapeutic suppression of translation initiation factor eIF4E expression reduces tumor growth without toxicity. The Journal of clinical investigation *117*, 2638-2648.
Grimmler, M., Otter, S., Peter, C., Muller, F., Chari, A., and Fischer, U. (2005). Unrip, a factor implicated in cap-independent translation, associates with the cytosolic SMN complex and influences its intracellular localization. Human molecular genetics *14*, 3099-3111.
Gruner, S., Peter, D., Weber, R., Wohlbold, L., Chung, M.Y., Weichenrieder, O., Valkov, E., Igreja, C., and Izaurralde, E. (2016). The Structures of eIF4E-eIF4G Complexes Reveal an Extended Interface to Regulate Translation Initiation. Molecular cell *64*, 467-479.
Grzmil, M., Rzymski, T., Milani, M., Harris, A.L., Capper, R.G., Saunders, N.J., Salhan, A., Ragoussis, J., and Norbury, C.J. (2010). An oncogenic role of eIF3e/INT6 in human breast cancer. Oncogene *29*, 4080-4089.
Guichard, S.M., Curwen, J., Bihani, T., D'Cruz, C.M., Yates, J.W., Grondine, M., Howard, Z., Davies, B.R., Bigley, G., Klinowska, T.*, et al.* (2015). AZD2014, an Inhibitor of mTORC1 and mTORC2, Is Highly Effective in ER+ Breast Cancer When Administered Using Intermittent or Continuous Schedules. Molecular cancer therapeutics *14*, 2508-2518.
Gupta, S.V., Sass, E.J., Davis, M.E., Edwards, R.B., Lozanski, G., Heerema, N.A., Lehman, A., Zhang, X., Jarjoura, D., Byrd, J.C.*, et al.* (2011). Resistance to the translation initiation inhibitor silvestrol is mediated by ABCB1/P-glycoprotein overexpression in acute lymphoblastic leukemia cells. The AAPS journal *13*, 357-364.
Hafner, M., Max, K.E., Bandaru, P., Morozov, P., Gerstberger, S., Brown, M., Molina, H., and Tuschl, T. (2013). Identification of mRNAs bound and regulated by human LIN28 proteins and molecular requirements for RNA recognition. RNA (New York, NY) *19*, 613-626.

Haghighat, A., Svitkin, Y., Novoa, I., Kuechler, E., Skern, T., and Sonenberg, N. (1996). The eIF4G-eIF4E complex is the target for direct cleavage by the rhinovirus 2A proteinase. Journal of virology *70*, 8444-8450.
Harding, H.P., Novoa, I., Zhang, Y., Zeng, H., Wek, R., Schapira, M., and Ron, D. (2000). Regulated translation initiation controls stress-induced gene expression in mammalian cells. Molecular cell *6*, 1099-1108.
Harding, H.P., Zhang, Y., and Ron, D. (1999). Protein translation and folding are coupled by an endoplasmic-reticulum-resident kinase. Nature *397*, 271-274.
Harding, H.P., Zhang, Y., Zeng, H., Novoa, I., Lu, P.D., Calfon, M., Sadri, N., Yun, C., Popko, B., Paules, R.*, et al.* (2003). An integrated stress response regulates amino acid metabolism and resistance to oxidative stress. Molecular cell *11*, 619-633.
Harms, U., Andreou, A.Z., Gubaev, A., and Klostermeier, D. (2014). eIF4B, eIF4G and RNA regulate eIF4A activity in translation initiation by modulating the eIF4A conformational cycle. Nucleic acids research *42*, 7911-7922.
Hart, L.S., Cunningham, J.T., Datta, T., Dey, S., Tameire, F., Lehman, S.L., Qiu, B., Zhang, H., Cerniglia, G., Bi, M.*, et al.* (2012). ER stress-mediated autophagy promotes Myc-dependent transformation and tumor growth. The Journal of clinical investigation *122*, 4621-4634.
Haydon, M.S., Googe, J.D., Sorrells, D.S., Ghali, G.E., and Li, B.D. (2000). Progression of eIF4e gene amplification and overexpression in benign and malignant tumors of the head and neck. Cancer *88*, 2803-2810.
Heesom, K.J., Avison, M.B., Diggle, T.A., and Denton, R.M. (1998). Insulin-stimulated kinase from rat fat cells that phosphorylates initiation factor 4E-binding protein 1 on the rapamycin-insensitive site (serine-111). The Biochemical journal *336 (Pt 1)*, 39-48.
Hellen, C.U., and Sarnow, P. (2001). Internal ribosome entry sites in eukaryotic mRNA molecules. Genes & development *15*, 1593-1612.
Henss, L., Scholz, T., Grunweller, A., and Schnierle, B.S. (2018). Silvestrol Inhibits Chikungunya Virus Replication. Viruses *10*.
Hernandez, G., Han, H., Gandin, V., Fabian, L., Ferreira, T., Zuberek, J., Sonenberg, N., Brill, J.A., and Lasko, P. (2012). Eukaryotic initiation factor 4E-3 is essential for meiotic chromosome segregation, cytokinesis and male fertility in Drosophila. Development (Cambridge, England) *139*, 3211-3220.
Hernandez, G., and Vazquez-Pianzola, P. (2005). Functional diversity of the eukaryotic translation initiation factors belonging to eIF4 families. Mechanisms of development *122*, 865-876.
Hernandez, G., Vazquez-Pianzola, P., Zurbriggen, A., Altmann, M., Sierra, J.M., and Rivera-Pomar, R. (2004). Two functionally redundant isoforms of Drosophila melanogaster eukaryotic initiation factor 4B are involved in cap-dependent translation, cell survival, and proliferation. European journal of biochemistry / FEBS *271*, 2923-2936.
Hershey, J.W. (2015). The role of eIF3 and its individual subunits in cancer. Biochimica et biophysica acta *1849*, 792-800.
Hershey, J.W., Sonenberg, N., and Mathews, M.B. (2012). Principles of translational control: an overview. Cold Spring Harbor perspectives in biology *4*.
Hinnebusch, A.G. (2014). The scanning mechanism of eukaryotic translation initiation. Annual review of biochemistry *83*, 779-812.

Hinnebusch, A.G., and Lorsch, J.R. (2012). The mechanism of eukaryotic translation initiation: new insights and challenges. Cold Spring Harbor perspectives in biology *4*.
Hiraishi, H., Oatman, J., Haller, S.L., Blunk, L., McGivern, B., Morris, J., Papadopoulos, E., Gutierrez, W., Gordon, M., Bokhari, W.*, et al.* (2014). Essential role of eIF5-mimic protein in animal development is linked to control of ATF4 expression. Nucleic acids research *42*, 10321-10330.
Hirsch, C.A. (1967). Quantitative determination of the ribosomal ribonucleic acid content of liver and Novikoff hepatoma from fed and from fasted rats. The Journal of biological chemistry *242*, 2822-2827.
Hoeffer, C.A., Santini, E., Ma, T., Arnold, E.C., Whelan, A.M., Wong, H., Pierre, P., Pelletier, J., and Klann, E. (2013). Multiple components of eIF4F are required for protein synthesis-dependent hippocampal long-term potentiation. Journal of neurophysiology *109*, 68-76.
Holz, M.K., Ballif, B.A., Gygi, S.P., and Blenis, J. (2005). mTOR and S6K1 mediate assembly of the translation preinitiation complex through dynamic protein interchange and ordered phosphorylation events. Cell *123*, 569-580.
Hong, D.S., Kurzrock, R., Oh, Y., Wheler, J., Naing, A., Brail, L., Callies, S., Andre, V., Kadam, S.K., Nasir, A.*, et al.* (2011). A phase 1 dose escalation, pharmacokinetic, and pharmacodynamic evaluation of eIF-4E antisense oligonucleotide LY2275796 in patients with advanced cancer. Clin Cancer Res *17*, 6582-6591.
Hood, K.A., West, L.M., Northcote, P.T., Berridge, M.V., and Miller, J.H. (2001). Induction of apoptosis by the marine sponge (Mycale) metabolites, mycalamide A and pateamine. Apoptosis : an international journal on programmed cell death *6*, 207-219.
Hsieh, A.C., Liu, Y., Edlind, M.P., Ingolia, N.T., Janes, M.R., Sher, A., Shi, E.Y., Stumpf, C.R., Christensen, C., Bonham, M.J.*, et al.* (2012). The translational landscape of mTOR signalling steers cancer initiation and metastasis. Nature *485*, 55-61.
Hua, H., Kong, Q., Zhang, H., Wang, J., Luo, T., and Jiang, Y. (2019). Targeting mTOR for cancer therapy. Journal of hematology & oncology *12*, 71.
Huang, J., and Manning, B.D. (2009). A complex interplay between Akt, TSC2 and the two mTOR complexes. Biochemical Society transactions *37*, 217-222.
Hunt, S.L., Hsuan, J.J., Totty, N., and Jackson, R.J. (1999). unr, a cellular cytoplasmic RNA-binding protein with five cold-shock domains, is required for internal initiation of translation of human rhinovirus RNA. Genes & development *13*, 437-448.
Hwang, S.K., Baker, A.R., Young, M.R., and Colburn, N.H. (2014). Tumor suppressor PDCD4 inhibits NF-kappaB-dependent transcription in human glioblastoma cells by direct interaction with p65. Carcinogenesis *35*, 1469-1480.
Iacono, M., Mignone, F., and Pesole, G. (2005). uAUG and uORFs in human and rodent 5'untranslated mRNAs. Gene *349*, 97-105.
Ilic, N., Utermark, T., Widlund, H.R., and Roberts, T.M. (2011). PI3K-targeted therapy can be evaded by gene amplification along the MYC-eukaryotic translation initiation factor 4E (eIF4E) axis. Proceedings of the National Academy of Sciences of the United States of America *108*, E699-708.
Imataka, H., Olsen, H.S., and Sonenberg, N. (1997). A new translational regulator with homology to eukaryotic translation initiation factor 4G. The EMBO journal *16*, 817-825.
Ingolia, N.T., Lareau, L.F., and Weissman, J.S. (2011). Ribosome profiling of mouse embryonic stem cells reveals the complexity and dynamics of mammalian proteomes. Cell *147*, 789-802.

Ishikawa, C., Tanaka, J., Katano, H., Senba, M., and Mori, N. (2013). Hippuristanol reduces the viability of primary effusion lymphoma cells both in vitro and in vivo. Marine drugs *11*, 3410-3424.
Iwasaki, S., Floor, S.N., and Ingolia, N.T. (2016). Rocaglates convert DEAD-box protein eIF4A into a sequence-selective translational repressor. Nature *534*, 558-561.
Iwasaki, S., Iwasaki, W., Takahashi, M., Sakamoto, A., Watanabe, C., Shichino, Y., Floor, S.N., Fujiwara, K., Mito, M., Dodo, K., *et al.* (2019). The Translation Inhibitor Rocaglamide Targets a Bimolecular Cavity between eIF4A and Polypurine RNA. Mol Cell *73*, 738-748 e739.
Jacinto, E., Loewith, R., Schmidt, A., Lin, S., Ruegg, M.A., Hall, A., and Hall, M.N. (2004). Mammalian TOR complex 2 controls the actin cytoskeleton and is rapamycin insensitive. Nature cell biology *6*, 1122-1128.
Jackson, R.J., and Standart, N. (1990). Do the poly(A) tail and 3' untranslated region control mRNA translation? Cell *62*, 15-24.
Jafari, R., Almqvist, H., Axelsson, H., Ignatushchenko, M., Lundback, T., Nordlund, P., and Martinez Molina, D. (2014). The cellular thermal shift assay for evaluating drug target interactions in cells. Nature protocols *9*, 2100-2122.
Jang, S.K., Davies, M.V., Kaufman, R.J., and Wimmer, E. (1989). Initiation of protein synthesis by internal entry of ribosomes into the 5' nontranslated region of encephalomyocarditis virus RNA in vivo. Journal of virology *63*, 1651-1660.
Joshi, B., Cameron, A., and Jagus, R. (2004). Characterization of mammalian eIF4E-family members. European journal of biochemistry / FEBS *271*, 2189-2203.
Joyce, C.E., Yanez, A.G., Mori, A., Yoda, A., Carroll, J.S., and Novina, C.D. (2017). Differential Regulation of the Melanoma Proteome by eIF4A1 and eIF4E. Cancer research *77*, 613-622.
Kahvejian, A., Svitkin, Y.V., Sukarieh, R., M'Boutchou, M.N., and Sonenberg, N. (2005). Mammalian poly(A)-binding protein is a eukaryotic translation initiation factor, which acts via multiple mechanisms. Genes & development *19*, 104-113.
Kang, S.A., Pacold, M.E., Cervantes, C.L., Lim, D., Lou, H.J., Ottina, K., Gray, N.S., Turk, B.E., Yaffe, M.B., and Sabatini, D.M. (2013). mTORC1 phosphorylation sites encode their sensitivity to starvation and rapamycin. Science (New York, NY) *341*, 1236566.
Kearse, M.G., and Wilusz, J.E. (2017). Non-AUG translation: a new start for protein synthesis in eukaryotes. Genes & development *31*, 1717-1731.
Keshwani, M.M., Gao, X., and Harris, T.K. (2009). Mechanism of PDK1-catalyzed Thr-229 phosphorylation of the S6K1 protein kinase. The Journal of biological chemistry *284*, 22611-22624.
Kim, J., Kundu, M., Viollet, B., and Guan, K.L. (2011). AMPK and mTOR regulate autophagy through direct phosphorylation of Ulk1. Nature cell biology *13*, 132-141.
Kimball, S.R. (1999). Eukaryotic initiation factor eIF2. The international journal of biochemistry & cell biology *31*, 25-29.
Kimball, S.R., Fabian, J.R., Pavitt, G.D., Hinnebusch, A.G., and Jefferson, L.S. (1998). Regulation of guanine nucleotide exchange through phosphorylation of eukaryotic initiation factor eIF2alpha. Role of the alpha- and delta-subunits of eiF2b. The Journal of biological chemistry *273*, 12841-12845.
King, M.L., Chiang, C.-C., Limng, H.-C., Fujita, E., Ochiai, M., and McPhail, A.T. (1982a). X-Ray Crystal Structure of Rocaglamide, a Novel Antileukemic I H-Cyclopenta[b] benzofuran from Aglaia elliptifolia. J Chem Sco Chem Commun *20*, 1150-1151.

King, M.L., Chiang, C.C., Ling, H.C., Fujita, E., Ochiai, M., and McPhail, A.T. (1982b). X-Ray crystal-structure of rocaglamide, a novel antileukemic 1H-cyclopenta[b]benzofuran from Aglaia elliptifolia. J Chem Soc Chem Commun, 1150-1151.
Kogure, T., Kinghorn, A.D., Yan, I., Bolon, B., Lucas, D.M., Grever, M.R., and Patel, T. (2013). Therapeutic potential of the translation inhibitor silvestrol in hepatocellular cancer. PloS one *8*, e76136.
Kong, T., Xue, Y., Cencic, R., Zhu, X., Monast, A., Fu, Z., Pilon, V., Sangwan, V., Guiot, M.C., Foulkes, W.D.*, et al.* (2019). eIF4A inhibitors suppress cell cycle feedback response and acquired resistance to CDK4/6 inhibition in cancer. Molecular cancer therapeutics.
Korneeva, N.L., Lamphear, B.J., Hennigan, F.L., and Rhoads, R.E. (2000). Mutually cooperative binding of eukaryotic translation initiation factor (eIF) 3 and eIF4A to human eIF4G-1. The Journal of biological chemistry *275*, 41369-41376.
Koromilas, A.E., Lazaris-Karatzas, A., and Sonenberg, N. (1992a). mRNAs containing extensive secondary structure in their 5' non-coding region translate efficiently in cells overexpressing initiation factor eIF-4E. EMBO J *11*, 4153-4158.
Koromilas, A.E., and Mounir, Z. (2013). Control of oncogenesis by eIF2alpha phosphorylation: implications in PTEN and PI3K-Akt signaling and tumor treatment. Future oncology *9*, 1005-1015.
Koromilas, A.E., Roy, S., Barber, G.N., Katze, M.G., and Sonenberg, N. (1992b). Malignant transformation by a mutant of the IFN-inducible dsRNA-dependent protein kinase. Science (New York, NY) *257*, 1685-1689.
Kozak, M. (1979). Inability of circular mRNA to attach to eukaryotic ribosomes. Nature *280*, 82-85.
Kozak, M. (1987). An analysis of 5'-noncoding sequences from 699 vertebrate messenger RNAs. Nucleic acids research *15*, 8125-8148.
Kozak, M. (1989). The scanning model for translation: an update. The Journal of cell biology *108*, 229-241.
Kozak, M. (1991). A short leader sequence impairs the fidelity of initiation by eukaryotic ribosomes. Gene expression *1*, 111-115.
Kozak, M. (2001). Constraints on reinitiation of translation in mammals. Nucleic acids research *29*, 5226-5232.
Kozel, C., Thompson, B., Hustak, S., Moore, C., Nakashima, A., Singh, C.R., Reid, M., Cox, C., Papadopoulos, E., Luna, R.E.*, et al.* (2016). Overexpression of eIF5 or its protein mimic 5MP perturbs eIF2 function and induces ATF4 translation through delayed re-initiation. Nucleic acids research *44*, 8704-8713.
Krishnamoorthy, T., Pavitt, G.D., Zhang, F., Dever, T.E., and Hinnebusch, A.G. (2001). Tight binding of the phosphorylated alpha subunit of initiation factor 2 (eIF2alpha) to the regulatory subunits of guanine nucleotide exchange factor eIF2B is required for inhibition of translation initiation. Molecular and cellular biology *21*, 5018-5030.
Kudla, G., Lipinski, L., Caffin, F., Helwak, A., and Zylicz, M. (2006). High guanine and cytosine content increases mRNA levels in mammalian cells. PLoS biology *4*, e180.
Kumar, P., Hellen, C.U., and Pestova, T.V. (2016). Toward the mechanism of eIF4F-mediated ribosomal attachment to mammalian capped mRNAs. Genes & development *30*, 1573-1588.
Kuznetsov, G., Xu, Q., Rudolph-Owen, L., Tendyke, K., Liu, J., Towle, M., Zhao, N., Marsh, J., Agoulnik, S., Twine, N.*, et al.* (2009). Potent in vitro and in vivo anticancer activities of des-methyl,

des-amino pateamine A, a synthetic analogue of marine natural product pateamine A. Molecular cancer therapeutics *8*, 1250-1260.
Lahr, R.M., Fonseca, B.D., Ciotti, G.E., Al-Ashtal, H.A., Jia, J.J., Niklaus, M.R., Blagden, S.P., Alain, T., and Berman, A.J. (2017). La-related protein 1 (LARP1) binds the mRNA cap, blocking eIF4F assembly on TOP mRNAs. eLife *6*.
Langmead, B., Trapnell, C., Pop, M., and Salzberg, S.L. (2009). Ultrafast and memory-efficient alignment of short DNA sequences to the human genome. Genome Biol *10*, R25.
Laplante, M., and Sabatini, D.M. (2012). mTOR signaling in growth control and disease. Cell *149*, 274-293.
Larsson, O., Li, S., Issaenko, O.A., Avdulov, S., Peterson, M., Smith, K., Bitterman, P.B., and Polunovsky, V.A. (2007). Eukaryotic translation initiation factor 4E induced progression of primary human mammary epithelial cells along the cancer pathway is associated with targeted translational deregulation of oncogenic drivers and inhibitors. Cancer research *67*, 6814-6824.
Larsson, O., Morita, M., Topisirovic, I., Alain, T., Blouin, M.J., Pollak, M., and Sonenberg, N. (2012). Distinct perturbation of the translatome by the antidiabetic drug metformin. Proc Natl Acad Sci U S A *109*, 8977-8982.
Lazaris-Karatzas, A., Montine, K.S., and Sonenberg, N. (1990). Malignant transformation by a eukaryotic initiation factor subunit that binds to mRNA 5' cap. Nature *345*, 544-547.
Lee, K.H., Nishimura, S., Matsunaga, S., Fusetani, N., Horinouchi, S., and Yoshida, M. (2005). Inhibition of protein synthesis and activation of stress-activated protein kinases by onnamide A and theopederin B, antitumor marine natural products. Cancer science *96*, 357-364.
Leibiger, C., Kosyakova, N., Mkrtchyan, H., Glei, M., Trifonov, V., and Liehr, T. (2013). First molecular cytogenetic high resolution characterization of the NIH 3T3 cell line by murine multicolor banding. J Histochem Cytochem *61*, 306-312.
Lemaire, P.A., Anderson, E., Lary, J., and Cole, J.L. (2008). Mechanism of PKR Activation by dsRNA. Journal of molecular biology *381*, 351-360.
Lemm, I., and Ross, J. (2002). Regulation of c-myc mRNA decay by translational pausing in a coding region instability determinant. Molecular and cellular biology *22*, 3959-3969.
Leppek, K., Das, R., and Barna, M. (2018). Functional 5' UTR mRNA structures in eukaryotic translation regulation and how to find them. Nature reviews Molecular cell biology *19*, 158-174.
Lewis, J.D., Izaurralde, E., Jarmolowski, A., McGuigan, C., and Mattaj, I.W. (1996). A nuclear cap-binding complex facilitates association of U1 snRNP with the cap-proximal 5' splice site. Genes & development *10*, 1683-1698.
Li, J., Kim, S.G., and Blenis, J. (2014). Rapamycin: one drug, many effects. Cell metabolism *19*, 373-379.
Li, Q., Imataka, H., Morino, S., Rogers, G.W., Jr., Richter-Cook, N.J., Merrick, W.C., and Sonenberg, N. (1999). Eukaryotic translation initiation factor 4AIII (eIF4AIII) is functionally distinct from eIF4AI and eIF4AII. Molecular and cellular biology *19*, 7336-7346.
Li, W., Belsham, G.J., and Proud, C.G. (2001a). Eukaryotic initiation factors 4A (eIF4A) and 4G (eIF4G) mutually interact in a 1:1 ratio in vivo. The Journal of biological chemistry *276*, 29111-29115.
Li, W., Ross-Smith, N., Proud, C.G., and Belsham, G.J. (2001b). Cleavage of translation initiation factor 4AI (eIF4AI) but not eIF4AII by foot-and-mouth disease virus 3C protease: identification of the eIF4AI cleavage site. FEBS letters *507*, 1-5.

Liang, S., Zhou, Y., Chen, Y., Ke, G., Wen, H., and Wu, X. (2014). Decreased expression of EIF4A1 after preoperative brachytherapy predicts better tumor-specific survival in cervical cancer. International journal of gynecological cancer : official journal of the International Gynecological Cancer Society *24*, 908-915.
Liberman, N., Gandin, V., Svitkin, Y.V., David, M., Virgili, G., Jaramillo, M., Holcik, M., Nagar, B., Kimchi, A., and Sonenberg, N. (2015). DAP5 associates with eIF2beta and eIF4AI to promote Internal Ribosome Entry Site driven translation. Nucleic acids research *43*, 3764-3775.
Lin, C.J., Nasr, Z., Premsrirut, P.K., Porco, J.A., Jr., Hippo, Y., Lowe, S.W., and Pelletier, J. (2012). Targeting Synthetic Lethal Interactions between Myc and the eIF4F Complex Impedes Tumorigenesis. Cell Reports *1*, 325-333.
Lin, D., Pestova, T.V., Hellen, C.U., and Tiedge, H. (2008). Translational control by a small RNA: dendritic BC1 RNA targets the eukaryotic initiation factor 4A helicase mechanism. Molecular and cellular biology *28*, 3008-3019.
Linder, P., and Jankowsky, E. (2011). From unwinding to clamping - the DEAD box RNA helicase family. Nature reviews Molecular cell biology *12*, 505-516.
Lindqvist, L., Imataka, H., and Pelletier, J. (2008a). Cap-dependent eukaryotic initiation factor-mRNA interactions probed by cross-linking. RNA (New York, NY) *14*, 960-969.
Lindqvist, L., Oberer, M., Reibarkh, M., Cencic, R., Bordeleau, M.E., Vogt, E., Marintchev, A., Tanaka, J., Fagotto, F., Altmann, M.*, et al.* (2008b). Selective pharmacological targeting of a DEAD box RNA helicase. PloS one *3*, e1583.
Linero, F.N., Thomas, M.G., Boccaccio, G.L., and Scolaro, L.A. (2011). Junin virus infection impairs stress-granule formation in Vero cells treated with arsenite via inhibition of eIF2alpha phosphorylation. The Journal of general virology *92*, 2889-2899.
Liu, F., Putnam, A., and Jankowsky, E. (2008). ATP hydrolysis is required for DEAD-box protein recycling but not for duplex unwinding. Proceedings of the National Academy of Sciences of the United States of America *105*, 20209-20214.
Liu, T., Nair, S.J., Lescarbeau, A., Belani, J., Peluso, S., Conley, J., Tillotson, B., O'Hearn, P., Smith, S., Slocum, K.*, et al.* (2012). Synthetic silvestrol analogues as potent and selective protein synthesis inhibitors. Journal of medicinal chemistry *55*, 8859-8878.
Liwak, U., Thakor, N., Jordan, L.E., Roy, R., Lewis, S.M., Pardo, O.E., Seckl, M., and Holcik, M. (2012). Tumor suppressor PDCD4 represses internal ribosome entry site-mediated translation of antiapoptotic proteins and is regulated by S6 kinase 2. Molecular and cellular biology *32*, 1818-1829.
Llacer, J.L., Hussain, T., Marler, L., Aitken, C.E., Thakur, A., Lorsch, J.R., Hinnebusch, A.G., and Ramakrishnan, V. (2015). Conformational Differences between Open and Closed States of the Eukaryotic Translation Initiation Complex. Molecular cell *59*, 399-412.
Llacer, J.L., Hussain, T., Saini, A.K., Nanda, J.S., Kaur, S., Gordiyenko, Y., Kumar, R., Hinnebusch, A.G., Lorsch, J.R., and Ramakrishnan, V. (2018). Translational initiation factor eIF5 replaces eIF1 on the 40S ribosomal subunit to promote start-codon recognition. eLife *7*.
Loh, P.G., Yang, H.S., Walsh, M.A., Wang, Q., Wang, X., Cheng, Z., Liu, D., and Song, H. (2009). Structural basis for translational inhibition by the tumour suppressor Pdcd4. The EMBO journal *28*, 274-285.
Lopez, M.S., Kliegman, J.I., and Shokat, K.M. (2014). The logic and design of analog-sensitive kinases and their small molecule inhibitors. Methods in enzymology *548*, 189-213.

Lorsch, J.R., and Herschlag, D. (1998). The DEAD box protein eIF4A. 1. A minimal kinetic and thermodynamic framework reveals coupled binding of RNA and nucleotide. Biochemistry *37*, 2180-2193.
Low, W., Harries, M., Ye, H., Du, M.Q., Boshoff, C., and Collins, M. (2001). Internal ribosome entry site regulates translation of Kaposi's sarcoma-associated herpesvirus FLICE inhibitory protein. Journal of virology *75*, 2938-2945.
Low, W.K., Dang, Y., Bhat, S., Romo, D., and Liu, J.O. (2007). Substrate-dependent targeting of eukaryotic translation initiation factor 4A by pateamine A: negation of domain-linker regulation of activity. Chemistry & biology *14*, 715-727.
Low, W.K., Dang, Y., Schneider-Poetsch, T., Shi, Z., Choi, N.S., Merrick, W.C., Romo, D., and Liu, J.O. (2005). Inhibition of eukaryotic translation initiation by the marine natural product pateamine A. Molecular cell *20*, 709-722.
Lu, L., Han, A.P., and Chen, J.J. (2001). Translation initiation control by heme-regulated eukaryotic initiation factor 2alpha kinase in erythroid cells under cytoplasmic stresses. Molecular and cellular biology *21*, 7971-7980.
Luan, Z., He, Y., He, F., and Chen, Z. (2015). Rocaglamide overcomes tumor necrosis factor-related apoptosis-inducing ligand resistance in hepatocellular carcinoma cells by attenuating the inhibition of caspase-8 through cellular FLICE-like-inhibitory protein downregulation. Molecular medicine reports *11*, 203-211.
Lucas, D.M., Edwards, R.B., Lozanski, G., West, D.A., Shin, J.D., Vargo, M.A., Davis, M.E., Rozewski, D.M., Johnson, A.J., Su, B.N., *et al.* (2009). The novel plant-derived agent silvestrol has B-cell selective activity in chronic lymphocytic leukemia and acute lymphoblastic leukemia in vitro and in vivo. Blood *113*, 4656-4666.
Macejak, D.G., and Sarnow, P. (1991). Internal initiation of translation mediated by the 5' leader of a cellular mRNA. Nature *353*, 90-94.
Mahon, F.X., Belloc, F., Lagarde, V., Chollet, C., Moreau-Gaudry, F., Reiffers, J., Goldman, J.M., and Melo, J.V. (2003). MDR1 gene overexpression confers resistance to imatinib mesylate in leukemia cell line models. Blood *101*, 2368-2373.
Malina, A., Mills, J.R., Cencic, R., Yan, Y., Fraser, J., Schippers, L.M., Paquet, M., Dostie, J., and Pelletier, J. (2013). Repurposing CRISPR/Cas9 for in situ functional assays. Genes & development *27*, 2602-2614.
Malka-Mahieu, H., Girault, I., Rubington, M., Leriche, M., Welsch, C., Kamsu-Kom, N., Zhao, Q., Desaubry, L., Vagner, S., and Robert, C. (2016). Synergistic effects of eIF4A and MEK inhibitors on proliferation of NRAS-mutant melanoma cell lines. Cell cycle (Georgetown, Tex) *15*, 2405-2409.
Maquat, L.E. (2005). Nonsense-mediated mRNA decay in mammals. Journal of cell science *118*, 1773-1776.
Marash, L., and Kimchi, A. (2005). DAP5 and IRES-mediated translation during programmed cell death. Cell death and differentiation *12*, 554-562.
Marchetti, A., Buttitta, F., Pellegrini, S., Bertacca, G., and Callahan, R. (2001). Reduced expression of INT-6/eIF3-p48 in human tumors. International journal of oncology *18*, 175-179.
Marcotrigiano, J., Gingras, A.C., Sonenberg, N., and Burley, S.K. (1997). Cocrystal structure of the messenger RNA 5' cap-binding protein (eIF4E) bound to 7-methyl-GDP. Cell *89*, 951-961.

Marintchev, A., Edmonds, K.A., Marintcheva, B., Hendrickson, E., Oberer, M., Suzuki, C., Herdy, B., Sonenberg, N., and Wagner, G. (2009). Topology and regulation of the human eIF4A/4G/4H helicase complex in translation initiation. Cell *136*, 447-460.
Marintchev, A., and Wagner, G. (2004). Translation initiation: structures, mechanisms and evolution. Quarterly reviews of biophysics *37*, 197-284.
Martindale, D.W., Wilson, M.D., Wang, D., Burke, R.D., Chen, X., Duronio, V., and Koop, B.F. (2000). Comparative genomic sequence analysis of the Williams syndrome region (LIMK1-RFC2) of human chromosome 7q11.23. Mammalian genome : official journal of the International Mammalian Genome Society *11*, 890-898.
Mayeur, G.L., and Hershey, J.W. (2002). Malignant transformation by the eukaryotic translation initiation factor 3 subunit p48 (eIF3e). FEBS letters *514*, 49-54.
Mayr, C. (2017). Regulation by 3'-Untranslated Regions. Annual review of genetics *51*, 171-194.
Mayr, C., and Bartel, D.P. (2009). Widespread shortening of 3'UTRs by alternative cleavage and polyadenylation activates oncogenes in cancer cells. Cell *138*, 673-684.
Mayr, C., Hemann, M.T., and Bartel, D.P. (2007). Disrupting the pairing between let-7 and Hmga2 enhances oncogenic transformation. Science (New York, NY) *315*, 1576-1579.
Mazroui, R., Sukarieh, R., Bordeleau, M.E., Kaufman, R.J., Northcote, P., Tanaka, J., Gallouzi, I., and Pelletier, J. (2006). Inhibition of ribosome recruitment induces stress granule formation independently of eukaryotic initiation factor 2alpha phosphorylation. Molecular biology of the cell *17*, 4212-4219.
Meijer, H.A., Kong, Y.W., Lu, W.T., Wilczynska, A., Spriggs, R.V., Robinson, S.W., Godfrey, J.D., Willis, A.E., and Bushell, M. (2013). Translational repression and eIF4A2 activity are critical for microRNA-mediated gene regulation. Science (New York, NY) *340*, 82-85.
Merrick, W.C. (2015). eIF4F: a retrospective. The Journal of biological chemistry *290*, 24091-24099.
Methot, N., Pause, A., Hershey, J.W., and Sonenberg, N. (1994). The translation initiation factor eIF-4B contains an RNA-binding region that is distinct and independent from its ribonucleoprotein consensus sequence. Molecular and cellular biology *14*, 2307-2316.
Methot, N., Song, M.S., and Sonenberg, N. (1996). A region rich in aspartic acid, arginine, tyrosine, and glycine (DRYG) mediates eukaryotic initiation factor 4B (eIF4B) self-association and interaction with eIF3. Molecular and cellular biology *16*, 5328-5334.
Meyuhas, O., and Kahan, T. (2015). The race to decipher the top secrets of TOP mRNAs. Biochimica et biophysica acta *1849*, 801-811.
Mine, N., Yamamoto, S., Kufe, D.W., Von Hoff, D.D., and Kawabe, T. (2014). Activation of Nrf2 pathways correlates with resistance of NSCLC cell lines to CBP501 in vitro. Molecular cancer therapeutics *13*, 2215-2225.
Moerke, N.J., Aktas, H., Chen, H., Cantel, S., Reibarkh, M.Y., Fahmy, A., Gross, J.D., Degterev, A., Yuan, J., Chorev, M., *et al.* (2007). Small-molecule inhibition of the interaction between the translation initiation factors eIF4E and eIF4G. Cell *128*, 257-267.
Morino, S., Imataka, H., Svitkin, Y.V., Pestova, T.V., and Sonenberg, N. (2000). Eukaryotic translation initiation factor 4E (eIF4E) binding site and the middle one-third of eIF4GI constitute the core domain for cap-dependent translation, and the C-terminal one-third functions as a modulatory region. Molecular and cellular biology *20*, 468-477.

Morita, M., Ler, L.W., Fabian, M.R., Siddiqui, N., Mullin, M., Henderson, V.C., Alain, T., Fonseca, B.D., Karashchuk, G., Bennett, C.F., *et al.* (2012). A novel 4EHP-GIGYF2 translational repressor complex is essential for mammalian development. Molecular and cellular biology *32*, 3585-3593.
Morris, C., Tomimatsu, N., Richard, D.J., Cluet, D., Burma, S., Khanna, K.K., and Jalinot, P. (2012). INT6/EIF3E interacts with ATM and is required for proper execution of the DNA damage response in human cells. Cancer research *72*, 2006-2016.
Morris, D.R., and Geballe, A.P. (2000). Upstream open reading frames as regulators of mRNA translation. Molecular and cellular biology *20*, 8635-8642.
Nagaraj, N., Wisniewski, J.R., Geiger, T., Cox, J., Kircher, M., Kelso, J., Paabo, S., and Mann, M. (2011). Deep proteome and transcriptome mapping of a human cancer cell line. Molecular systems biology *7*, 548.
Nakamura, Y., Endo, K., Adachi, H., and Ishiguro, A. (2009). RNA aptamers to translational components. Progress in molecular biology and translational science *90*, 369-395.
Newman, Z.R., Young, J.M., Ingolia, N.T., and Barton, G.M. (2016). Differences in codon bias and GC content contribute to the balanced expression of TLR7 and TLR9. Proceedings of the National Academy of Sciences of the United States of America *113*, E1362-1371.
Niedzwiecka, A., Marcotrigiano, J., Stepinski, J., Jankowska-Anyszka, M., Wyslouch-Cieszynska, A., Dadlez, M., Gingras, A.C., Mak, P., Darzynkiewicz, E., Sonenberg, N., *et al.* (2002). Biophysical studies of eIF4E cap-binding protein: recognition of mRNA 5' cap structure and synthetic fragments of eIF4G and 4E-BP1 proteins. Journal of molecular biology *319*, 615-635.
Nielsen, P.J., and Trachsel, H. (1988). The mouse protein synthesis initiation factor 4A gene family includes two related functional genes which are differentially expressed. The EMBO journal *7*, 2097-2105.
Niesen, F.H., Berglund, H., and Vedadi, M. (2007). The use of differential scanning fluorimetry to detect ligand interactions that promote protein stability. Nature protocols *2*, 2212-2221.
Nojima, T., Hirose, T., Kimura, H., and Hagiwara, M. (2007). The interaction between cap-binding complex and RNA export factor is required for intronless mRNA export. The Journal of biological chemistry *282*, 15645-15651.
Northcote, P.T., Blunt, J.W., and Munro, M.H.G. (1991). Pateamine: a potent cytotoxin from the New Zealand marine sponge, Mycale sp. Tetrahedron Lett *32*, 6411-6414.
Novac, O., Guenier, A.S., and Pelletier, J. (2004). Inhibitors of protein synthesis identified by a high throughput multiplexed translation screen. Nucleic acids research *32*, 902-915.
Nupponen, N.N., Porkka, K., Kakkola, L., Tanner, M., Persson, K., Borg, A., Isola, J., and Visakorpi, T. (1999). Amplification and overexpression of p40 subunit of eukaryotic translation initiation factor 3 in breast and prostate cancer. The American journal of pathology *154*, 1777-1783.
Obayashi, E., Luna, R.E., Nagata, T., Martin-Marcos, P., Hiraishi, H., Singh, C.R., Erzberger, J.P., Zhang, F., Arthanari, H., Morris, J., *et al.* (2017). Molecular Landscape of the Ribosome Pre-initiation Complex during mRNA Scanning: Structural Role for eIF3c and Its Control by eIF5. Cell reports *18*, 2651-2663.
Oberer, M., Marintchev, A., and Wagner, G. (2005). Structural basis for the enhancement of eIF4A helicase activity by eIF4G. Genes & development *19*, 2212-2223.
Ohlmann, T., Rau, M., Morley, S.J., and Pain, V.M. (1995). Proteolytic cleavage of initiation factor eIF-4 gamma in the reticulocyte lysate inhibits translation of capped mRNAs but enhances that of uncapped mRNAs. Nucleic acids research *23*, 334-340.

Olson, C.M., Donovan, M.R., Spellberg, M.J., and Marr, M.T., 2nd (2013). The insulin receptor cellular IRES confers resistance to eIF4A inhibition. eLife *2*, e00542.
Osborne, M.J., Volpon, L., Kornblatt, J.A., Culjkovic-Kraljacic, B., Baguet, A., and Borden, K.L. (2013). eIF4E3 acts as a tumor suppressor by utilizing an atypical mode of methyl-7-guanosine cap recognition. Proceedings of the National Academy of Sciences of the United States of America *110*, 3877-3882.
Pabis, M., Neufeld, N., Steiner, M.C., Bojic, T., Shav-Tal, Y., and Neugebauer, K.M. (2013). The nuclear cap-binding complex interacts with the U4/U6.U5 tri-snRNP and promotes spliceosome assembly in mammalian cells. RNA (New York, NY) *19*, 1054-1063.
Palamarchuk, A., Efanov, A., Maximov, V., Aqeilan, R.I., Croce, C.M., and Pekarsky, Y. (2005). Akt phosphorylates and regulates Pdcd4 tumor suppressor protein. Cancer research *65*, 11282-11286.
Pan, L., Woodard, J.L., Lucas, D.M., Fuchs, J.R., and Kinghorn, A.D. (2014). Rocaglamide, silvestrol and structurally related bioactive compounds from Aglaia species. Nat Prod Rep *31*, 924-939.
Papadopoulos, E., Jenni, S., Kabha, E., Takrouri, K.J., Yi, T., Salvi, N., Luna, R.E., Gavathiotis, E., Mahalingam, P., Arthanari, H.*, et al.* (2014). Structure of the eukaryotic translation initiation factor eIF4E in complex with 4EGI-1 reveals an allosteric mechanism for dissociating eIF4G. Proceedings of the National Academy of Sciences of the United States of America *111*, E3187-3195.
Pardo, O.E., Arcaro, A., Salerno, G., Tetley, T.D., Valovka, T., Gout, I., and Seckl, M.J. (2001). Novel cross talk between MEK and S6K2 in FGF-2 induced proliferation of SCLC cells. Oncogene *20*, 7658-7667.
Pardo, O.E., and Seckl, M.J. (2013). S6K2: The Neglected S6 Kinase Family Member. Frontiers in oncology *3*, 191.
Park, E.H., Zhang, F., Warringer, J., Sunnerhagen, P., and Hinnebusch, A.G. (2011). Depletion of eIF4G from yeast cells narrows the range of translational efficiencies genome-wide. BMC genomics *12*, 68.
Passmore, L.A., Schmeing, T.M., Maag, D., Applefield, D.J., Acker, M.G., Algire, M.A., Lorsch, J.R., and Ramakrishnan, V. (2007). The eukaryotic translation initiation factors eIF1 and eIF1A induce an open conformation of the 40S ribosome. Molecular cell *26*, 41-50.
Paulin, F.E., Campbell, L.E., O'Brien, K., Loughlin, J., and Proud, C.G. (2001). Eukaryotic translation initiation factor 5 (eIF5) acts as a classical GTPase-activator protein. Current biology : CB *11*, 55-59.
Pause, A., Methot, N., Svitkin, Y., Merrick, W.C., and Sonenberg, N. (1994). Dominant negative mutants of mammalian translation initiation factor eIF-4A define a critical role for eIF-4F in cap-dependent and cap-independent initiation of translation. The EMBO journal *13*, 1205-1215.
Pavan, I.C., Yokoo, S., Granato, D.C., Meneguello, L., Carnielli, C.M., Tavares, M.R., do Amaral, C.L., de Freitas, L.B., Paes Leme, A.F., Luchessi, A.D.*, et al.* (2016). Different interactomes for p70-S6K1 and p54-S6K2 revealed by proteomic analysis. Proteomics *16*, 2650-2666.
Pelletier, J., and Sonenberg, N. (1985). Insertion mutagenesis to increase secondary structure within the 5' noncoding region of a eukaryotic mRNA reduces translational efficiency. Cell *40*, 515-526.
Pelletier, J., and Sonenberg, N. (1988). Internal initiation of translation of eukaryotic mRNA directed by a sequence derived from poliovirus RNA. Nature *334*, 320-325.
Pelletier, J., and Sonenberg, N. (2019). The Organizing Principles of Eukaryotic Ribosome Recruitment. Annu Rev Biochem *88*, 307-335.

Peng, C., Knebel, A., Morrice, N.A., Li, X., Barringer, K., Li, J., Jakes, S., Werneburg, B., and Wang, L. (2007). Pim kinase substrate identification and specificity. Journal of biochemistry *141*, 353-362.
Perkins, D.J., and Barber, G.N. (2004). Defects in translational regulation mediated by the alpha subunit of eukaryotic initiation factor 2 inhibit antiviral activity and facilitate the malignant transformation of human fibroblasts. Molecular and cellular biology *24*, 2025-2040.
Pesole, G., Mignone, F., Gissi, C., Grillo, G., Licciulli, F., and Liuni, S. (2001). Structural and functional features of eukaryotic mRNA untranslated regions. Gene *276*, 73-81.
Pestova, T.V., and Kolupaeva, V.G. (2002). The roles of individual eukaryotic translation initiation factors in ribosomal scanning and initiation codon selection. Genes & development *16*, 2906-2922.
Pestova, T.V., Lomakin, I.B., Lee, J.H., Choi, S.K., Dever, T.E., and Hellen, C.U. (2000). The joining of ribosomal subunits in eukaryotes requires eIF5B. Nature *403*, 332-335.
Pestova, T.V., Shatsky, I.N., and Hellen, C.U. (1996). Functional dissection of eukaryotic initiation factor 4F: the 4A subunit and the central domain of the 4G subunit are sufficient to mediate internal entry of 43S preinitiation complexes. Mol Cell Biol *16*, 6870-6878.
Peter, D., Igreja, C., Weber, R., Wohlbold, L., Weiler, C., Ebertsch, L., Weichenrieder, O., and Izaurralde, E. (2015). Molecular architecture of 4E-BP translational inhibitors bound to eIF4E. Molecular cell *57*, 1074-1087.
Philippe, L., Vasseur, J.J., Debart, F., and Thoreen, C.C. (2018). La-related protein 1 (LARP1) repression of TOP mRNA translation is mediated through its cap-binding domain and controlled by an adjacent regulatory region. Nucleic acids research *46*, 1457-1469.
Pincheira, R., Chen, Q., and Zhang, J.T. (2001). Identification of a 170-kDa protein over-expressed in lung cancers. British journal of cancer *84*, 1520-1527.
Pisarev, A.V., Kolupaeva, V.G., Yusupov, M.M., Hellen, C.U., and Pestova, T.V. (2008). Ribosomal position and contacts of mRNA in eukaryotic translation initiation complexes. The EMBO journal *27*, 1609-1621.
Pisareva, V.P., Pisarev, A.V., Komar, A.A., Hellen, C.U., and Pestova, T.V. (2008). Translation initiation on mammalian mRNAs with structured 5'UTRs requires DExH-box protein DHX29. Cell *135*, 1237-1250.
Polier, G., Neumann, J., Thuaud, F., Ribeiro, N., Gelhaus, C., Schmidt, H., Giaisi, M., Kohler, R., Muller, W.W., Proksch, P.*, et al.* (2012). The natural anticancer compounds rocaglamides inhibit the Raf-MEK-ERK pathway by targeting prohibitin 1 and 2. Chemistry & biology *19*, 1093-1104.
Poulin, F., Gingras, A.C., Olsen, H., Chevalier, S., and Sonenberg, N. (1998). 4E-BP3, a new member of the eukaryotic initiation factor 4E-binding protein family. The Journal of biological chemistry *273*, 14002-14007.
Powles, T., Wheater, M., Din, O., Geldart, T., Boleti, E., Stockdale, A., Sundar, S., Robinson, A., Ahmed, I., Wimalasingham, A.*, et al.* (2016). A Randomised Phase 2 Study of AZD2014 Versus Everolimus in Patients with VEGF-Refractory Metastatic Clear Cell Renal Cancer. European urology *69*, 450-456.
Preiss, T., Muckenthaler, M., and Hentze, M.W. (1998). Poly(A)-tail-promoted translation in yeast: implications for translational control. RNA (New York, NY) *4*, 1321-1331.
Presnyak, V., Alhusaini, N., Chen, Y.H., Martin, S., Morris, N., Kline, N., Olson, S., Weinberg, D., Baker, K.E., Graveley, B.R.*, et al.* (2015). Codon optimality is a major determinant of mRNA stability. Cell *160*, 1111-1124.

Price, N., and Proud, C. (1994). The guanine nucleotide-exchange factor, eIF-2B. Biochimie *76*, 748-760.
Protter, D.S.W., and Parker, R. (2016). Principles and Properties of Stress Granules. Trends in cell biology *26*, 668-679.
Proudfoot, N.J. (2011). Ending the message: poly(A) signals then and now. Genes & development *25*, 1770-1782.
Puighermanal, E., Biever, A., Pascoli, V., Melser, S., Pratlong, M., Cutando, L., Rialle, S., Severac, D., Boubaker-Vitre, J., Meyuhas, O., *et al.* (2017). Ribosomal Protein S6 Phosphorylation Is Involved in Novelty-Induced Locomotion, Synaptic Plasticity and mRNA Translation. Frontiers in molecular neuroscience *10*, 419.
Qian, Z., Hussein, A.-H., and Laurent, D. (2016). Recent Advances in the Synthesis of Flavaglines, a Family of Potent Bioactive Natural Compounds Originating from Traditional Chinese Medicine. Eur J Org Chem *2016*, 5908 - 5916.
Qin, X., Jiang, B., and Zhang, Y. (2016). 4E-BP1, a multifactor regulated multifunctional protein. Cell cycle (Georgetown, Tex) *15*, 781-786.
Radtke, K., English, L., Rondeau, C., Leib, D., Lippe, R., and Desjardins, M. (2013). Inhibition of the host translation shutoff response by herpes simplex virus 1 triggers nuclear envelope-derived autophagy. Journal of virology *87*, 3990-3997.
Rajalingam, K., Wunder, C., Brinkmann, V., Churin, Y., Hekman, M., Sievers, C., Rapp, U.R., and Rudel, T. (2005). Prohibitin is required for Ras-induced Raf-MEK-ERK activation and epithelial cell migration. Nat Cell Biol *7*, 837-843.
Ramirez-Valle, F., Braunstein, S., Zavadil, J., Formenti, S.C., and Schneider, R.J. (2008). eIF4GI links nutrient sensing by mTOR to cell proliferation and inhibition of autophagy. The Journal of cell biology *181*, 293-307.
Rasmussen, S.B., Kordon, E., Callahan, R., and Smith, G.H. (2001). Evidence for the transforming activity of a truncated Int6 gene, in vitro. Oncogene *20*, 5291-5301.
Raught, B., and Gingras, A.C. (1999). eIF4E activity is regulated at multiple levels. The international journal of biochemistry & cell biology *31*, 43-57.
Raught, B., Peiretti, F., Gingras, A.C., Livingstone, M., Shahbazian, D., Mayeur, G.L., Polakiewicz, R.D., Sonenberg, N., and Hershey, J.W. (2004). Phosphorylation of eucaryotic translation initiation factor 4B Ser422 is modulated by S6 kinases. The EMBO journal *23*, 1761-1769.
Ravindar, K., Reddy, M.S., Lindqvist, L., Pelletier, J., and Deslongchamps, P. (2010). Efficient Synthetic Approach to Potent Antiproliferative Agent Hippuristanol via Hg(II)-Catalyzed Spiroketalization. Org Lett *12*, 4420-4423.
Ravindar, K., Reddy, M.S., Lindqvist, L., Pelletier, J., and Deslongchamps, P. (2011). Synthesis of the Antiproliferative Agent Hippuristanol and Its Analogues via Suarez Cyclizations and Hg(II)-Catalyzed Spiroketalizations. J Org Chem.
Ribeiro, N., Thuaud, F., Nebigil, C., and Desaubry, L. (2012). Recent advances in the biology and chemistry of the flavaglines. Bioorg Med Chem *20*, 1857-1864.
Richter, J.D. (1999). Cytoplasmic polyadenylation in development and beyond. Microbiology and molecular biology reviews : MMBR *63*, 446-456.
Rinker-Schaeffer, C.W., Graff, J.R., De Benedetti, A., Zimmer, S.G., and Rhoads, R.E. (1993). Decreasing the level of translation initiation factor 4E with antisense RNA causes reversal of ras-

mediated transformation and tumorigenesis of cloned rat embryo fibroblasts. International journal of cancer Journal international du cancer *55*, 841-847.
Robert, F., Roman, W., Bramoulle, A., Fellmann, C., Roulston, A., Shustik, C., Porco, J.A., Jr., Shore, G.C., Sebag, M., and Pelletier, J. (2014). Translation initiation factor eIF4F modifies the dexamethasone response in multiple myeloma. Proceedings of the National Academy of Sciences of the United States of America *111*, 13421-13426.
Robichaud, N., Del Rincon, S.V., Huor, B., Alain, T., Petruccelli, L.A., Hearnden, J., Goncalves, C., Grotegut, S., Spruck, C.H., Furic, L.*, et al.* (2014). Phosphorylation of eIF4E promotes EMT and metastasis via translational control of SNAIL and MMP-3. Oncogene.
Robichaud, N., del Rincon, S.V., Huor, B., Alain, T., Petruccelli, L.A., Hearnden, J., Goncalves, C., Grotegut, S., Spruck, C.H., Furic, L.*, et al.* (2015). Phosphorylation of eIF4E promotes EMT and metastasis via translational control of SNAIL and MMP-3. Oncogene *34*, 2032-2042.
Roche, S.P., Cencic, R., Pelletier, J., and Porco, J.A., Jr. (2010). Biomimetic photocycloaddition of 3-hydroxyflavones: synthesis and evaluation of rocaglate derivatives as inhibitors of eukaryotic translation. Angewandte Chemie (International ed in English) *49*, 6533-6538.
Rodrigo, C.M., Cencic, R., Roche, S.P., Pelletier, J., and Porco, J.A. (2012). Synthesis of rocaglamide hydroxamates and related compounds as eukaryotic translation inhibitors: synthetic and biological studies. Journal of medicinal chemistry *55*, 558-562.
Rogers, G.W., Jr., Komar, A.A., and Merrick, W.C. (2002). eIF4A: the godfather of the DEAD box helicases. Progress in nucleic acid research and molecular biology *72*, 307-331.
Rogers, G.W., Jr., Richter, N.J., and Merrick, W.C. (1999). Biochemical and kinetic characterization of the RNA helicase activity of eukaryotic initiation factor 4A. The Journal of biological chemistry *274*, 12236-12244.
Rogozin, I.B., Kochetov, A.V., Kondrashov, F.A., Koonin, E.V., and Milanesi, L. (2001). Presence of ATG triplets in 5' untranslated regions of eukaryotic cDNAs correlates with a 'weak' context of the start codon. Bioinformatics (Oxford, England) *17*, 890-900.
Rom, E., Kim, H.C., Gingras, A.C., Marcotrigiano, J., Favre, D., Olsen, H., Burley, S.K., and Sonenberg, N. (1998). Cloning and characterization of 4EHP, a novel mammalian eIF4E-related cap-binding protein. The Journal of biological chemistry *273*, 13104-13109.
Romo, D., Rzasa, R.M., Shea, H.A., Park, K., Langenhan, J.M., Sun, L., Akhiezer, A., and Liu, J.O. (1998). Total synthesis and immunosuppressive activity of (-)-pateamine A and related compounds: Implementation of a β-lactam-based macrocyclization. Journal of the American Chemical Society *120*, 12237-12254.
Rosenwald, I.B., Chen, J.J., Wang, S., Savas, L., London, I.M., and Pullman, J. (1999). Upregulation of protein synthesis initiation factor eIF-4E is an early event during colon carcinogenesis. Oncogene *18*, 2507-2517.
Rozovsky, N., Butterworth, A.C., and Moore, M.J. (2008). Interactions between eIF4AI and its accessory factors eIF4B and eIF4H. RNA (New York, NY) *14*, 2136-2148.
Rubio, C.A., Weisburd, B., Holderfield, M., Arias, C., Fang, E., DeRisi, J.L., and Fanidi, A. (2014). Transcriptome-wide characterization of the eIF4A signature highlights plasticity in translation regulation. Genome biology *15*, 476.
Ruggero, D., Montanaro, L., Ma, L., Xu, W., Londei, P., Cordon-Cardo, C., and Pandolfi, P.P. (2004). The translation factor eIF-4E promotes tumor formation and cooperates with c-Myc in lymphomagenesis. Nature medicine *10*, 484-486.

Rush, J., Moritz, A., Lee, K.A., Guo, A., Goss, V.L., Spek, E.J., Zhang, H., Zha, X.M., Polakiewicz, R.D., and Comb, M.J. (2005). Immunoaffinity profiling of tyrosine phosphorylation in cancer cells. Nature biotechnology *23*, 94-101.

Ruvinsky, I., Katz, M., Dreazen, A., Gielchinsky, Y., Saada, A., Freedman, N., Mishani, E., Zimmerman, G., Kasir, J., and Meyuhas, O. (2009). Mice deficient in ribosomal protein S6 phosphorylation suffer from muscle weakness that reflects a growth defect and energy deficit. PloS one *4*, e5618.

Ruvinsky, I., Sharon, N., Lerer, T., Cohen, H., Stolovich-Rain, M., Nir, T., Dor, Y., Zisman, P., and Meyuhas, O. (2005). Ribosomal protein S6 phosphorylation is a determinant of cell size and glucose homeostasis. Genes & development *19*, 2199-2211.

Sabatini, D.M. (2006). mTOR and cancer: insights into a complex relationship. Nature reviews Cancer *6*, 729-734.

Sabatini, D.M., Erdjument-Bromage, H., Lui, M., Tempst, P., and Snyder, S.H. (1994). RAFT1: a mammalian protein that binds to FKBP12 in a rapamycin-dependent fashion and is homologous to yeast TORs. Cell *78*, 35-43.

Sachs, A.B., Davis, R.W., and Kornberg, R.D. (1987). A single domain of yeast poly(A)-binding protein is necessary and sufficient for RNA binding and cell viability. Molecular and cellular biology *7*, 3268-3276.

Sadlish, H., Galicia-Vazquez, G., Paris, C.G., Aust, T., Bhullar, B., Chang, L., Helliwell, S.B., Hoepfner, D., Knapp, B., Riedl, R.*, et al.* (2013). Evidence for a functionally relevant rocaglamide binding site on the eIF4A-RNA complex. ACS chemical biology *8*, 1519-1527.

Saeki, T., Nomizu, T., Toi, M., Ito, Y., Noguchi, S., Kobayashi, T., Asaga, T., Minami, H., Yamamoto, N., Aogi, K.*, et al.* (2007). Dofequidar fumarate (MS-209) in combination with cyclophosphamide, doxorubicin, and fluorouracil for patients with advanced or recurrent breast cancer. Journal of clinical oncology : official journal of the American Society of Clinical Oncology *25*, 411-417.

Saini, A.K., Nanda, J.S., Lorsch, J.R., and Hinnebusch, A.G. (2010). Regulatory elements in eIF1A control the fidelity of start codon selection by modulating tRNA(i)(Met) binding to the ribosome. Genes & development *24*, 97-110.

Sandberg, R., Neilson, J.R., Sarma, A., Sharp, P.A., and Burge, C.B. (2008). Proliferating cells express mRNAs with shortened 3' untranslated regions and fewer microRNA target sites. Science (New York, NY) *320*, 1643-1647.

Saradhi, U.V., Gupta, S.V., Chiu, M., Wang, J., Ling, Y., Liu, Z., Newman, D.J., Covey, J.M., Kinghorn, A.D., Marcucci, G.*, et al.* (2011). Characterization of silvestrol pharmacokinetics in mice using liquid chromatography-tandem mass spectrometry. The AAPS journal *13*, 347-356.

Sarbassov, D.D., Ali, S.M., Kim, D.H., Guertin, D.A., Latek, R.R., Erdjument-Bromage, H., Tempst, P., and Sabatini, D.M. (2004). Rictor, a novel binding partner of mTOR, defines a rapamycin-insensitive and raptor-independent pathway that regulates the cytoskeleton. Current biology : CB *14*, 1296-1302.

Sarbassov, D.D., Ali, S.M., Sengupta, S., Sheen, J.H., Hsu, P.P., Bagley, A.F., Markhard, A.L., and Sabatini, D.M. (2006). Prolonged rapamycin treatment inhibits mTORC2 assembly and Akt/PKB. Molecular cell *22*, 159-168.

Sarbassov, D.D., Guertin, D.A., Ali, S.M., and Sabatini, D.M. (2005). Phosphorylation and regulation of Akt/PKB by the rictor-mTOR complex. Science (New York, NY) *307*, 1098-1101.

Sato, K., Masuda, T., Hu, Q., Tobo, T., Gillaspie, S., Niida, A., Thornton, M., Kuroda, Y., Eguchi, H., Nakagawa, T.*, et al.* (2019). Novel oncogene 5MP1 reprograms c-Myc translation initiation to drive malignant phenotypes in colorectal cancer. EBioMedicine *44*, 387-402.
Saxton, R.A., and Sabatini, D.M. (2017). mTOR Signaling in Growth, Metabolism, and Disease. Cell *168*, 960-976.
Scheper, G.C., van der Knaap, M.S., and Proud, C.G. (2007). Translation matters: protein synthesis defects in inherited disease. Nature reviews Genetics *8*, 711-723.
Scheper, G.C., van Kollenburg, B., Hu, J., Luo, Y., Goss, D.J., and Proud, C.G. (2002). Phosphorylation of eukaryotic initiation factor 4E markedly reduces its affinity for capped mRNA. The Journal of biological chemistry *277*, 3303-3309.
Schewe, D.M., and Aguirre-Ghiso, J.A. (2009). Inhibition of eIF2alpha dephosphorylation maximizes bortezomib efficiency and eliminates quiescent multiple myeloma cells surviving proteasome inhibitor therapy. Cancer research *69*, 1545-1552.
Schmid, P., Zaiss, M., Harper-Wynne, C., Ferreira, M., Dubey, S., Chan, S., Makris, A., Nemsadze, G., Brunt, A.M., Kuemmel, S.*, et al.* (2019). Fulvestrant Plus Vistusertib vs Fulvestrant Plus Everolimus vs Fulvestrant Alone for Women With Hormone Receptor-Positive Metastatic Breast Cancer: The MANTA Phase 2 Randomized Clinical Trial. JAMA oncology.
Schreiber, K.H., Ortiz, D., Academia, E.C., Anies, A.C., Liao, C.Y., and Kennedy, B.K. (2015). Rapamycin-mediated mTORC2 inhibition is determined by the relative expression of FK506-binding proteins. Aging cell *14*, 265-273.
Schutz, P., Bumann, M., Oberholzer, A.E., Bieniossek, C., Trachsel, H., Altmann, M., and Baumann, U. (2008). Crystal structure of the yeast eIF4A-eIF4G complex: an RNA-helicase controlled by protein-protein interactions. Proceedings of the National Academy of Sciences of the United States of America *105*, 9564-9569.
Schwanhausser, B., Busse, D., Li, N., Dittmar, G., Schuchhardt, J., Wolf, J., Chen, W., and Selbach, M. (2011). Global quantification of mammalian gene expression control. Nature *473*, 337-342.
Sen, N.D., Zhou, F., Harris, M.S., Ingolia, N.T., and Hinnebusch, A.G. (2016). eIF4B stimulates translation of long mRNAs with structured 5' UTRs and low closed-loop potential but weak dependence on eIF4G. Proceedings of the National Academy of Sciences of the United States of America *113*, 10464-10472.
Sengoku, T., Nureki, O., Nakamura, A., Kobayashi, S., and Yokoyama, S. (2006). Structural basis for RNA unwinding by the DEAD-box protein Drosophila Vasa. Cell *125*, 287-300.
Shabalina, S.A., Ogurtsov, A.Y., Rogozin, I.B., Koonin, E.V., and Lipman, D.J. (2004). Comparative analysis of orthologous eukaryotic mRNAs: potential hidden functional signals. Nucleic acids research *32*, 1774-1782.
Shadrick, W.R., Ndjomou, J., Kolli, R., Mukherjee, S., Hanson, A.M., and Frick, D.N. (2013). Discovering new medicines targeting helicases: challenges and recent progress. Journal of biomolecular screening *18*, 761-781.
Shah, O.J., Ghosh, S., and Hunter, T. (2003). Mitotic regulation of ribosomal S6 kinase 1 involves Ser/Thr, Pro phosphorylation of consensus and non-consensus sites by Cdc2. The Journal of biological chemistry *278*, 16433-16442.
Shah, P., Ding, Y., Niemczyk, M., Kudla, G., and Plotkin, J.B. (2013). Rate-limiting steps in yeast protein translation. Cell *153*, 1589-1601.

Shahbazian, D., Parsyan, A., Petroulakis, E., Topisirovic, I., Martineau, Y., Gibbs, B.F., Svitkin, Y., and Sonenberg, N. (2010). Control of cell survival and proliferation by mammalian eukaryotic initiation factor 4B. Mol Cell Biol *30*, 1478-1485.
Shahbazian, D., Roux, P.P., Mieulet, V., Cohen, M.S., Raught, B., Taunton, J., Hershey, J.W., Blenis, J., Pende, M., and Sonenberg, N. (2006). The mTOR/PI3K and MAPK pathways converge on eIF4B to control its phosphorylation and activity. The EMBO journal *25*, 2781-2791.
Shatsky, I.N., Terenin, I.M., Smirnova, V.V., and Andreev, D.E. (2018). Cap-Independent Translation: What's in a Name? Trends in biochemical sciences *43*, 882-895.
Shi, J., Kahle, A., Hershey, J.W., Honchak, B.M., Warneke, J.A., Leong, S.P., and Nelson, M.A. (2006). Decreased expression of eukaryotic initiation factor 3f deregulates translation and apoptosis in tumor cells. Oncogene *25*, 4923-4936.
Shveygert, M., Kaiser, C., Bradrick, S.S., and Gromeier, M. (2010). Regulation of eukaryotic initiation factor 4E (eIF4E) phosphorylation by mitogen-activated protein kinase occurs through modulation of Mnk1-eIF4G interaction. Molecular and cellular biology *30*, 5160-5167.
Silvera, D., Arju, R., Darvishian, F., Levine, P.H., Zolfaghari, L., Goldberg, J., Hochman, T., Formenti, S.C., and Schneider, R.J. (2009). Essential role for eIF4GI overexpression in the pathogenesis of inflammatory breast cancer. Nat Cell Biol *11*, 903-908.
Silvera, D., Formenti, S.C., and Schneider, R.J. (2010). Translational control in cancer. Nature reviews Cancer *10*, 254-266.
Singh, P., Wedeken, L., Waters, L.C., Carr, M.D., and Klempnauer, K.H. (2011). Pdcd4 directly binds the coding region of c-myb mRNA and suppresses its translation. Oncogene *30*, 4864-4873.
Sinvani, H., Haimov, O., Svitkin, Y., Sonenberg, N., Tamarkin-Ben-Harush, A., Viollet, B., and Dikstein, R. (2015). Translational tolerance of mitochondrial genes to metabolic energy stress involves TISU and eIF1-eIF4GI cooperation in start codon selection. Cell metabolism *21*, 479-492.
Sladic, R.T., Lagnado, C.A., Bagley, C.J., and Goodall, G.J. (2004). Human PABP binds AU-rich RNA via RNA-binding domains 3 and 4. European journal of biochemistry / FEBS *271*, 450-457.
Smit, S., Yarus, M., and Knight, R. (2006). Natural selection is not required to explain universal compositional patterns in rRNA secondary structure categories. RNA (New York, NY) *12*, 1-14.
Smurnyy, Y., Cai, M., Wu, H., McWhinnie, E., Tallarico, J.A., Yang, Y., and Feng, Y. (2014). DNA sequencing and CRISPR-Cas9 gene editing for target validation in mammalian cells. Nat Chem Biol *10*, 623-625.
Sokabe, M., and Fraser, C.S. (2017). A helicase-independent activity of eIF4A in promoting mRNA recruitment to the human ribosome. Proc Natl Acad Sci U S A *114*, 6304-6309.
Sokabe, M., Fraser, C.S., and Hershey, J.W. (2012). The human translation initiation multi-factor complex promotes methionyl-tRNAi binding to the 40S ribosomal subunit. Nucleic acids research *40*, 905-913.
Somaiah, R., Ravindar, K., Cencic, R., Pelletier, J., and Deslongchamps, P. (2014). Synthesis of the antiproliferative agent hippuristanol and its analogues from hydrocortisone via Hg(II)-catalyzed spiroketalization: structure-activity relationship. J Med Chem *57*, 2511-2523.
Sporn, M.B., and Liby, K.T. (2012). NRF2 and cancer: the good, the bad and the importance of context. Nature reviews Cancer *12*, 564-571.
Stone, S.D., Lajkiewicz, N.J., Whitesell, L., Hilmy, A., and Porco, J.A., Jr. (2015). Biomimetic kinetic resolution: highly enantio- and diastereoselective transfer hydrogenation of aglain ketones to access flavagline natural products. J Am Chem Soc *137*, 525-530.

Sui, H., Fan, Z.Z., and Li, Q. (2012). Signal transduction pathways and transcriptional mechanisms of ABCB1/Pgp-mediated multiple drug resistance in human cancer cells. The Journal of international medical research *40*, 426-435.
Sun, R., Cheng, E., Velasquez, C., Chang, Y., and Moore, P.S. (2019). Mitosis-related phosphorylation of the eukaryotic translation suppressor 4E-BP1 and its interaction with eukaryotic translation initiation factor 4E (eIF4E). The Journal of biological chemistry *294*, 11840-11852.
Sun, Y., Atas, E., Lindqvist, L.M., Sonenberg, N., Pelletier, J., and Meller, A. (2014a). Single-molecule kinetics of the eukaryotic initiation factor 4AI upon RNA unwinding. Structure (London, England : 1993) *22*, 941-948.
Sun, Y., Atas, E., Lindqvist, L.M., Sonenberg, N., Pelletier, J., and Meller, A. (2014b). Single-Molecule Kinetics of the Eukaryotic Initiation Factor 4AI upon RNA Unwinding. Structure (London, England : 1993).
Suo, J., Medina, D., Herrera, S., Zheng, Z.Y., Jin, L., Chamness, G.C., Contreras, A., Gutierrez, C., Hilsenbeck, S., Umar, A.*, et al.* (2015). Int6 reduction activates stromal fibroblasts to enhance transforming activity in breast epithelial cells. Cell & bioscience *5*, 10.
Suzuki, C., Garces, R.G., Edmonds, K.A., Hiller, S., Hyberts, S.G., Marintchev, A., and Wagner, G. (2008). PDCD4 inhibits translation initiation by binding to eIF4A using both its MA3 domains. Proceedings of the National Academy of Sciences of the United States of America *105*, 3274-3279.
Svitkin, Y.V., Herdy, B., Costa-Mattioli, M., Gingras, A.C., Raught, B., and Sonenberg, N. (2005). Eukaryotic translation initiation factor 4E availability controls the switch between cap-dependent and internal ribosomal entry site-mediated translation. Molecular and cellular biology *25*, 10556-10565.
Svitkin, Y.V., Pause, A., Haghighat, A., Pyronnet, S., Witherell, G., Belsham, G.J., and Sonenberg, N. (2001). The requirement for eukaryotic initiation factor 4A (eIF4A) in translation is in direct proportion to the degree of mRNA 5' secondary structure. RNA *7*, 382-394.
Tamburini, J., Green, A.S., Bardet, V., Chapuis, N., Park, S., Willems, L., Uzunov, M., Ifrah, N., Dreyfus, F., Lacombe, C.*, et al.* (2009). Protein synthesis is resistant to rapamycin and constitutes a promising therapeutic target in acute myeloid leukemia. Blood *114*, 1618-1627.
Tang, L., Morris, J., Wan, J., Moore, C., Fujita, Y., Gillaspie, S., Aube, E., Nanda, J., Marques, M., Jangal, M.*, et al.* (2017). Competition between translation initiation factor eIF5 and its mimic protein 5MP determines non-AUG initiation rate genome-wide. Nucleic acids research *45*, 11941-11953.
Tao, S., Wang, S., Moghaddam, S.J., Ooi, A., Chapman, E., Wong, P.K., and Zhang, D.D. (2014). Oncogenic KRAS confers chemoresistance by upregulating NRF2. Cancer research *74*, 7430-7441.
Tauber, D., Tauber, G., Khong, A., Van Treeck, B., Pelletier, J., and Parker, R. (2019). Modulation of RNA condensation by the eIF4A RNA helicase. bioRxiv, 689802.
Tecle, H., Shao, J., Li, Y., Kothe, M., Kazmirski, S., Penzotti, J., Ding, Y.H., Ohren, J., Moshinsky, D., Coli, R.*, et al.* (2009). Beyond the MEK-pocket: can current MEK kinase inhibitors be utilized to synthesize novel type III NCKIs? Does the MEK-pocket exist in kinases other than MEK? Bioorg Med Chem Lett *19*, 226-229.
Teng, Y., Gao, M., Wang, J., Kong, Q., Hua, H., Luo, T., and Jiang, Y. (2014). Inhibition of eIF2alpha dephosphorylation enhances TRAIL-induced apoptosis in hepatoma cells. Cell death & disease *5*, e1060.
Thakur, A., and Hinnebusch, A.G. (2018). eIF1 Loop 2 interactions with Met-tRNAi control the accuracy of start codon selection by the scanning preinitiation complex. Proceedings of the National Academy of Sciences of the United States of America *115*, E4159-e4168.

Theissen, B., Karow, A.R., Kohler, J., Gubaev, A., and Klostermeier, D. (2008). Cooperative binding of ATP and RNA induces a closed conformation in a DEAD box RNA helicase. Proceedings of the National Academy of Sciences of the United States of America *105*, 548-553.
Thoreen, C.C., Chantranupong, L., Keys, H.R., Wang, T., Gray, N.S., and Sabatini, D.M. (2012). A unifying model for mTORC1-mediated regulation of mRNA translation. Nature *485*, 109-113.
Thoreen, C.C., Kang, S.A., Chang, J.W., Liu, Q., Zhang, J., Gao, Y., Reichling, L.J., Sim, T., Sabatini, D.M., and Gray, N.S. (2009). An ATP-competitive mammalian target of rapamycin inhibitor reveals rapamycin-resistant functions of mTORC1. The Journal of biological chemistry *284*, 8023-8032.
Thuaud, F., Ribeiro, N., Nebigil, C.G., and Desaubry, L. (2013). Prohibitin ligands in cell death and survival: mode of action and therapeutic potential. Chemistry & biology *20*, 316-331.
Thurner, C., Witwer, C., Hofacker, I.L., and Stadler, P.F. (2004). Conserved RNA secondary structures in Flaviviridae genomes. The Journal of general virology *85*, 1113-1124.
Tiedge, H., Fremeau, R.T., Jr., Weinstock, P.H., Arancio, O., and Brosius, J. (1991). Dendritic location of neural BC1 RNA. Proceedings of the National Academy of Sciences of the United States of America *88*, 2093-2097.
Todt, D., Moeller, N., Praditya, D., Kinast, V., Friesland, M., Engelmann, M., Verhoye, L., Sayed, I.M., Behrendt, P., Dao Thi, V.L.*, et al.* (2018). The natural compound silvestrol inhibits hepatitis E virus (HEV) replication in vitro and in vivo. Antiviral research *157*, 151-158.
Tomonaga, T., Matsushita, K., Yamaguchi, S., Oh-Ishi, M., Kodera, Y., Maeda, T., Shimada, H., Ochiai, T., and Nomura, F. (2004). Identification of altered protein expression and post-translational modifications in primary colorectal cancer by using agarose two-dimensional gel electrophoresis. Clinical cancer research : an official journal of the American Association for Cancer Research *10*, 2007-2014.
Tomoo, K., Shen, X., Okabe, K., Nozoe, Y., Fukuhara, S., Morino, S., Ishida, T., Taniguchi, T., Hasegawa, H., Terashima, A.*, et al.* (2002). Crystal structures of 7-methylguanosine 5'-triphosphate (m(7)GTP)- and P(1)-7-methylguanosine-P(3)-adenosine-5',5'-triphosphate (m(7)GpppA)-bound human full-length eukaryotic initiation factor 4E: biological importance of the C-terminal flexible region. The Biochemical journal *362*, 539-544.
Topisirovic, I., Ruiz-Gutierrez, M., and Borden, K.L. (2004). Phosphorylation of the eukaryotic translation initiation factor eIF4E contributes to its transformation and mRNA transport activities. Cancer Res *64*, 8639-8642.
Treiber, T., Treiber, N., and Meister, G. (2019). Regulation of microRNA biogenesis and its crosstalk with other cellular pathways. Nature reviews Molecular cell biology *20*, 5-20.
Tremblay, F., and Marette, A. (2001). Amino acid and insulin signaling via the mTOR/p70 S6 kinase pathway. A negative feedback mechanism leading to insulin resistance in skeletal muscle cells. The Journal of biological chemistry *276*, 38052-38060.
Truitt, M.L., Conn, C.S., Shi, Z., Pang, X., Tokuyasu, T., Coady, A.M., Seo, Y., Barna, M., and Ruggero, D. (2015). Differential Requirements for eIF4E Dose in Normal Development and Cancer. Cell *162*, 59-71.
Tschopp, C., Knauf, U., Brauchle, M., Zurini, M., Ramage, P., Glueck, D., New, L., Han, J., and Gram, H. (2000). Phosphorylation of eIF-4E on Ser 209 in response to mitogenic and inflammatory stimuli is faithfully detected by specific antibodies. Molecular cell biology research communications : MCBRC *3*, 205-211.

Tsokanos, F.F., Albert, M.A., Demetriades, C., Spirohn, K., Boutros, M., and Teleman, A.A. (2016). eIF4A inactivates TORC1 in response to amino acid starvation. The EMBO journal *35*, 1058-1076.
Tsumuraya, T., Ishikawa, C., Machijima, Y., Nakachi, S., Senba, M., Tanaka, J., and Mori, N. (2011). Effects of hippuristanol, an inhibitor of eIF4A, on adult T-cell leukemia. Biochemical pharmacology *81*, 713-722.
Tung, M.C., Lin, P.L., Wang, Y.C., He, T.Y., Lee, M.C., Yeh, S.D., Chen, C.Y., and Lee, H. (2015). Mutant p53 confers chemoresistance in non-small cell lung cancer by upregulating Nrf2. Oncotarget *6*, 41692-41705.
Ueda, T., Sasaki, M., Elia, A.J., Chio, II, Hamada, K., Fukunaga, R., and Mak, T.W. (2010). Combined deficiency for MAP kinase-interacting kinase 1 and 2 (Mnk1 and Mnk2) delays tumor development. Proceedings of the National Academy of Sciences of the United States of America *107*, 13984-13990.
van Gorp, A.G., van der Vos, K.E., Brenkman, A.B., Bremer, A., van den Broek, N., Zwartkruis, F., Hershey, J.W., Burgering, B.M., Calkhoven, C.F., and Coffer, P.J. (2009). AGC kinases regulate phosphorylation and activation of eukaryotic translation initiation factor 4B. Oncogene *28*, 95-106.
Van Treeck, B., Protter, D.S.W., Matheny, T., Khong, A., Link, C.D., and Parker, R. (2018). RNA self-assembly contributes to stress granule formation and defining the stress granule transcriptome. Proceedings of the National Academy of Sciences of the United States of America *115*, 2734-2739.
Vandamme, T., Beyens, M., de Beeck, K.O., Dogan, F., van Koetsveld, P.M., Pauwels, P., Mortier, G., Vangestel, C., de Herder, W., Van Camp, G.*, et al.* (2016). Long-term acquired everolimus resistance in pancreatic neuroendocrine tumours can be overcome with novel PI3K-AKT-mTOR inhibitors. British journal of cancer *114*, 650-658.
Vassilenko, K.S., Alekhina, O.M., Dmitriev, S.E., Shatsky, I.N., and Spirin, A.S. (2011). Unidirectional constant rate motion of the ribosomal scanning particle during eukaryotic translation initiation. Nucleic acids research *39*, 5555-5567.
Vattem, K.M., and Wek, R.C. (2004). Reinitiation involving upstream ORFs regulates ATF4 mRNA translation in mammalian cells. Proceedings of the National Academy of Sciences of the United States of America *101*, 11269-11274.
Vaysse, C., Philippe, C., Martineau, Y., Quelen, C., Hieblot, C., Renaud, C., Nicaise, Y., Desquesnes, A., Pannese, M., Filleron, T.*, et al.* (2015). Key contribution of eIF4H-mediated translational control in tumor promotion. Oncotarget *6*, 39924-39940.
Velasquez, C., Cheng, E., Shuda, M., Lee-Oesterreich, P.J., Pogge von Strandmann, L., Gritsenko, M.A., Jacobs, J.M., Moore, P.S., and Chang, Y. (2016). Mitotic protein kinase CDK1 phosphorylation of mRNA translation regulator 4E-BP1 Ser83 may contribute to cell transformation. Proceedings of the National Academy of Sciences of the United States of America *113*, 8466-8471.
Villa, N., Do, A., Hershey, J.W., and Fraser, C.S. (2013). Human eukaryotic initiation factor 4G (eIF4G) protein binds to eIF3c, -d, and -e to promote mRNA recruitment to the ribosome. The Journal of biological chemistry *288*, 32932-32940.
Virgili, G., Frank, F., Feoktistova, K., Sawicki, M., Sonenberg, N., Fraser, C.S., and Nagar, B. (2013). Structural analysis of the DAP5 MIF4G domain and its interaction with eIF4A. Structure (London, England : 1993) *21*, 517-527.
Visa, N., Izaurralde, E., Ferreira, J., Daneholt, B., and Mattaj, I.W. (1996). A nuclear cap-binding complex binds Balbiani ring pre-mRNA cotranscriptionally and accompanies the ribonucleoprotein particle during nuclear export. The Journal of cell biology *133*, 5-14.

Vukmirovic, M., Manojlovic, Z., and Stefanovic, B. (2013). Serine-threonine kinase receptor-associated protein (STRAP) regulates translation of type I collagen mRNAs. Mol Cell Biol *33*, 3893-3906.
Wabnitz, P.D., DE), Gehling, Matthias (Leichlingen, DE), Henkel, Thomas (Wuppertal, DE), Schmitz, Lienhard M. (Marburg, DE) (2012). INHIBITORS OF HIF-1 PROTEIN ACCUMULATION (United States: INTERMED DISCOVERY GMBH (Dortmund, DE)).
Walton, G.M., and Gill, G.N. (1975). Nucleotide regulation of a eukaryotic protein synthesis initiation complex. Biochimica et biophysica acta *390*, 231-245.
Wander, S.A., Hennessy, B.T., and Slingerland, J.M. (2011). Next-generation mTOR inhibitors in clinical oncology: how pathway complexity informs therapeutic strategy. The Journal of clinical investigation *121*, 1231-1241.
Wang, H., Iacoangeli, A., Popp, S., Muslimov, I.A., Imataka, H., Sonenberg, N., Lomakin, I.B., and Tiedge, H. (2002). Dendritic BC1 RNA: functional role in regulation of translation initiation. The Journal of neuroscience : the official journal of the Society for Neuroscience *22*, 10232-10241.
Wang, H., Ru, Y., Sanchez-Carbayo, M., Wang, X., Kieft, J.S., and Theodorescu, D. (2013). Translation initiation factor eIF3b expression in human cancer and its role in tumor growth and lung colonization. Clinical cancer research : an official journal of the American Association for Cancer Research *19*, 2850-2860.
Wang, X., Flynn, A., Waskiewicz, A.J., Webb, B.L., Vries, R.G., Baines, I.A., Cooper, J.A., and Proud, C.G. (1998). The phosphorylation of eukaryotic initiation factor eIF4E in response to phorbol esters, cell stresses, and cytokines is mediated by distinct MAP kinase pathways. The Journal of biological chemistry *273*, 9373-9377.
Weingarten-Gabbay, S., Elias-Kirma, S., Nir, R., Gritsenko, A.A., Stern-Ginossar, N., Yakhini, Z., Weinberger, A., and Segal, E. (2016). Comparative genetics. Systematic discovery of cap-independent translation sequences in human and viral genomes. Science (New York, NY) *351*.
Wek, R.C., Jiang, H.Y., and Anthony, T.G. (2006). Coping with stress: eIF2 kinases and translational control. Biochemical Society transactions *34*, 7-11.
Wen, F., Zhou, R., Shen, A., Choi, A., Uribe, D., and Shi, J. (2012). The tumor suppressive role of eIF3f and its function in translation inhibition and rRNA degradation. PloS one *7*, e34194.
Wendel, H.G., De Stanchina, E., Fridman, J.S., Malina, A., Ray, S., Kogan, S., Cordon-Cardo, C., Pelletier, J., and Lowe, S.W. (2004). Survival signalling by Akt and eIF4E in oncogenesis and cancer therapy. Nature *428*, 332-337.
Wendel, H.G., Silva, R.L., Malina, A., Mills, J.R., Zhu, H., Ueda, T., Watanabe-Fukunaga, R., Fukunaga, R., Teruya-Feldstein, J., Pelletier, J., *et al.* (2007). Dissecting eIF4E action in tumorigenesis. Genes & development *21*, 3232-3237.
Wethmar, K., Barbosa-Silva, A., Andrade-Navarro, M.A., and Leutz, A. (2014). uORFdb--a comprehensive literature database on eukaryotic uORF biology. Nucleic acids research *42*, D60-67.
Wilbert, M.L., Huelga, S.C., Kapeli, K., Stark, T.J., Liang, T.Y., Chen, S.X., Yan, B.Y., Nathanson, J.L., Hutt, K.R., Lovci, M.T., *et al.* (2012). LIN28 binds messenger RNAs at GGAGA motifs and regulates splicing factor abundance. Molecular cell *48*, 195-206.
Wilkie, G.S., Dickson, K.S., and Gray, N.K. (2003). Regulation of mRNA translation by 5'- and 3'-UTR-binding factors. Trends in biochemical sciences *28*, 182-188.

Wilson, M.C., Sawicki, S.G., White, P.A., and Darnell, J.E., Jr. (1978). A correlation between the rate of poly(A) shortening and half-life of messenger RNA in adenovirus transformed cells. Journal of molecular biology *126*, 23-36.
Wilson, T.R., Longley, D.B., and Johnston, P.G. (2006). Chemoresistance in solid tumours. Annals of oncology : official journal of the European Society for Medical Oncology / ESMO *17 Suppl 10*, x315-324.
Wolfe, A.L., Singh, K., Zhong, Y., Drewe, P., Rajasekhar, V.K., Sanghvi, V.R., Mavrakis, K.J., Jiang, M., Roderick, J.E., Van der Meulen, J.*, et al.* (2014). RNA G-quadruplexes cause eIF4A-dependent oncogene translation in cancer. Nature *513*, 65-70.
Wolking, S., Schaeffeler, E., Lerche, H., Schwab, M., and Nies, A.T. (2015). Impact of Genetic Polymorphisms of ABCB1 (MDR1, P-Glycoprotein) on Drug Disposition and Potential Clinical Implications: Update of the Literature. Clinical pharmacokinetics *54*, 709-735.
Wu, D., Matsushita, K., Matsubara, H., Nomura, F., and Tomonaga, T. (2011). An alternative splicing isoform of eukaryotic initiation factor 4H promotes tumorigenesis in vivo and is a potential therapeutic target for human cancer. International journal of cancer Journal international du cancer *128*, 1018-1030.
Wu, Y., Giaisi, M., Kohler, R., Chen, W.M., Krammer, P.H., and Li-Weber, M. (2017). Rocaglamide breaks TRAIL-resistance in human multiple myeloma and acute T-cell leukemia in vivo in a mouse xenogtraft model. Cancer letters *389*, 70-77.
Xie, M., Li, M., Vilborg, A., Lee, N., Shu, M.D., Yartseva, V., Sestan, N., and Steitz, J.A. (2013). Mammalian 5'-capped microRNA precursors that generate a single microRNA. Cell *155*, 1568-1580.
Yan, X., Hoek, T.A., Vale, R.D., and Tanenbaum, M.E. (2016). Dynamics of Translation of Single mRNA Molecules In Vivo. Cell *165*, 976-989.
Yanagiya, A., Svitkin, Y.V., Shibata, S., Mikami, S., Imataka, H., and Sonenberg, N. (2009). Requirement of RNA binding of mammalian eukaryotic translation initiation factor 4GI (eIF4GI) for efficient interaction of eIF4E with the mRNA cap. Molecular and cellular biology *29*, 1661-1669.
Yang, D.Q., and Kastan, M.B. (2000). Participation of ATM in insulin signalling through phosphorylation of eIF-4E-binding protein 1. Nature cell biology *2*, 893-898.
Yang, H.S., Jansen, A.P., Komar, A.A., Zheng, X., Merrick, W.C., Costes, S., Lockett, S.J., Sonenberg, N., and Colburn, N.H. (2003a). The transformation suppressor Pdcd4 is a novel eukaryotic translation initiation factor 4A binding protein that inhibits translation. Molecular and cellular biology *23*, 26-37.
Yang, H.S., Knies, J.L., Stark, C., and Colburn, N.H. (2003b). Pdcd4 suppresses tumor phenotype in JB6 cells by inhibiting AP-1 transactivation. Oncogene *22*, 3712-3720.
Yang, J., Wang, J., Chen, K., Guo, G., Xi, R., Rothman, P.B., Whitten, D., Zhang, L., Huang, S., and Chen, J.L. (2013a). eIF4B phosphorylation by pim kinases plays a critical role in cellular transformation by Abl oncogenes. Cancer research *73*, 4898-4908.
Yang, L., Guell, M., Byrne, S., Yang, J.L., De Los Angeles, A., Mali, P., Aach, J., Kim-Kiselak, C., Briggs, A.W., Rios, X.*, et al.* (2013b). Optimization of scarless human stem cell genome editing. Nucleic Acids Res *41*, 9049-9061.
Yao, J.C., Shah, M.H., Ito, T., Bohas, C.L., Wolin, E.M., Van Cutsem, E., Hobday, T.J., Okusaka, T., Capdevila, J., de Vries, E.G.*, et al.* (2011). Everolimus for advanced pancreatic neuroendocrine tumors. The New England journal of medicine *364*, 514-523.

Yoder-Hill, J., Pause, A., Sonenberg, N., and Merrick, W.C. (1993). The p46 subunit of eukaryotic initiation factor (eIF)-4F exchanges with eIF-4A. The Journal of biological chemistry *268*, 5566-5573.
Young, N.P., Stumpf, C.R., Chen, J., Chiang, G.G., Thompson, P.A., and Webster, K.R. (2019). Abstract 4343: A focused CRISPR screen to identify synthetic lethal interactions with the novel eIF4A inhibitor eFT226 in KRAS driven NSCLC. Cancer research *79*, 4343-4343.
Yueh, H., Gao, Q., Porco, J.A., Jr., and Beeler, A.B. (2017). A photochemical flow reactor for large scale syntheses of aglain and rocaglate natural product analogues. Bioorg Med Chem *25*, 6197-6202.
Zhang, L., Kasif, S., Cantor, C.R., and Broude, N.E. (2004). GC/AT-content spikes as genomic punctuation marks. Proceedings of the National Academy of Sciences of the United States of America *101*, 16855-16860.
Zhang, L., Pan, X., and Hershey, J.W. (2007). Individual overexpression of five subunits of human translation initiation factor eIF3 promotes malignant transformation of immortal fibroblast cells. The Journal of biological chemistry *282*, 5790-5800.
Zhang, P., McGrath, B.C., Reinert, J., Olsen, D.S., Lei, L., Gill, S., Wek, S.A., Vattem, K.M., Wek, R.C., Kimball, S.R.*, et al.* (2002). The GCN2 eIF2alpha kinase is required for adaptation to amino acid deprivation in mice. Molecular and cellular biology *22*, 6681-6688.
Zhang, W., Chu, J., Cyr, A.M., Yueh, H., Brown, L.E., Wang, T.T., Pelletier, J., and Porco, J.A. (2019). Intercepted Retro-Nazarov Reaction: Syntheses of Amidino-Rocaglate Derivatives and Their Biological Evaluation as eIF4A Inhibitors. J Am Chem Soc.
Zhao, C., He, R., Shen, M., Zhu, F., Wang, M., Liu, Y., Chen, H., Li, X., and Qin, R. (2019). PINK1/Parkin-Mediated Mitophagy Regulation by Reactive Oxygen Species Alleviates Rocaglamide A-Induced Apoptosis in Pancreatic Cancer Cells. Frontiers in pharmacology *10*, 968.
Zheng, H.C. (2017). The molecular mechanisms of chemoresistance in cancers. Oncotarget *8*, 59950-59964.
Zindy, P., Berge, Y., Allal, B., Filleron, T., Pierredon, S., Cammas, A., Beck, S., Mhamdi, L., Fan, L., Favre, G.*, et al.* (2011). Formation of the eIF4F translation-initiation complex determines sensitivity to anticancer drugs targeting the EGFR and HER2 receptors. Cancer research *71*, 4068-4073.
Zuberek, J., Kubacka, D., Jablonowska, A., Jemielity, J., Stepinski, J., Sonenberg, N., and Darzynkiewicz, E. (2007). Weak binding affinity of human 4EHP for mRNA cap analogs. RNA (New York, NY) *13*, 691-697.